

SCHOOL OF
CIVIL ENGINEERING

INDIANA

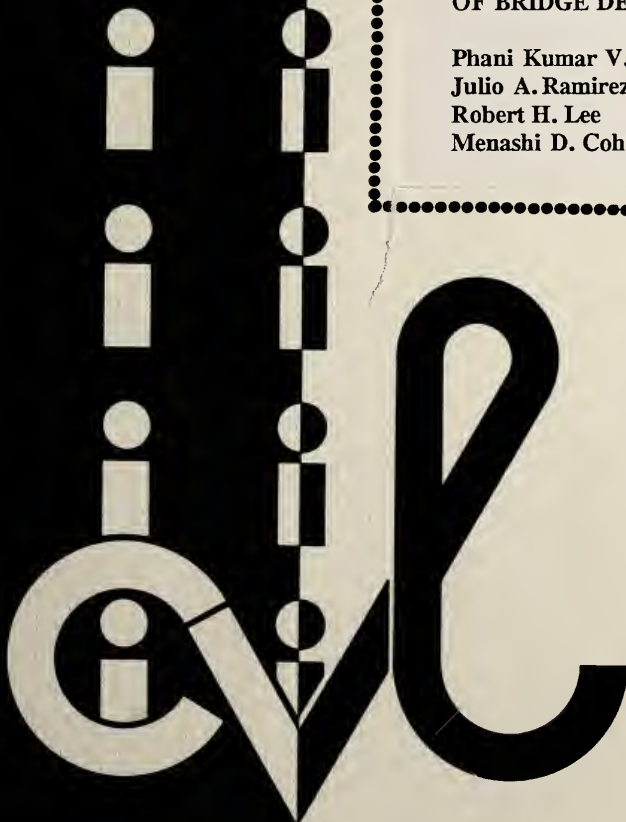
DEPARTMENT OF TRANSPORTATION

JOINT HIGHWAY RESEARCH PROJECT

FHWA/IN/JHRP-94/11
Final Report

STAY-IN-PLACE DECK FORMS -
HORIZONTAL SHEAR STRENGTH
OF BRIDGE DECK PANELS - PART 2

Phani Kumar V. V. Nukala
Julio A. Ramirez
Robert H. Lee
Menashi D. Cohen



PURDUE UNIVERSITY



JOINT HIGHWAY RESEARCH PROJECT

FHWA/IN/JHRP-94/11

Final Report

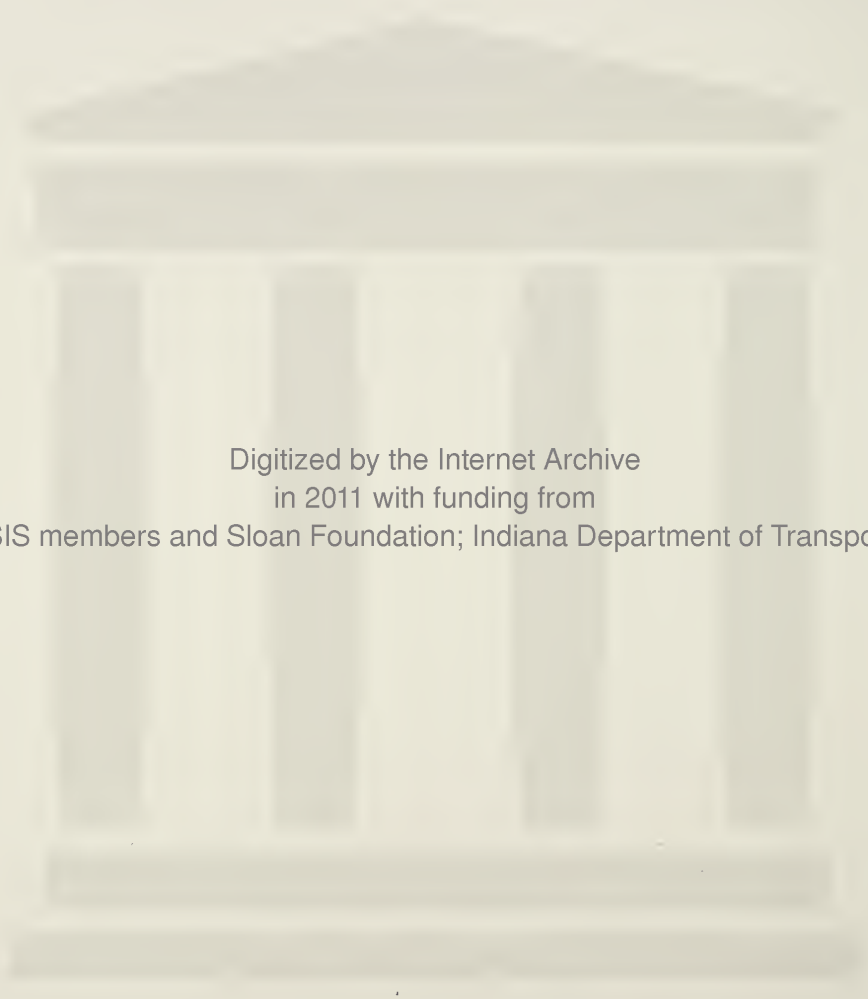
**STAY-IN-PLACE DECK FORMS -
HORIZONTAL SHEAR STRENGTH
OF BRIDGE DECK PANELS - PART 2**

Phani Kumar V. V. Nukala

Julio A. Ramirez

Robert H. Lee

Menashi D. Cohen



Digitized by the Internet Archive
in 2011 with funding from
LYRASIS members and Sloan Foundation; Indiana Department of Transportation

<http://www.archive.org/details/stayinplacedeckf00nuka>

1. Report No. FHWA/TN/JHRP-94/11	2. Government Accession No.	3. Recipient's Catalog No.	
4. Title and Subtitle Stay-in-Place Deck Forms - Horizontal Shear Strength on Bridge Deck Panels - Part 2		5. Report Date August 28, 1995	
		6. Performing Organization Code	
7. Author(s) Phani Kumar V. V. Nukala, Julio A. Ramirez, Robert H. Lee and Menashi Cohen		8. Performing Organization Report No. FHWA/TN/JHRP-94/11	
9. Performing Organization Name and Address Joint Highway Research Project Civil Engineering Building Purdue University West Lafayette, Indiana 47907-1284		10. Work Unit No.	
		11. Contract or Grant No.	
12. Sponsoring Agency Name and Address Indiana Department of Transportation Indiana Government Center North 100 North Senate Avenue Indianapolis, IN 46204		13. Type of Report and Period Covered Final Report Executive Summary July 1, 1992 - June 30, 1994	
		14. Sponsoring Agency Code	
15. Supplementary Notes Conducted in cooperation with the U.S. Department of Transportation, Federal Highway Administration.			
16. Abstract One of the most economic methods of bridge deck construction consists of prestressed concrete deck panels used in stay-in-place forms in conjunction with the cast-in-place concrete topping instead of the traditional monolithic roadway deck slabs. The performance of this type of deck as a composite unit is only possible if the horizontal shear stress resulting from bending of the deck is effectively transferred across the interface of the two elements. It is assumed that horizontal shear stresses are transmitted across the interface due to bond between the precast panel and cast-in-place concrete acting in conjunction with the horizontal shear connectors provided across the interface. Presently the Indiana Department of Transportation requires a minimum of 20 shear connectors regardless of the panel dimensions. The shear connectors are placed across a broom finished deck panel surface. Broom finish with approximately 0.05 to 0.075 in. (1.27 to 1.91 mm) total amplitude deformations is specified instead of a raked finish with a total amplitude of 0.25 in. (6.35 mm) because of the reduced 2.5 in (63.5 mm) thickness of the panels used in Indiana. This study focuses on the evaluation of the horizontal shear strength across a broom finished interface. Experiments were undertaken on six precast prestressed deck panels with composite cast-in-place concrete topping. All the specimens were 8 ft. x 8 ft. (2.4 m x 2.4 m) and 2.5 in. (63.5 mm) thick precast prestressed panels with a 5.5 in (140 mm) topping slab. Specimens 1 and 5 had no shear connectors and Specimens 2, 3 and 6 had four shear connectors across the interface. Specimen 4 had four shear connectors and the top of the precast panel was sprayed with a bond breaking agent (form oil) to eliminate chemical bonding between the precast panel and cast-in-place concrete topping. The test results indicated that shear connectors are not required to achieve adequate composite action at service and ultimate load levels in panels with broom finished top surface. This finding is limited to situations where the nominal average shear stress does not exceed 115 psi. A minimum of 4 shear connectors will likely be provided for handling purposes. A comparison of the performance of the specimens in this study with and without shear connectors indicates that specimens with four shear connectors were stiffer near failure load. The minimum of 4 connectors did not significantly increase the load carrying capacity of the panels tested. Lubrication of the interface in Specimen 4 resulted in a 10% decrease in ultimate capacity as compared to that of companion Specimen 3. But the failure load in Specimen 4 was 82% higher than the predicted value based on development length requirements (strand slip criteria).			
17. Key Words precast, prestressed, deck panels, horizontal shear, shear connectors, friction, strength, and detailing		18. Distribution Statement No restrictions. This document is available to the public through the National Technical Information Service, Virginia, 22161	
19. Security Classif. (of this report) Unclassified	20. Security Classif. (of this page) Unclassified	21. No. of Pages 226	22. Price

FINAL REPORT

STAY-IN-PLACE DECK FORMS-HORIZONTAL SHEAR STRENGTH
ON BRIDGE DECK PANELS - PART 2

by

Phani Kumar V. V. Nukala

Julio A. Ramirez

Robert H. Lee

and

Menashi Cohen
Purdue University
Department of Civil Engineering

Joint Highway Research Project

Project No: C-36-56EE
File No: 7-4-31

In cooperation with the
Indiana Department of Transportation

and

Federal Highway Administration

The contents of this report reflect the views of the author who is responsible for the facts and the accuracy of the data presented herein. The contents do not necessarily reflect the official views or policies of the Federal Highway Administration and the Indiana Department of Transportation. This report does not constitute a standard, specification or regulation.

Purdue University
West Lafayette, IN 47907
August 28, 1995

STAY IN PLACE DECK FORMS - HORIZONTAL SHEAR STRENGTH OF BRIDGE DECK PANELS - PART 2

IMPLEMENTATION REPORT

1. General

The use of precast concrete for new bridge construction and for the rehabilitation of deteriorated bridges is economically and structurally attractive. Durability, ease and speed of construction, together with reduced need for maintenance are all advantages in using precast concrete. Precast prestressed concrete bridge deck panels are used with CIP concrete to provide a convenient and cost effective method of construction for concrete bridge decks. In this study, emphasis is placed on the behavior of stay-in-place precast panels in conjunction with CIP decks under the action of applied loads. During the past 12 years the construction cost of bridge decks in Indiana has been reduced by the use of these stay-in-place deck forms.

The main objective of this study was to evaluate the horizontal shear friction requirements for prestressed deck panels in bridge construction with broom finished top surface. Currently INDOT requires a total of 20 shear connectors across the interface regardless of panel dimensions. This study addresses the specific INDOT concerns dealing with the number of horizontal shear connectors required in precast panels with broom finished top surface. The issues of potential separation of the precast prestressed panel from the cast-in-place portion of the deck, as well as the adequate development of positive moment and shear capacities of the composite section were examined experimentally.

2. Research Program

To accomplish the objective of this study, an experimental program consisting of six full-scale composite stay-in-place deck slabs was conducted. These specimens had different interface characteristics including different amounts of horizontal shear reinforcement across the interface. Specimens 1-4 had 18 prestressing strands representing a practical upper limit on the amount of flexural reinforcement in this type of member. These specimens were tested to evaluate the potential maximum horizontal shear demand. Specimen 4 had a lubricated interface with form oil to simulate extreme lack of cleanliness during construction. This ensures the elimination of chemical bond between the precast panel and the cast-in-place topping. Specimens 5 and 6 had 12 prestressing strands. These last two specimens were used to evaluate the effect of repeated loading due to an increase in mean shear stress at the interface. In addition, these specimens were intended to evaluate the amount of shear to be transferred in deck panels designed according to AASHTO for HS20 loading.

All six composite specimens consisted of a 2.5 in. thick precast prestressed panels with a 5.5 in. thick CIP reinforced concrete topping slab. This provided an 8 in. standard full deck

thickness as commonly used in Indiana. The longitudinal dimension of the panel depends on the spacing of longitudinal bridge girders. A panel length equal to 8 ft was chosen as it falls in the range of medium to wide girder spacing. A width of 8 ft. was chosen as it represents the upper practical limit due to handling considerations. The prestressing strands were Lo-Lax, Grade 270, with a 3/8 in. diameter. The mild reinforcing steel in the panel was Grade 60 and met the requirements of ASTM A-615. Welded wire fabric was according to ASTM A-497 requirements. Panels were roughened in the direction parallel to the strands so as to minimize the reduction in section modulus. The broom finished surface provided deformation with approximately 0.05 to 0.075 in. amplitude. This is less than the standard raked surface amplitude of 0.25 in. Strands were prestressed to about 17.5 kips (corrected for slip loss which was estimated to be approximately 0.3 kips) approximately equal to $0.75 f_{pu}$, where f_{pu} is the ultimate strand tensile strength. Each panel had a single layer of welded wire fabric located directly on top of the prestressing strands. In addition, these panels contained five #3 reinforcing bars placed at 6 in., 18 in. and 48 in. from either end of the panel.

The reinforcement in the CIP slab was nominal and placed in the concrete to take care of the temperature and shrinkage stresses. The transverse reinforcement consisted of #5 bars spaced at 9 in. on centers supported on 1.75 in. high bar chairs spaced at approximately 2 ft on centers. The bar chairs rested directly on the top surface of the precast panels. The longitudinal reinforcement parallel to the prestressing strands consisted of #5 bars spaced at 6 in. on centers, placed on top of the transverse reinforcement. All reinforcing bars were ASTM A615-90, Grade 60 bars. These bars were not epoxy-coated and the clear cover to the top bars was 2.5 inches. End cover was 3 inches. The design concrete compressive strength was 4000 psi.

These specimens were tested under static and cyclic loadings. All loads were applied by hydraulic actuators. Static load tests were performed at regular intervals of repeated loading. The specimens were tested under repeated loading to simulate traffic effects on the horizontal shear strength of the panel at the interface between the precast panel and the cast-in-place portion of the deck. Following cyclic loading, the specimens were monotonically loaded to failure.

When the load is applied over the wheel foot print, it has been found that punching shear usually governs the ultimate strength of the slab in a monotonic loading situation. In these cases the full flexural capacity of the panels would not be achieved and thus the maximum uniform horizontal shear stress at the interface is not developed across the entire width of the panel. Thus to find the horizontal shear capacity of the panel, the loading area was extended over the entire width of the panel. In this study, horizontal shear capacity was also examined in the limit of flexural failure of the specimen. The load was distributed over an area of 10 in. x 96 in.

The performance of the deck system was obtained by evaluating the following data:

- 1) Load versus deflection characteristics
- 2) Interface slip characteristics
- 3) Load versus strand slip characteristics
- 4) Behavior under cyclic loading

5) Load versus strain at various locations of the specimens

To obtain the above data, instrumentation was provided at appropriate locations. During all the static load tests, strains and deflection were monitored. To observe the cyclic loading effect on these specimens, intermediate static tests were performed at regular intervals, during these static tests behavior of these specimens was observed. Data collected at the end of each of these intermediate static tests were analyzed to observe the effect of cyclic loading on stiffness and ductility characteristics of steel and concrete elements in the specimen.

3. Findings from Experimental Program

3.1 Strand Development

Strand development lengths necessary to attain the full strength of strands were not obtained experimentally on a quantitative basis. However, a qualitative evaluation of the strand development lengths was obtained by monitoring the ends of selected strands for their slip relative to the panel ends. Slippage of prestressing strands was observed in all of the ultimate monotonic loading cycles of the six specimens. Specimens 3 and 4 showed a significant difference in their loads (P_{ssmin}) at which strand slip in the monitored strands was observed, when compared with the loads at which strands slipped in Specimens 1 and 2. In these specimens, strand slip might have occurred earlier than observed in some of the non-monitored strands. However, in all the specimens a minimum reserve capacity of about 22.5% above that of the strand slip loads observed was noted at failures. The strand slip loads for the first four specimens were within 4.17 to 5.87 times the service load of 26.4 kips (equivalent to standard AASHTO wheel load with a 30% impact factor). In Specimens 5 and 6 this ratio was 3.60 and 3.79 respectively (see Table 4.9). These ratios in the last two specimens roughly correspond to the same stress level at the strand locations as that of Specimens 1-4.

3.2 Interface Slip

Composite behavior between the precast panels and the reinforced concrete topping slab is assumed to exist for conventional analysis of these types of bridge decks. For the equivalent service level wheel load of 26.4 kips, that was applied to all the specimens, and for the equivalent factored wheel load equal to 57.3 kips, interface slip was not observed. In Specimens 1-4, significant slip at the interface occurred only at maximum load levels. In these cases, the minimum ratio of significant slip load to the ultimate load was about 0.8. No interface slip was observed in Specimens 5 and 6.

3.3 Load Deflection Behavior

The load versus deflection behavior of the composite slab specimens was linear elastic at both the equivalent wheel service and factored load levels. The midspan slab deflections were quite small at both of these load levels. Just before the failure of specimens, LVDTs were removed to prevent them from getting damaged. In the case of the first four specimens whose failure occurred in shear mode, the deflections recorded by LVDTs were within a range of 0.4

to 0.55 inches. At failure, deflection recorded by the micro profiler of the controller, was in the range of 0.9 to 1.0 inch. These readings were confirmed with the readings obtained in the case of Specimen 2, where the LVDTs were not removed prior to failure of the specimen. The load-deflection behavior of Specimens 5 and 6 was the same as the previous four panels for the majority of the loading cycle. The behavior was linear elastic at both the service load level and the factored load level. Just before failure, the measured deflection was about 1.8 inches in both specimens. This larger deflection was due to their ductile flexural mode of failure compared to the sudden beam-shear mode failure in the first four specimens. Load versus deflection behavior in general can be separated into three main stages. In Stage 1, deflection varied linearly up to cracking load. In a few cases this crack did not appear over the entire width of the specimen up to a higher load level. In Stage 2, which is post-cracking stage, deflection varied at a much faster rate than in Stage 1. Load versus deflection behavior in this stage can also be roughly described as linear. Near the maximum load level, there was a sudden increase in deflection for very small increments in load. This signified the end of Stage 2 and beginning of Stage 3. In Stage 3, deflection increased rapidly with small increments in load up to failure.

3.4 Strains in Reinforcement and Concrete

Strain gages were placed at various locations on the prestressing strands, on the concrete deck and also on the CIP bars. In Specimens 1-4 load versus strand strain characteristics were linear, both at the equivalent wheel service load and at the equivalent wheel factored load levels. Even at the factored load level, strain was below $7000\text{ }\mu\epsilon$ which is below the elastic limit of the strand steel. Hence strands were not loaded into their inelastic range at equivalent wheel factored loads. Once the load exceeded cracking levels, as expected, there was a sudden change in strain value. In the strands where slippage was observed, there was either a reduction in strain or constant strain. In the strands where slippage was not observed, there was an increase in strain with increasing load level and at the time of failure, the stress in the strands reached almost their ultimate capacity. In Specimens 5 and 6, similar behavior was observed except that at the ultimate load levels, due to ductile flexural behavior, the stress in the strands was much higher. Some of the strands in these last two specimens fractured at failure.

Load versus strain readings from gages located at the top of the CIP slab varied linearly up to the flexural cracking load. With further increase in load, strain increased suddenly. Near maximum load levels, there was a sudden increase in strain, it increased rapidly for very small increments in load up to failure. In Specimens 1-4, failing in beam-shear mode, strain recorded at failure was barely $2800\text{ }\mu\epsilon$. In Specimens 5 and 6 failing in flexural mode, the strain recorded at failure was well over $3000\text{ }\mu\epsilon$. In fact, the average strain recorded in these specimens on the failure side was about $3500\text{ }\mu\epsilon$.

Strain gages were placed on CIP bars parallel to the strands only in Specimens 3, 4, 5 and 6. Load versus strain gage readings located on the CIP bars did not show significant strain value during the earlier stages of loading. In fact, these bars were under compression up to a load of 110 kips in Specimens 3 and 4. Strain value at this load was about $-50\text{ }\mu\epsilon$. With further increase in load, strain in the bars changed from compressive to tensile. This tensile strain in the bars

increased non-linearly with increasing load up to near ultimate load level. At ultimate, the strain increased very rapidly and in Specimen 3, the strain observed at failure on the failure side was well over 3000 $\mu\epsilon$, indicating yielding in the bars. In Specimen 4, strain observed at failure was about 950 $\mu\epsilon$. This could be due to sudden splitting failure which caused separation at the interface. In Specimens 5 and 6, the bars were under compression up to a load of 80 kips. With further increases in load, these compressive strains became tensile strains. At the ultimate load, the average strain recorded in the bars was about 3500 $\mu\epsilon$ with as much as 6000 $\mu\epsilon$ in certain bars.

3.5 Horizontal Shear Connectors

Specimens 1 and 5 did not have any horizontal shear connectors. Specimens 2,3,4 and 6 had four shear connectors. In all the specimens, strain in shear connectors was not significant until a significant slip occurred at the interface. Significant amount of interface slip was observed only in Specimens 1-4 near the ultimate load level and hence the effect of the shear connectors was observed only at the maximum load level. Minimum load at which interface slip occurred in Specimens 1-4 was about 5.68 times the equivalent wheel service load level of 26.4 kips and 2.6 times the factored load of 57.3 kips. Near failure, strain in one of the shear connectors of Specimen 3, reached its yield capacity. This suggests that shear connectors were effective at the ultimate load, though not enough to prevent failure.

3.6 Crack Patterns

The crack patterns on either side of the loading point were symmetrical for most of the loading cycles. Near the ultimate load level, a number of cracks appeared on one side of the loading point indicating the impending failure on that side of specimen. In Specimens 1-4, failing in beam-shear mode, the principal diagonal failure crack emanated from one of the pre-existing cracks and progressed towards the interface. Cracks propagated along the interface up to the compressive region of the reaction point and from there the bottom tip of this diagonal crack propagated towards the reaction point and the top tip progressed towards the loading point. Propagation of this critical crack occurred suddenly at the maximum load causing this diagonal crack to extend from the bottom fiber near the reaction point to the top fiber near loading point. In Specimens 5 and 6, where failure occurred in a ductile flexural mode, the crack pattern was symmetrical even at the ultimate loads except that crack widths were wider on the failure side. Failure occurred in a typical flexural mode with cracks extending into the concrete compression block and finally causing the crushing of concrete. Some of the prestressing strands were fractured at failure. The crack patterns, indicated that full composite behavior existed between the precast panel and CIP topping slab almost up to failure of specimens.

3.7 Effects of Cyclic Loading

Load versus deflection characteristics obtained after each intermediate static test performed during cyclic loading of the specimens showed negligible effect of cyclic loading on the stiffness of the deck slab. During this cyclic loading, specimens stayed below elastic limit

and hence there was not any significant effect of cyclic loading observed in any of the measurements taken.

4. Conclusions

The primary objectives of this study were to evaluate the performance of thin precast prestressed concrete panels with broom finish surface and to determine if horizontal shear friction reinforcement is needed to ensure adequate composite behavior between the panel and the CIP portion of the bridge deck. The issues of potential separation of the precast prestressed panel from the cast-in-place portion of the deck, as well as the adequate development of positive moment and shear capacities of the composite bridge section were examined experimentally.

Failure occurred in beam-shear-compression mode in Specimens 1-4. In Specimens 5 and 6 a ductile flexural mode was observed. The specimens with 18 prestressing strands had a larger flexural capacity than shear capacity, whereas Specimens 5 and 6 with 12 prestressing strands had a lower flexural capacity than shear capacity and hence failure occurred in flexural mode. From the first four specimens, a limit on the nominal horizontal shear strength across the interface with broom finish can be established. This nominal horizontal shear strength across the interface was obtained with the minimum capacity of those specimens which failed in shear mode. The extreme condition of lubricated interface with form oil in the case of Specimen 4 had no appreciable deleterious effect. The roughness of the interface was sufficient to maintain composite action in this test. Hence from the first specimen capacity of 160 kips, nominal horizontal shear strength obtained was about 123 psi. Based on the minimum load of 150 kips at which interface slip was observed in Specimens 1-4, a lower limit for nominal horizontal shear strength can be established as 115 psi. Therefore, with a broom finish, an interface horizontal shear stress of 115 psi can be transferred without shear connectors.

The following additional conclusions are drawn from the experimental tests:

- 1) Slippage of prestressing strands was recorded during the final monotonic cycle to failure for all specimens. However, a minimum reserve capacity of at least 29% at failure above that of the strand slip loads observed and at least 11% at strand slip loads above the strand slip loads calculated by current AASHTO procedures were observed in all the specimens.
- 2) All the specimens showed composite behavior to failure. Interface slip was not observed at the equivalent service load of 26.4 kips (117.5 kN) nor at the equivalent factored wheel load of 57.3 kips (255 kN). Interface slip in the first four specimens with 18 strands occurred only at failure loads at least 54% above the predicted AASHTO capacity controlled by development length. No interface slips were recorded in Specimens 5 and 6 with 12 strands.

- 3) Specimens with shear connectors were stiffer near ultimate loads than those without shear connectors (Specimens 1 and 5) but having the same number of strands. Specimens 3 and 4 were stiffer than specimens 1 and 2 due to less prestress loss.
- 4) Cyclic loading did not have any appreciable effect on the stiffness of deck slabs.

5. Implementation

No shear connectors are needed in stay-in-place precast prestressed deck panels with broom finished surface if the nominal average horizontal shear stress at the interface is less than 115 psi.

6. Needed Research

Additional research into the behavior of composite bridge deck slabs constructed with precast prestressed concrete panels includes the following topics :

- 1) Continuity of composite slabs across the bridge girders
- 2) Non-destructive field load tests of a composite bridge deck to monitor behavior
- 3) Non-destructive evaluation of an existing composite bridge deck slab for potential reinforcement corrosion and integrity of composite behavior .
- 4) Effects of shrinkage of concrete in the cast-in-place topping slab on the development of cracks in the composite slab.

Final Report

STAY IN PLACE DECK FORMS - HORIZONTAL SHEAR STRENGTH
OF BRIDGE DECK PANELS - PART 2

Phani Kumar V.V. Nukala

Julio A. Ramirez

Robert H. Lee

and

Menashi Cohen

Joint Highway Research Project

Project No: C-36-56EE

File No: 7-4-31

Conducted in Cooperation with the

Indiana Department of Transportation

and

Federal Highway Administration

The contents of this report reflect the view of the authors who are responsible for the facts and the accuracy of the data presented herein. The contents do not necessarily reflect the official views of policies of the Federal Highway Administration and the Indiana Department of Transportation. This report does not constitute a standard, specification or regulation.

Purdue University
West Lafayette, IN 47907
August 28, 1995

ACKNOWLEDGEMENTS

This report is based on a thesis submitted by Phani Kumar V.V. Nukala in partial fulfillment of the requirements for the degree of Master of Science in Civil Engineering in the Graduate School at Purdue University. Mr. Nukala wishes to express his gratitude to Professor Julio A. Ramirez, chairman of his graduate committee, for his guidance, encouragement, and continuous support throughout this research. Thanks are extended to the advisory committee members, especially S. Herrin, R. Smutzer, and D. Andrewski for their suggestions and helpful comments.

The study presented in this report was conducted at the Karl H. Kettelhut Structural Engineering Laboratory of Purdue University. The research was sponsored by the Indiana Department of Transportation and Federal Highway Administration, and The HydroConduit Corporation. The support of the Prestressed Concrete Institute through the Daniel P. Jenny Research Fellowship is also deeply appreciated. The conclusions and opinions expressed in this report are solely those of the authors and do not necessarily reflect the views of the sponsors.

EXECUTIVE SUMMARY

One of the most economic methods of bridge deck construction consists of prestressed concrete deck panels used as stay-in-place forms in conjunction with the cast-in-place concrete topping instead of the traditional monolithic roadway deck slabs. The stay-in-place panels act as composite members spanning the opening between the longitudinal bridge girders. The performance of this type of deck as a composite unit is only possible if the horizontal shear stress resulting from bending of the deck is effectively transferred across the interface of the two elements.

In general, it is assumed that horizontal shear stresses are transmitted across the interface due to bond between the precast panel and cast-in-place concrete acting in conjunction with the horizontal shear connectors provided across the interface. These horizontal shear connectors act as a combination of dowel and clamping reinforcement once the slip occurs at the interface. Presently the Indiana Department of Transportation requires a minimum of 20 shear connectors regardless of the panel dimensions. The shear connectors are placed across a broom or wire brush finished deck panel surface. Broom or wire brush finish with approximately 0.05 to 0.075 in. (1.27 to 1.91 mm) total amplitude deformations is specified instead of a raked finish with a total amplitude of 0.25 in. (6.35 mm) because of the reduced 2.5 in (63.5 mm) thickness of the panels used in Indiana. This study focuses on the evaluation of the horizontal shear strength across a broom finished interface.

Experiments were undertaken on six precast prestressed check panels with composite cast-in-place concrete topping. All the specimens were 8 ft. x 8 ft. (2.4 m x 2.4 m) and 2.5 in. (6.4 mm) thick precast prestressed panel with a 5.5 in (140 mm) topping slab. Specimens 1 and 5

had no shear connectors and Specimens 2,3 and 6 had four shear connectors across the interface. Specimen 4 had four shear connectors and the top of the precast panel was sprayed with a bond breaking agent (form oil) to eliminate chemical bonding between the precast panel and the cast-in-place concrete topping. Specimens 1-4 were reinforced with 18-3/8" (9.5 mm) diameter, Grade 270 low-relaxation strands. This amount represents a practical upper limit for reinforcement in the maximum width, 8 ft. (2.4 m), panel used in Indiana. Specimens 1-4 allowed performance evaluation of this type of composite structure under the potential maximum horizontal shear demand. Specimens 5 and 6 were reinforced with only 12 strands. These last two specimens were used to study the effect of repeated loading under a higher mean shear stress at the interface. This mean shear stress represents the level transferred in deck panels designed for HS20 loading on an 8 ft. (2.4m) simple span.

The test results indicated that shear connectors are not required to achieve adequate composite action at service and ultimate load levels in panels with broom or with wire brush finished top surface. This finding is limited to situations where the nominal average shear stress does not exceed 115 psi. A minimum of 4 shear connectors will likely be provided for handling purposes. A comparison of the performance of the specimens in this study with and without shear connectors indicates that specimens with four shear connectors were stiffer near failure load. The minimum of 4 connectors did not significantly increase the load carrying capacity of the panels tested.

Lubrication of the interface in Specimen 4 resulted in a 10% decrease in ultimate capacity as compared to that of companion Specimen 3. But the failure load in specimen 4 was 82% higher than the predicted value based on development length requirements (strand slip criteria).

Yielding of the shear connectors was observed at failure in the case of Specimen 3 failing in beam shear mode. Strand slip was observed in all the specimens tested. The measured initial slip load was always greater than the calculated load based on available anchorage of the strands. Specimens 5 and 6 failed in flexure, and their failure load exceed the predicted flexural capacity. Shear connectors provided across the interface of Specimen 6 were not strained significantly in the flexure failure mode.

All the specimens were subjected to 1,000,000 cycles of repeated load prior to the final monotonic cycle to failure. The repeated loading had no significant effect on the service load performance as indicated by crack patterns and load vs. deflection.

PREFACE

It is suggested that the reader be selective in choosing which chapter to read, depending on the depth of his/her interest in this subject. A general understanding of the report can be obtained by considering only Chapter 5 or Chapters 1 and 5. A general literature review on previous studies performed on the subject of horizontal shear strength transfer across concrete interfaces is given in Chapter 2. Those interested in details of specimen design and fabrication, test set-up and instrumentation are referred to Chapter 3. A detailed explanation about the behavior of the specimens during test is included in Chapter 4.

TABLE OF CONTENTS

	Page
Cover Page	i
ACKNOWLEDGEMENTS	ii
EXECUTIVE SUMMARY	iii
PREFACE	vi
TABLE OF CONTENTS	vii
LIST OF TABLES	xi
LIST OF FIGURES	xii
CHAPTER 1 - INTRODUCTION	1
1.1 Background Information	1
1.2 Objective	3
1.3 Scope	4
CHAPTER 2 - LITERATURE REVIEW	5
2.1 Introduction	5
2.2 Previous Studies	5
2.3 Detailing Practices by other DOTs	11
2.4 Current Design Specifications AASHTO / ACI	11
2.5 Summary	12
CHAPTER 3- EXPERIMENTAL PROGRAM	14
3.1 Introduction	14
3.2 Geometric Conditions	14

3.2.1	Prestressed Concrete Panels	16
3.2.2	Concrete Topping Slab	18
3.3	Experimental Procedure	19
3.3.1	Test Set-Up	19
3.3.2	Loading Pattern	20
3.3.3	Instrumentation	21
3.4	Summary	24
CHAPTER 4 - EXPERIMENTAL RESULTS		35
4.1	Material Properties	35
4.1.1	Properties of Concrete	35
4.1.1.1	Specimen 1 and Specimen 2 (Set 1)	35
4.1.1.2	Specimen 3 and Specimen 4 (Set 2)	37
4.1.1.3	Specimen 5 and Specimen 6 (Set 3)	38
4.1.2	Steel Properties	39
4.2	Strand Slip Results	40
4.2.1	Specimen 1 - Panel with 18 strands and no shear connectors	45
4.2.2	Specimen 2 - Panel with 18 strands and four shear connectors	45
4.2.3	Specimen 3 - Panel with 18 strands and four shear connectors	46
4.2.4	Specimen 4 - Panel with 18 strands, Four Shear Connectors and a Lubricated Interface	47
4.2.5	Specimen 5 - Panel with 12 strands and without any shear connectors	48
4.2.6	Specimen 6 - Panel with 12 strands and four shear connectors	49
4.3	Composite Behavior of Deck Slabs	49
4.3.1	Interface Slip	52
4.3.1.1	Specimen 1 - Panel with 18 strands and without any shear connectors	52
4.3.1.2	Specimen 2 - Panel with 18 strands and with four shear connectors	52
4.3.1.3	Specimen 3 - Panel with 18 strands and with four shear connectors	53
4.3.1.4	Specimen 4 - Panel with 18 strands and with Lubricated Interface	53
4.3.1.5	Specimen 5 - Panel with 12 strands and without any shear connectors	53
4.3.1.6	Specimen 6 - Panel with 12 strands and	

	with four shear connectors	54
4.4	Load versus Deflection Characteristics	54
4.4.1	Specimen 1 - Panel with 18 strands and without any shear connectors	54
4.4.2	Specimen 2 - Panel with 18 strands and with four shear connectors	55
4.4.3	Specimen 3 - Panel with 18 strands and with four shear connectors	56
4.4.4	Specimen 4 - Panel with 18 strands and with Lubricated Interface	57
4.4.5	Specimen 5 - Panel with 12 strands and without any shear connectors	57
4.4.6	Specimen 6 - Panel with 12 strands and with four shear connectors	58
4.5	Load versus Strand Strain Results	59
4.5.1	Specimen 1 - Panel with 18 strands and without any shear connectors	59
4.5.2	Specimen 2 - Panel with 18 strands and with four shear connectors	60
4.5.3	Specimen 3 - Panel with 18 strands and with four shear connectors	61
4.5.4	Specimen 4 - Panel with 18 strands and with Lubricated Interface	62
4.5.5	Specimen 5 - Panel with 12 strands and without any shear connectors	63
4.5.6	Specimen 6 - Panel with 12 strands and with four shear connectors	64
4.6	Load versus Concrete Strain Results	64
4.6.1	Load versus Strain at Strand Level	65
4.6.2	Load versus Strain at 5 in. from top of CIP	67
4.6.3	Load versus Strain at top of CIP Slab	68
4.6.4	Load versus Interface Strain Results	70
4.6.5	Load versus CIP Reinforcement Strain Results	72
4.6.6	Behavior of Horizontal Shear Connectors	74
4.7	Crack Patterns	76
4.7.1	Specimen 1 - Panel with 18 strands and without any shear connectors	76
4.7.2	Specimen 2 - Panel with 18 strands and with four shear connectors	77
4.7.3	Specimen 3 - Panel with 18 strands and with four shear connectors	77
4.7.4	Specimen 4 - Panel with 18 strands and with Lubricated Interface	77

4.7.5	Specimen 5 - Panel with 12 strands and without any shear connectors	78
4.7.6	Specimen 6 - Panel with 12 strands and with four shear connectors	79
4.7.7	Summary of Crack Pattern Observation	79
4.8	Effect of Cyclic Loading on the Behavior of Deck Panels	79
4.8.1	Cyclic Load versus Stiffness of Deck Panel	80
4.8.2	Cyclic Load versus Strain in the strands	80
4.8.3	Cyclic Load versus Overall Behavior of the Specimen	81
4.9	Summary	82
CHAPTER 5 - SUMMARY, CONCLUSIONS AND RECOMMENDATIONS		202
5.1	General	202
5.2	Research Program	203
5.3	Findings From Experimental Program	205
5.3.1	Strand Development	205
5.3.2	Interface Slip	206
5.3.3	Load-Deflection Behavior	207
5.3.4	Strains in Reinforcement and Concrete	208
5.3.5	Horizontal Shear Connectors	209
5.3.6	Crack Patterns	210
5.3.7	Effects of Cyclic Loading	210
5.4	Conclusions	211
5.5	Recommendations	212
5.6	Needed Research	213
LIST OF REFERENCES		214
APPENDIX A: Sample Calculations		217

LIST OF TABLES

Table	Page
3.1 Description of specimens	15
4.1 Variation in concrete compressive strength with age of concrete	36
4.2 Variation in concrete compressive strength with age of concrete	36
4.3 Variation in concrete compressive strength with age of concrete	37
4.4 Variation in concrete compressive strength with age of concrete	37
4.5 Variation in concrete compressive strength with age of concrete	38
4.6 Variation in concrete compressive strength with age of concrete	39
4.7 Estimated Capacities of Specimens based on AASHTO	41
4.8 Load Capacities of various Specimens	43
4.9 Actual Ultimate Capacities versus Service Loads and Factored Loads	44

LIST OF FIGURES

Figure	Page
3.1 Geometrical Characteristics of Deck Slab	25
3.2 Typical detail of a panel with 4 stirrups a) Plan b) Section AA	26
3.3 Cross Section Details of Bridge Deck	27
3.4 Loading frame details a) Elevation b) Plan	28
3.5 LVDT Locations on the sides for measuring deflections	29
3.6 Strain Gage Locations on the sides of the deck	29
3.7 Strain gage Locations on top of the CIP slab	30
3.8 Strain gage and Dial gage locations on the prestressing strands	
a) Details of Specimens 1 and 2	31
b) Details of Specimens 3 and 4	32
c) Details of Specimens 5 and 6	32
3.9 Strain Gage Locations on top of the Precast Panel	
a) Details of Specimens 3 and 4 b) Details of Specimens 5 and 6	33
3.10 Slip gage locations on the sides of the Deck	34
3.11 Slip Gage Details	34
4.1 Concrete compressive strength versus age of concrete	83
4.2 Concrete compressive strength versus age of concrete	84

4.3	Concrete compressive strength versus age of concrete	85
4.4	Load versus Strand Slip at #S10 of Specimen 1	86
4.5	Load versus Strand Slip at #S13 of Specimen 1	87
4.6	Load versus Strand Slip at #N17 of Specimen 1	88
4.7	Load versus Strand Slip at #N2 of Specimen 2	89
4.8	Load versus Strand Slip at #S2 of Specimen 2	90
4.9	Load versus Strand Slip at #S10 of Specimen 2	91
4.10	Load versus Strand Slip at #S6 of Specimen 3	92
4.11	Load versus Strand Slip at #S9 of Specimen 3	93
4.12	Load versus Strand Slip at #S17 of Specimen 3	94
4.13	Load versus Strand Slip at #N6 of Specimen 4	95
4.14	Load versus Strand Slip at #N17 of Specimen 4	96
4.15	Load versus Strand Slip at #N4 of Specimen 5	97
4.16	Load versus Strand Slip at #N6 of Specimen 5	98
4.17	Load versus Strand Slip at #S6 of Specimen 6	99
4.18	Inclined crack in Reinforced Concrete beams similar to that observed in Deck panel	100
4.19	Strain distribution across the depth of Specimen 1	101
4.20	Strain distribution across the depth of Specimen 2	102
4.21	Strain distribution across the depth of Specimen 3	103
4.22	Strain distribution across the depth of Specimen 4	104
4.23	Strain distribution across the depth of Specimen 5	105

4.24	Strain distribution across the depth of Specimen 6	106
4.25	Load versus Slip at the interface of Specimen 1	107
4.26	Load versus Slip at the interface of Specimen 2	108
4.27	Load versus Slip at the interface of Specimen 3	109
4.28	Load versus Slip at the interface of Specimen 4	110
4.29	Load versus Slip at the interface of Specimen 5	111
4.30	Load versus Slip at the interface of Specimen 6	112
4.31	Load versus Deflection characteristics of Specimen 1	113
4.32	Load versus Deflection characteristics of Specimen 2	114
4.33	Load versus Deflection characteristics of Specimen 3	115
4.34	Load versus Deflection characteristics of Specimen 4	116
4.35	Load versus Deflection characteristics of Specimen 5	117
4.36	Load versus Deflection characteristics of Specimen 6	118
4.37	Comparison of Load versus Deflection characteristics of various specimens	119
4.38	Load versus Strain in the strand at #C10 of Specimen 1	120
4.39	Load versus Strain in the strand at #C13 of Specimen 1	121
4.40	Load versus Strain in the strand at #C17 of Specimen 1	122
4.41	Load versus Average strain in the strand of Specimen 2 after 500,000 cycles	123
4.42	Load versus Strain in the strand at #C2 of Specimen 2	124
4.43	Load versus Strain in the strand at #C6 of Specimen 2	125

4.44	Load versus Strain in the strand at #C9 of Specimen 2	126
4.45	Load versus Average strain in strands of Specimen 3 after 500,000 cycles	127
4.46	Load versus Strain in the strand at #C5 of Specimen 3	128
4.47	Load versus Strain in the strand at #C17 of Specimen 3	129
4.48	Load versus Average strain in strands of Specimen 4 after 600,000 cycles	130
4.49	Load versus Average strain in the strands of Specimen 4	131
4.50	Load versus Strain in the strand at #C10 of Specimen 5	132
4.51	Load versus Strain in the strand at #C11 of Specimen 5	133
4.52	Load versus Strain in the strand at #C2 of Specimen 6	134
4.53	Load versus Strain in the strand at #C8 of Specimen 6	135
4.54	Load versus Strain in the strand at #C10 of Specimen 6	136
4.55	Load versus Strain at strand level of Specimen 1	137
4.56	Load versus Strain at strand level of Specimen 2	138
4.57	Load versus Strain at strand level of Specimen	139
4.58	Load versus Average strain at strand level of Specimen 4	140
4.59	Load versus Strain at strand level of Specimen 5	141
4.60	Load versus Strain at strand level of Specimen 6	142
4.61	Load versus Strain at CIP gage level of Specimen 1	143
4.62	Load versus Strain at CIP gage level of Specimen 2	144
4.63	Load versus Strain at CIP gage level of Specimen 3	145

4.64	Load versus Strain at CIP gage level of Specimen 4	146
4.65	Load versus Strain at CIP gage level of Specimen 5	147
4.66	Load versus Strain at CIP gage level of Specimen 6	148
4.67	Load versus Strain at the top of CIP slab (SSE6) of Specimen 1	149
4.68	Load versus Strain at the top of CIP slab (SNE6) of Specimen 1	150
4.69	Load versus Strain at the top of CIP slab (SNE1) of Specimen 2	151
4.70	Load versus Strain at the top of CIP slab (SNE4) of Specimen 2	152
4.71	Load versus Strain at the top of CIP slab (SSE6) of Specimen 2	153
4.72	Load versus Strain at the top of CIP slab (SSE5) of Specimen 3	154
4.73	Load versus Strain at the top of CIP slab (SNE5) of Specimen 3	155
4.74	Load versus Strain at the top of CIP slab (SSE5) of Specimen 4	156
4.75	Load versus Strain at the top of CIP slab (SSE6) of Specimen 4	157
4.76	Load versus Strain at the top of CIP slab (SSE6) of Specimen 5	158
4.77	Load versus Strain at the top of CIP slab (SNE6) of Specimen 5	159
4.78	Load versus Strain at the top of CIP slab (SNE2) of Specimen 6	160
4.79	Load versus Strain at the top of CIP slab (SSE5) of Specimen 6	161
4.80	Load versus Strain at the top of CIP slab (SNE6) of Specimen 6	162
4.81	Load versus Strain at the interface at #PC9 of Specimen 3	163
4.82	Load versus Strain at the interface at #PC9 of Specimen 4	164
4.83	Load versus Strain at the interface at #PC6 of Specimen 5	165
4.84	Load versus Strain at the interface at #PC2 of Specimen 6	166
4.85	Load versus Strain at the interface at #PC3 of Specimen 6	167

4.86	Load versus Strain in the CIP Bar on southern side of Specimen 3	168
4.87	Load versus Strain in the CIP Bar on northern side of Specimen 3	169
4.88	Load versus Strain in the CIP Bar on southern side of Specimen 4	170
4.89	Load versus Strain in the CIP Bar on northern side of Specimen 4	171
4.90	Load versus Strain in the CIP Bar on northern side of Specimen 5	172
4.91	Load versus Strain in the CIP Bar on southern side of Specimen 6	173
4.92	Load versus Strain in the CIP Bar on northern side of Specimen 6	174
4.93	Load versus Strain in the horizontal shear connectors of Specimen 2	175
4.94	Load versus Strain in the horizontal shear connectors of Specimen	176
4.95	Load versus Strain in the horizontal shear connectors of Specimen 4	177
4.96	Crack Patterns of Specimen 1 a) West Side View b) East Side View	178
4.97	Crack Patterns of Specimen 2 a) West Side View b) East Side View	179
4.98	Crack Patterns of Specimen 3 a) West Side View b) East Side View	180
4.99	Crack Patterns of Specimen 4 a) West Side View b) East Side View	181
4.100	Crack Patterns of Specimen 5 a) West Side View b) East Side View	182
4.101	Crack Patterns of Specimen 6 a) West Side View b) East Side View	183
4.102	Effect of Cyclic Loading on Deflection of Specimen 1	184
4.103	Effect of Cyclic Loading on Deflection of Specimen 2	185
4.104	Effect of Cyclic Loading on Deflection of Specimen 3	186
4.105	Effect of Cyclic Loading on Deflection of Specimen 4	187
4.106	Effect of Cyclic Loading on Deflection of Specimen 5	188
4.107	Effect of Cyclic Loading on Deflection of Specimen 6	189

4.108	Effect of Cyclic Loading on Average Strain in strands of Specimen 5 . . .	190
4.109	Effect of Cyclic Loading on Average Strain in strands of Specimen 6 . . .	191
4.110	Effect of Cyclic Loading on Average Strain at the top of CIP slab of Specimen 1	192
4.111	Effect of Cyclic Loading on Average Strain at the top of CIP slab of Specimen 2	193
4.112	Effect of Cyclic Loading on Average Strain at the top of CIP slab of Specimen 3	194
4.113	Effect of Cyclic Loading on Average Strain at the top of CIP slab of Specimen 4	195
4.114	Effect of Cyclic Loading on Average Strain at the top of CIP slab of Specimen 5	196
4.115	Effect of Cyclic Loading on Average Strain at the top of CIP slab of Specimen 6	197
4.116	Effect of Cyclic Loading on Average Strain at strand level of Specimen 2	198
4.117	Effect of Cyclic Loading on Average Strain at strand level of Specimen 6	199
4.118	Effect of Cyclic Loading on Average Strain at CIP gage level of Specimen 4	200
4.119	Effect of Cyclic Loading on Average Strain at the interface of Specimen 3	201

CHAPTER 1 - INTRODUCTION

1.1 Background Information

One of the most popular methods of bridge construction consists of prestressed concrete or steel girders supporting a roadway deck. Although timber decks were used originally, today reinforced concrete is the most common deck because of its ease of construction, smoothness and durability. A major problem for bridge engineers has been the deterioration of reinforced concrete bridge decks. Many design and maintenance techniques have been developed in an attempt to reduce the maintenance and replacement costs on bridge decks. Some of these are overlays, impregnation of the concrete to reduce its permeability, increasing the depth of cover over the reinforcing steel, and use of epoxy-coated steel.

The use of precast concrete for new bridge construction and for the rehabilitation of deteriorated bridges is economically and structurally amenable to today's system engineering concepts. Precast products can be used for some or most of the components of a bridge's superstructure and/or substructure. Durability, ease and speed of construction together with reduced need for maintenance are all advantages in using precast concrete. During the past 12 years precast prestressed concrete bridge deck panels have been used with cast-in-place concrete in Indiana and other states to provide a convenient and cost effective method of construction for concrete bridge decks. These panels span the opening between the longitudinal bridge girders and serve as permanent forms for the cast-in-place concrete topping that completes the bridge deck. The precast concrete panels and the concrete topping become composite and the panels contain all of the required positive moment reinforcement between the longitudinal bridge girders. In

Indiana, currently the use of precast panels is only allowed in bridge decks supported by prestressed I - beams.

Full composite action with the cast-in-place concrete of the deck is achieved by means of interface shear strength of the panel's roughened surface . In a deck panel where shear connectors are provided, it is assumed that interface shear strength is achieved by shear connectors acting as a combination of dowel and clamping reinforcement along with the panel's roughened surface. The Indiana Department of Transportation (INDOT) specifies that the top of the panel be broom or wire brush finished in the direction of strands instead of the raked finished with 0.25 in. full amplitude deformation. This is due to the 2.5 in. total thickness of panel used in the state. The broom or wire brush finishing results in a total amplitude deformation of about 0.05 to 0.075 in. Mechanical shear connectors, as is the case with stirrups protruding above the surface of the panel, have been shown to be unnecessary to achieve composite action and to transfer the necessary horizontal shear across the interface when a roughened raked type surface with a total amplitude deformation of 0.25 in. is provided [3]. However for the current broom finish specified by INDOT, a minimum amount of mechanical shear connectors is specified by INDOT. Therefore, due to the reduced amplitude deformation of the broom finish and to further account for possible presence of contaminants on the panel surface, 20 mechanical shear connectors are specified by INDOT regardless of the panel dimensions. A maximum standard panel width of 8 ft. is used, with the panel length being a function of the girder spacing. Practically, a minimum number of four shear connectors would be necessary for handling of the precast panels.

1.2 Objective

The main objective of this study is to evaluate the composite section performance of precast prestressed deck panels with a wire brush or broom finished top surface. This evaluation includes the performance of this type of bridge deck section under static and repeated loading. This study addresses the specific concerns raised by INDOT dealing with the number of horizontal shear connectors required in precast deck panels with broom finished top surface. The issues of potential separation of the precast prestressed panel from the cast-in-place portion of the deck, as well as the adequate development of positive moment and shear capacities of the composite bridge section are examined experimentally. The performance of the deck system was obtained by evaluating the following data :

- (1) Load versus deflection characteristics
- (2) Load versus strand slip characteristics
- (3) Cyclic behavior of the panels
- (4) Interface slip characteristics of the panels
- (5) Strains at various locations in the concrete and the reinforcement

The dimensions of all deck panels were 8 ft x 8 ft x 2.5 inches with typical amounts of prestressing and mild steel reinforcement. The 8 foot width and length represent the standard panel width used in Indiana and a medium range girder spacing respectively. The concrete strengths of the panels based on current INDOT standards were 5000 psi for 28 days and 4000 psi for transfer of prestressing.

1.3 Scope

This study consists of 3 tasks. Task 1 is a survey of the relevant previous research in the field. Task 2 consists of a thorough experimental investigation of the composite behavior and various other aspects related to it. Task 3 deals with the analysis of data obtained during the experimental investigation. This work is presented in subsequent chapters of this report. Chapter 2 deals with the survey of previous research related to this study. In Chapter 3 the experimental program is described. Chapter 4 analyzes the data obtained during this experimental investigation. Chapter 5 gives the final conclusions and recommendations based on the study findings.

CHAPTER 2 - LITERATURE REVIEW

2.1 Introduction

Previous research on precast prestressed deck panels in conjunction with cast-in-place topping concrete slab systems has involved various aspects of their behavior and performance. In the following sections, details relevant to the present study, detailing practices that are followed by other DOTs, and current AASHTO / ACI, [1,2] design specifications are discussed.

2.2 Previous Studies

In 1975, Barker [3] presented an overview of research findings involving precast prestressed panel forms in bridge deck construction. He examined the behavior of two types of specimens. The first type had a raked finish with the depth of depression equal to 1/4 in. The second type had essentially the same raked finish, but in addition had reinforcing bars extending through the top surface to provide shear reinforcement. He showed that specimens with and without the shear connectors developed adequate bond to insure composite action. There was no indication that the shear reinforcement increased the bond performance under normal service load conditions. However, there was some indication that the panels with shear reinforcement were tougher under cyclic loading and appeared to be stiffer under higher static loads. He concluded that shear reinforcement was not worth the expense of installation. Here shear reinforcement was not needed to help the bond between cast-in-place topping slab and the precast panel. However, he stated that to insure composite action the interface must be free of contaminants.

Regarding development length of prestressing strands, for a 3/8 in. diameter strands, the development length required was concluded to be about 20 inches. The amount of development length required depended mostly on the surface conditions of the strands, the method used while detensioning, the strand size and the concrete strength. Cyclic loading did not have an appreciable effect on strand development length or panel stiffness. He concluded that use of precast prestressed concrete panels results in an economical deck system and fast deck construction, and if properly executed, they result in high quality decks with increased durability.

In the same year, Kluge and Sawyer [16] performed a feasibility study on using composite decks for slab and girder bridges. They concluded that panels could be used as a composite part of the bridge decks. The composite slab and pretensioning strands may be designed for ultimate capacity as a pretensioned slab of the same depth to resist the main ultimate positive bending moment specified by AASHTO. To achieve the composite behavior, horizontal shear stresses must be transferred across the interface of the precast panel and the cast-in-place deck and this interface must be free of contaminants.

Gustaferro et al [6] examined the performance of prestressed concrete deck system on the Illinois Tollway after 25 years of service. They concluded that stay-in-place precast prestressed bridge deck slabs have performed very well and did not create any problems. In fact, the performance was so good that the Illinois Tollway used them in new bridges on the East-West Tollway expansion which was constructed in 1970.

Jones and Furr [36] studied prestress strand development length. They also studied the effects of cyclic loading on the development length of prestressing strands and panel stiffness. They used 3/8 in. diameter, 7 wire strands, having lengths equal to 68 in. and 108 in. embedded

in light and normal weight concrete. The strands were clean and rust free. The strands were detensioned at an initial prestress of 162 ksi. Their conclusion was that an average of 22 in. of development length was needed for 3/8 in. diameter strand and the type of concrete used had insignificant effect on the amount of development length required. They also concluded that cyclic loading had negligible effect on strand development length and panel stiffness.

Buckner and Turner [18] examined the performance of full span panel form bridges under repetitive loading. All of the specimens tested in their experimental program were simply supported, and performed satisfactorily for 2 million cycles of repetitive load. Visible cracks did not develop in the concrete specimens and there was no measurable increase in the width of any preexisting crack during the cyclic loading period. Primary failure mode was a ductile flexural mode and there was no indication of fatigue in the reinforcement. Bond between the topping slab and the roughened interface surfaces of the panels provided the only means of shear connection. Adequate composite action was obtained by roughening (1/8" full amplitude deformation) the top surface of the precast panel. Differences in serviceability and strength characteristics of flat precast panels and beveled-edge panels were negligible. The thickness of the topping slab relative to the total thickness of the deck did not effect the fatigue strength of the composite deck up to 2 million cycles. They concluded that for HS20-44 live loads, adequate shear transfer strength can be obtained by providing a 5 in. topping slab reinforced transversely with #4 Grade 60 bars spaced at 12 in. on centers even under the existence of longitudinal crack in the topping slab over the panel.

Barnoff et al [17] examined the behavior of a full scale prestressed bridge with precast deck panels. The conclusions made in this study were :

- (1) The assumption of full composite action between the plank forms and the topping slab while designing the deck is a valid assumption as full composite behavior was observed at both service loads and overloads.
- (2) The deck utilizing precast prestressed concrete planks was slightly more flexible than the conventional deck, thereby allowing larger beam deflection, but resulting in smaller live load moments in the slab. But this slight difference in behavior does not justify a separate procedure to determine design moments in decks with precast prestressed panels.
- (3) Full composite action was developed between the precast panel and the cast-in-place topping. Mechanical shear connectors are not required if the panel surface is given a scored finish. No quantitative reference to the degree of roughness provided by the scored finish was given.
- (4) Cyclic loading was not shown to have any detrimental effect on the performance of panels.
- (5) The Plane Section assumption appears to be valid even under loads 3.5 times the design load.
- (6) Precast prestressed panel had substantially more strength than was indicated by the design calculations.
- (7) Failure of the precast prestressed deck panels did not occur until a 60 kip wheel load on tandem axles was applied, whereas a 20 kip wheel load produced cracking in the conventional slab. Reinforcing steel did not yield in either deck.
- (8) The deck constructed with 3 in. deck panels and 4.5 in. topping slab failed by diagonal tension in both the laboratory and field tests. Failure load in the laboratory was 110 kips

from a single simulated wheel load on a 4 ft wide continuity assembly. On the experimental bridge, failure resulted from 60 kip wheel loads applied on tandem axles spaced at 4 ft centers.

Klinger and Bieschke [15] examined the performance of deck panels with and without strand extensions. They concluded that under static and fatigue axle loads about twice as large as AASHTO design load levels, both the panels with and without panel strand extensions behaved satisfactorily.

Ross Bryan Associates, Inc., has presented recommendations [5] on the design, production, shipping and handling, and erection of the panels. A design example using the AASHTO specifications and several design aids were included in their report.

Hanson [14] conducted two different kinds of tests. They were pushoff tests and girder tests. Both of the tests showed similar slip versus shearing stress characteristics. At slips of about 0.005 in. at the contact surface, the girder deflection curves began to deviate from the initial smooth curve. Slip observed in the girder tests was higher than the slip observed in any of the pushoff tests before bond failure. The girder and pushoff tests reported a maximum shearing stress of 500 psi to insure composite action in the case of rough interface and 300 psi for smooth interface. Regarding the contribution of shear connectors, he concluded that approximately 175 psi shear capacity may be added for each 1% of shear reinforcement across the joint. These shear connectors were effective only after the interface slip commenced. Girder tests indicated that when bond is absent at the connection interface, roughness can contribute up to 150 psi towards shear strength. Finally he concluded that shear reinforcement across the interface was effective only at large relative displacements (> 0.005 in.) at the interface.

Paulay et al [37] in their comprehensive test series on horizontal construction joints in cast-in-place reinforced concrete with inter-layer reinforcement concluded that, for design purposes, contribution from the dowel action of the reinforcement should be ignored as significant dowel forces can be generated only after excessive slip along a joint.

Seible and Latham [12, 13] concluded that the horizontal load transfer behavior of overlaid reinforced concrete slabs used frequently in bridge deck rehabilitation depends largely on the interface surface preparation. They also noted that the horizontal shear connector reinforcement provided across a rough and clean horizontal construction joint interface, between the bridge deck and the overlay cannot be effective unless delamination and interface slip occur. Due to the in - plane stiffness of both the deck and overlay, relative interlayer slip in the construction joint can only occur when large regions of delamination grow together and provide a continuously delaminated region between the point of load application and slab boundaries. Furthermore, the amount of minimum dowel reinforcement currently required by AASHTO (0.083 % for Grade 60 dowels) is not sufficient to control the horizontal slip after the onset of delamination. They also concluded that small topological changes in the interface (about 0.125 in. deep at 1 in. spacing) suffice to provide monolithic behavior up to critical flexural yield limit states, which make dowels virtually ineffective. In the few cases where critical nominal horizontal shear stress levels are exceeded and delamination is possible, dowel reinforcement with an increased minimum reinforcement ratio of 0.2% must be provided. It was further concluded that change in behavior from monolithic to that of lubricated or unbonded occurs only when the delamination zones from the loading and reaction points meet each other. Since a complete delamination in a bridge deck is very unlikely to occur under traffic loads, relative interlayer slip

in the construction joint cannot occur and hence the dowel reinforcement across the interlayer is ineffective in contributing towards the transfer of horizontal shear.

2.3 Detailing Practices by other DOTs

The U. S. Department Of Transportation (USDOT) and the FHWA structures division provided information regarding the usage of precast prestressed deck panels in various states. Information regarding these concrete bridge deck panels is provided in Table 2.1. Out of the 17 states that use precast panels, information from only 13 states was available. Out of these 13 states, 7 use four or no shear connectors across the interface to transfer horizontal shear stresses between the precast panel and the cast - in - place topping slab. Out of these 7 states, three states (Tennessee, Virginia, and Georgia) use 1/8 in. depressions on the top surface of the precast panel to give rough interface characteristics to the interface. Kansas, Minnesota, and North Carolina use 1/4 in. depressions on the top surface of the precast panel to roughen the interface for better bond characteristics. Iowa uses wire - finish to roughen the surface of the precast panel.

2.4 Current Design Specifications AASHTO / ACI

Current design practice based on AASHTO, 1992, recommends that the nominal horizontal shear strength across an interface (or a joint) can be considered as the following :

- (1) When contact surface is clean, free of laitance, and intentionally roughened, shear strength V_{nh} shall not be taken greater than $80b_vd$, in pounds.
- (2) If minimum ties are provided between interconnected elements with an area not less than $50 b_v s / f_y$ and with spacing "s" not exceeding four times the least web width of the

supporting element nor 24 inches, and contact surface is clean and free of laitance, but not intentionally roughened, shear strength V_{nh} shall not be taken greater than $80b_v d$, in pounds.

- (3) If minimum ties are provided as above, and the contact surface is clean, free of laitance, and intentionally roughened to a full amplitude of approximately 1/4 in., shear strength V_{nh} shall not be taken greater than $350b_v d$, in pounds.
- (4) For each percent of tie reinforcement crossing the contact surface in excess of the minimum stipulated in (2), shear strength V_{nh} may be increased by $(160f_y/40,000)b_v d$, in pounds.

As an example, for Grade 60 rebar dowels, minimum required shear connector steel area gives a dowel to contact area ratio of 0.08%. This is equivalent to 20, #4, Grade 60 shear connectors for a panel width of 8 ft. Cost associated with the dowel reinforcement especially in the rehabilitation projects, amounts to approximately 15 - 20% of the total rehabilitation cost [12,13].

2.5 Summary

It is evident that the number of shear connectors required in a precast panel depends on the preparation of the surface and that shear connectors are not required if the surface is given a scored finish with an amplitude deformation of 0.25 in. In the state of Indiana, in precast prestressed deck panels a broom finish is specified instead of a raked finish with 0.25 in. amplitude deformations. This is due to the reduced 2.5 in. thickness of the panels. The review of available detailing practices by 13 DOT's indicates that the states using 4 or less shear

connectors require a minimum amplitude depression between 0.125" and 0.25 inch with the exception of Iowa which uses brush wire finish interface. The decrease in roughness and the irregular pattern of deformations associated with broom finish (approximate maximum depression of 0.05 in.) justify the evaluation of the available bond across the interface. To date, no experimental information is available on the horizontal shear strength detailing required to achieve composite behavior in precast deck panels with broom or wire brush finished top under static and repeated loading. This study addresses the horizontal shear strength of precast prestressed deck panels with a broom finished surface and examines the need for shear connectors across this interface to obtain composite action. In the following chapters, details of the experimental program and the analysis of the data obtained during this experimental investigation are presented.

CHAPTER 3 - EXPERIMENTAL PROGRAM

3.1 Introduction

The experimental program consisted of testing six full-scale composite stay - in -place deck slabs. The specimens had different interface properties including different amounts of horizontal shear reinforcement across the interface. The first four had 18 prestressing strands representing an upper practical limit for the amount of flexural reinforcement in this type of member and the maximum possible horizontal shear demand. The last two specimens with 12 prestressing strands were used to evaluate the effect of repeated loading due to an increase in mean shear stress at the interface. In this chapter, specimen detailing and scope of the experimental program and procedures are discussed.

3.2 Geometric Conditions

All six composite specimens consisted of a 2.5 in. thick precast prestressed panel with a 5.5 in. thick cast - in - place reinforced concrete topping slab. This provided an 8 in. standard full deck thickness, as commonly used in Indiana. The details of various specimens are given in Table 3.1. Figure 3.1 shows the geometrical characteristics of the composite specimens. Deck panel plan and elevation details are shown in Fig. 3.2. Locations of shear connectors are also indicated on Fig. 3.2. In this study, four panels (Specimens 2,3,4,6) had 4 shear connectors representing a minimum practical limit for handling. The remaining two panels (Specimens 1 and 5) had no shear connectors. In Specimen, 4, bond was interrupted by applying a coating of form oil in order to assess the contribution of the shear connectors under conditions of bond

Table 3.1 - Description of specimens

Specimen	Description of Specimen	28 days Concrete Strength		Total Prestress Loss (%)
		Precast (psi)	CIP (psi)	
1	Specimen with 18 strands and no shear connectors	7850	6932	14.8
2	Specimen with 18 strands and four shear connectors	7850	6932	14.9
3	Specimen with 18 strands and four shear connectors	5647	5747	12.3
4	Specimen with lubricated interface, 18 strands, and four shear connectors	5647	5747	13
5	Specimen with 12 strands and no shear connectors	6857	5657	14.9
6	Specimen with 12 strands and four shear connectors	6857	5657	15

Note : 1 in. = 25.4 mm; 1 psi = 0.00689 MPa.

deterioration.

A typical transverse section of a bridge superstructure is shown in Fig. 3.3. The precast panels rest right on top of longitudinal bridge girders and then the topping slab is poured on top of the deck panels. Although strand extensions were not needed [15], these extensions are typically used to anchor these deck panels. The panels provide the entire positive moment reinforcement in the transverse direction of the bridge deck. The topping slab contains nominal reinforcement to take care of the temperature and shrinkage stresses as well as negative moment reinforcement in the transverse and longitudinal directions if continuity for live load is provided. Indiana has a standard panel width not to exceed 8 ft. The longitudinal dimension (length) of the panel depends on the spacing of longitudinal bridge girders. For the specimens tested in this study a panel length of 8 ft was chosen as it falls in the range of medium to upper girder spacing. In general, the wider and longer deck panels are more susceptible to damage during shipping and handling.

Based on the previous considerations the selected dimensions of the composite specimens were 8 ft x 8 ft x 8 inches. Though the cast-in-place topping slab offers restraint against rotation and thus inducing negative moments at the ends of the precast panel, the specimens were tested in the simply supported condition. This in fact is the worst possible case for the precast element in terms of loading.

3.2.1 Prestressed Concrete Panels

The dimensions of the precast panels were 8 ft x 8 ft x 2.5 inches with typical amounts of prestressing and mild steel reinforcement. The panels were cast with low slump concrete mixes

and aggregate sizes not larger than 3/4 in. to ensure proper consolidation. In Indiana, the specified concrete compressive strength at transfer is 4000 psi and the minimum 28 day strength is 5000 psi with a minimum panel thickness of 2.5 inches in a concrete bridge deck with a total minimum thickness of 8 inches. The mild reinforcing steel was Grade 60 and met the requirements of ASTM A-615. The prestressing strands were seven wire Lo-Lax Grade 270 with a 3/8 in. diameter. Welded wire fabric (3 x 15 D7 x W4) met ASTM A-497 requirements. Panel surface was roughened in the direction parallel to the strands so as to minimize the reduction in the section modulus. The panel surface was broom finished. The mix quantities per cubic yard of concrete were 649 lbs of cement (Portland Cement Type I), 1415 lbs of fine aggregate (natural sand), 1655 lbs of coarse aggregate with a maximum aggregate size not larger than 3/4 in. to ensure proper consolidation and 233 lbs of water. Air entrained content was 8.5% and concrete slump was 3 to 3.5 inches.

Precast panels in Specimens 1-4 contained 18 prestressing strands positioned at mid-depth of the panel. The panels in specimens 5 and 6 had 12 strands of same type and size positioned at mid - depth of the panel. Spacing between the strands in each panel varied as the prestressing bed had a fixed strand spacing. But spacing was symmetrical on either side of the center line of the panel. The strands were extended 6 in. beyond the panel end on either side of the panel. Before the concrete was poured, the strands were prestressed to about 17.5 kips (corrected for slip loss which was estimated to be approximately 0.3 kips) approximately equal to $0.75 f_{pu}$, where f_{pu} is the strand ultimate tensile strength.

Each panel had a single layer of welded wire fabric located directly on top of the prestressing strands. In addition five #3 reinforcing bars placed at 6 in., 18 in., and 48 in. from

either end of the panel. These bars are provided to improve transverse load distribution. The panels were designed to support their own dead load, the weight of the cast - in - place concrete and a construction live load of 50 psf along with the effects of prestressing. At this stage, since the concrete is not fully set, the panels have to be designed as non - composite, simply supported slabs spanning between longitudinal bridge girders. Precast deck panels, unlike metal deck forms, continue to serve structural function after the construction of the deck is completed.

3.2.2 Concrete Topping Slab (CIP)

The 5.5 in. thick topping slab provided a total composite slab thickness of 8 in. Reinforcement in the CIP topping was similar to that specified for a conventional 8 in. bridge deck. The transverse reinforcement consisted of #5 bars spaced at 9 in. on centers supported on 1.75 in. high bar chairs spaced at approximately 2 ft on centers. These bar chairs rested directly on the top surface of the precast panels. The longitudinal reinforcement (parallel to span) consisted of #5 bars spaced at 6 in. on centers placed on top of the transverse reinforcement. All reinforcing bars were ASTM A615 - 90, Grade 60 bars. These bars were not epoxy coated and the clear cover for the above bars was 2.5 inches. End cover in the case of these bars was 3 in. from the sides of the specimen. This reinforcement was nominal and placed in the concrete to take care of the temperature and shrinkage stresses. The design concrete compressive strength of this slab was 4000 psi. The approximate quantities of various components per cubic yard of concrete mix were 658 lbs of cement (Portland Cement Type I), 1360 lbs of fine aggregate (natural sand), 1850 lbs of coarse aggregate (gravel) and about 250 lbs of water. The amount of air entrainment for the topping slab was about 6% and the slump was between 3 and 4 inches.

The overall topping slab dimensions were 8 ft x 8 ft x 5.5 inches.

3.3 Experimental Procedure

3.3.1 Test set - up and sequence of load application

The test set up is shown in Fig. 3.4. The two columns are 12 ft apart and support a cross beam. The cross beam in turn supports two hydraulic actuators. The load is distributed to the specimen by means of a spreader beam, which distributes the load over the entire width of the panel. Though in the actual bridge deck the cast - in - place concrete offers restraint against rotation inducing negative moments at the ends of the precast panel, specimens were tested in the simply supported condition. This in fact is the worst possible case, as in the simply supported panel the effects of loading for positive moment and shear are more severe than in an end restrained panel.

Static load tests were performed at regular intervals between repeated loading applications. The specimens were tested under repeated loading to simulate traffic effects on the horizontal shear strength of the panel at the interface between the precast panel and the cast-in-place portion of the deck. The stress range for the repeated loading in Specimens 1-4 was from 26.4 kips (corresponding to an equivalent concentrated load producing the same positive midspan moment as that of an HS20 wheel load with an impact factor of 30% (see Appendix) to 38.2 kips (corresponding to a tensile stress of $6\sqrt{f'_c}$ at the bottom fiber of the precast panel) for Stage 1. Stage 1 consisted of 600,000 cycles of repeated loading. At the end of Stage 1, the specimens were loaded monotonically until first flexural cracking was observed. In Stage 2, the specimens

were cycled between 2.4 kips (corresponding to all superimposed dead load) to 28.8 kips (corresponding to a tensile stress of $3\sqrt{f'_c}$ at the bottom fiber of the precast panel). Intermediate monotonic cycles were performed at regular intervals. Stage 2 was repeated for 400,000 cycles. After the 1,000,000 cycles were completed, Specimen 1-4 were tested monotonically to failure. Specimens 5 and 6 were loaded up to first flexural cracking prior to beginning their cyclic loading. Repeated loading followed using the same loads as in Stage 2 for Specimens 1-4 up to a total of 1,000,000 cycles. The upper limit of 28.8 kips corresponded to a stress of $7.5\sqrt{f'_c}$ at the bottom fiber of the precast panel in the last two specimens. Specimens 5 and 6 were designed to evaluate the effect of lower prestressing and higher stress level at the panel interface.

3.3.2 Loading Pattern

Earlier, it was found that punching shear [19] usually governs the ultimate strength of the slab in a monotonic loading situation when the load is distributed over the wheel foot print. In these cases if the full flexural capacity of the panels is not achieved, maximum uniform horizontal shear stress at the interface across the width of the panel is not developed. Thus to find the horizontal shear capacity of the panel, it was felt necessary to extend the loading area over the entire width of the panel.

For this purpose, load was distributed over an area of 10 in. x 96 in. The first four specimens were used to evaluate the ultimate horizontal shear strength of a precast panel with a broom finished interface and the last two specimens were used to observe the behavior of specimens under flexural failure. Loads were applied by hydraulic actuators. These hydraulic

actuators were manufactured by MTS (Material Testing Systems). This equipment contained MTS 458.20 micro console, 458.13 AC controller, 458.11 DC controller and 458.91 micro profiler. The two hydraulic actuators were connected to two different beam elements about 2 ft long. The short beams in turn were supported by a 10 inch wide spreader beam to distribute the load uniformly over the entire 8 ft. width of the specimen. These two actuators were operated synchronously by adjusting both the AC and DC controllers. Test program was keyed in through the micro profiler and various data pertaining to the actuators was displayed on the micro console.

3.3.3 Instrumentation

Instrumentation was placed to monitor strains and deflections at various locations. To obtain the vertical deflections, three LVDTs were placed on the sides of the panel at distances 2.5 ft, 4 ft and 5.5 ft respectively from either of the supported edges, as shown in Fig. 3.5. These readings were used to obtain load versus deflection characteristics of the deck slab.

Strain gages were used to measure the strains on the sides of the specimen and the prestressing strands. Strain distribution across the section can be used to examine the behavior of the composite specimen. Under the applied loading the curvature for both the panel and the topping slab has to be the same, if vertical separation between the panel and the topping slab does not occur. According to the plane section hypothesis, a plane section perpendicular to the neutral axis before bending should remain plane and perpendicular to neutral axis after bending also, even in the case of composite panels. This composite behavior can be achieved only if the strains at the interface are continuous and if the strain distribution is linear across the entire depth of the composite section. Once the two deck elements start behaving independently, owing to the

curvature change due to the vertical separation which also causes horizontal slip at the interface between the cast - in - place slab and the precast panel, the strain distribution across the entire depth of the composite section will not be linear. Hence for determining the strain distribution across the entire depth of the composite section at least three strain measurements across the depth of the deck are necessary.

Strain gages were placed on the sides of the panel at a depth of 5 in. from the top of the deck, at the prestressing strand level as shown in Fig. 3.6 and also on the top of the concrete surface as shown in Fig. 3.7. The strain gages were located at a distance of 3 ft from both supports. Strain gages placed on concrete surface were manufactured by Micro Measurements Division and of type EA - 06 - 20CBW - 120 with a gage factor of $2.09 \pm 0.5\%$ and with a transverse sensitivity of $-1.1 \pm 0.2\%$. Strain measurements on the prestressing strands were used to verify prestressing losses and to examine the behavior of the panel. On the prestressing strands, strain gages were placed at mid - section. On some strands two more strain gages were placed on either side of mid - section at a distance of 6 in. as shown in Fig. 3.8. These strain gages were manufactured by Micro Measurements Division and of type EA - 06 - 062DN - 350 with a gage factor of $2.08 \pm 0.5\%$, and with a transverse sensitivity of $(0.7 \pm 0.2)\%$. To find the amount of strand slip, which might occur as the loading increases, dial gages were placed on the strands as shown in Fig. 3.8.

Strain gages were also placed on the rebars located in cast - in - place topping slab. These strain gages were placed at a distance of 3 ft. from both supports. These gages were in line with the gages placed on the sides of panels and also on top of the deck slab and were used to determine the rebar contribution to the flexural and shear capacity of the composite specimen.

These gages were placed only in Specimens 3-6. The gages used were of type CEA - 06 - 125UN - 350, with a gage factor of $2.105 \pm 0.5\%$ and with a transverse sensitivity of $(0.2 \pm 0.2)\%$.

Interface strain gages were placed at mid - section of the top surface of precast panel. These strain gages were placed to estimate the immediate loss following detensioning the prestressing strands as well as the total loss prior to casting of the topping slab. Usually during the operation of pouring concrete for topping slab, these interface gages get damaged and useless beyond this point. These gages were placed in the last four specimens only. The location of these gages can be seen in Fig. 3.9.

To determine the slip between the cast - in - place concrete slab and the prestressed panel, LVDTs were used as slip gages. Slip between the cast - in - place slab and the prestressed panel is associated with diminishing composite behavior between the cast - in - place (CIP) slab and the precast panel. There will be separation between the CIP slab and the precast panel when the deck loses composite action. This separation usually does not occur at the supports and the loading point due to the compressive stress flow. Hence the separation and thereby slip would only take place in between the points which are, d , effective depth of the slab, away from the loading point and the support reactions. To measure this slip, slip gages were placed as shown in Fig. 3.10. Slip gage details are shown in Fig. 3.11.

In the case of panels where shear connectors were used, strain gages were placed on the shear connectors in an attempt to evaluate their effectiveness when the slip occurs between the CIP and the precast panel. These shear connectors act as a combination of dowel and clamping reinforcement once the slip occurs at the interface. It was found [7] that the behavior of a dowel

was mostly elastic (both in the bar and in the embedment) for shear forces not exceeding 40% of the ultimate capacity. Near the collapse loads, more than 50% of the dowel section was plastisized over a bar length close to two diameters with a peak at one diameter from the shear plane. Hence on the shear connectors, strain gages were placed at a distance of one diameter from the shear plane. Strain gages can be placed either above or below the shear plane. In all the specimens where shear connectors were provided, strain gages were kept above the shear plane. Strain gages placed on these shear connectors consisted of two different types. First type was CEA - 06 - 125UN - 350 with previously described set of values and was used in specimens 2 and 6. The second type was EA - 06 - 250BG - 120, with a gage factor of $2.075 \pm 0.5\%$ and a transverse sensitivity of $(0.4 \pm 0.2)\%$. This second type of strain gages were used in specimens 3 and 4.

3.4 Summary

In this chapter, the geometrical characteristics of the specimens and the experimental program involved are discussed. In the following chapter, data obtained during this experimental investigation is analyzed to examine the behavior of specimens. This analysis includes the examination of the composite behavior at ultimate, evaluation of the effectiveness of the shear connectors, interface slip characteristics, cracking, deflection and effects of repeated loading.

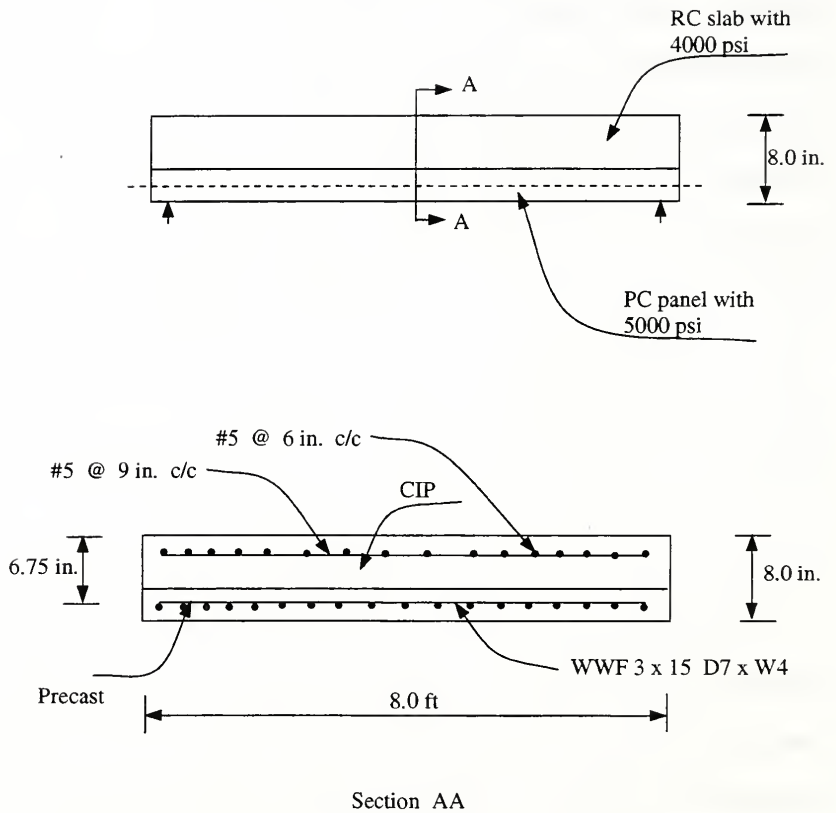


Figure 3.1 - Geometrical characteristics of deck slab

Note: 1 in. = 25.4 mm

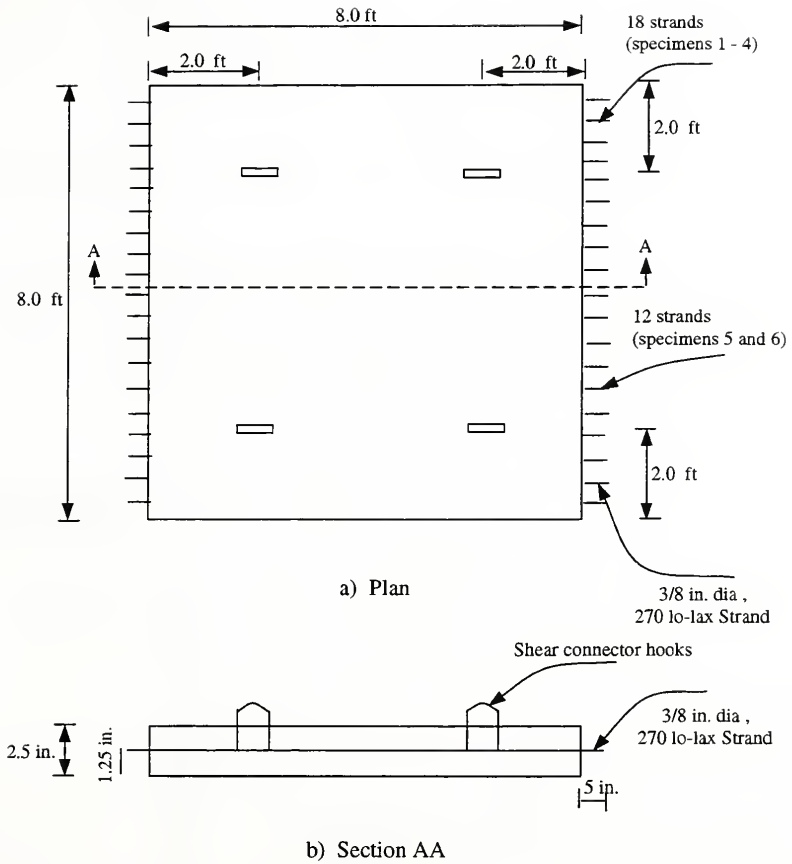


Figure 3.2 - Typical detail of a panel with 4 stirrups a) Plan b) Section AA

Note: 1 in. = 25.4 mm

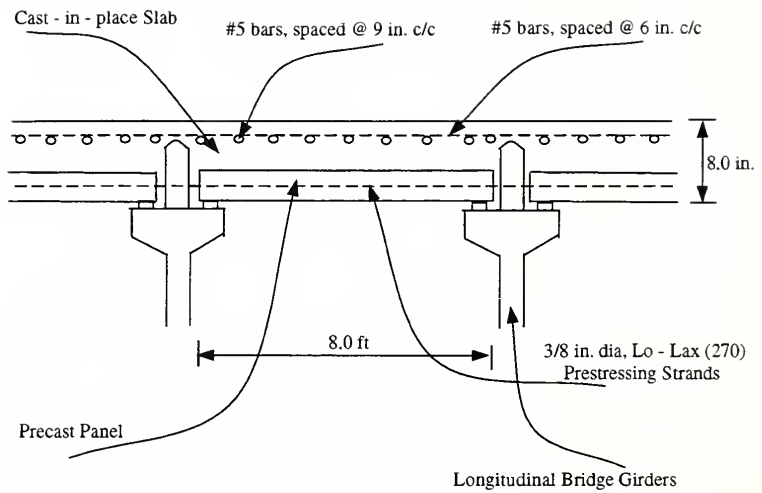


Figure 3.3 - Cross section details of bridge deck

Note: 1 in. = 25.4 mm

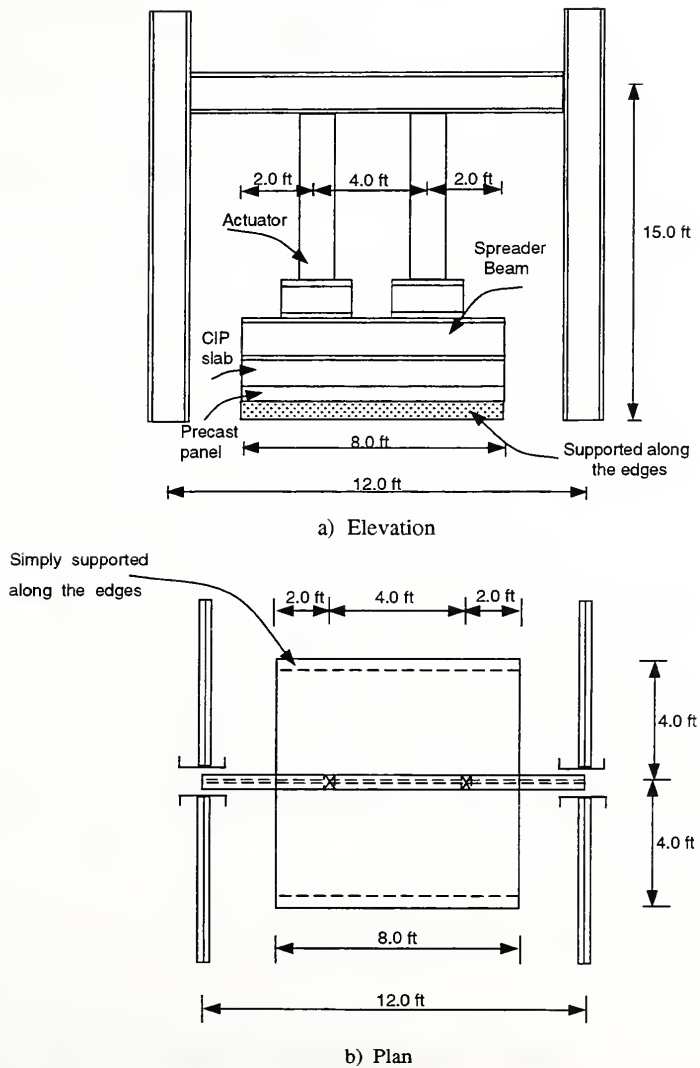


Figure 3.4 - Loading frame details a) Elevation b) Plan

Note: 1 in. = 25.4 mm

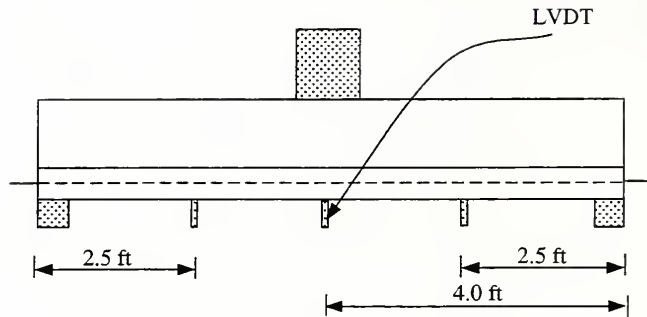


Figure 3.5 LVDT Locations on the sides for measuring deflections

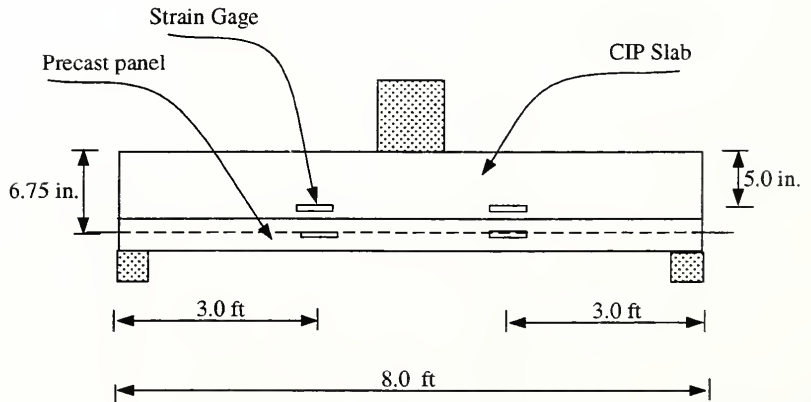
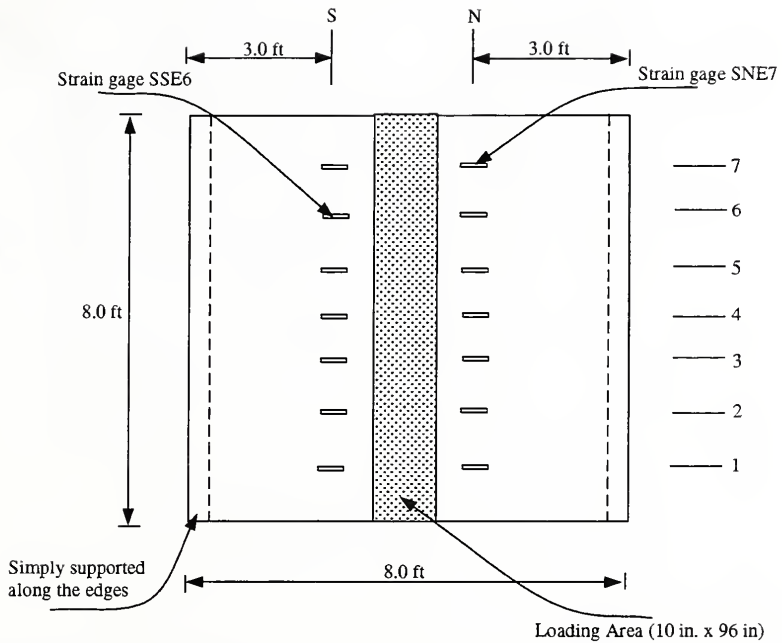
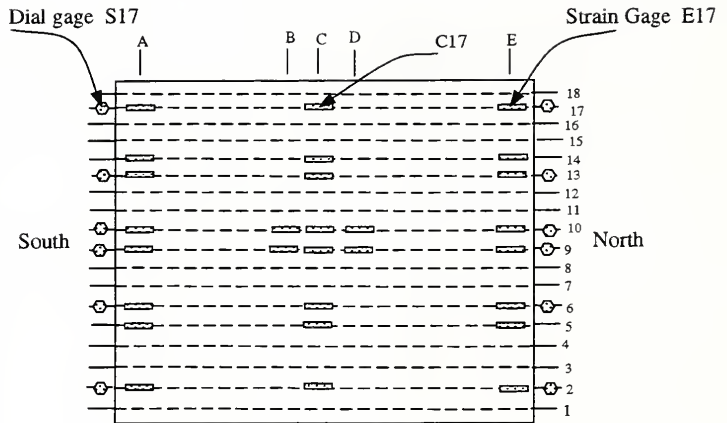


Figure 3.6 Strain Gage Locations on the sides of the deck



Note : Strain gages are identified according to the grid shown.

Figure 3.7 - Strain gage Locations on top of the CIP slab



Note: A and E are 6 in. away from edges
 B and D are 3.5 ft. away from edges
 C is 4.0 ft away from edges

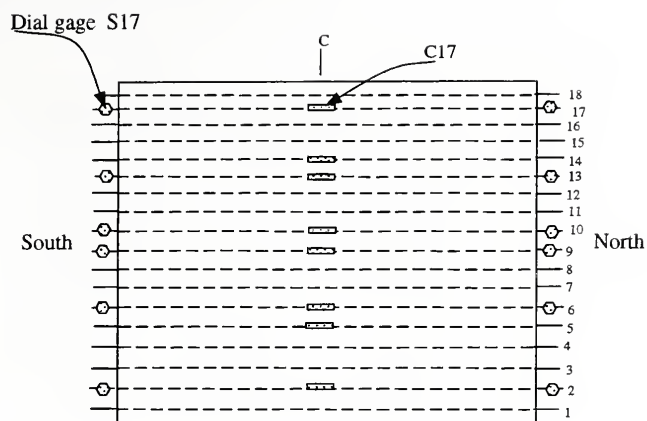
a) Details of Specimens 1 and 2

Figure 3.8 Strain gage and Dial gage locations on the prestressing strands

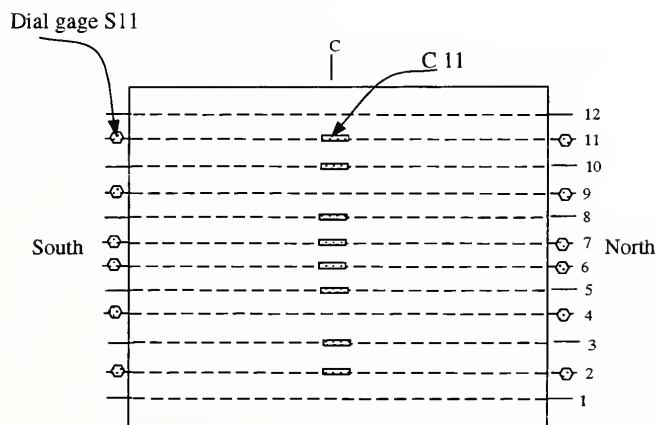
a) Details of Specimens 1 and 2

b) Details of Specimens 3 and 4

c) Details of Specimens 5 and 6

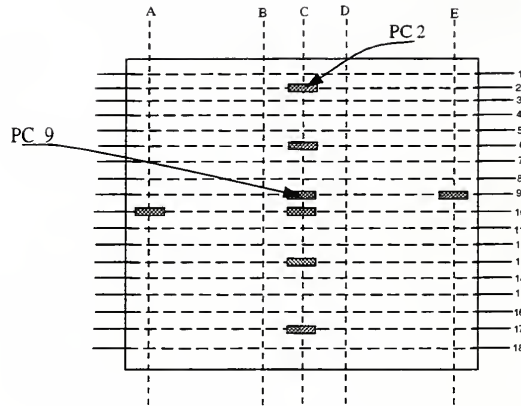


b) Details of Specimens 3 and 4

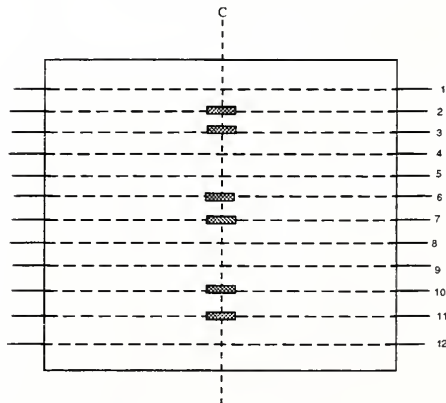


c) Details of Specimens 5 and 6

Figure 3.8, continued



a) Details of Specimens 3 and 4



b) Details of Specimens 5 and 6


Note :  Represents strain gage location.

Figure 3.9 Strain Gage Locations on top of the Precast Panel

a) Details of Specimens 3 and 4

b) Details of Specimens 5 and 6

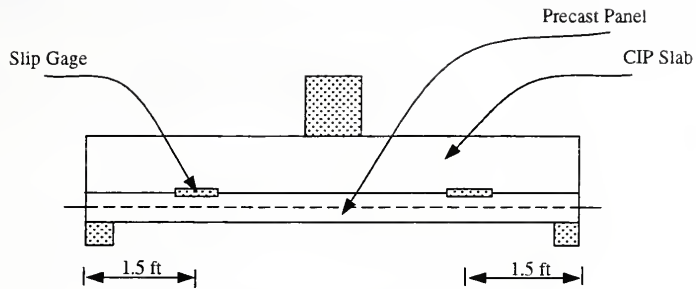


Figure 3.10 Slip gage locations on the sides of the Deck

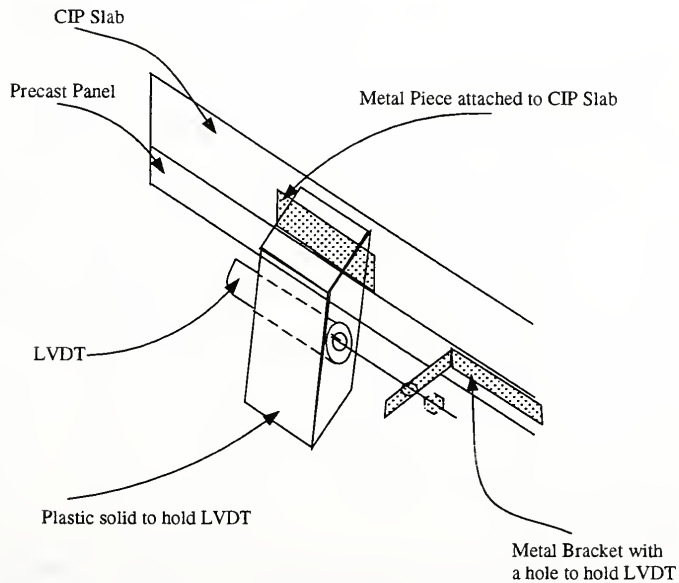


Figure 3.11 Slip Gage Details

CHAPTER 4 - EXPERIMENTAL RESULTS

4.1 Material Properties

4.1.1 Properties of Concrete

Concrete compressive strength, f'_c , and modulus of elasticity were established for the concrete used in the precast panels and cast-in-place (CIP) topping slabs. The modulus of rupture, f_r , for each type of concrete was determined by testing 6 in. square concrete prisms with one-third point loading on an 18 in. span. Cylinder strengths of both the precast panel and the CIP slab concrete were determined after 3, 7, 14, 21 and 28 days of casting of the slabs. Ultimate compressive strength and variation of compressive strength with age of concrete were determined from the concrete test cylinders. These results were plotted in Figs. 4.1 to 4.3.

The specimens were prepared in three sets. The first set contained Specimen 1 and Specimen 2. The second set contained Specimen 3 and Specimen 4, and the third set contained Specimen 5 and Specimen 6. Precast prestressed concrete and cast-in-place reinforced concrete properties for each set are listed in the Tables 4.1 to 4.6.

4.1.1.1 Specimen 1 and Specimen 2 (Set 1)

For the precast panel

Date on which precast panel was cast	= 02 / 05 / 93
Date on which prestressing strands were detensioned	= 02 / 08 / 93
Slump of concrete	= 3.25 inches
Air content	= 5.2 %
Concrete compressive strength on 02 / 08 / 93	= 4320 psi

Table 4.1 Variation in concrete compressive strength with age of concrete

Date (mo/dd/yr)	Age of Concrete (days)	Concrete Compressive Strength (psi)
02 / 08 / 93	3	4320
02 / 12 / 93	7	6378
02 / 19 / 93	14	6844
02 / 26 / 93	21	7781
03 / 05 / 93	28	7850
06 / 21 / 93	136	8323

The modulus of rupture calculated from the concrete compressive strength was 684 psi.

The tests on flexural beams gave a modulus rupture of 919 psi.

For the CIP topping slab,

Slump = 4.0 inches
Air content = 6.0 %

Table 4.2 Variation in concrete compressive strength with age of concrete

Date (mo/dd/yr)	Age of Concrete (days)	Concrete Compressive Strength (psi)
04 / 05 / 93	4	5364
04 / 08 / 93	7	5930
04 / 15 / 93	14	6826
04 / 22 / 93	21	6838
04 / 29 / 93	28	6932
06 / 21 / 93	81	7239

The modulus of rupture calculated from the concrete compressive strength was 638 psi.

The tests on flexural beams gave a modulus rupture of 765 psi.

4.1.1.2 Specimen 3 and Specimen 4 (Set 2)

For the precast panel

Date on which precast panel was cast = 07 / 31 / 93
Date on which prestressing strands were detensioned = 08 / 04 / 93
Slump of concrete = 4.25 inches
Air content = 7.8 %
Concrete compressive strength on 08 / 04 / 93 = 4155 psi

Table 4.3 Variation in concrete compressive strength with age of concrete

Date (mo/dd/yr)	Age of Concrete (days)	Concrete Compressive Strength (psi)
08 / 04 / 93	4	4155
08 / 10 / 93	10	4904
08 / 24 / 93	24	5175
08 / 31 / 93	31	5647
10 / 11 / 93	72	6826

The modulus of rupture calculated from the concrete compressive strength was 619 psi.

The tests on flexural beams gave a modulus rupture of 930 psi.

For the CIP topping slab,

Slump = 4.0 inches
Air content = 6.0 %

Table 4.4 Variation in concrete compressive strength with age of concrete

Date (mo/dd/yr)	Age of Concrete (days)	Concrete Compressive Strength (psi)
08 / 30 / 93	3	3584
09 / 03 / 93	7	4279
09 / 10 / 93	14	4680
09 / 24 / 93	28	5747
10 / 11 / 93	45	6343

The modulus of rupture calculated from the concrete compressive strength was 597 psi.

The tests on flexural beams gave a modulus rupture of 536 psi.

4.1.1.3 Specimen 5 and Specimen 6 (Set 3)

For the precast panel

Date on which precast panel was cast = 10 / 07 / 93
Date on which prestressing strands were detensioned = 10 / 12 / 93
Slump of concrete = 4.0 inches
Air content = 5.6 %
Concrete compressive strength on 10 / 10 / 93 = 4750 psi

Table 4.5 Variation in concrete compressive strength with age of concrete

Date (mo/dd/yr)	Age of Concrete (days)	Concrete Compressive Strength (psi)
10 / 10 / 93	3	4750
10 / 14 / 93	7	5368
10 / 21 / 93	14	5821
10 / 28 / 93	21	6319
11 / 04 / 93	28	6857
11 / 19 / 93	43	7032

The modulus of rupture calculated from the concrete compressive strength was 629 psi.

The tests on flexural beams gave a modulus rupture of 830 psi.

For the CIP topping slab,

Slump = 4.0 inches
Air content = 6.0 %

Table 4.6 Variation in concrete compressive strength with age of concrete

Date (mo/dd/yr)	Age of Concrete (days)	Concrete Compressive Strength (psi)
11 / 08 / 93	3	3822
11 / 12 / 93	7	4329
11 / 19 / 93	14	4957
11 / 26 / 93	21	5334
12 / 03 / 93	28	5657

The modulus of rupture calculated from the concrete compressive strength was 564 psi.

The tests on flexural beams gave a modulus rupture of 592 psi.

4.1.2 Steel Properties

The prestressing strands were Lo-Lax Grade 270 with a 3/8 in. diameter. These strands were given an initial prestress of 3 kips per strand to lift the strands off the bed so that the strain gages can be placed. The specified load per strand was 17.2 kips.

Nominal area of strand	= 0.085 in ²
Modulus of Elasticity	= 28,500 ksi
Load at 1% elongation	= 22,050 lbs
Elongation at 17,230 lbs	= 0.00712 in/in
Ultimate elongation	= 5.47%
Ultimate load	= 23,840 lbs
Slip loss	= 0.25 in.
Gage length	= 2451 in.
Correction for slip loss (from Hooke's law)	= 247 lbs
Total load per strand	= 17,447 lbs
Ultimate strength of strands	= 280.47 ksi
Computed elongation (e)	= 14.36 in.
Corrected elongation ($e_c = e + \text{slip loss}$)	= 14.61 in.
Minimum elongation ($0.95 \times e_c$)	= 13.875 in.
Maximum elongation ($1.05 \times e_c$)	= 15.25 in.

The shear connectors provided across the interface were #4, Grade 60, epoxy coated bars and met the requirements of ASTM A615-90. The actual yield strength of these bars was 74,500 psi and that of ultimate strength was 116,000 psi.

Reinforcement provided in CIP topping slab to take care of temperature and shrinkage stresses was #5, Grade 60 and met the requirements of ASTM A615-90. The actual yield strength was 75,500 psi. The ultimate strength was 116,600 psi with a maximum elongation of 9.0%.

4.2 Strand Slip Results

Strand development lengths necessary to attain the full strength of the strands were not obtained experimentally on a quantitative basis. But a qualitative evaluation of the strand development lengths can be obtained by monitoring the ends of the selected strands for their slip relative to the panel ends. This slippage occurs when the actual bond stresses between the strand and the surrounding concrete exceed the bond strength along some portion of the strand development length. Dial gages were placed on selected strands to monitor the relative displacement between the strand and the panel ends. Load and strand slip results were plotted against each other for all the specimens. Due to the sensitivity of the dial gages, strand slips were presumed to occur when there was a significant deviation from the initial reading. Strand slip load was recorded to be the load at which any of the monitored strands showed a significant slip. But this cannot be taken exactly as the slip load because slip might have occurred earlier in any of those non-monitored strands.

Estimated capacities of the specimens based on AASHTO guidelines are shown in Table 4.7. In this table, cracking load was calculated using the average modulus of rupture of the

Table 4.7 - Estimated Capacities of Specimens

Specimen	Cracking Load (kips)	Strand Slip Capacity [#] (kips)	Flexural Capacity* (kips)	Horizontal Shear Capacity (kips)	Beam-Shear Capacity (kips)
1 to 4	60	99	158	98	158
5 and 6	40	62	128	98	158

Note : 1 kip = 4.46 kN.

- Strand Slip capacity based on the Development length criterion of AASHTO.

* - Flexural Capacity including the contribution from the CIP rebars and the wire mesh.

concrete. Strand slip capacity was calculated based on the development length requirements of AASHTO. Ultimate flexural capacity of the panel included the contributions from the CIP rebars, wire mesh placed in precast panel, and using the ultimate tensile strength of the strands. Horizontal shear capacity was assumed to be $80b_vd$ even though some amount of shear reinforcement across the interface was provided in some cases. Similarly vertical shear capacity was calculated based on a nominal shear stress of $2\sqrt{f'_c}$ over the vertical section. In all these cases dead load effects were subtracted to represent the amount of live load that can be taken by the specimen before failure occurs.

Observed load capacities of various specimens are listed in Table 4.8. In this table, the load at which the specimen cracked, the strand slip load at which the strands started slipping, the ultimate load of the specimen, the cracking load ratio, the strand slip load ratio, the ultimate load ratios between the actually applied loads and the theoretically estimated strand slip capacity based on AASHTO, and the ratio corresponding failure mode capacities (either beam-shear or flexural capacity including the contributions from CIP rebars and wire mesh) taken from Table 4.7 are shown. Along with these, ratios of experimentally observed ultimate to strand slip load levels and ultimate to cracking load levels are also shown. Failure modes were also listed in the last column. Beam-shear capacities of the specimens were improved by the dowel action provided by the horizontal longitudinal reinforcement in CIP. This also explains the higher failure capacities of Specimens 3 and 4 in beam-shear mode.

Comparison of ultimate capacities of all the specimens with service loads and factored loads was shown in Table 4.9. In Table 4.9 cracking loads, strand slip loads, and ultimate capacities of all specimens are compared with the equivalent service loads and equivalent factored loads (see Appendix).

Table 4.8 - Load Capacities of various Specimens

Specimen	Test Values			Test / Predicted Values				Load ratios		Type of Failure Mode
	Crack- ing Load (kips) (a)	Strand Slip Load (kips) (b)	Ultimate Load (kips) (c)	Crackin g Load ratio	Strand Slip Load ratio	Ultimate Load ratio [#]	Ultimate Load ratio [*]	(c) ----- (b)	(c) ----- (b)	
1	60	115	160	1.00	1.16	1.62	1.01	1.39	2.67	Shear
2	65	110	170	1.08	1.11	1.72	1.07	1.54	2.62	Shear
3	75	155	200	1.25	1.56	2.02	1.26	1.29	2.67	Shear
4	65	140	180	1.08	1.41	1.82	1.14	1.29	2.77	Shear
5	47.5	95	130	1.18	1.53	2.10	1.01	1.37	2.74	Flexure
6	50	100	140	1.25	1.61	2.26	1.09	1.40	2.80	Flexure

Note : 1 kip = 4.46 kN; # - Taking Strand Slip Load as ultimate load; * - Taking Failure Mode Capacity;

Table 4.9 - Actual Ultimate Capacities versus Service Loads and Factored Loads

Specimen	Test Values			<div> <div>(a)</div> <div>(b)</div> <div>(c)</div> </div> <div> <div>divided by</div> <div>Service Load (= 26.4 kips)</div> </div>			<div> <div>(a)</div> <div>(b)</div> <div>(c)</div> </div> <div> <div>divided by</div> <div>Factored Load (= 57.3 kips)</div> </div>		
	Cracking Load (kips) (a)	Strand Slip Load (kips) (b)	Ultimate Load (kips) (c)						
1	60	115	160	2.27	4.36	6.06	1.05	2.00	2.79
2	65	110	170	2.46	4.17	6.44	1.13	1.92	2.97
3	75	155	200	2.84	5.87	7.57	1.31	2.70	3.49
4	65	140	180	2.46	5.30	6.82	1.13	2.44	3.14
5	47.5	95	130	1.80	3.60	4.92	0.83	1.66	2.27
6	50	100	140	1.89	3.79	5.30	0.87	1.75	2.44

Note : 1 kip = 4.46 kN.

4.2.1 Specimen 1 - Panel with 18 strands and no shear connectors

Even after a million cycles of repeated loading the strands did not slip by a significant amount. After the million cycles of repeated loading the panel was subjected to monotonic loading. Strand slip readings were monitored during this monotonic loading. Slips occurred neither at the factored loads nor at the flexural cracking load at which bottom fiber of the precast panel cracked. The slippage that occurred in various strands had different characteristics. In cases like S10, S13 and N17 gages there was a gradual slip in the strands. The final slips that were obtained from these dial gages at the ultimate load were of the order of one inch. From these gage readings, it can be seen that failure of the specimen occurred on the southern side. There was a considerable amount of strength remaining in the slab at the time the first strand slip was noticed. The ratio of load at which strand slip was observed in any of the monitored strands (P_{ssmin}) to the ultimate load at which the slab failed in diagonal tension failure (i.e shear failure) is about 0.736. This indicates that the first strand slip in any of the monitored strands had occurred approximately at three fourths the capacity of the slab. The ratio of P_{ssmin} to the factored load is about 2.06 which indicates that strand slip had not occurred in any of the strands until a load level twice as high as the design factored load, which in turn indicates that the strand slips had not occurred until about 4.46 times the service load. Load versus strand slips are shown in Figs. 4.4 to 4.6.

4.2.2 Specimen 2 - Panel with 18 strands and four shear connectors

As in the case of panel without any shear connectors, this panel also did not show by a significant amount of slip even after a million cycles of repeated loading. During the monotonic

loading which was conducted after a million cycles of repeated loading, slip occurred neither at the factored loads nor at the flexural cracking load at which the bottom fiber of the precast panel cracked. The slippage that occurred had different characteristics. In this panel some of the strand ends showed a gradual slip and some showed sudden slip. Load vs strand slip results of the 2nd, and 10th strands were plotted. These plots show a gradual slip of these strands with increasing load beginning at 110 kips. The dial gages located at the ends of strand 2 and strand 10 showed similar slip characteristics as well as the same amount. The final slip obtained from these dial gages at the ultimate load was of the order of 0.16 inch.

There was a considerable amount of strength remaining in the slab at the time the first strand slip was noticed. The ratio of the load at which strand slip was noticed in the monitored strands (P_{ssmin}) to the ultimate load at which the slab failed in diagonal tension failure (i.e shear failure) is about 0.675. This indicates that the first strand slip in any of the monitored strands had occurred approximately at two thirds of the final capacity of the slab. The ratio of P_{ssmin} to the factored load is about 2.01 which indicates that strand slip had not occurred in any of the strands up to about twice as much load as the factored load which in turn indicates that the strand slips occurred at about 4.36 times the service load. Load versus strand slips for panel with four shear connectors are shown in Figs. 4.7 to 4.9.

4.2.3 Specimen 3 - Panel with 18 strands and four shear connectors

Similar to Specimen 2 which had 18 strands with four shear connectors across the interface, this panel also did not show signs of slip even after a million cycles of repeated

loading. During the monotonic loading which was conducted after a million cycles of repeated loading, slips occurred neither at the factored loads nor at the flexural cracking load at which the bottom fiber of the precast panel cracked. In this panel same as in Specimens 1 and 2, some of the strand ends showed a gradual slip and some showed sudden slip at the ultimate load. Load versus slip results were plotted. Slip of the monitored strands started at 155 kips instead of 110 kips as in the Specimen 2. This could be a misinterpretation in regards to the bond strength of the strands because slip might have occurred earlier than this load in strands that were not monitored. The dial gages located at the ends of strands 6, 9 and 10 clearly showed that the imminent failure was to occur on the south side of the specimen. The final slips that were obtained from these dial gages at the ultimate load were of the order of 0.4 inches. There was a considerable amount of strength remaining in the slab at the time the first strand slip was noticed. The ratio of load at which strand slip was noticed in the monitored strands (P_{ssmin}) to the ultimate load at which the slab failed in diagonal tension failure (i.e shear failure) was about 0.775. This indicates that the first strand slip in any of the monitored strands had occurred approximately at three fourths the capacity of the slab. The ratio of P_{ssmin} to the factored load was about 2.71 which in turn indicates that the strand slips had not occurred up to about 5.87 times the service load. Load versus strand slip results for this panel are shown in Figs. 4.10 to 4.12.

4.2.4 Specimen 4 - Panel with 18 strands, Four Shear Connectors and a Lubricated Interface

This panel with 18 strands, having four shear connectors across the lubricated interface showed similar strand-slip characteristics as the previous three panels. There was no significant strand slip in any of the monitored strands during the cyclic loading stage of the specimen.

During the monotonic loading stage that followed the million cycles of fatigue life, strand slip was not observed until a load level of 140 kips. This load level was 2.48 times the factored load level which in turn indicates that strand slip load was 5.3 times that of service load. The dial gages that were located on the north side clearly indicated in advance the impending failure on the north side. The final slips that were obtained from the dial gages located on the north side on the 6th, 9th, 10th, 13th and 17th strands were of the order of 0.6 inches. Similar to the previous panels there was a considerable amount of strength remaining in the slab at the time the first strand slip was noticed. The ratio of load at which strand slip was noticed in any of the monitored strands (P_{ssmin}) to the ultimate load at which slab failed in shear failure mode was about 0.775. This also indicates a reserve capacity of about 25% in the slab from the point at which first strand slip was noticed. Load versus slip results for this specimen are shown in Figs. 4.13 and 4.14.

4.2.5 Specimen 5 - Panel with 12 strands and without any shear connectors

This panel with 12 strands and without any shear connectors across the interface showed similar strand-slip characteristics as the previous four panels. There was no significant strand slip in any of the monitored strands during the cyclic loading stage of the specimen. During the monotonic loading stage that followed the million cycles of loading, strand slips were not observed until a load level of 95 kips. This load level was 1.66 times that of factored load level which in turn indicates that strand slip load was 3.6 times that of service load. The final slips that were obtained from the dial gages were of the order of 0.8 inches. Similar to the previous panels there was a considerable amount of strength remaining in the slab at the time the first

strand slip was noticed. The ratio of load at which strand slip was noticed in any of the monitored strands (P_{ssmin}) to the ultimate load at which slab failed in flexural failure mode was about 0.731. This also indicates a reserve capacity of about 25% in the slab from the point at which first strand slip was noticed. Load versus slip results for this specimen are shown in Figs. 4.15 and 4.16.

4.2.6 Specimen 6 - Panel with 12 strands and four shear connectors

This panel with 12 strands and four shear connectors across the interface showed similar strand-slip characteristics as the previous five panels. There was no significant strand slip in any of the monitored strands during the cyclic loading stage of the specimen. During the monotonic loading stage that followed the million cycles of fatigue life, strand slips were not observed until a load level of 100 kips. This load level was 1.75 times that of factored load level which in turn indicates that strand slip load was 3.8 times that of service load. The final slips that were obtained from the dial gages were of the order of 0.4 inches. Similar to the previous panels there was a considerable amount of strength remaining in the slab at the time the first strand slip was noticed. The ratio of load at which strand slip was noticed in any of the monitored strands (P_{ssmin}) to the ultimate load at which slab failed in flexural failure mode was about 0.714. This also indicates a reserve capacity of about 25% in the slab from the point at which first strand slip was noticed. Load versus slip results for this specimen is shown in Fig. 4.17.

4.3 Composite Behavior of Deck Slabs

For the precast panel and the cast-in-place slab to act together, transfer of horizontal shear

stress across the interface without significant interface slip must take place. Hence, the interface slip is a good indicator of the composite deck behavior under the applied loading. Horizontal shear across the interface is transferred by the interface bond strength between the precast panel and the cast-in-place slab before the interface slip occurs and by any shear connectors across the interface, once the interface slip commences.

This composite behavior of the specimens can also be noticed in the strain distributions across the depth of various specimens. These strain distributions were linear until significant diagonal cracking occurred, at which stage redistribution of stresses and strains occurred due to the release in energy near the crack tip vicinity. A typical diagonal crack similar to that observed in deck panels is shown in Fig. 4.18. The internal force mechanism is the same as that proposed by Krefeld et al [26]. As can be seen clearly from this free body diagram, at Section 2-2, tensile stresses exist at A above the diagonal tension crack, and compressive stresses exist at A, right below diagonal crack. Hence the strain measurements indicated an increase in neutral axis depth at Section 2-2, once the diagonal cracking propagated into the CIP slab. Strain distributions across the depth for various specimens are plotted in Figs. 4.19 to 4.24.

In the case of Specimens 1-4 with 18 strands, when load was applied, flexural cracks initiated at mid-span of the deck after the load exceeded the flexural cracking load of the precast panel. As the load increased further, these cracks propagated throughout the entire thickness of the precast panel and further across the interface into the cast-in-place slab without progressing along the interface. This suggests that at this load level the slab was behaving as a composite member. As the loading increased further, flexural cracks were observed at places away from the mid-span. These cracks propagated vertically for sometime as flexural cracks and later propagated

diagonally as diagonal tension cracks towards the loading point. As the load increased, a number of diagonal cracks were observed. Near the ultimate load the diagonal cracks started to propagate along the interface. As expected these interface cracks appeared in the region away from the compressive flow of the concentrated loads (under the point load and supports). These cracks propagated towards the ends of the panel until they met the compressive flow region of the support reaction and when they encountered this region they started propagating towards the support reaction point. This indicates that entire span length is not effective in resisting the horizontal shear between the precast panel and the cast-in-place slab. These specimens failed in shear failure mode. There was not significant slip at the interface until near the ultimate load on the specimen. At the ultimate load where the panel failed in diagonal tension failure or shear failure, there was a sudden noticeable slip at the interface.

In Specimens 5 and 6 with 12 strands, when load was applied, flexural cracks initiated at mid-span of the deck after the load exceeded the flexural cracking load of the precast panel. As the load increased further, cracks propagated throughout the entire thickness of the precast panel and further across the interface into the cast-in-place slab without progressing along the interface. This suggests that at this load level the slab was behaving as a composite member. As the loading increased further, flexural cracks were observed at places away from the mid-span. These new cracks were confined to 1.5 ft on either side of the mid-span. These cracks propagated vertically and towards the loading point. There was not much diagonal cracking observed until near the ultimate capacity of the specimen. As the load increased further, there was a significant increase in deflection for small load increments suggesting a ductile failure. At loads approaching failure, a new crack emanated from one of the pre-existing cracks and started propagating

downwards towards the interface. This crack was similar to the crack that initiated failure in the first four specimens. Before it could reach the interface the specimen failed in flexural mode leading to excessive deflection. Interface slip was not significant even at the ultimate load.

4.3.1 Interface Slip

As mentioned above, interface slips were not observed until load levels approaching ultimate capacity in the case of Specimens 1-4. Interface slip was not observed even at the ultimate load levels in the case of Specimens 5 and 6 with 12 strands. In the case of the Specimens 1-4, at ultimate loads, interface slip occurred in the critical region, between d , effective depth of slab, away from the loading point and the support reactions.

4.3.1.1 Specimen 1 - Panel with 18 strands and without any shear connectors

In this panel, interface slip occurred suddenly just at the ultimate load. Just before failure, interface slip of the order of 0.002 in. was observed. But immediately after failure, the interface slip measured to 0.1 in. Load versus interface slips are plotted in Fig. 4.25.

4.3.1.2 Specimen 2 - Panel with 18 strands and with four shear connectors

In this case, slip gage readings deviated from the initial no slip behavior at about 100 kips. At this point a crack crossed between the fixed ends of the slip gage. Hence in this case slip gage must have been recording the crack width rather than the interface slip. This was verified by readings obtained from a different slip gage located at the opposite side of the specimen. Load versus interface slips are plotted in Fig. 4.26.

4.3.1.3 Specimen 3 - Panel with 18 strands and with four shear connectors

There was not significant slip at the interface in this panel even at the ultimate load levels. Interface slips of the order of 0.001 were observed at the ultimate load. These slip gage readings suggest that the specimen was behaving as a composite deck even at the ultimate load levels. Load versus interface slips are plotted in Fig. 4.27.

4.3.1.4 Specimen 4 - Panel with 18 strands and with Lubricated Interface

In this specimen, the entire interface between the precast panel and the cast-in-place topping slab was lubricated with form oil. Interface slips of the order of 0.01 in. were observed at the ultimate load levels. At ultimate load, there was splitting along the interface for about 6 inches. This splitting occurred in the critical slip region mentioned earlier. Top of the splitting surface was smooth and in fact the prestressed panel separated from the cast-in-place topping slab over those 6 in. along the entire width of the specimen (see Fig. 4.105). All this was observed only immediately after the failure of the specimen in beam-shear mode. This splitting was not observed before the failure of the specimen. Load versus interface slips are plotted in Fig. 4.28.

4.3.1.5 Specimen 5 - Panel with 12 strands and without any shear connectors

Interface slip of the order of 0.0008 was observed at the ultimate load levels. This specimen failed in a ductile flexural mode. From the above value of interface slip, we could conclude that this specimen behaved as a composite deck slab throughout the entire range of loading life. Load versus interface slips are plotted in Fig. 4.29.

4.3.1.6 Specimen 6 - Panel with 12 strands and with four shear connectors

In this specimen interface slip of the order of 0.0008 in. was observed at ultimate load levels. The specimen failed in a ductile flexural mode. Composite behavior was observed over the entire loading cycle. Load versus interface slips are plotted in Fig. 4.30.

4.4 Load versus Deflection Characteristics

Load versus mid-span deflection of the specimens roughly showed a tri-linear behavior. As the load increased, deflection at mid-span also increased linearly with the applied load conforming to the uncracked section stiffness. As the load increased further and reached flexural cracking load of the precast panel, there was a slight reduction in the slope of the linear behavior that was observed thereafter. This linear behavior of the deflection with the applied load corresponded to that of cracked stiffness of the composite deck slab. As the load further increased, deviation from the linear behavior between the load and deflection was observed. This indicates a change in the stiffness of the deck slab. Deflection varied from there on with a very mild slope (very large increase in deflection was observed for relatively small increments in load) until the LVDTs were removed due to excessive deflections of the deck slab near its ultimate capacity. Load versus deflection characteristics of all specimens are plotted until the loads at which LVDTs were removed. The actual failure loads are listed in Table 4.8.

4.4.1 Specimen 1 - Panel with 18 strands and without any shear connectors

In this specimen, deflection varied linearly up to 60 kips corresponding to the flexural tensile capacity of the precast panel. This indicates the end of Stage 1 in which the deck was

behaving as an uncracked specimen. Once cracking of the specimen occurred, there was a reduction in the stiffness of the deck slab. In this Stage 2, deflection varied roughly in a linear fashion with increasing load. As the load reached 110 kips, there was a sudden increase in deflection for relatively small increments in load. This terminated the Stage 2. From this point onwards, deflection increased quite rapidly with the load and the LVDTs were removed before the ultimate failure of the specimen to prevent damage to the instrumentation due to the excessive observed deflections. The final deflection recorded by the LVDTs was 0.4 inches. Load versus deflection characteristics are shown in Fig. 4.31.

4.4.2 Specimen 2 - Panel with 18 strands and with four shear connectors

In this specimen, deflection varied linearly up to 65 kips corresponding to the flexural cracking capacity of the precast panel. This indicates the end of Stage 1 in which the deck was behaving as an uncracked specimen. This specimen showed slight non-linear behavior between 65 kips and 85 kips. A close look at the load versus strain in the various prestressing strands indicated that there was sudden increase in strain in the strands located at the middle of the panel. This indicates that the specimen should have cracked in the middle of the panel at the mid-span. Cracks were observed on the sides of the specimen only after the load level reached about 85 kips. Hence 65 kips was taken as the cracking load. This crack must have initiated in the panel underside and eventually propagated to the sides of the specimen where it could be visually detected. This also explains slight non-linear behavior of the specimen between 65 kips and 85 kips. As the load increased further, deflection varied linearly with the applied load up to about 140 kips. This was the end of Stage 2. After this load level, deflection increased at a relatively

rapid rate and deflection LVDTs were removed at a load level of about 160 kips. Ultimate failure of the specimen occurred in beam-shear mode at 170 kips and the maximum deflection noted by LVDTs before they were removed was of the order of 1.0 inch. Load versus deflection characteristics are shown in Fig. 4.32.

4.4.3 Specimen 3 - Panel with 18 strands and with four shear connectors

In this specimen, deflection varied linearly up to 75 kips corresponding to the flexural tensile capacity of the precast panel. This indicates the end of Stage 1 in which the deck was behaving as an uncracked specimen. This specimen showed slight non-linear behavior between 75 kips and 100 kips. A close look at the load versus strain in the various prestressing strands indicated that there was sudden increase in strain in the strands located near the middle of the panel. This indicates that the specimen should have cracked in the middle of the panel at the mid-span same as in the case of Specimen 2. Cracks were observed on the sides of the specimen at about 90 kips. Hence 75 kips was taken as the cracking load and this also explains slight non-linear behavior of the specimen between 65 kips and 85 kips. As the load increased further, deflection varied linearly with the applied load until 180 kips. This was the end of Stage 2. At this load, LVDTs were removed and the load was increased until failure. Failure of the specimen in beam-shear mode, occurred at 200 kips and the maximum deflection recorded by the LVDTs before removal was about 0.4 inches. Stage 3 was not observed in this specimen probably because LVDTs were removed before it reached that load level. Load versus deflection characteristics are shown in Fig. 4.33.

4.4.4 Specimen 4 - Panel with 18 strands and with Lubricated Interface

In this specimen, deflection varied linearly up to 65 kips at which the tensile capacity of the precast panel reached. This indicates the end of Stage 1 with the deck was behaving as an uncracked specimen. This specimen showed slight non-linear behavior between 65 kips and 90 kips. A close look at the load versus strain in the various prestressing strands indicated that there was sudden increase in strain in the strands located at the middle of the panel. This indicates that the specimen should have cracked in the middle of the panel at the mid-span. Cracks were observed on the sides of the specimen at about 85 kips. Hence 65 kips was taken as the cracking load and this also explains slight non-linear behavior of the specimen between 65 kips and 85 kips. As the load increased further, deflection varied linearly with the applied load until 170 kips. This was the end of Stage 2. As the load increased further, large deflection increments were observed for small increments in load. At this load level, LVDTs were removed and the load was increased up to failure. Failure of the specimen in beam-shear mode, occurred at 180 kips and the maximum deflection noted by LVDTs before they were removed was about 0.55 inches. Load versus deflection characteristics are shown in Fig. 4.34.

4.4.5 Specimen 5 - Panel with 12 strands and without any shear connectors

In this specimen, deflection varied linearly up to 47.5 kips corresponding to first flexural cracking of the precast panel. This indicates the end of Stage 1 with the deck behaving as an uncracked specimen. This specimen showed slight non-linear behavior between 47.5 kips and 75 kips. A close look at the load versus strain in the various prestressing strands indicated that there was sudden increase in strain in the strands located at the middle of the panel. Cracks were

observed on the sides of the specimen at about 75 kips. Hence 47.5 kips was taken as the cracking load and this also explains slight non-linear behavior of the specimen between 47.5 kips and 75 kips. As the load increased further, deflection varied linearly with the applied load up to 120 kips. This was the end of Stage 2. As the load increased further, large deflection increments were observed for small increments in load. At this load, LVDTs were removed and the load was increased up to failure. Failure occurred in ductile flexural mode at 130 kips and the maximum deflection noted was about 2.0 inches. Load versus deflection characteristics are shown in Fig. 4.35.

4.4.6 Specimen 6 - Panel with 12 strands and with four shear connectors

In this specimen, deflection varied linearly up to 50 kips corresponding to the flexural tensile capacity of the precast panel. This indicates the end of Stage 1 with the deck behaving as an uncracked specimen. This specimen also showed slight non-linear behavior between 50 kips and 75 kips. Cracks were observed on the sides of the specimen at about 75 kips. Hence 50 kips was taken as the cracking load and this also explains the slight non-linear behavior of the specimen between 50 kips and 75 kips. As the load increased further, deflection varied linearly with the applied load up to 120 kips. This was the end of Stage 2. As the load increased further, large deflection increments were observed for small increments in load. After the end of Stage 2 slight non-linear behavior was observed up to a load level of 135 kips with large increments in deflection. At this load, LVDTs were removed and the load was increased to failure. Failure of the specimen in ductile flexural mode, occurred at 140 kips and the maximum deflection noted was about 1.8 inches. Load versus deflection characteristics are given in Fig. 4.36.

Comparison of load versus deflection characteristics of various specimens was also made and load versus deflection characteristics are shown in Fig. 4.37. Specimen 3 and Specimen 4 showed higher stiffness than the other four specimens and deviated at an early stage from the other four plots. This was due to the lower prestress loss in these two specimens compared to Specimens 1 and 2.

4.5 Load versus Strand Strain Results

Before casting of the precast panels, the strands were pretensioned to a load of 3 kips at which point strain gages were placed on the strands. They were then pretensioned to an extra 14.2 kips (total = 17.2 kips) which corresponds to the maximum prestressing limit ($0.75 f_{pu} = 202.5$ ksi). Strain gages at this point of time recorded a reading of $5800 \mu\epsilon$ corresponding to a force of 14.2 kips. After detensioning of the strands, there was an initial loss in the prestress. The average immediate prestress loss was about $200 \mu\epsilon$ (equivalent prestress force loss = $E_s A_s (200 \mu\epsilon) = 0.485$ kips) . In the following graphs, this initial strain along with other prestress losses was deducted to show the effect of applied load only.

4.5.1 Specimen 1 - Panel with 18 strands and without any shear connectors

Load versus strand strains are plotted for some specified strands. Strains in the strands increased linearly up to cracking load (60 kips) at which the bottom fiber of the precast panel cracked and the load was transferred to the strand. At this point there was a change in the stiffness of the slab and thus there was a change in the slope of the load versus strain plot. This behavior can be observed from the readings that were obtained from strain gages located at the

center of the strands 10, 13 and 17 and designated as C10, C13 and C17 respectively in Figure 3.8. As the load increased further, strains varied linearly until the load reached 110 kips at which some of the strands began to slip. After this load, strain in the strands underwent large increases for small changes in load. The strain at 110 kips was about $1500 \mu\epsilon$ and maximum strain at failure was about $4000 \mu\epsilon$ (Strain in the strand at zero live load i.e strain due to pretension is not included). This strain along with initial prestress, approximately $9600 \mu\epsilon$, corresponds to an ultimate stress of 248 ksi in the strands. Load versus strains in the prestressing strands, due to superimposed loading only, at corresponding gage locations are shown in Figs. 4.38 to 4.40.

4.5.2 Specimen 2 - Panel with 18 strands and with four shear connectors

Load versus strand strains are plotted for some specified strands. Strains in the strands increased linearly up to cracking load. In this case though the first crack might have appeared in the middle of the mid-span at 65 kips, this crack did not appear over the entire width of the mid-span. Consequently, load versus average strand strain plot did not show a significant deviation from the original slope until 85 kips at which cracks appeared on the sides at mid-span. Between 60 kips and 85 kips, cracks started propagating over the entire width of the specimen. This can be observed clearly from the load versus average strand strain characteristics of the panel shown in Fig. 4.41, obtained from the readings from the monotonic test conducted after 500,000 cycles of repeated loading. Same conclusion can be drawn from the two plots of the strain distributions across the depth of the specimen with 0.75 times average strand strain being considered as the strain at the mid-height of the precast panel in one case and average strain obtained from the surface gages located at mid-height of the precast panel in the other. In the

case where 0.75 times average strand strain was considered as mid-height precast panel strain, strain distribution across the depth was not linear after 60 kips.

Once cracking along the face of the specimen at midspan section started, the stresses were transferred to the strands at this section. Thus there was an increase in the strand strains causing the strain distribution across the depth to be a distorted one. In the other case where average strain obtained from the surface gages located at the mid-height of the precast panel was used, the strain distribution across the depth of the specimen was linear indicating that concrete has not cracked at the sides of the specimen. Hence at a load of 85 kips there was a change in the stiffness of the slab and thus there was a change in the slope of the load versus strain plot. This behavior can be observed from the readings that were obtained from strain gages located at the center of the strands 2, 6 and 9 and designated as C2, C6 and C9 respectively. As the load increased further, strains varied linearly until the load reached 140 kips. After this load, strain in the strands started to undergo large changes for small changes in load. The average strain at 140 kips was about 3100 $\mu\epsilon$, and average maximum strain due to superimpose loading only, at failure was about 3600 $\mu\epsilon$. This strain along with initial pretension, corresponds to an ultimate stress of 240 ksi in the strands. This can be observed in the plots shown in Figs. 4.42 to 4.44.

4.5.3 Specimen 3 - Panel with 18 strands and with four shear connectors

Load versus strand strains were plotted for some specified strands. Strains in the strands increased linearly until the cracking load (75 kips) at which the bottom fiber of the precast panel cracked and the load was transferred to the strand. At this point there was a change in the stiffness of the slab and thus there was a change in the slope of the load versus strain plot. As

mentioned earlier in the load versus deflection characteristics of this specimen, cracks did not appear on the sides of the specimen until 90 kips. Between 75 kips and 90 kips, cracks started propagating over the entire width of the specimen. This can be observed clearly from the load versus average strand strain characteristics of the panel as shown in Fig. 4.45, which was obtained from the readings obtained from the monotonic test conducted after 500,000 cycles of repeated loading. As the load increased further, cracks propagated over the entire width of the specimen at about 100 kips and there was a sudden increase in the strand strain at this load. As the load increased further, strains increased non-linearly with the load up to 180 kips. At this load the average strain in the strands was about 4700 $\mu\epsilon$. As the load increased further, there was a sudden increase in the strand strains for small increments in load. This behavior was observed in all the strands. The ultimate strand strain at the time of failure was of the order of 8000 $\mu\epsilon$. Load versus strains at corresponding gage locations are plotted in Figs. 4.46 and 4.47.

4.5.4 Specimen 4 - Panel with 18 strands and with Lubricated Interface

Load versus strand strains were plotted for some of the strands. Strains in the strands increased linearly up to cracking load (65 kips). At this point there was a change in the stiffness of the slab and thus there was a change in the slope of the load versus strain graph. As mentioned earlier in the load versus deflection characteristics of this specimen, cracks did not appear on the sides of the specimen up to 90 kips and at this load level cracks propagated over the entire width of the specimen with a sudden increase in the strand strain. Between 65 kips and 90 kips, cracks started propagating over the entire width of the specimen. This can be observed from the non-linear behavior of load versus the average strain plot between those two load limits

as shown in Fig. 4.48. This graph was obtained from the monotonic test conducted after 600,000 cycles of repeated loading. As the load further increased, strains increased non-linearly with the load up to 170 kips. At this load the average strain in the strands was about 4000 $\mu\epsilon$. As the load increased further, there was a sudden increase in the strand strains for small increments in load. This behavior was observed in all the strands. The ultimate strand strain at the time of failure was of the order of 8000 $\mu\epsilon$. Load versus strains at selected gage locations are shown in Fig. 4.49.

4.5.5 Specimen 5 - Panel with 12 strands and without shear connectors

The cracking load for this panel was 47.5 kips. Strain in the strands increased linearly up to cracking load with the stiffness corresponding to that of an uncracked deck slab. Cracks were not observed on the sides of the panel at this load. There was a change in the stiffness of the deck slab at this load level. As the load increased further, cracks started propagating along the width of the panel at mid-span. Cracks were observed on the sides of the panel at about 70 kips. Strain varied linearly between 47.5 kips and 75 kips. There was a change in the stiffness of the deck slab at this load level too. After this load level, strain in the strands started to increase at a relatively rapid pace. This behavior was observed until 120 kips load level. Behavior of these strand strains was approximately linear between 75 kips and 120 kips. At this load level, the average strain in the strands was 4000 $\mu\epsilon$. After this load level, strains in the strands increased considerably with small increments in load. The load at which the failure of this specimen occurred in a ductile flexural mode was 130 kips. Total ultimate strain obtained from the strain gages at this load level was of the order of 12000 $\mu\epsilon$. Load versus strand strain results are shown in Figs. 4.50 and 4.51.

4.5.6 Specimen 6 - Panel with 12 strands and with four shear connectors

The cracking load for this panel was 50 kips. Strains in the strands increased linearly up to cracking load with the stiffness corresponding to that of an uncracked deck slab. Cracks were not observed on the sides of the panel at this load. There was a change in the stiffness of the deck slab at this load level. As the load increased further, cracks started propagating along the width of the panel at mid-span. Cracks were observed on the sides of the panel at about 75 kips. Strains varied linearly between 50 kips and 75 kips. There was a change in the stiffness of the deck slab at 75 kips too. Beyond this load level, strain in the strands started to increase at a relatively rapid pace. This behavior was observed up to 120 kips. The strand strains varied in a non-linear fashion between 75 kips and 120 kips. At this load level, the average strain in the strands was 6000 $\mu\epsilon$. Beyond this load level, strains in the strands showed large increases for small increments in load. Ultimate load at which the failure of this specimen occurred in a ductile flexural mode was 140 kips. Total ultimate strain obtained from the strain gages at this load level was of the order of 16000 $\mu\epsilon$. Load versus strand strain results are shown in Figs. 4.52 to 4.54.

4.6 Load versus Concrete Strain Results

Strain gages were placed on the concrete deck slab at various locations. In this section, the behavior recorded by the strain gages placed at the strand level, on the sides of the specimens but in the cast-in-place slab, and on the top surface of topping slab are discussed. In the specimens where interface gages were placed on top of the precast panel, the behavior of these gages is also discussed.

4.6.1 Load versus Concrete Strain at Strand Level

In the case of Specimen 1, the average strain at the strand level increased linearly with the applied load up to a load level of 110 kips. After this load level, strain gages showed a decrease in their strain values due to the cracks that appeared in the near vicinity of these gages. When a crack forms or when it progresses, some amount of strain energy stored in the specimen will be released from the crack tip vicinity. Due to this release in energy there will be a drop in the strain of the concrete in the vicinity of crack. Load versus concrete strain at strand level are shown in Fig. 4.55.

In the case of Specimen 2, the average strain at the strand level increased linearly up to 80 kips and from there on, behavior of these gages was non-linear up to 110 kips. Again as in Specimen 1, these gages showed a decrease in their strain value. Load versus strain at strand level is shown in Fig. 4.56.

In Specimen 3, a behavior similar to that observed in the two previous panels was recorded. In the case of strain gage located on the north-west side (PC-NW), strain increased almost linearly up to a load level of 100 kips and it started to drop off after a load level of 110 kips. But in the case of strain gage located on north-east side (PC-NE), strain increased linearly up to 100 kips and there was slight decrease in strain at 110 kips and an increase after 130 kips. The increase in strain after 130 kips was sudden and large, up to 2000 $\mu\epsilon$. Load versus strain at strand level is shown in Fig. 4.57.

In Specimen 4, similar behavior was observed. Strains increased linearly up to 100 kips and then dropped off after 110 kips. This behavior was observed in all the four gages that were placed on the sides of the panel. In all the gages a drop off in the strain occurred at about

215 $\mu\epsilon$. This strain corresponds to flexural cracking of the panel indicating that a crack appeared in the vicinity of the gage. This was the same amount of strain observed in all the previous panels also corresponding to a load (110 kips) at which drop off occurred. Load versus strain at strand level is shown in Fig. 4.58.

In Specimen 5, strains increased linearly up to a load level of 70 kips. In the case of strain gage located on the north-east side (PC-NE), the strain increased suddenly after a load level of 80 kips. Similar behavior was observed in PC-SW (strain gage located on south-west side). In the case of strain gages located on north-west side (PC-NW), this increase occurred at 70 kips. After this sudden increase strain readings dropped off. This was observed in all the four gages. Load versus strain at strand level is shown in Fig. 4.59.

In Specimen 6 similar performance to that observed in Specimen 5. In these last two specimens strains dropped off at a load level of 80 kips corresponding to an average strain level of around 400 $\mu\epsilon$ in Specimen 5, and 120 $\mu\epsilon$ in Specimen 6. This value is different from the value shown in the Fig. 4.60 because it represents the average value obtained from all the gages located at strand level. Load versus strain at strand level characteristics are shown in Fig. 4.60.

From the above results it is clear that cracks were initiated or propagated in the vicinity of gages at about a strain level of 220 $\mu\epsilon$. These strain levels corresponded to different load levels depending upon the total number of the strands in the panels.

4.6.2 Load versus Strain at 5 in. from the Top of CIP Slab

In Specimen 1, strain increased linearly with the load up to 110 kips. After this load level there was a decrease in the strain due to cracks in the vicinity of the strain gages. The magnitude of average strain obtained before they dropped off was about 140 $\mu\epsilon$. Load versus strain at CIP gage level for this specimen is plotted in Fig. 4.61.

In Specimen 2, similar behavior was observed. Strains increased linearly up to a load level of 80 kips. Strain was non-linear between 80 kips and 110 kips. Strains dropped off at a load level of 110 kips. The average maximum strain noted before was again about 90 $\mu\epsilon$. Load versus strain at CIP gage level for this specimen is plotted in Fig. 4.62.

In Specimen 3, almost the same behavior was observed. Strains increased linearly up to a load of 110 kips. In the case of strain gage located on north-east side (CIP-NE), strains dropped off after a load level of 130 kips. In the case of CIP-NW, strain increased suddenly to about 4000 $\mu\epsilon$ immediately after 130 kips. In CIP-SE, strain dropped slightly after a load level of 110 kips and increased after a load level of 140 kips to about 400 $\mu\epsilon$. Similar behavior was observed in CIP-SW. The strain recorded at 110 kips was about 105 $\mu\epsilon$. Load versus strain at CIP gage level for this specimen is plotted in Fig. 4.63.

In Specimen 4, where the interface was lubricated, similar behavior was observed. Strains increased approximately linearly until a load level of 110 kips. At this load level the corresponding strain gage reading was about 110 $\mu\epsilon$. As the load increased further, there was a slight decrease in strain and at about 140 kips there was a sudden increase in strain. The strain gage located on north-east side (CIP-NE) recorded a value of 1000 $\mu\epsilon$. Load versus strain at CIP gage level for this specimen is given in Fig. 4.64.

In Specimen 5, the strain increased linearly with the applied load up to a load level of 80 kips. Strain recorded at this load level was about $115\ \mu\epsilon$. At this point strain decreased suddenly with the applied load indicating a crack propagation in the vicinity of gage. Only in the case of CIP-NE gage, strain increased suddenly after 80 kips. A crack propagated right through the location of the gage at about 90 kips. Load versus strain at CIP gage level for this specimen is plotted in Fig. 4.65. Similar behavior to that of Specimen 5 was observed in Specimen 6. Load versus strain at CIP gage level for Specimen 6 is shown in Fig. 4.66.

4.6.3 Load versus Strain at top of CIP Slab

In Specimen 1, strain at the top of CIP increased linearly up to 60 kips. The strain recorded at this load level was about $200\ \mu\epsilon$. As the load increased further, there was not appreciable change in the slope of the load versus strain plot. Strains increased with almost the same slope (stiffness) up to 110 kips. At this load level, strain gages recorded an average strain of about $400\ \mu\epsilon$. There was a sudden increase in the strain at this load level. Strains continued to increase in a non-linear fashion beyond this load level. This behavior was observed up to a load level of 130 kips at which point the strain recorded was about $950\ \mu\epsilon$. Loading of this specimen was stopped at this load level and the specimen was unloaded because it was thought that further loading of the specimen might make the stresses in the anchoring bolts of the frame exceed their yield capacity. After repairs to the frame were completed it was decided to reload the specimen up to its failure. Specimen 1 failed at a load level of 160 kips. But strain readings were plotted only up to 130 kips because the initial loading was found to have a significant influence on the amount of strain observed. Load versus strain at the top of CIP slab readings,

for this specimen, are shown in Figs. 4.67 and 4.68.

In Specimen 2, almost linear behavior was observed up to a load of 80 kips. Strain gages recorded a value of 350 $\mu\epsilon$ at this load level. As the load increased further, slight non-linear behavior was observed based on strain readings. There was a sudden increase in strain at about 110 kips. Non-linear behavior of strain continued up to a load of 150 kips. At this load level, the average strain was about 1000 $\mu\epsilon$. As the load further increased, strain started to increase at a rapid pace for very small increments in load. Ultimate failure of the specimen occurred at 170 kips. Strain recorded at ultimate load was about 2600 $\mu\epsilon$. Load versus strain at the top of CIP slab readings are shown in Figs. 4.69 to 4.71.

In Specimen 3, strains increased approximately in a linear fashion up to a load level of 100 kips. Strain recorded at this load level was about 300 $\mu\epsilon$. As the load increased further, strains increased non-linearly up to a load of 180 kips. Strain recorded at this load was about 1400 $\mu\epsilon$. As the load increased, strains increased at a rapid pace and the failure of the specimen occurred at a load level of 200 kips. Failure occurred on the south side and the strain recorded by gages located on this side was about 3000 $\mu\epsilon$. Gages located on the north side recorded about 2200 $\mu\epsilon$ at this load level. Load versus strain readings at the top of CIP slab are shown in Figs. 4.72 and 4.73.

In Specimen 4, strains increased linearly up to a load of 100 kips. At this load level, strain recorded was about 350 $\mu\epsilon$. As the load increased further, strain increased non-linearly. This behavior continued up to a load level of 170 kips with a corresponding strain of about 1050 $\mu\epsilon$. After this stage, strains increased at a rapid pace and at failure, which occurred at 180 kips, strain gages recorded a value of about 1600 $\mu\epsilon$. Failure of the specimen occurred on the north side.

Load versus strain readings at the top of CIP slab, are shown in Figs. 4.74 and 4.75.

In Specimen 5, strains increased almost linearly with the applied load up to 80 kips. Strain in the concrete was about 350 $\mu\epsilon$. Further increase in load caused a sudden increase in strain at 80 kips. Strain increased non-linearly with the applied load up to a load of 120 kips. The average strain recorded on the north side of the specimen at this load level was about 1500 $\mu\epsilon$. On the south side of the specimen the recorded strain was about 1200 $\mu\epsilon$. Strain increased rapidly with further increase in load and the ultimate failure of the specimen occurred at a load level of 130 kips on the north side. At this stage, the ultimate strain recorded by the gages located on the north side was above 3000 $\mu\epsilon$ and the average strain recorded was about 3400 $\mu\epsilon$. Strain recorded by the gages located on the south side of the panel was above 2500 $\mu\epsilon$ and the average of these gage readings was around 2700 $\mu\epsilon$. Failure of the specimen occurred in flexural mode on the north side. Load versus strain at the top of CIP slab are shown in Figs. 4.76 and 4.77.

In Specimen 6, strain increased almost linearly up to a load level of 80 kips. Strain recorded at this load was about 350 $\mu\epsilon$. Further increase in load caused the strains to increase non-linearly up to a load level of 115 kips. Average strain recorded by gages at this load level was about 1000 $\mu\epsilon$. Failure of the specimen occurred at 140 kips. Average strain recorded at this load level was about 2800 $\mu\epsilon$. Failure occurred on the south-side in flexural mode. Load versus strain at the top of CIP slab are shown in Figs. 4.78 to 4.80.

4.6.4 Load versus Interface Strain Results

Strain gages on the top of the precast panel were provided only in the case of Specimens 3, 4, 5 and 6. The location of these interface gages on top of precast panel are shown in Fig. 3.9.

The behavior of these interface gage readings with respect to load is discussed below.

In Specimen 3, strain increased linearly up to a load level of 100 kips. Strain corresponding to this load level was about 200 $\mu\epsilon$. Further increase in load caused the strain to increase rapidly for relatively small increments in load. At a load level of 120 kips, strain at these locations was about 3000 $\mu\epsilon$. Strain gages were damaged at this load level probably due to cracks propagating right through these gages. Load versus interface strain characteristics were shown in Fig. 4.81.

In Specimen 4, strain increased approximately in a linear fashion up to a load of 100 kips. Strain at this load level was about 100 $\mu\epsilon$. With further increase in load, strain remained the same up to a load of 100 kips. At this load level a sudden increase in strain was observed. In the case of gage #PC2, strain increased suddenly to a value of about 1500 $\mu\epsilon$. In the case of #PC9, strain increased to a value of about 3000 $\mu\epsilon$. In the case of gage #PC17, strain increased to a value of 1500 $\mu\epsilon$. All this just shows that, at a load level of 100 kips there was a sudden increase in strain at the interface and the values of strains observed at these points reflect the propagation of cracks in the vicinity of these gages. In the case of gage #PC9, higher strain was observed because a crack did not appear in its vicinity up to a load level of 130 kips. As soon as the crack appeared at 130 kips, there was a sudden drop in strain and in fact the strain gage was damaged probably due to crack passing through it. Load versus interface strain characteristics are shown in Fig. 4.82.

In Specimen 5, strain increased almost linearly with the applied load up to a load of 70 kips. This can be observed in the first monotonic loading which is shown along with other monotonic loading tests conducted at various levels of cyclic life in Fig. 4.83. This behavior

cannot be observed in the plots for the ultimate monotonic cycle. The reason behind this type of behavior is the opening of the cracks formed in the previous load cycles, at load levels below the load levels of previous cycles. Strain at 70 kips in the first monotonic cycle was noted to be about 120 $\mu\epsilon$. In the ultimate monotonic cycle, strain increased at a very rapid pace at about 70 kips. The final strain value attained by these strain gages was about 2600 $\mu\epsilon$. In some cases where the cracks passed through the vicinity of the gages, strain readings dropped off at an earlier load stage.

In Specimen 6, a behavior similar to that of Specimen 5 was observed. Strain at a load level of 70 kips was about 125 $\mu\epsilon$. After this load level, strain at the interface increased at a rapid pace. Most of the strain gages showed a decrease in strain probably due to the propagation of cracks in their vicinity. Load versus interface strain characteristics are shown in Figs. 4.84 and 4.85.

4.6.5 Load versus CIP Reinforcement Strain Results

Strain gages were placed on CIP re-bars only in Specimens 3, 4, 5 and 6. The behavior of these gages with the applied load is discussed next.

In Specimen 3, strains did not show significant deviation from the initial value until a load level of about 120 kips. Further increase in load caused an increase in the strain in a non-linear fashion. Strain in the monitored CIP bars increased with increasing load up to a load of 180 kips. The average strain in the CIP bars at this load level was about 1000 $\mu\epsilon$. At this load level, further increase in load caused strains to increase rapidly. Failure of the specimen occurred at a load level of 200 kips. The average strain recorded in the gages placed was about 3250 $\mu\epsilon$. The

maximum strain attained in these bars on the south side was 4000 $\mu\epsilon$. The average strain recorded in the gages placed on the north-side was about 2000 $\mu\epsilon$. The maximum strain that the gages on the north-side recorded was about 2200 $\mu\epsilon$. Failure of the specimen occurred on the south-side. Load versus CIP bar strain results are shown in Figs. 4.86 and 4.87.

In Specimen 4, initially, CIP bars were in compression. The compressive strains increased at a very slow rate up to a load of 110 kips. Strain in the bars at this load level was about -50 $\mu\epsilon$. Further increase in load caused the strains to change from compressive to tensile at a load of 130 kips. Further increase in load caused substantial increase in strain in these bars and this behavior continued up to a load of 170 kips. The average strain recorded at this load level was about 600 $\mu\epsilon$. Failure of the specimen occurred at a load of 180 kips. The corresponding strain in the bars was about 950 $\mu\epsilon$. Failure of the specimen occurred on the north-side. Load versus CIP bar strain results are shown in Figs. 4.88 and 4.89.

In Specimen 5, initially, CIP bars were in compression. These compressive strains increased at a very slow rate up to a load of 80 kips. The strain recorded at this load level was about -100 $\mu\epsilon$. Further increase in load resulted in tensile strains in the bars as the cracks propagated into the CIP slab. Strain in the bars was zero at a load of 90 kips. With further increase in load, strain varied non-linearly and the specimen failed at a load level of 130 kips. The corresponding strain in the CIP bars was about 3500 $\mu\epsilon$. The maximum strain recorded was about 6000 $\mu\epsilon$. Failure of the specimen occurred in flexural mode. Load versus CIP bar strain are given in Fig. 4.90.

Initially, in Specimen 6, CIP bars were in compression. These compressive strains increased at a very slow rate up to a load of 80 kips. The strain recorded at this load level was

about $-100 \mu\epsilon$. Further increase in load resulted in tensile strains in the bars as the cracks propagated into the CIP slab. Strain in the bars was zero at a load of 90 kips. As the load increased further, strains increased non-linearly up to a load of 130 kips. Average strain recorded at this load was about $2000 \mu\epsilon$. There was a sudden increase in strain with further increase in load. Failure of the specimen occurred at 140 kips. Average strain recorded at this load was about $3500 \mu\epsilon$. Failure of the specimen occurred in flexural mode. Load versus CIP bar strain results are shown in Figs. 4.91 and 4.92.

4.6.6 Behavior of Horizontal Shear Connectors

Specimens 1 and 5 did not contain horizontal shear connectors. All the other specimens contained four shear connectors. The behavior of these shear connectors in transferring the horizontal shear stress across the interface is discussed here.

In Specimen 2, strain in shear connectors did not show significant deviation up to a load of 90 kips. As the load increased further there was an increase in the strain up to $40 \mu\epsilon$. There was no further increase in strain with increase in load, up to a load of 160 kips. As the load increased further, there was a sudden increase in strain with the increasing applied load. Failure of the specimen occurred at 170 kips. Strain corresponding to this load was $200 \mu\epsilon$. This indicates that there was not enough slip at the interface to significantly activate shear reinforcement. This was due to the sudden failure of the specimen in shear at 170 kips rather than the slip aggravating the composite behavior and thereby the strength of the specimen. Load versus strain in the horizontal shear connectors is shown in Fig. 4.93.

In Specimen 3, strain increased almost linearly but at a very slow rate. This behavior was observed up to a load of 180 kips. Strain recorded by the strain gages at this load level was about 40 $\mu\epsilon$. At this load level, there was a sudden increase. Beyond this load level strain started increasing rapidly for small increments in load. Failure of the specimen occurred at a load of 200 kips. At this load level, the maximum strain recorded in shear connector #1 was about 500 $\mu\epsilon$, that recorded in shear connector #2 was about 2000 $\mu\epsilon$ and shear connector #3 recorded a value of 720 $\mu\epsilon$. From the above results, it is clear that the deck slab behaved as a composite member up to failure of the specimen. The resistance offered by shear connectors was insignificant as the failure of the specimen occurred as soon as strains increased rapidly. Load versus strain in the horizontal shear connectors is shown in Fig. 4.94.

In Specimen 4, only one of the four strain gages was not damaged. Strain recorded by this strain gage increased almost linearly up to a load of 50 kips and at this load level there was a sudden increase in strain up to 90 $\mu\epsilon$. Beyond this load level, strain in the shear connector started decreasing. Ultimate failure of the specimen occurred at 180 kips. At the time of failure there was a separation at the interface. Load versus strain in the horizontal shear connectors is shown in Fig. 4.95.

In Specimen 6, there was not any significant change in the strain from its initial value. Ultimate failure of the specimen occurred at 140 kips.

From the above results, it is clear that the horizontal shear stress across the interface can be transferred through the broom finished top surface of the precast panel even in the case of a lubricated interface. This interface roughness is adequate to transfer the needed shear stresses purposely to achieve member strength. Horizontal shear connectors across the interface were not

required to achieve the strength of the specimens in beam-shear or flexure. At the ultimate capacity of the deck slab, just before the failure was imminent, strains in the shear connectors reached their yield capacity in Specimen 3. But the resistance provided was not sufficient to stop the failure of the specimen as the mode of failure was different than that caused by interface slip.

4.7 Crack Patterns

As in most cases of failure, even though the loading was symmetrical, failure of the specimen occurred only on one side of the loading. Thus the crack pattern was not symmetrical. Composite behavior can also be justified by looking at the crack patterns. In this section crack patterns of all the specimens are discussed.

4.7.1 Specimen 1 - Panel with 18 strands and without any shear connectors

This specimen consisted of 18 strands and no shear connectors, cracks originated and propagated vertically into the precast slab as flexure cracks and when they encountered the interface there was no discontinuity in the propagation of these cracks. This suggests that the specimen behaved as a monolithic slab. Near the ultimate load, from the points where these cracks met the interface, new cracks started propagating along the interface. As expected the propagation of these cracks was confined to the region where the interface intersects the compressive flow region. When these interface cracks intercepted the compressive flow region they traversed towards the loading point. Finally at the ultimate load the diagonal tension cracks extended towards the loading point and the failure occurred with crushing of the concrete just near the loading point. This type of crack pattern was observed on both edges of the specimen.

Failure of the specimen occurred on the south-side of the specimen. Crack pattern for Specimen 1 is shown in Fig. 4.96.

4.7.2 Specimen 2 - Panel with 18 strands and with four shear connectors

Similar behavior to that of Specimen 1 was observed. Failure was sudden with the crack extending to the loading point. In this case there was no crushing of the concrete. The specimen failed when diagonal tension crack extended from the bottom fiber to the top most fiber of the cast-in-place concrete without any crushing of the concrete. Failure of the specimen occurred on the north side of the specimen. Crack pattern is shown in Fig. 4.97.

4.7.3 Specimen 3 - Panel with 18 strands and with four shear connectors

The crack patterns were identical to those of Specimen 2. Failure of Specimen 3 occurred on the south side and hence more cracks were observed on this side than the other. This was the only difference between these two specimens regarding the crack patterns. Crack pattern for this specimen can be seen in Fig. 4.98.

4.7.4 Specimen 4 - Panel with 18 strands and with Lubricated Interface

Similar behavior as in the previous three panels was observed in Specimen 4. Crack patterns were symmetrical on either side for most of the loading cycle. Near the ultimate load, cracks were observed more on one side of the loading point than the other. Near the failure load, from the points where these diagonal cracks met the interface, new cracks started propagating along the interface. As mentioned earlier, the propagation of these cracks was confined to the

critical region. At the ultimate load the failure was sudden with the diagonal tension crack extending to the loading point. There was separation of the precast panel from the top CIP slab at the interface in the slip critical region mentioned earlier. In fact, this separation was observed over the entire width of the specimen. Failure of the specimen occurred on the north-side of the specimen. Crack patterns for this specimen are shown in Fig. 4.99.

4.7.5 Specimen 5 - Panel with 12 strands and without shear connectors

Crack patterns were similar to previous panel crack patterns for most part of the loading cycle. Deviation from the previous crack patterns occurred near the ultimate load. As the load increased, cracks originated and propagated vertically into the precast slab as flexural cracks. When they encountered the interface there was no discontinuity in the propagation of these cracks and in fact these cracks propagated vertically right into the CIP slab. Near the ultimate load, a crack at a distance of about 1.5 ft from the center of the span and which originated and propagated earlier to a height of 4 in. from the bottom of the deck, started to propagate diagonally towards the loading point. At the time of failure, there was crushing of the concrete at the loading point and also there was failure of the concrete in compression. At the same time a crack was observed to propagate down towards the interface. Failure of the specimen occurred on the north-side and the failure occurred in flexural mode. Crack pattern for this specimen can be observed in Fig. 4.100.

4.7.6 Specimen 6 - Panel with 12 strands and with four shear connectors

Similar behavior to that of Specimen 5 was observed. Crack pattern was symmetrical on either side of the loading point for most part of the loading cycle. Near the ultimate load, more cracks were observed to emanate from the existing cracks on the south-side of the specimen. Crack pattern and behavior was identical to specimen 5 except that the failure of the specimen occurred on south-side as compared to north-side in specimen 5. Failure of the specimen occurred due to crushing and buckling (local) of the flexural compressive block of concrete. At the time of failure, a crack was observed to propagate down towards the interface. Failure of the specimen occurred in flexural mode. Crack pattern for this specimen can be observed in Fig. 4.101.

4.7.7 Summary of Crack Pattern Observation

From the above crack patterns it is clear that full composite behavior was observed between the precast panel and CIP topping slab up to the failure of Specimens 1-4. For majority of the loading cycle, cracks were symmetrical on either side of the loading point. Deviation from this behavior occurred near the failure load. In the first four specimens where the failure mode was shear, there was noticeable interface crack propagation near ultimate loads. In the Specimens 5 and 6 which failed in flexural mode, interface cracks were not observed.

4.8 Effect of Cyclic Loading on the Behavior of Deck Panels

In this section, effects of cyclic loading on the behavior of deck panels are discussed. In particular, deck panel's stiffness, ductility characteristics of strand steel and the fatigue in the concrete and steel are addressed. During the cyclic loading of the specimen, intermediate static

tests were performed at regular intervals. The behavior of specimens during these intermediate static tests were used to judge the effect of fatigue on various characteristics of the deck panel. In this section, behavior of a typical specimen under cyclic loading is explained.

4.8.1 Cyclic Load versus Stiffness of Deck Panel

Load versus deflection behavior of the specimens is graphed after various number of cycles. In Figs. 4.102 to 4.107, load versus deflection characteristics for each static test conducted at the beginning of the test, and at regular intervals thereafter are shown. From these plots, it can be seen clearly that cyclic loading had negligible effect on the load versus deflection characteristics of specimens and hence on their stiffness.

4.8.2 Cyclic Load versus Strain in the strands

Load versus strain in the strands were plotted for various static tests performed after various number of cycles as shown in Figs. 4.108 and 4.109. From these tests it can be seen that there was not any significant effect of cyclic loading before the specimen cracked. After the cracking of specimen occurred, there was some dispersion of data near the cracking load. This was expected because of the early opening of the pre-existing cracks during the static tests that followed the first cracking load test. In any case the dispersion was not significant to suggest any influence of cyclic loading on the strain in the strands. Strain increased almost linearly over the entire loading cycle. The same overall behavior was observed in all the strands though the amount of strain experienced was different in some. This was due to the fact that cracking occurred at various load levels along the width of the mid-span section. As soon as a crack

forms, stresses are transferred from the concrete to the steel strand at that location. At this point, the strain in the strand located at that cracked section will be more than the strain in the other strands where cracks had not appeared. This explains the different strain values in various strands near the cracking load. These strain values will be the same once the crack has formed over the entire width of the section in question.

4.8.3 Cyclic Load versus Overall Behavior of the Specimen

Strain values at various locations on the specimen were considered to evaluate the overall behavior of the specimen. For each specimen, load versus strain at the top of CIP slab are plotted, (See Figs. 4.110 to 4.115) for each intermediate static test performed. Strain showed a linear variation with the applied load before the cracking of the specimen occurred. There was no significant effect of cyclic load or number of cycles on these strain readings.

Load versus strain at strand level is also plotted in Figs. 4.116 and 4.117, for each intermediate static test performed. Strain varied linearly with the applied load up to the cracking load. There was not any significant effect of cyclic load or number of cycles on these strain readings.

Load versus strain on the sides of the CIP slab at 5 inches below the top of the slab was graphed for each intermediate static test performed. Strain varied approximately in a linear fashion with the applied load and there was not a noticeable effect of cyclic load or number of cycles on these strain readings. The dispersion in the data was about $10\ \mu\epsilon$ which was roughly the sensitivity of the strain gage. This behavior can be observed in Fig. 4.118.

The effect of cyclic loading on interface strain characteristics can be observed in Fig. 4.119. The stiffness of these plots was the same up to cracking of the specimen, and following

cracking there was a noticeable change in the stiffness. In all the monotonic tests performed after cracking the specimen, the same stiffness was observed. This indicates that the effect of cyclic loading was negligible on these strain readings.

4.9 Summary

The results of the experimental program consisting of testing six composite panel specimens have been presented. The following chapter summarizes the results from this study and conclusions and design recommendations are provided.

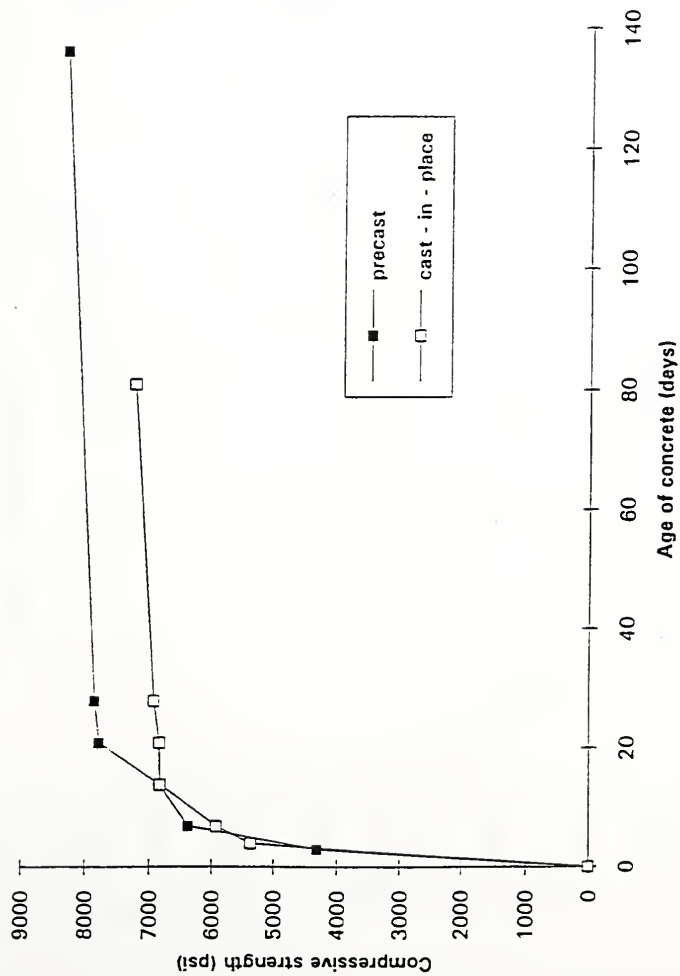


Figure 4.1 Concrete compressive strength versus age of concrete

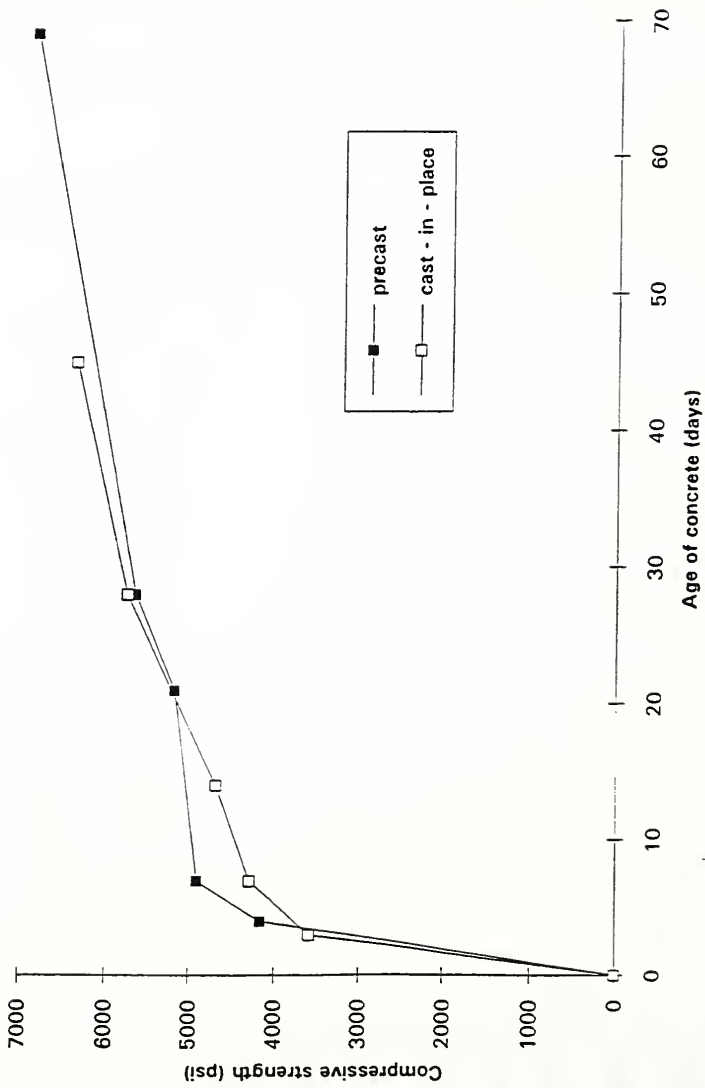


Figure 4.2 Concrete compressive strength versus age of concrete

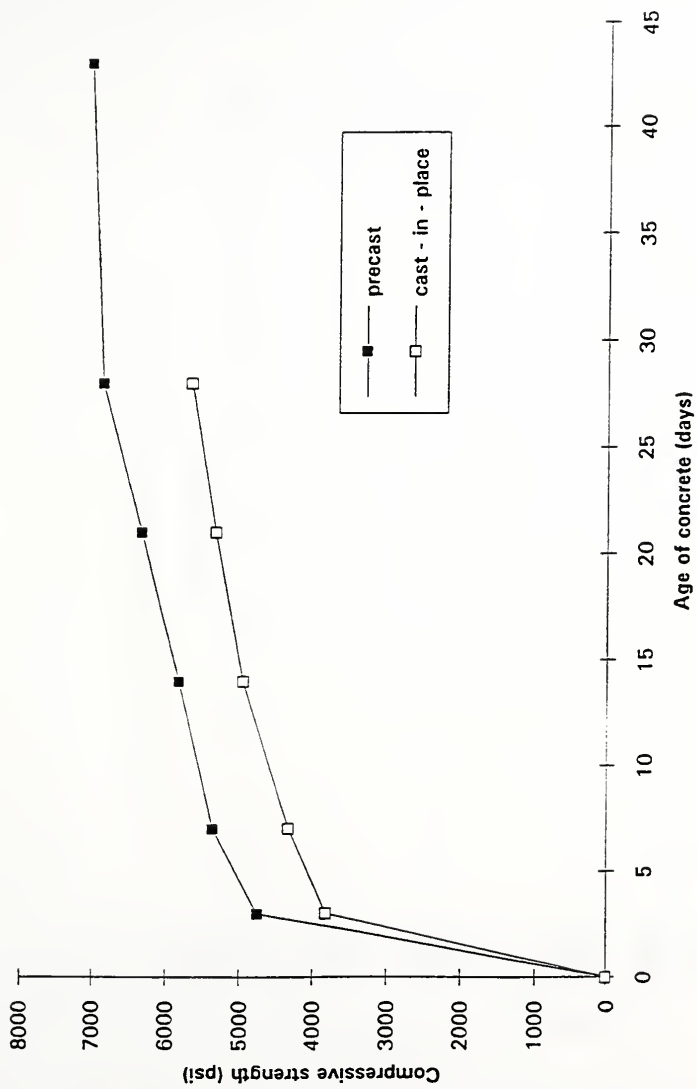


Figure 4.3 Concrete compressive strength versus age of concrete

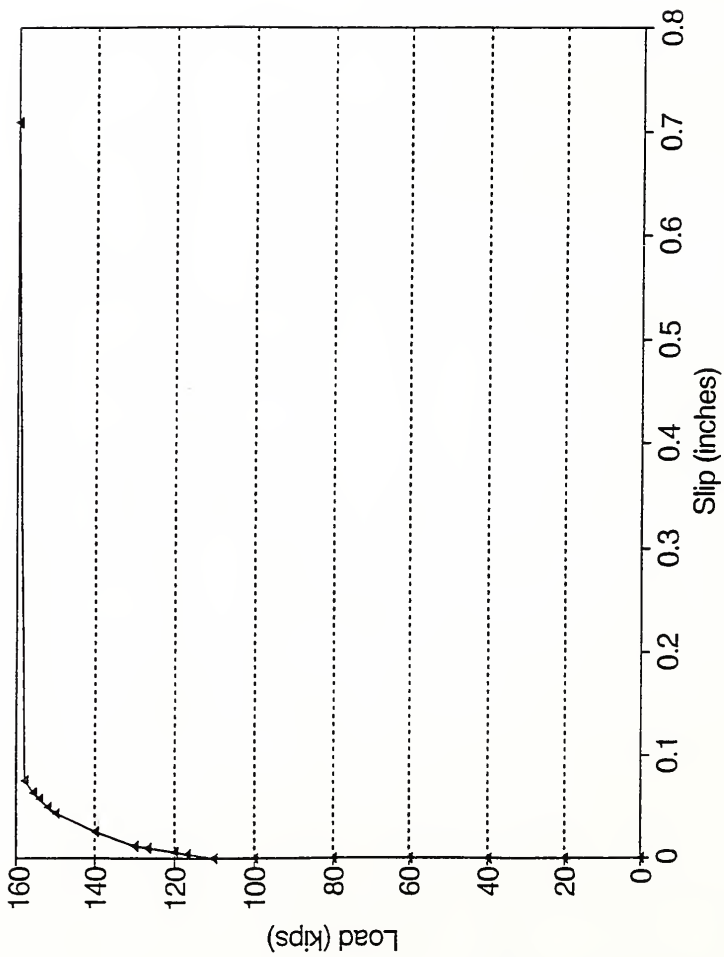


Figure 4.4 Load versus Strand Slip at #S10 of Specimen I

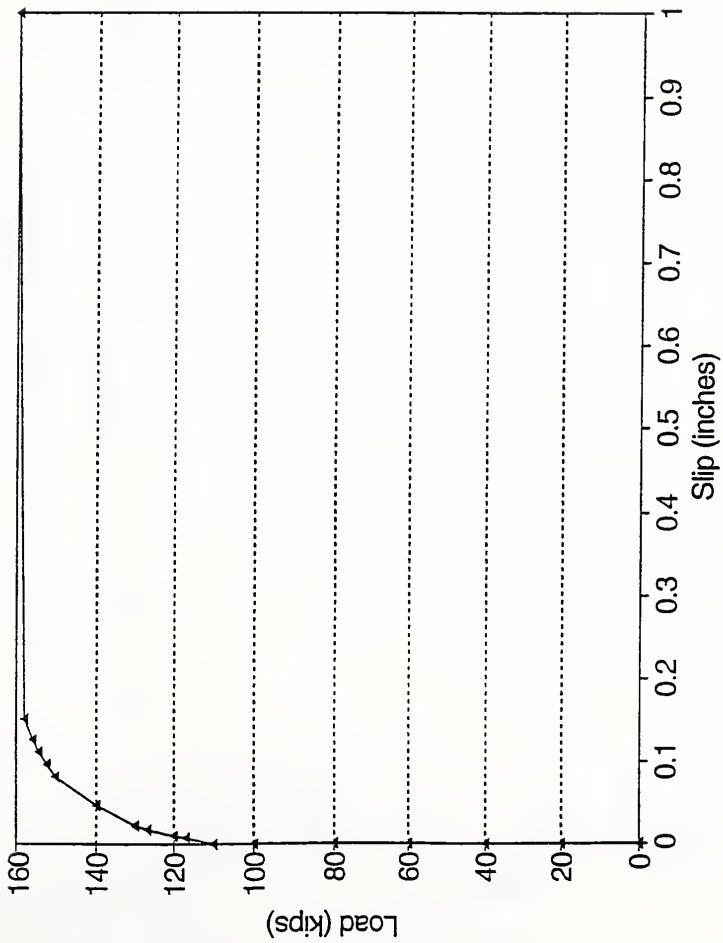


Figure 4.5 Load versus Strand Slip at #S13 of Specimen 1

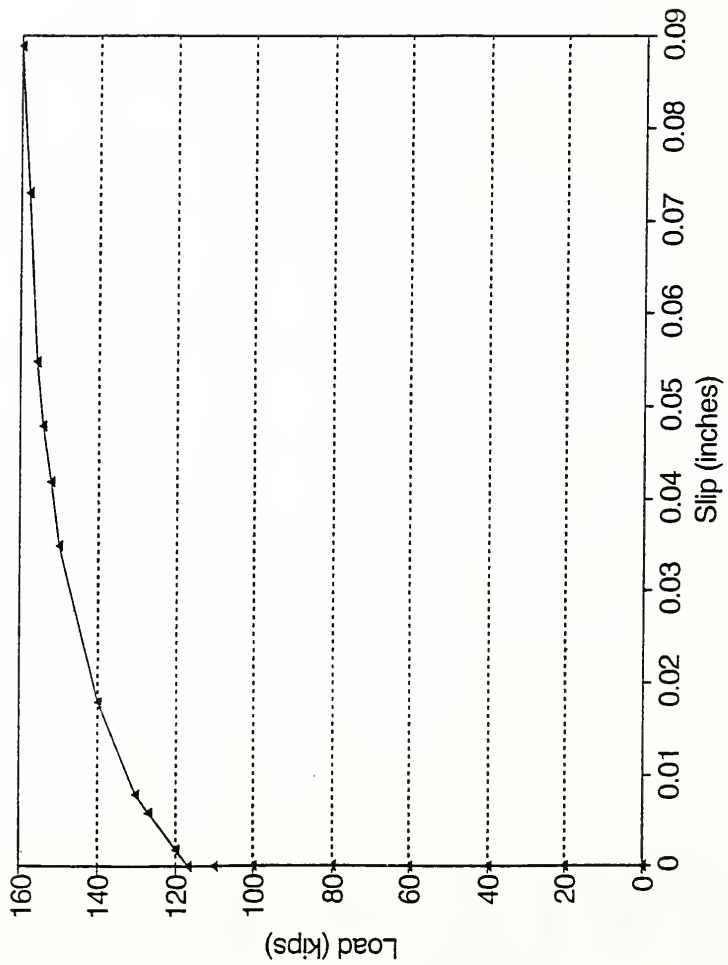


Figure 4.6 Load versus Strand Slip at #N17 of Specimen I

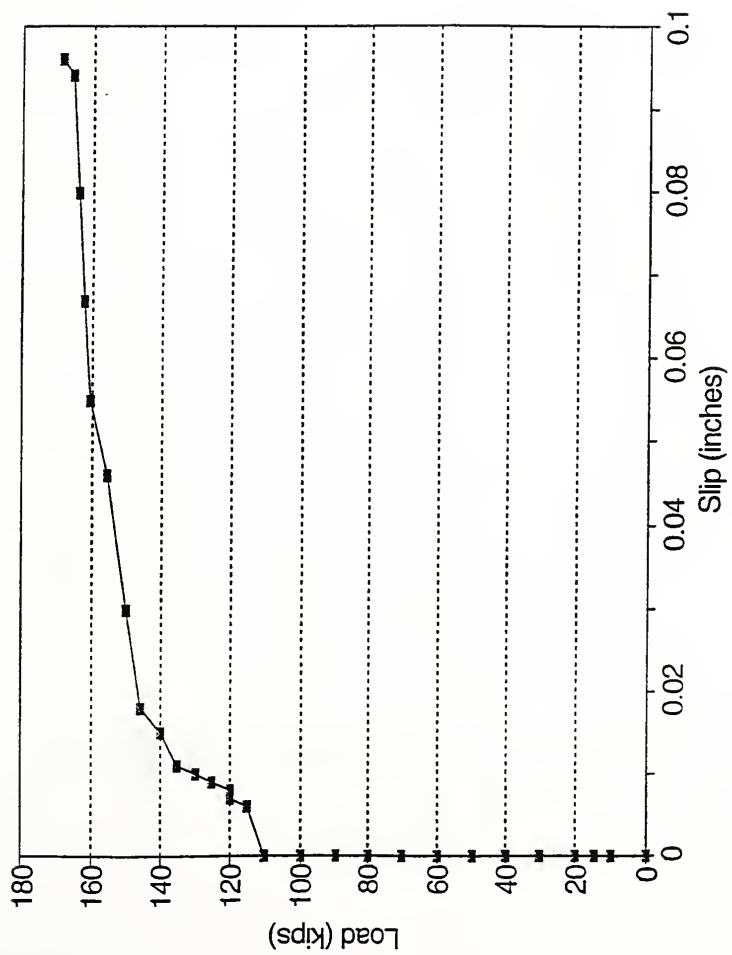


Figure 4.7 Load versus Strand Slip at #N2 of Specimen 2

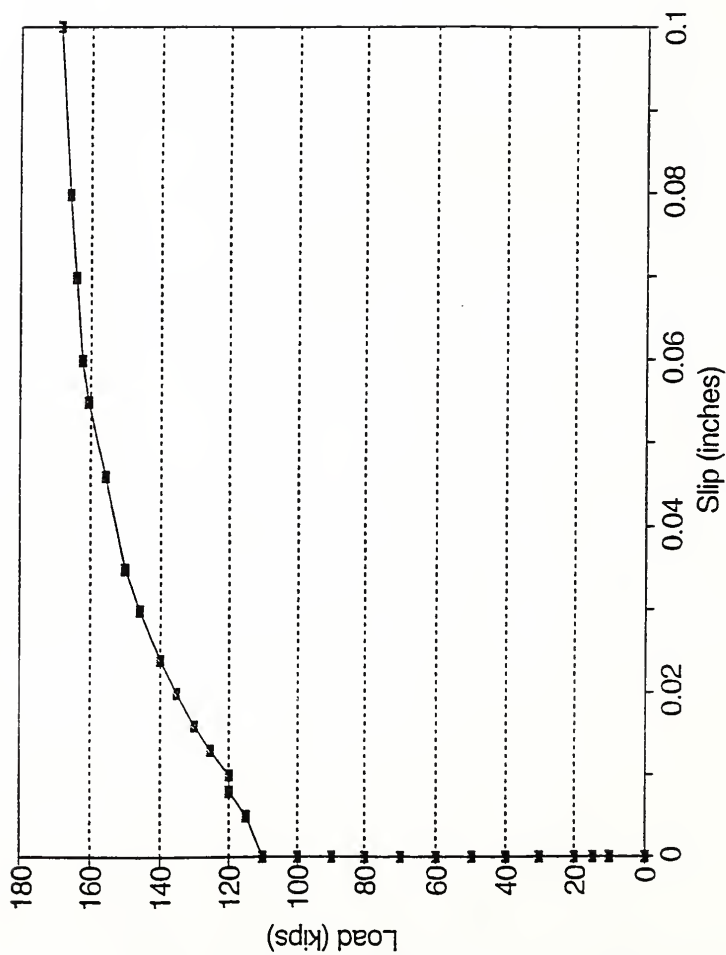


Figure 4.8 Load versus Strand Slip at #S2 of Specimen 2

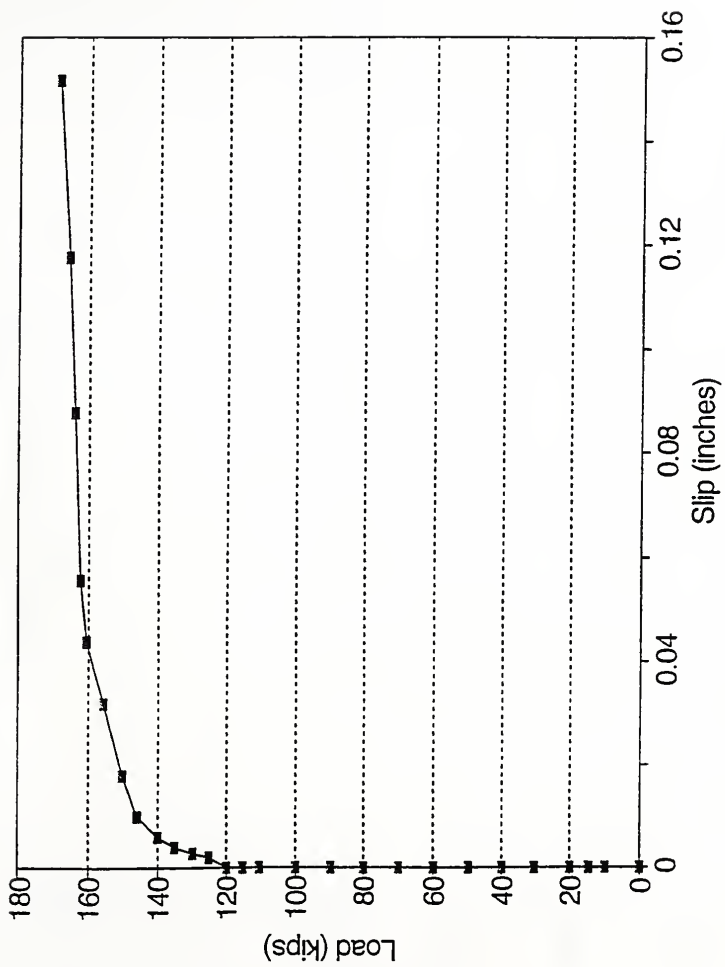


Figure 4.9 Load versus Strand Slip at #S10 of Specimen 2

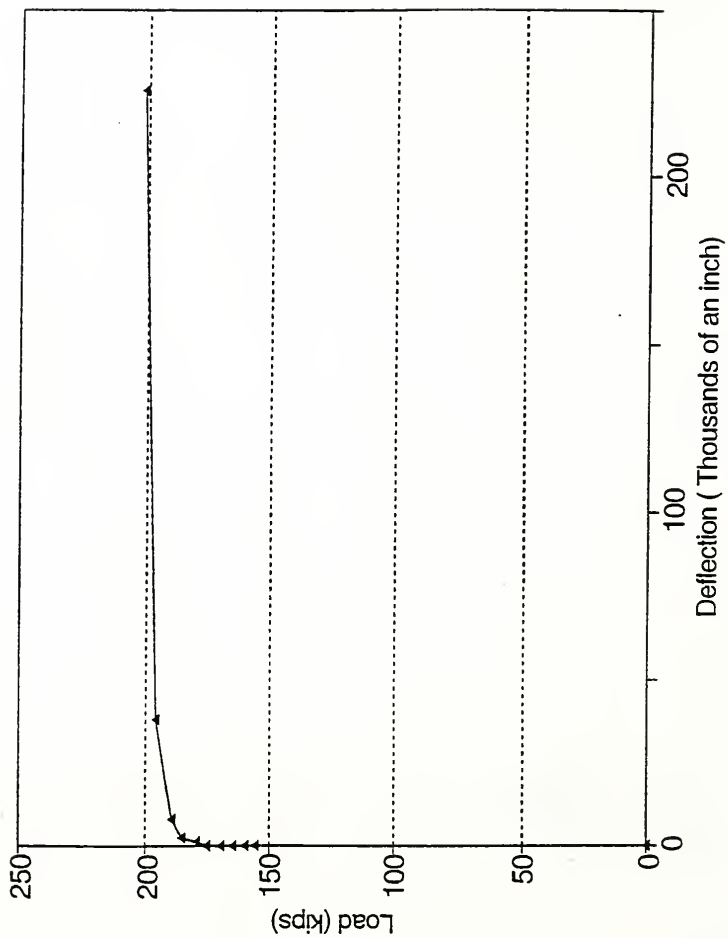


Figure 4.10 Load versus Strand Slip at #S6 of Specimen 3

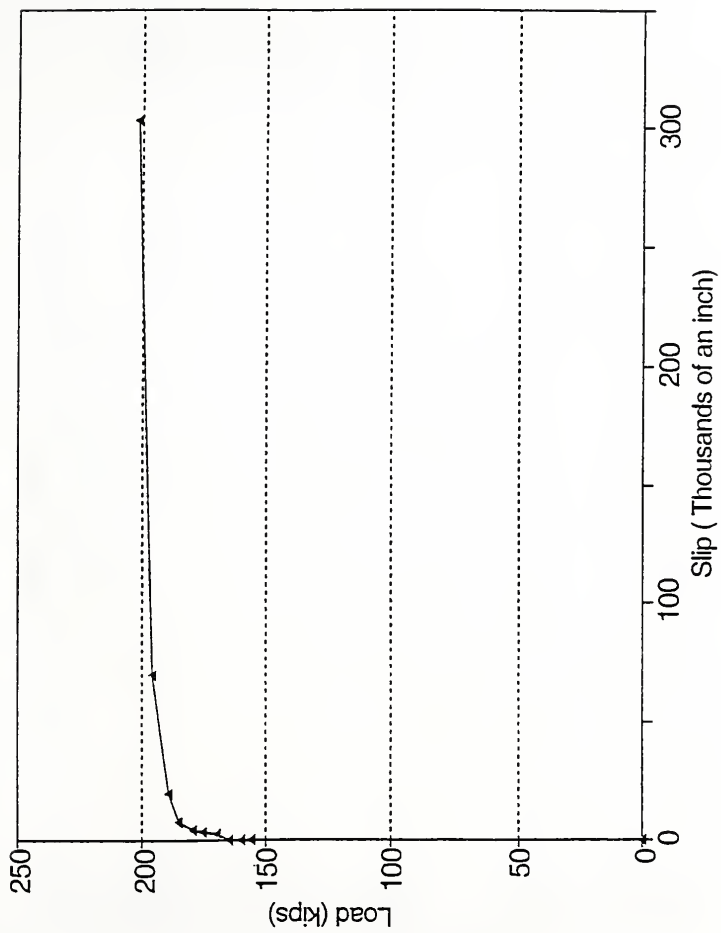


Figure 4.11 Load versus Strand Slip at #S9 of Specimen 3

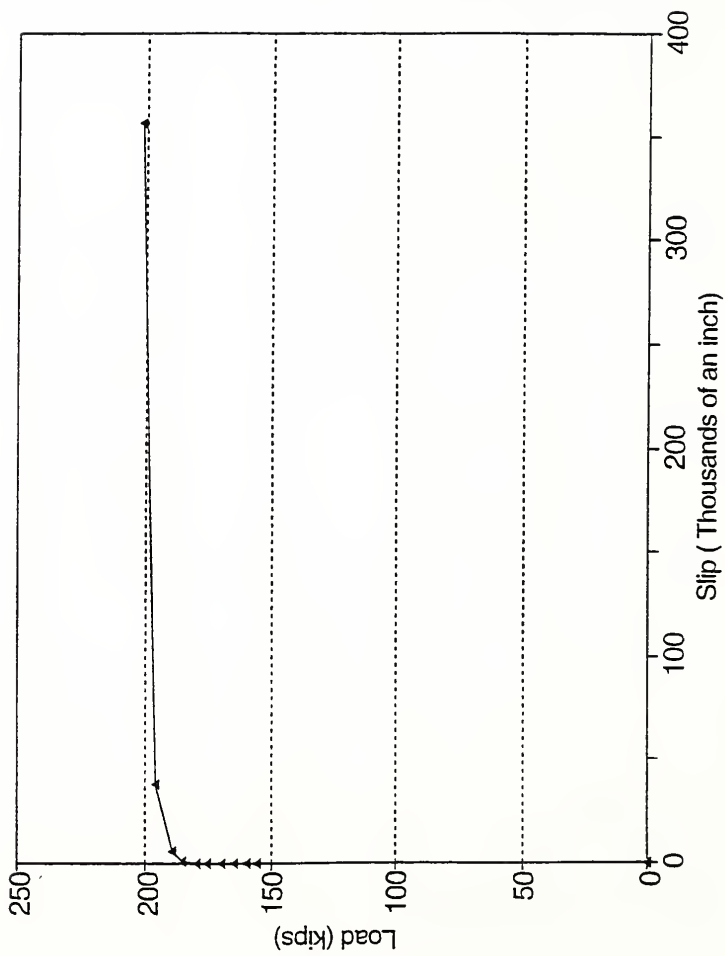


Figure 4.12 Load versus Strand Slip at #S17 of Specimen 3

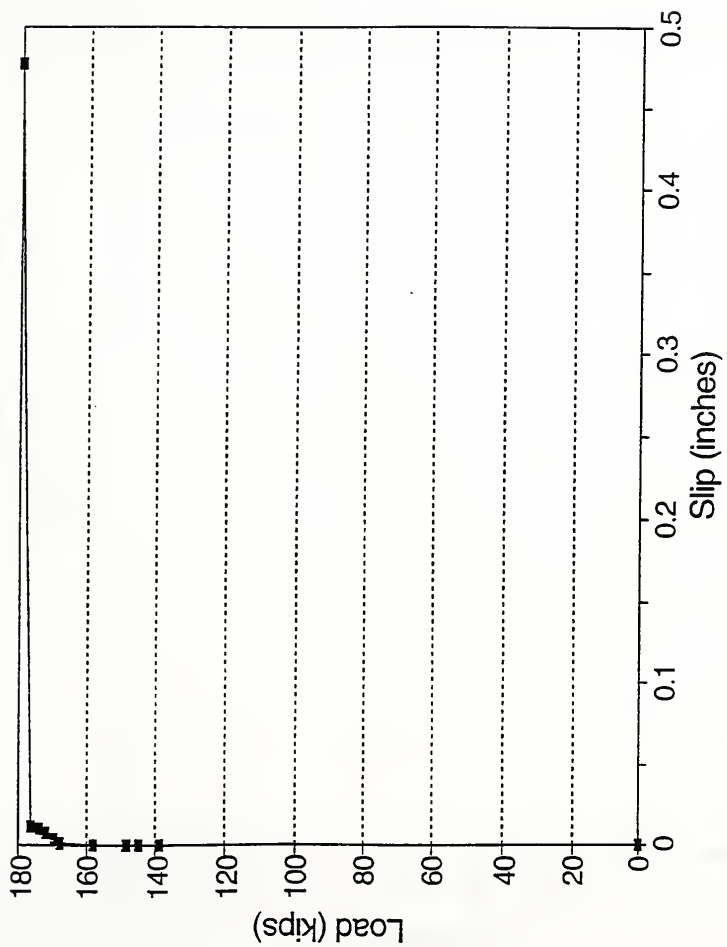


Figure 4.13 Load versus Strand Slip at #N6 of Specimen 4

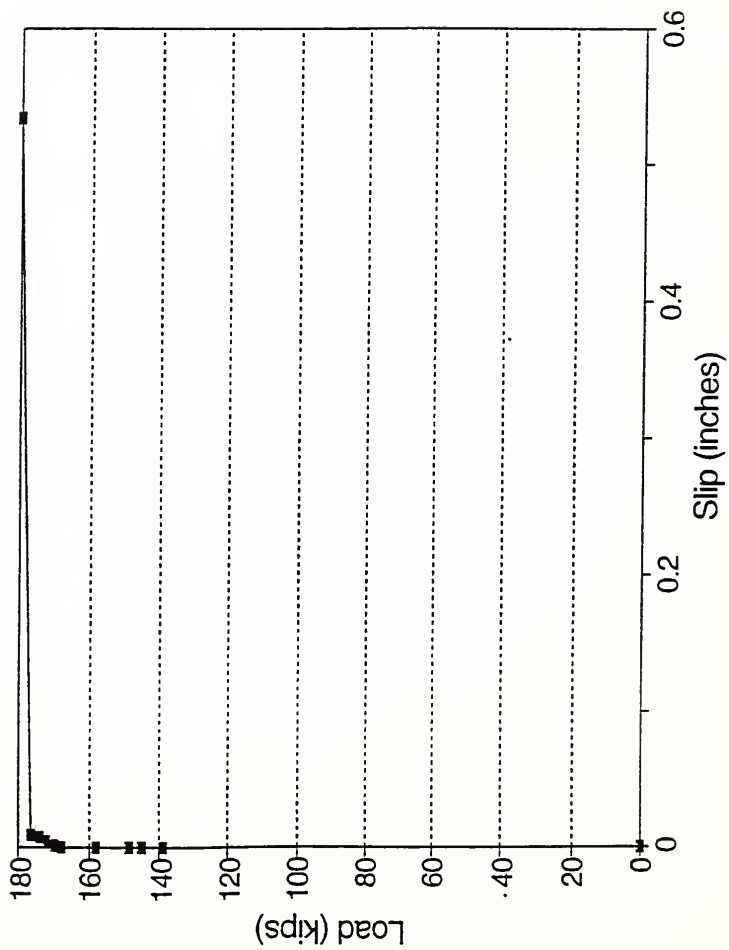


Figure 4.14 Load versus Strand Slip at #N17 of Specimen 4

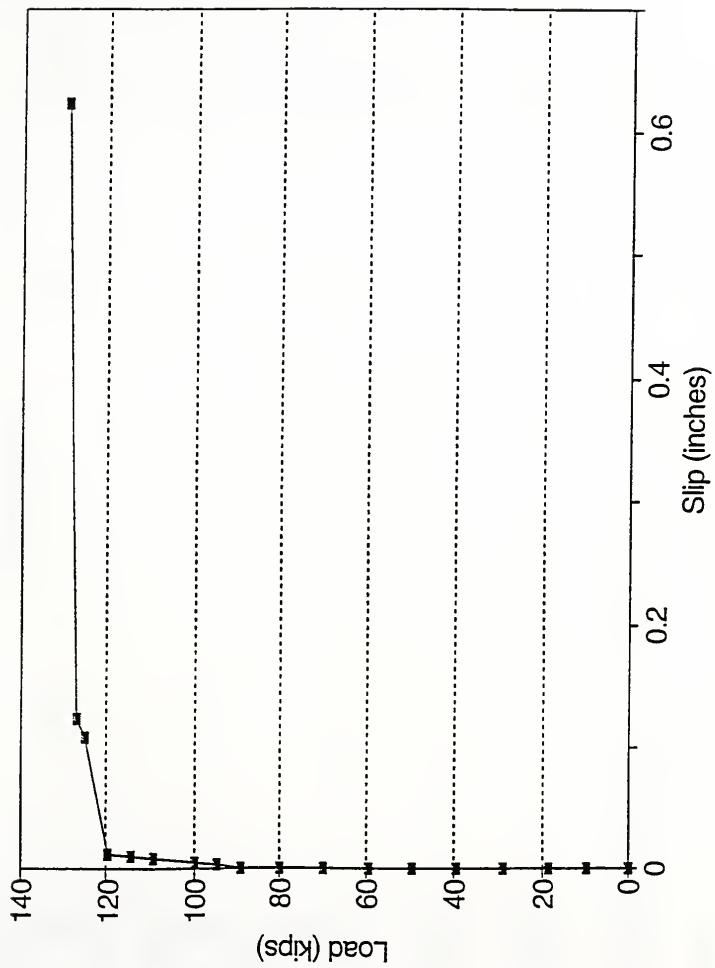


Figure 4.15 Load versus Strand Slip at #N4 of Specimen 5

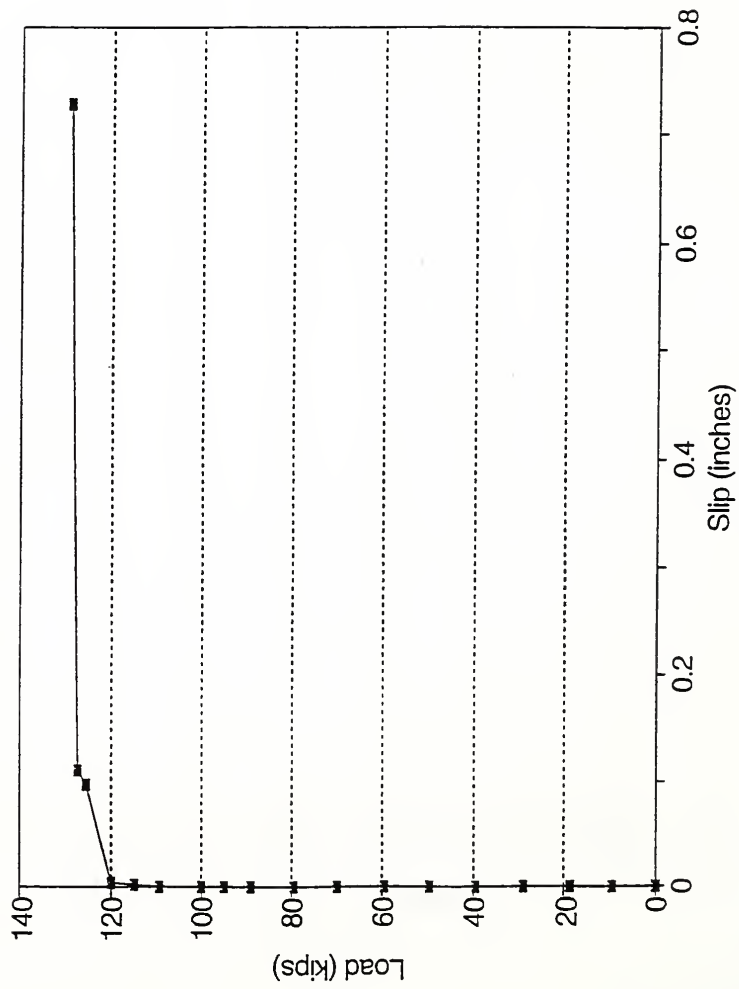


Figure 4.16 Load versus Strand Slip at #N6 of Specimen 5

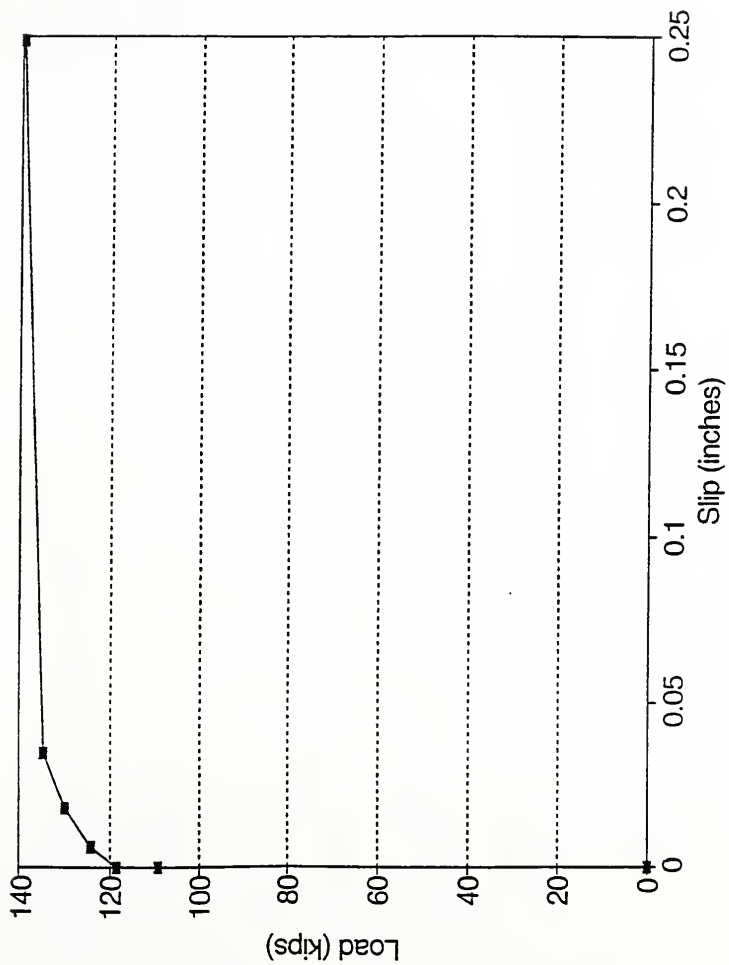


Figure 4.17 Load versus Strand Slip at #S6 of Specimen 6

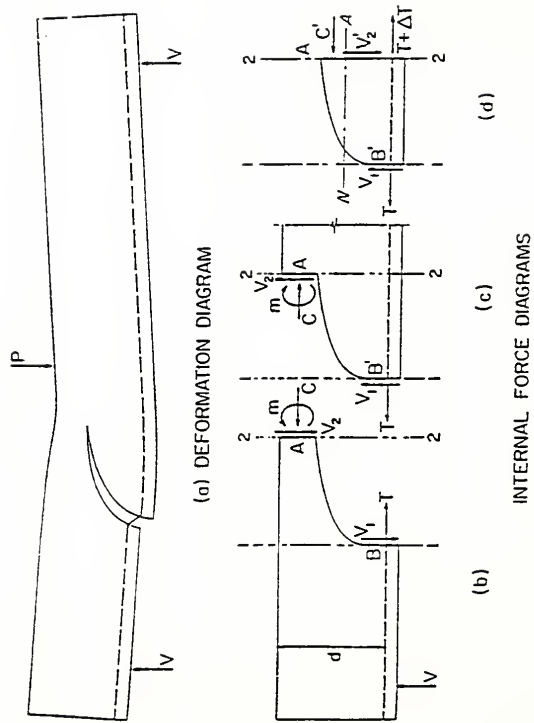


Figure 4.18 Inclined crack in Reinforced Concrete beams similar to that observed in Deck panel

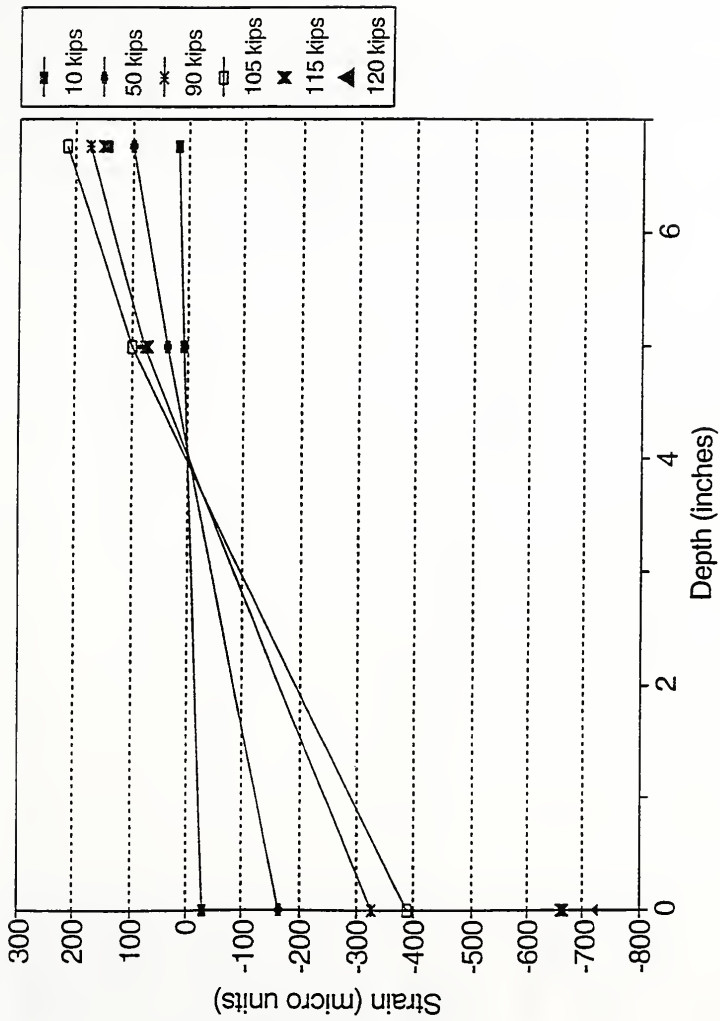


Figure 4.19 Strain distribution across the depth of Specimen I

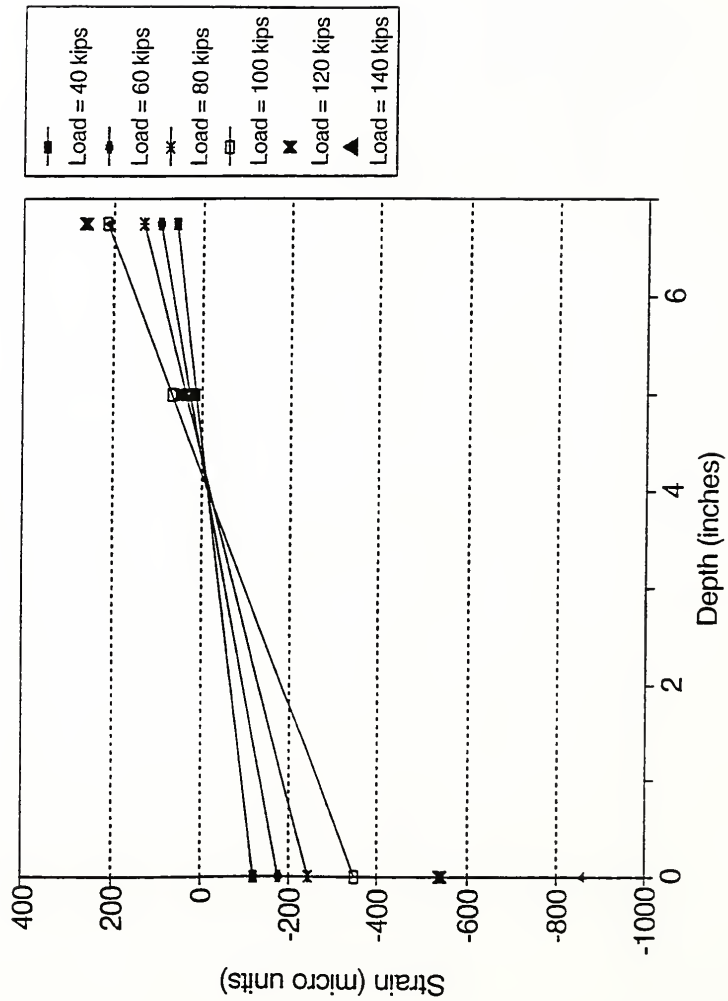


Figure 4.20 Strain distribution across the depth of Specimen 2

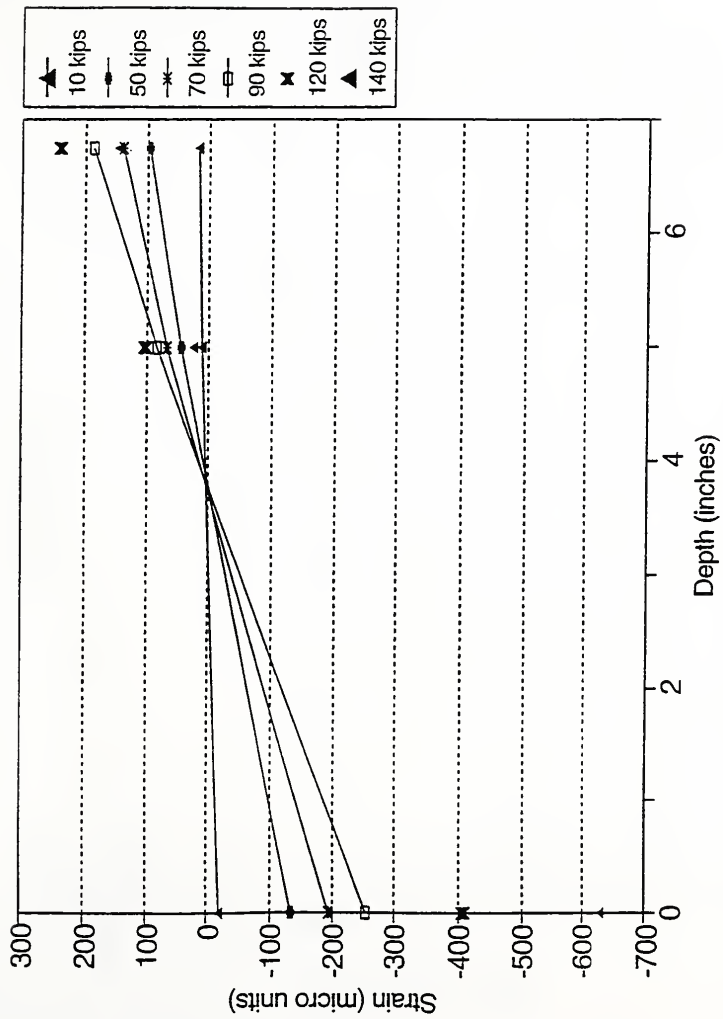


Figure 4.21 Strain distribution across the depth of Specimen 3

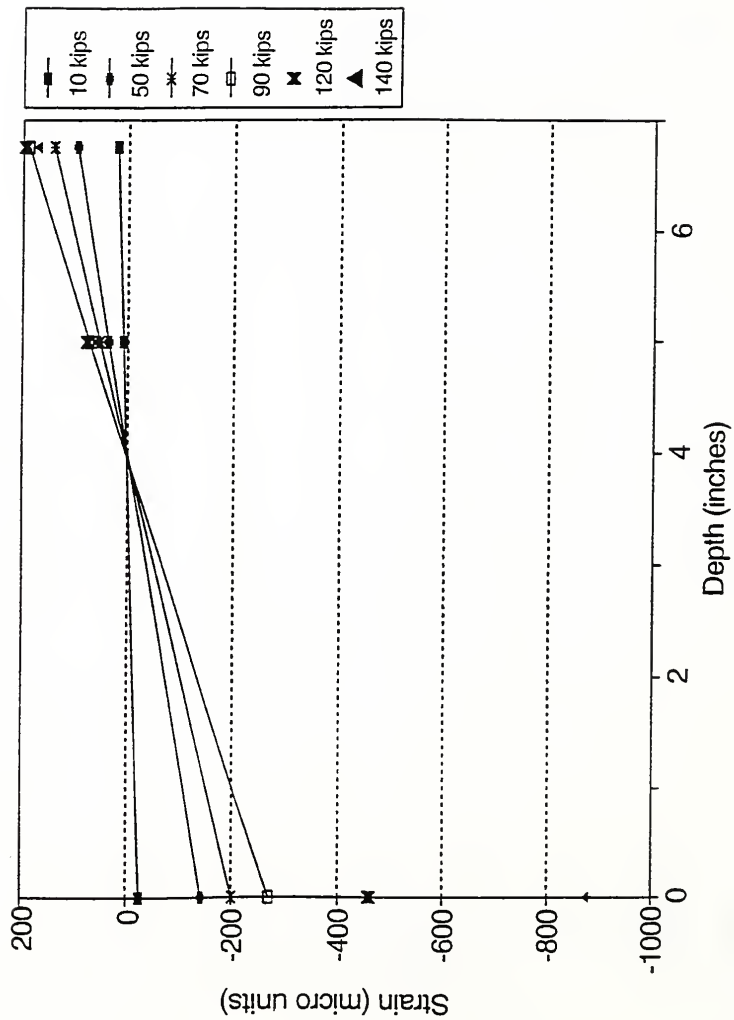


Figure 4.22 Strain distribution across the depth of Specimen 4

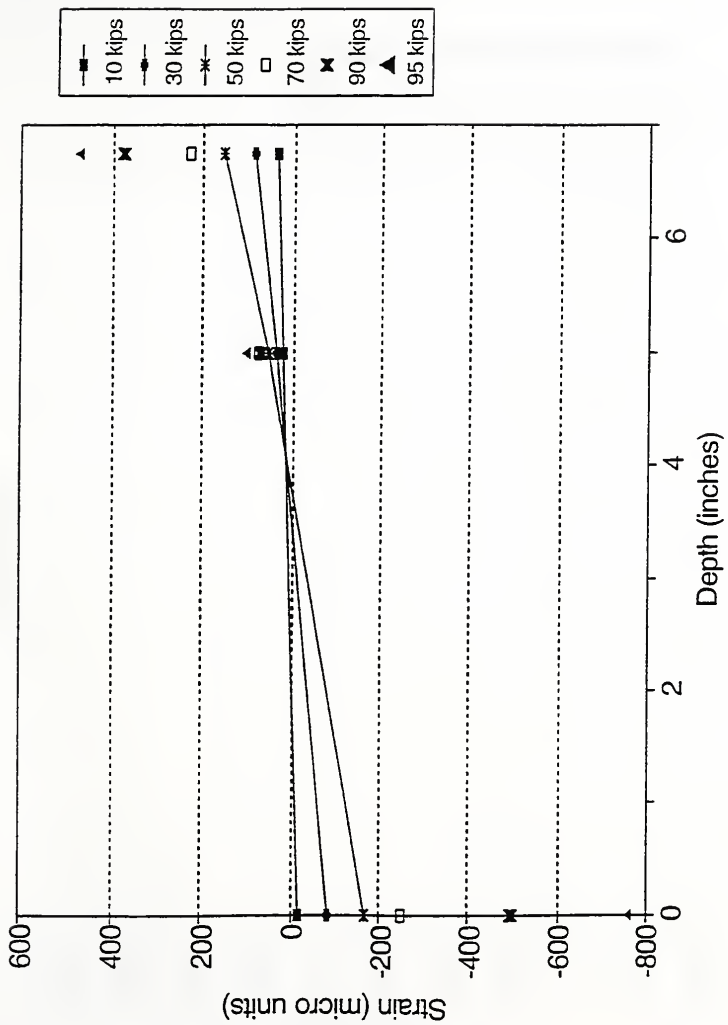


Figure 4.23 Strain distribution across the depth of Specimen 5

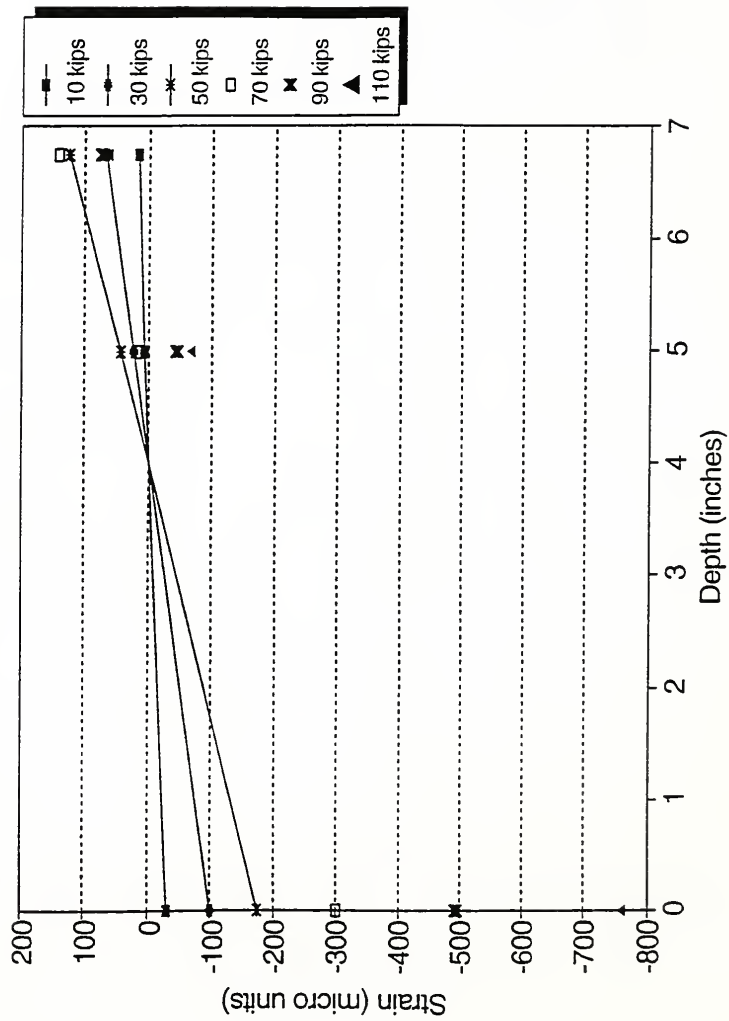


Figure 4.24 Strain distribution across the depth of Specimen 6

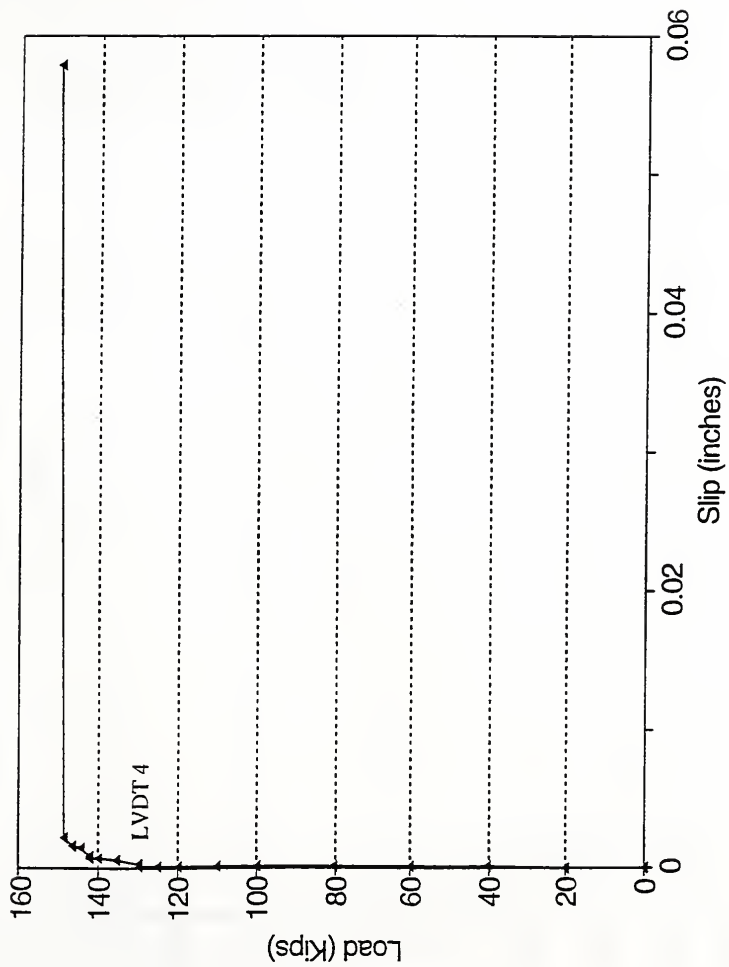


Figure 4.25 Load versus Slip at the interface of Specimen 1

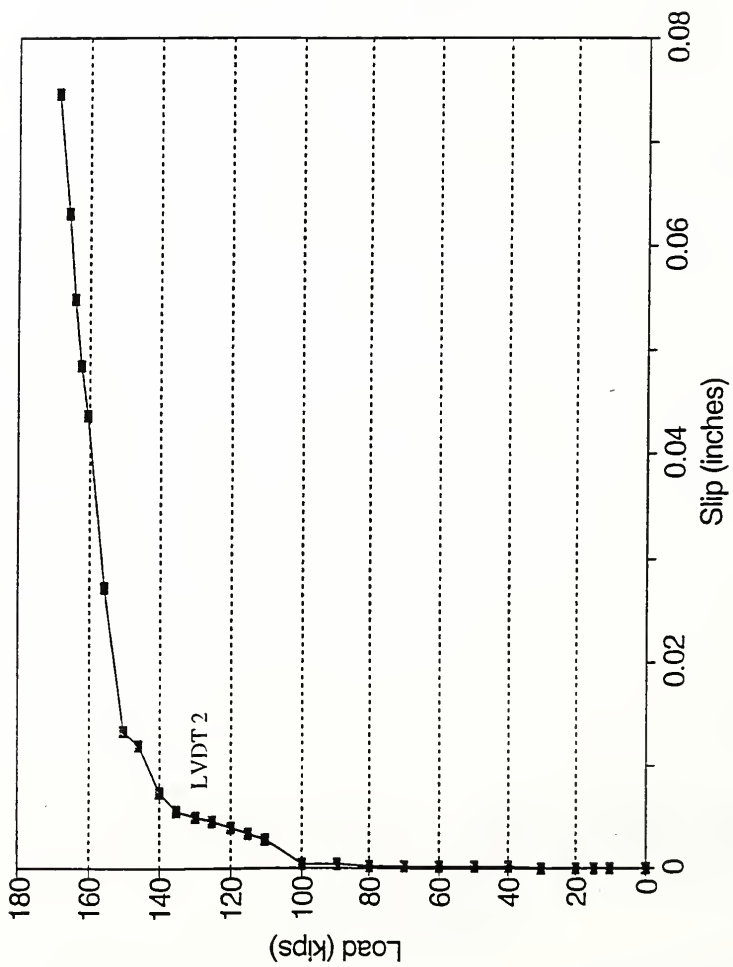


Figure 4.26 Load versus Slip at the interface of Specimen 2

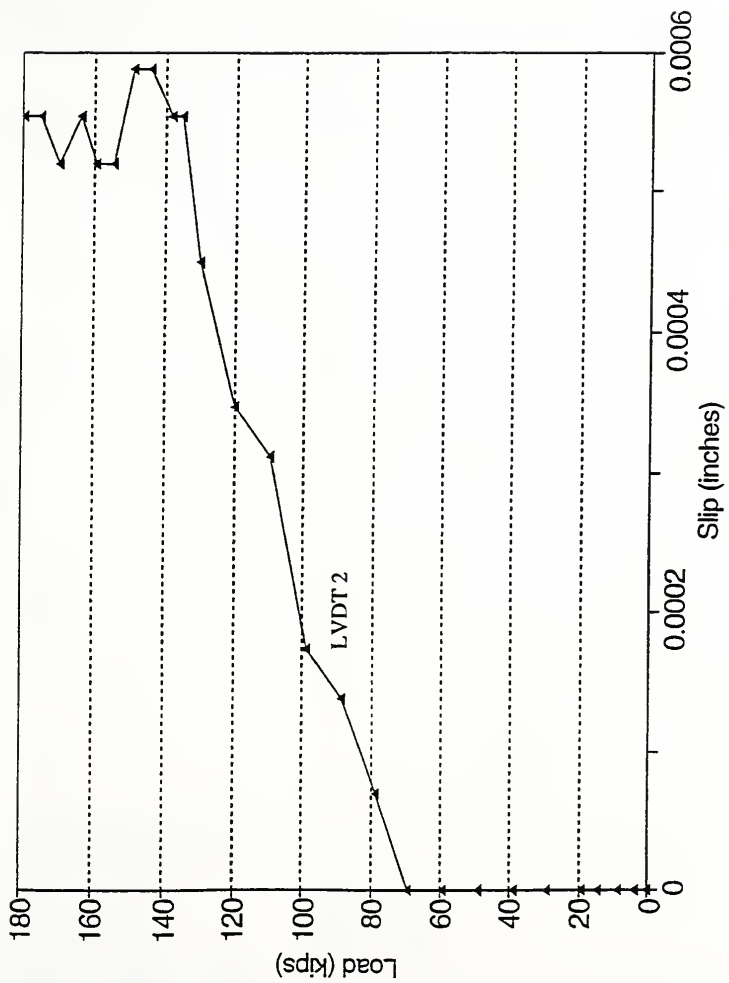


Figure 4.27 Load versus Slip at the interface of Specimen 3

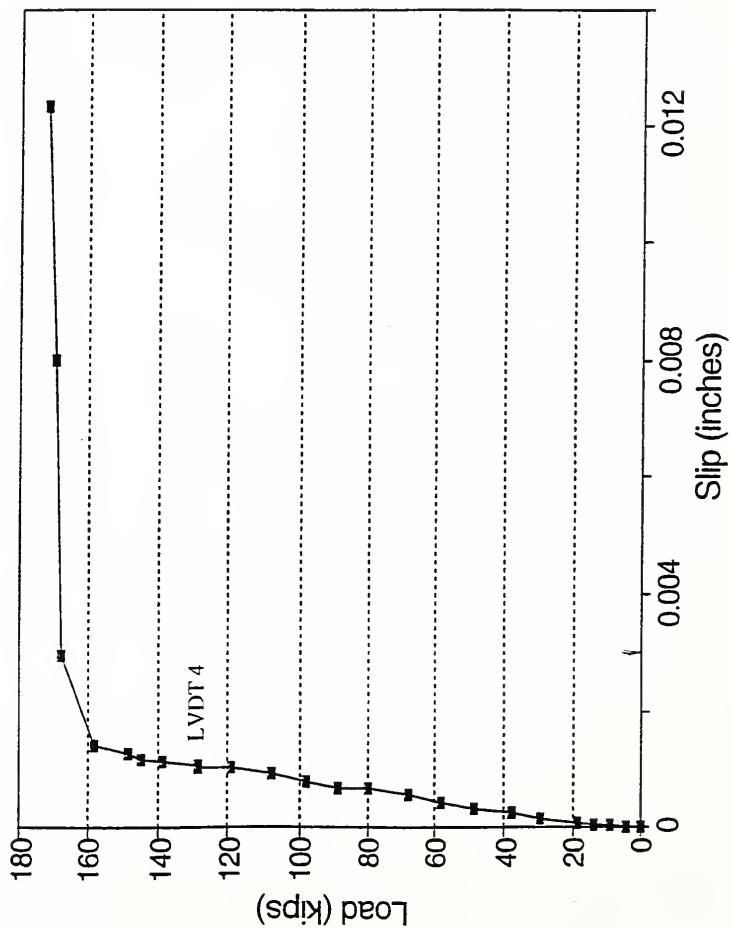


Figure 4.28 Load versus Slip at the interface of Specimen 4

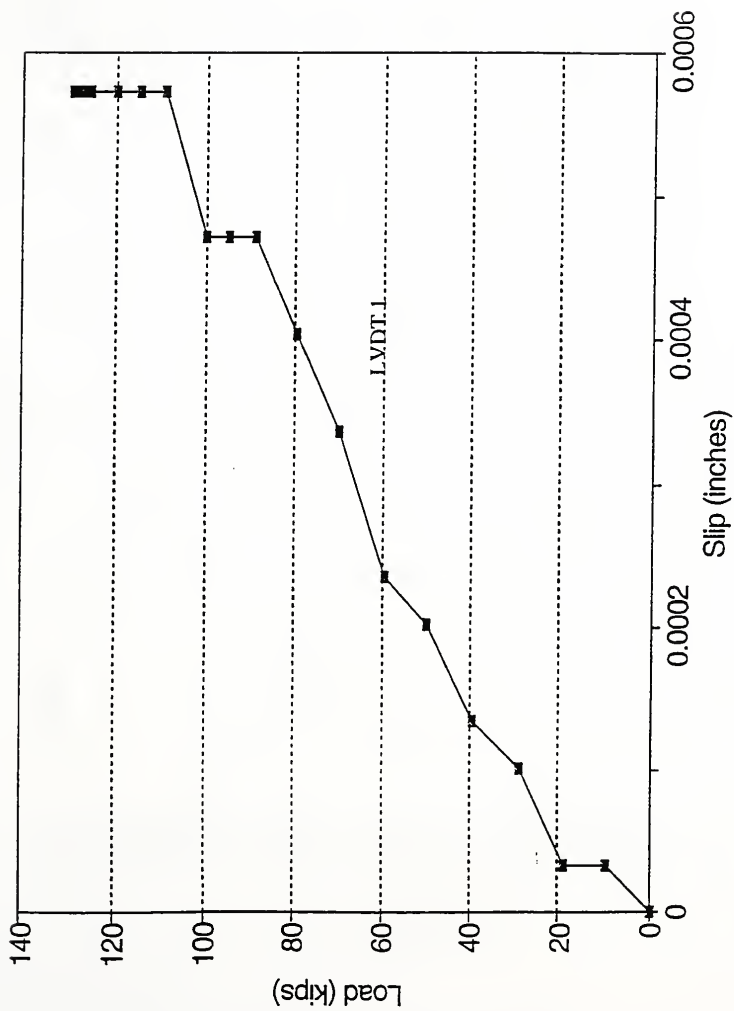


Figure 4.29 Load versus Slip at the interface of Specimen 5

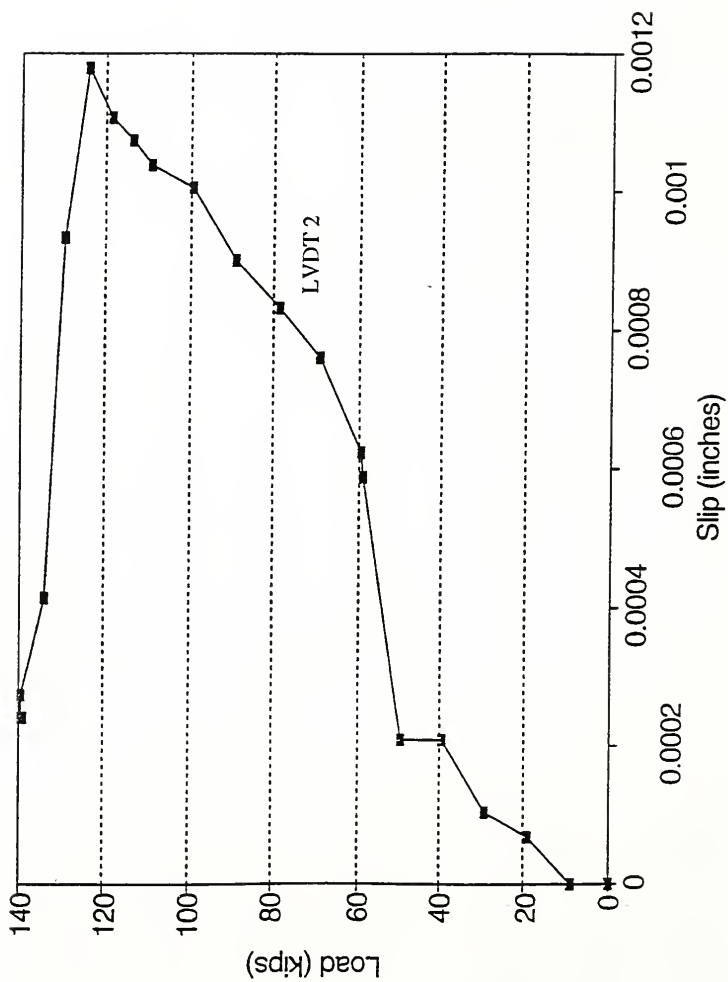


Figure 4.30 Load versus Slip at the interface of Specimen 6

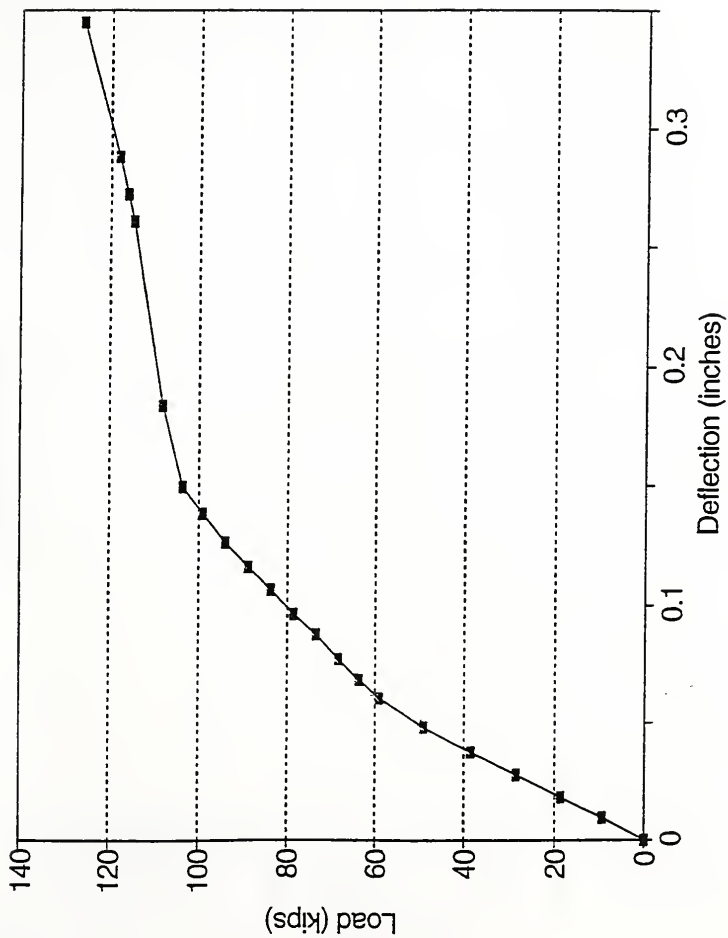


Figure 4.31 Load versus Deflection characteristics of Specimen 1

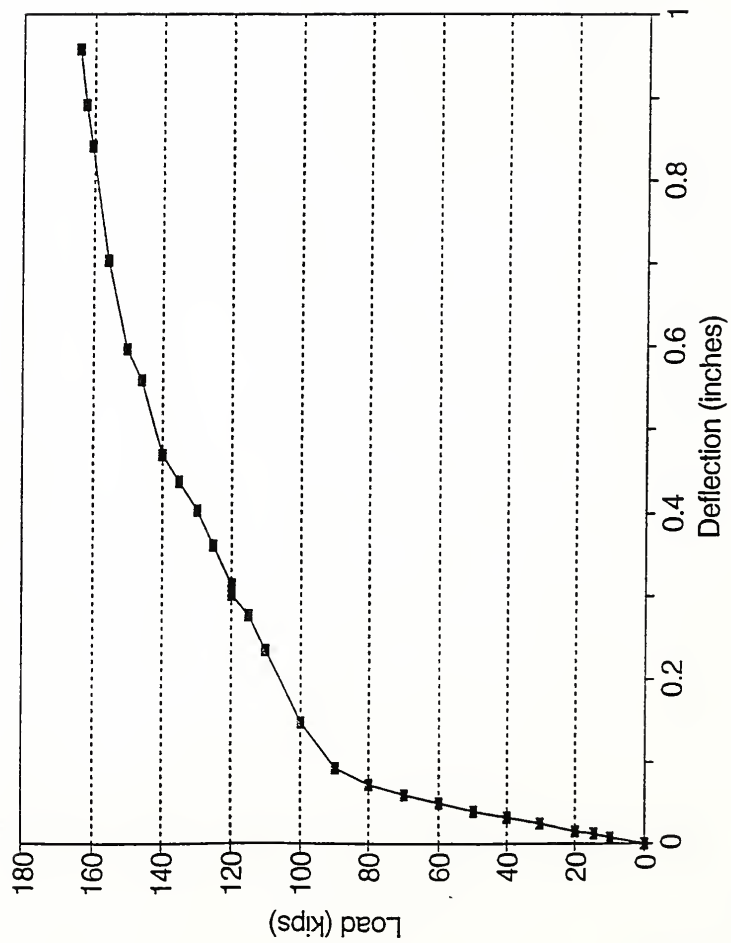


Figure 4.32 Load versus Deflection characteristics of Specimen 2

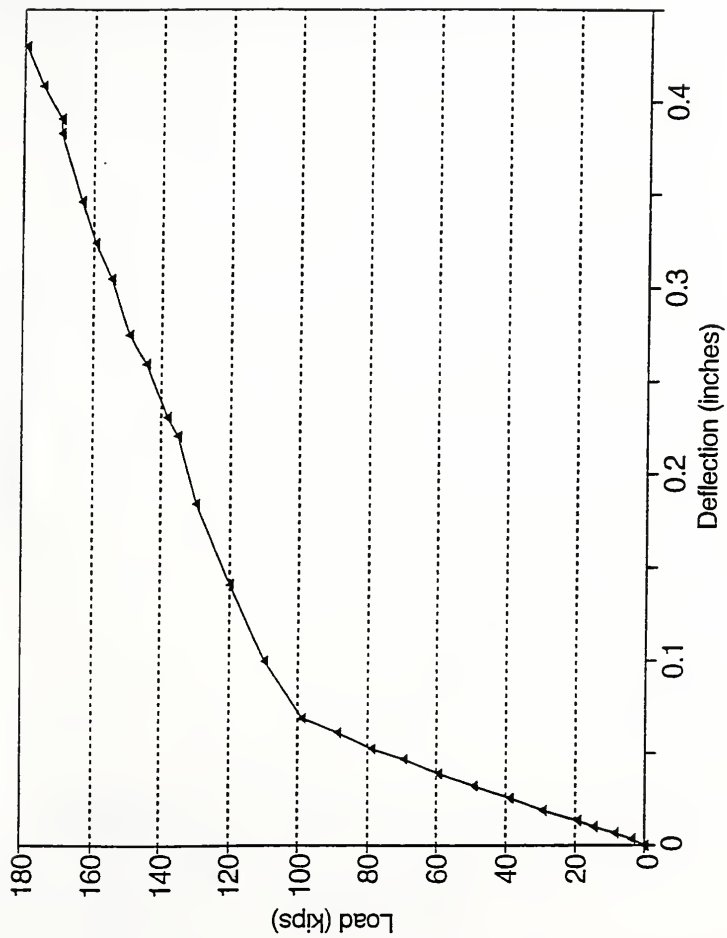


Figure 4.33 Load versus Deflection characteristics of Specimen 3

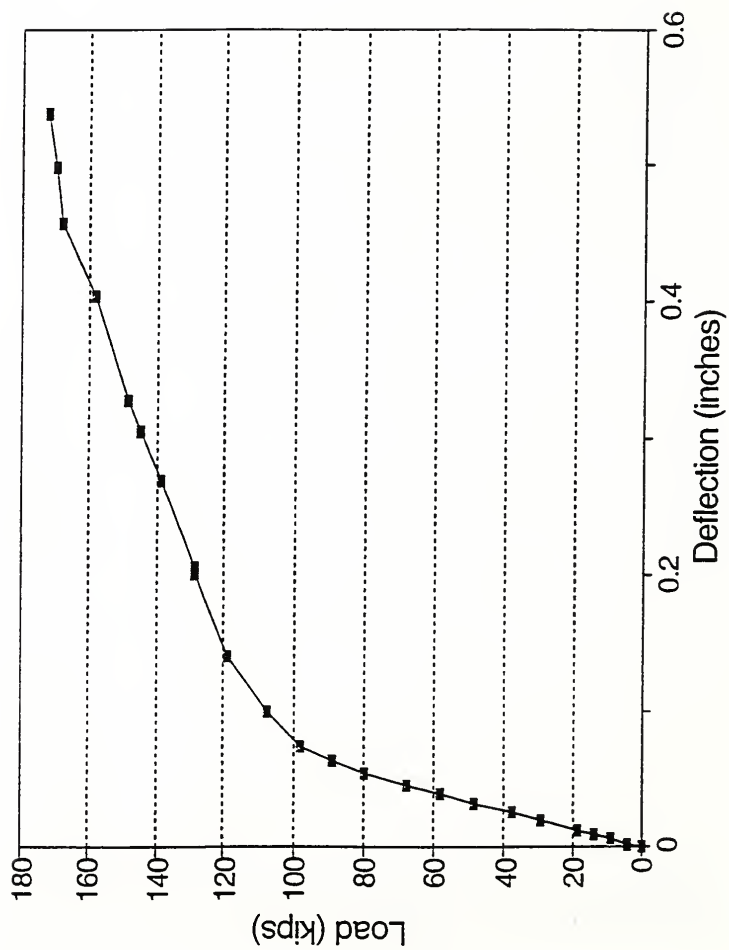


Figure 4.34 Load versus Deflection characteristics of Specimen 4

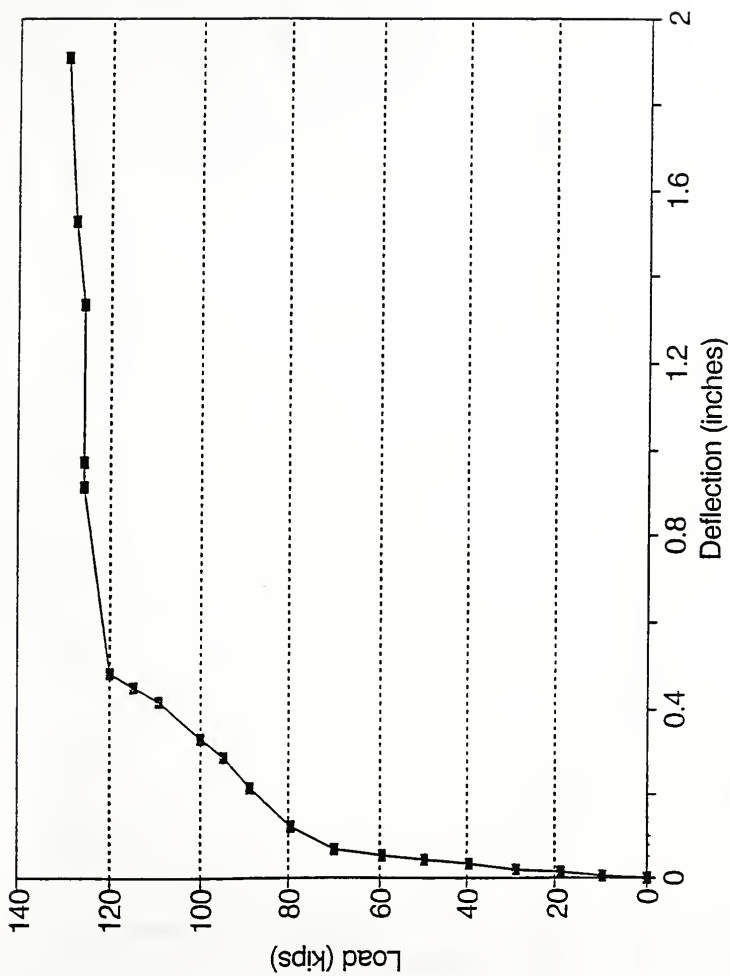


Figure 4.35 Load versus Deflection characteristics of Specimen 5

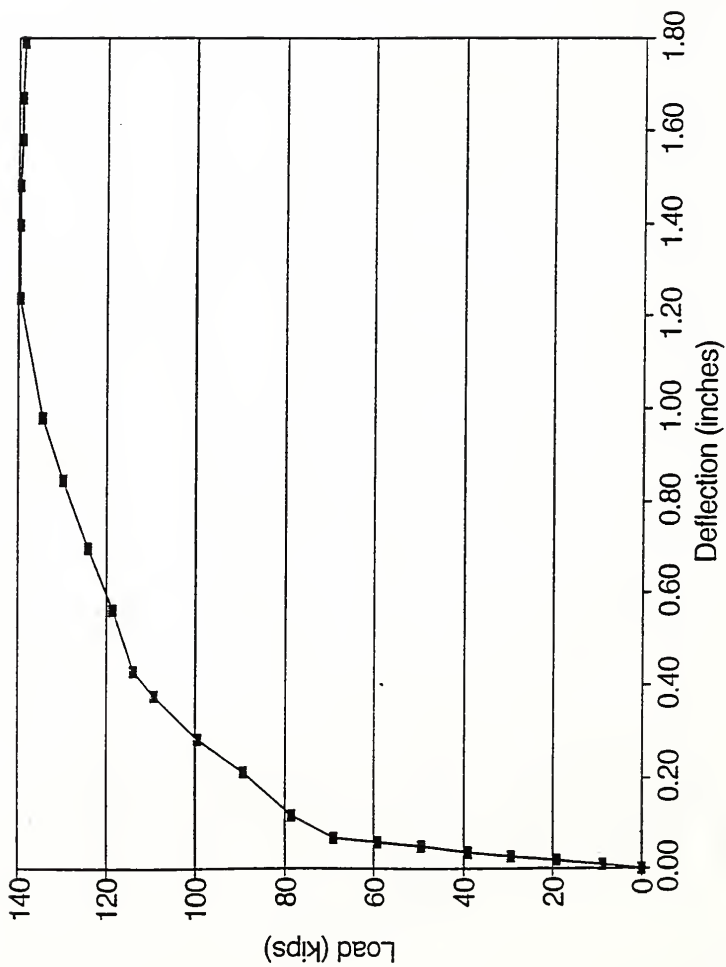


Figure 4.36 Load versus Deflection characteristics of Specimen 6

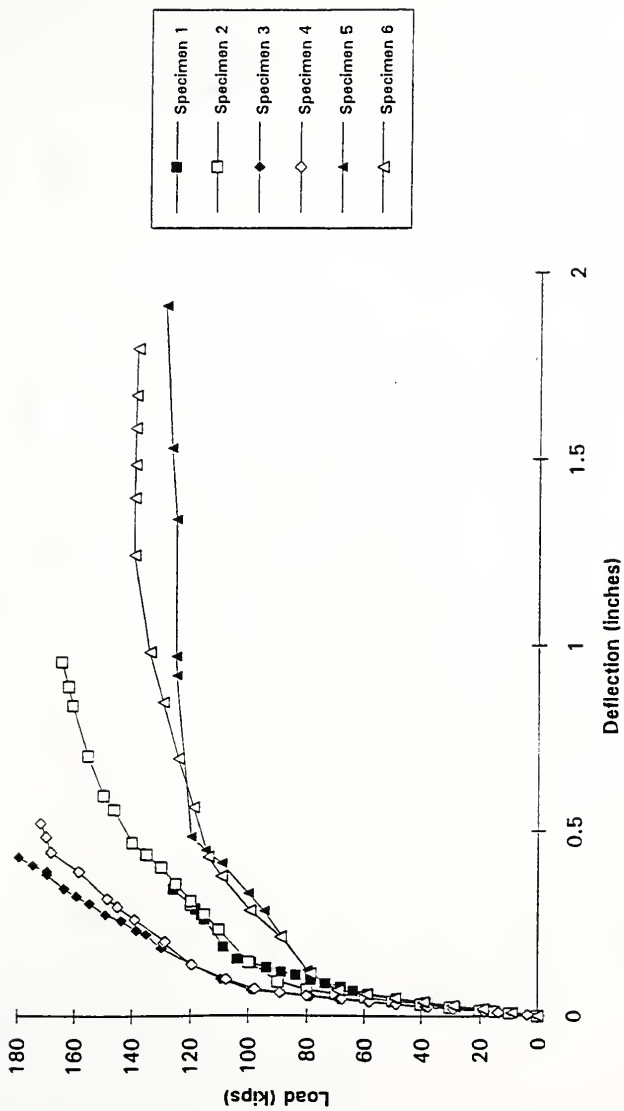


Figure 4.37 Comparison of Load versus Deflection characteristics of various specimens

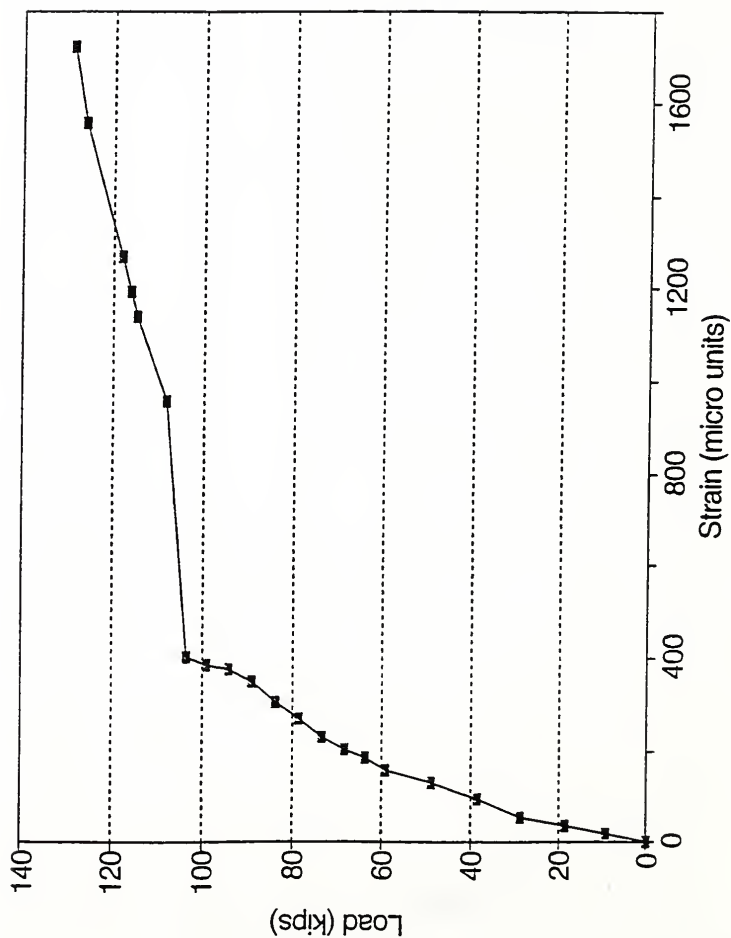


Figure 4.38 Load versus Strain in the strand at #C10 of Specimen 1

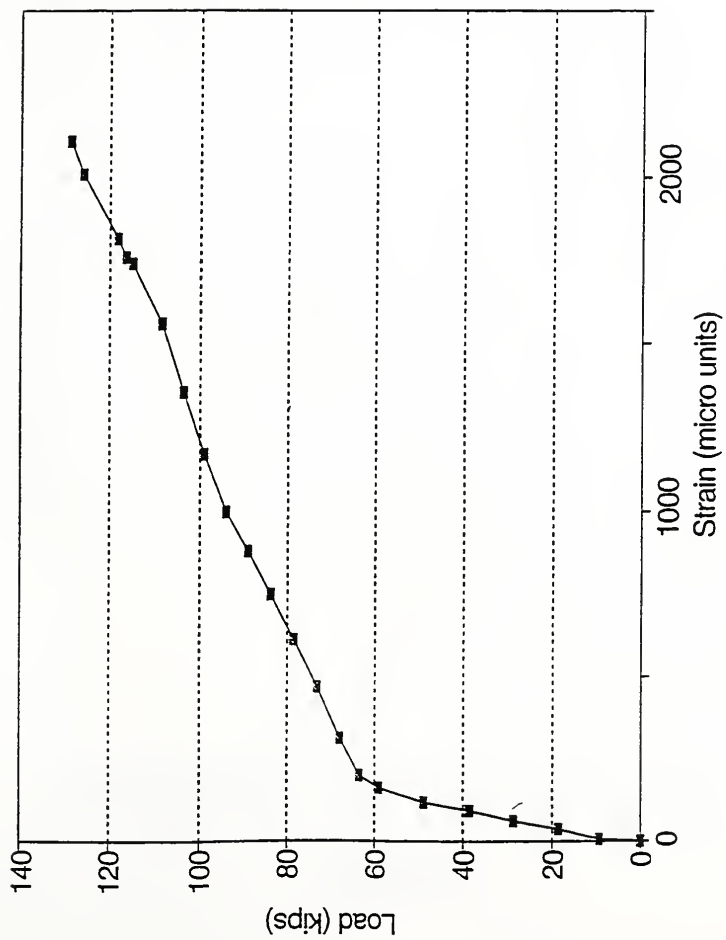


Figure 4.39 Load versus Strain in the strand at #C13 of Specimen 1

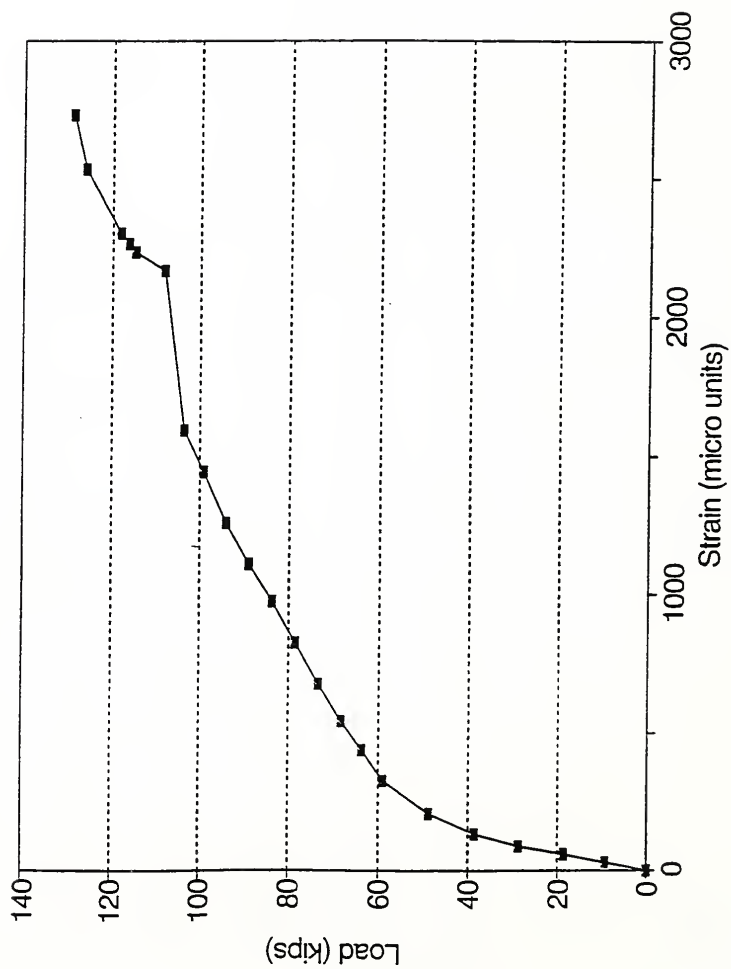


Figure 4.40 Load versus Strain in the strand at #C17 of Specimen 1

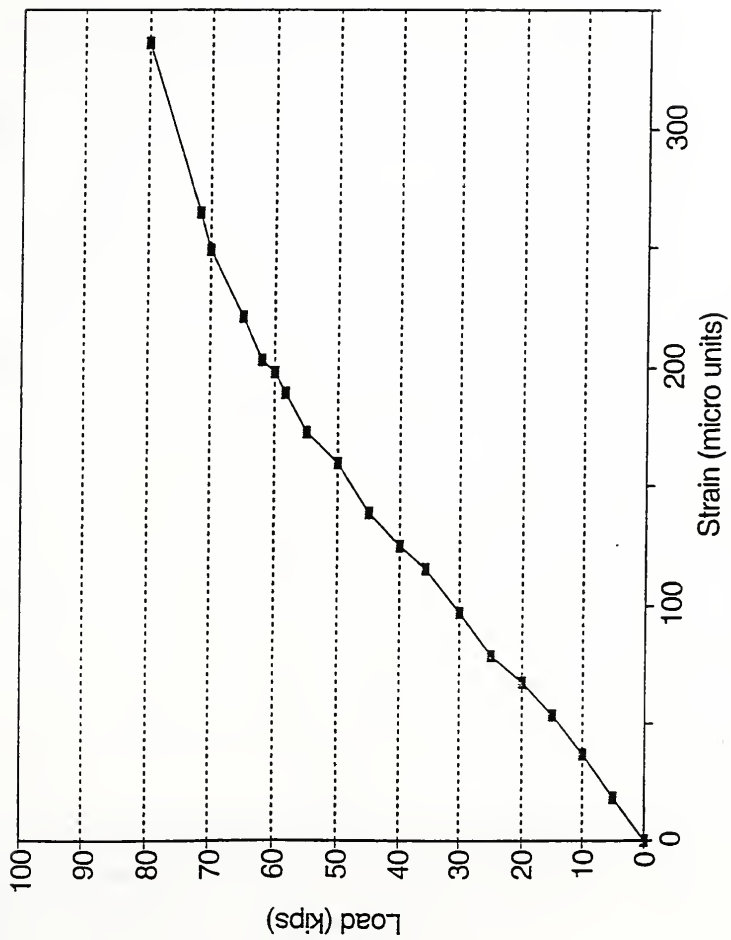


Figure 4.41 Load versus Average strain in the strand of Specimen 2 after 500,000 cycles

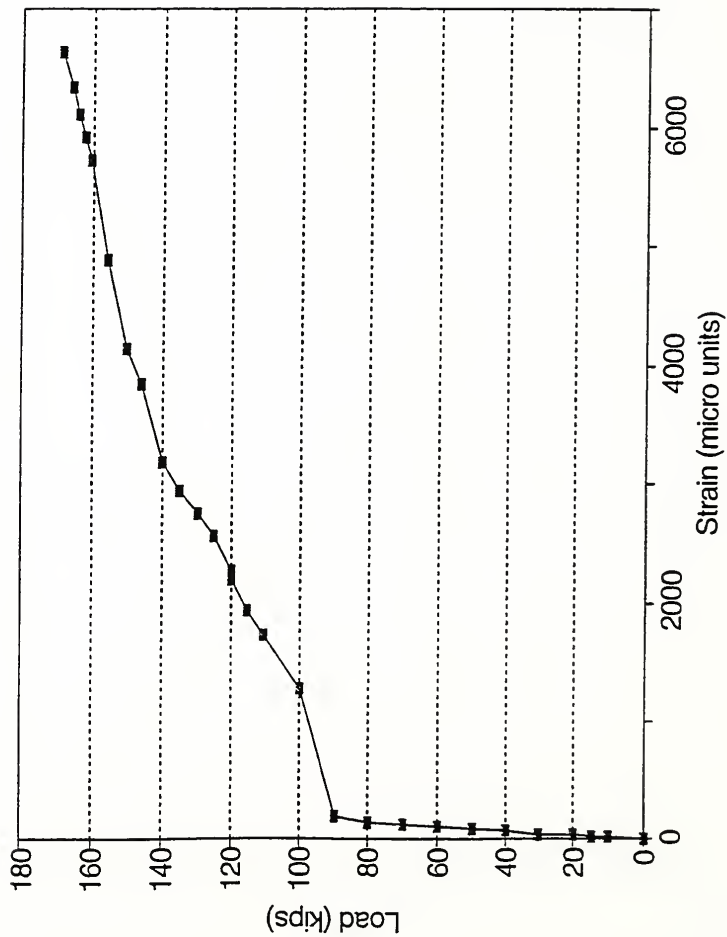


Figure 4.42 Load versus Strain in the strand at #C2 of Specimen 2

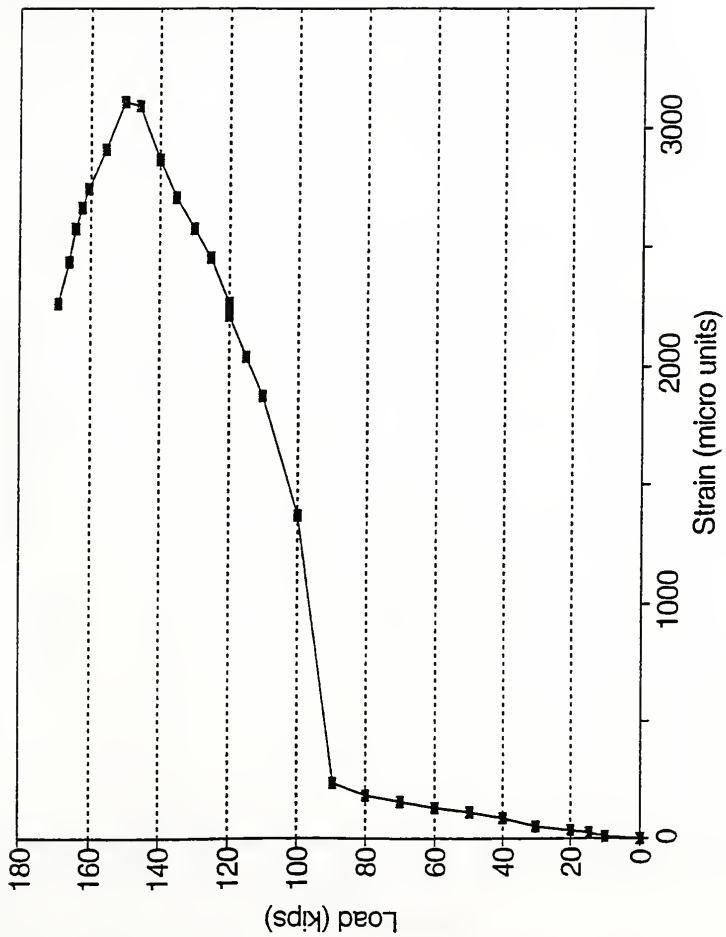


Figure 4.43 Load versus Strain in the strand at #C6 of Specimen 2

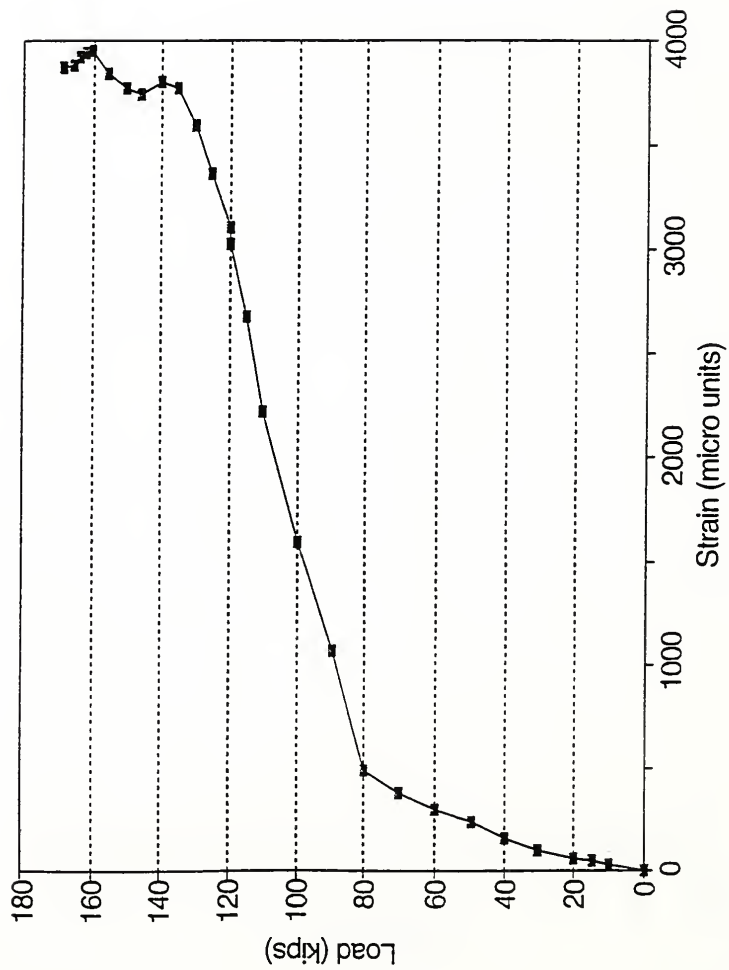


Figure 4.44 Load versus Strain in the strand at #C9 of Specimen 2

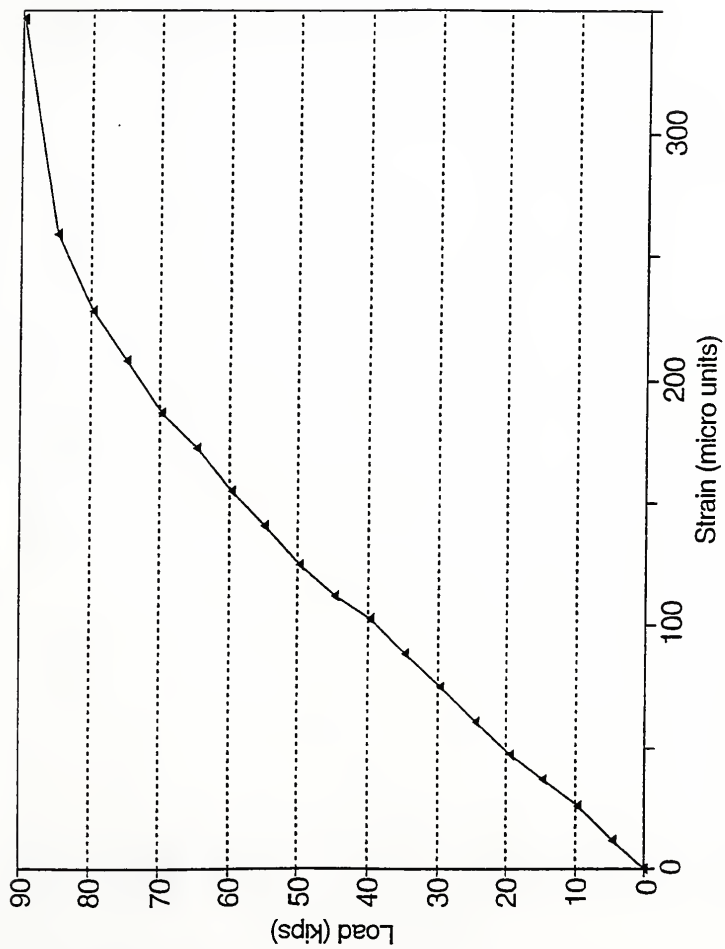


Figure 4.45 Load versus Average strain in strands of Specimen 3 after 500,000 cycles

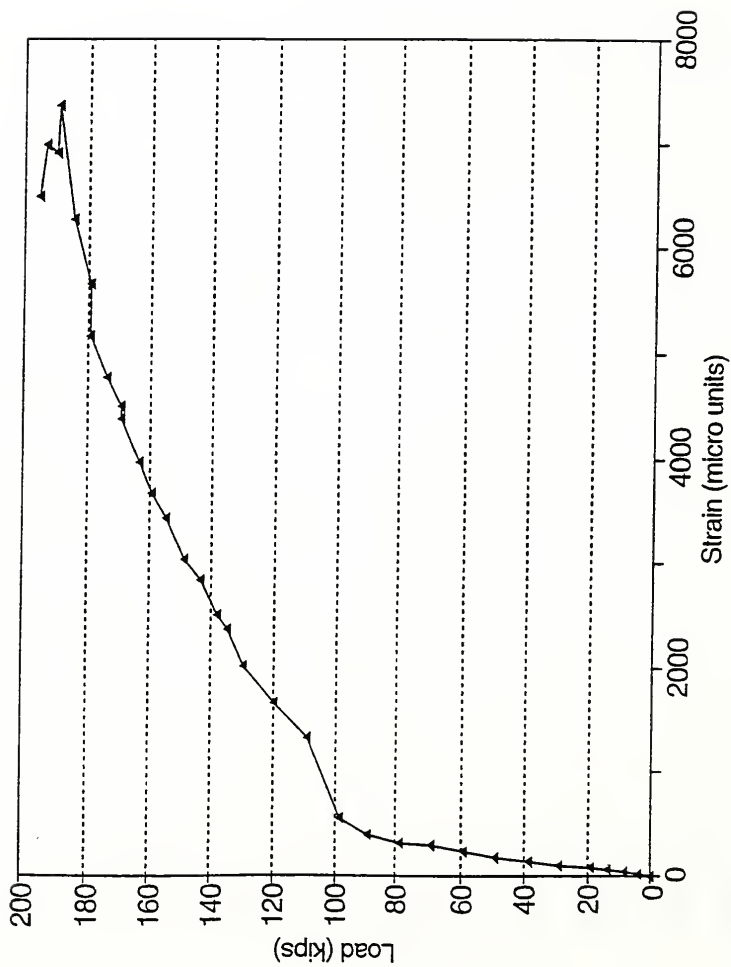


Figure 4.46 Load versus Strain in the strand at #C5 of Specimen 3

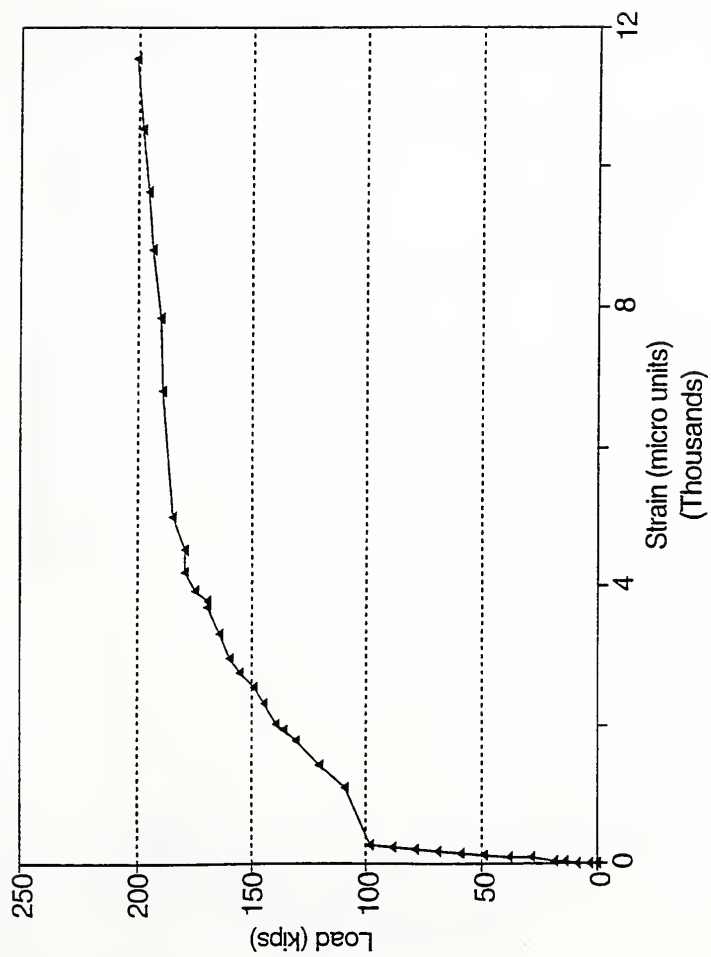


Figure 4.47 Load versus Strain in the strand at #C17 of Specimen 3

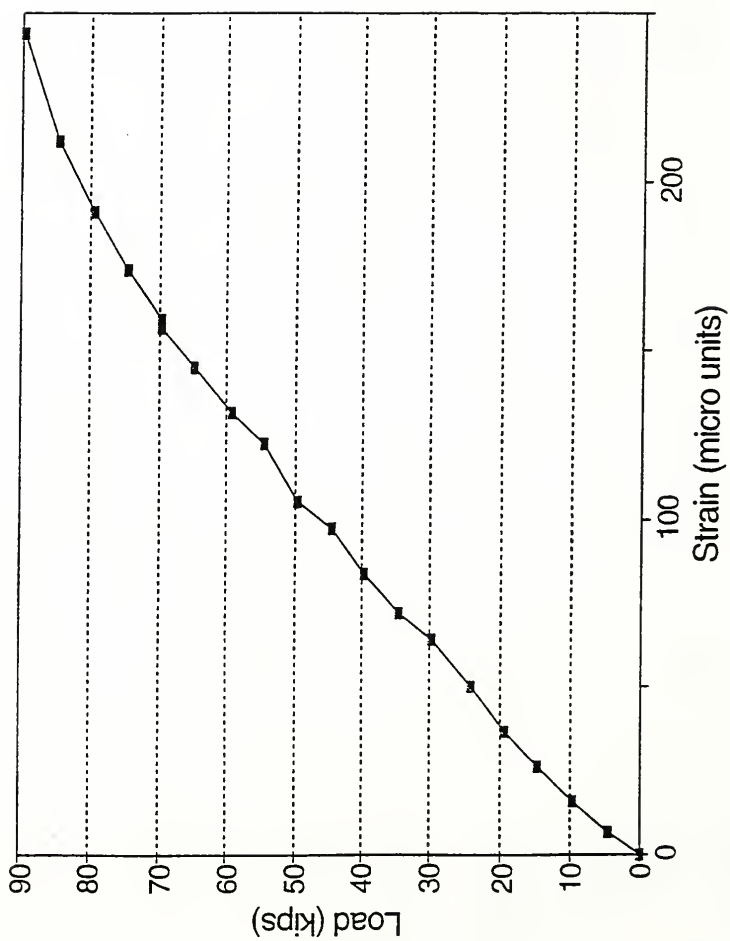


Figure 4.48 Load versus Average strain in strands of Specimen 4 after 600,000 cycles

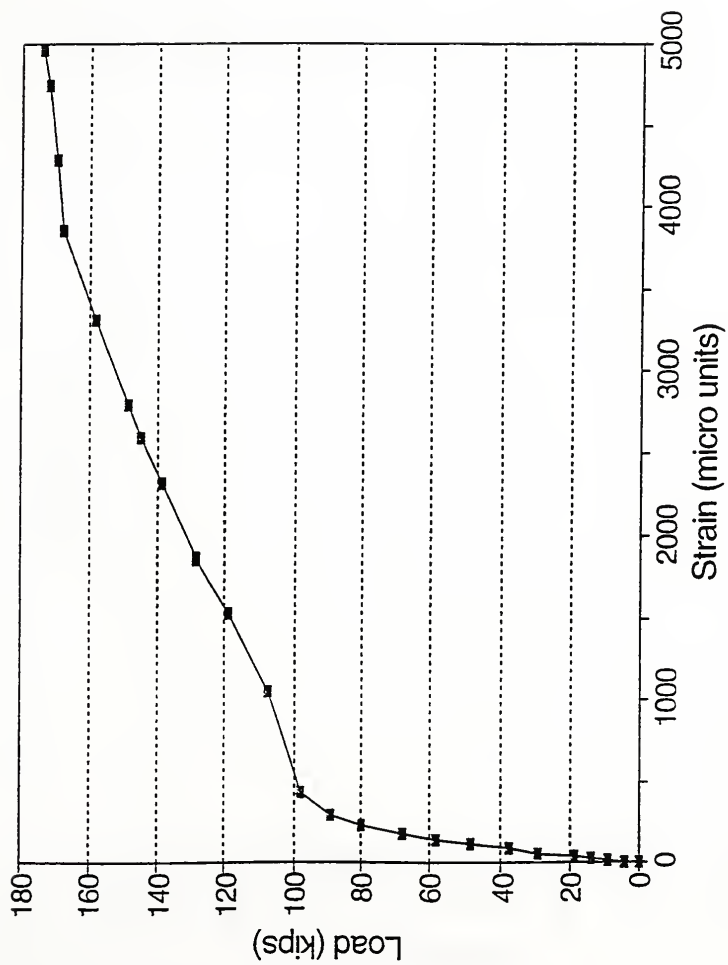


Figure 4.49 Load versus Average strain in the strands of Specimen 4

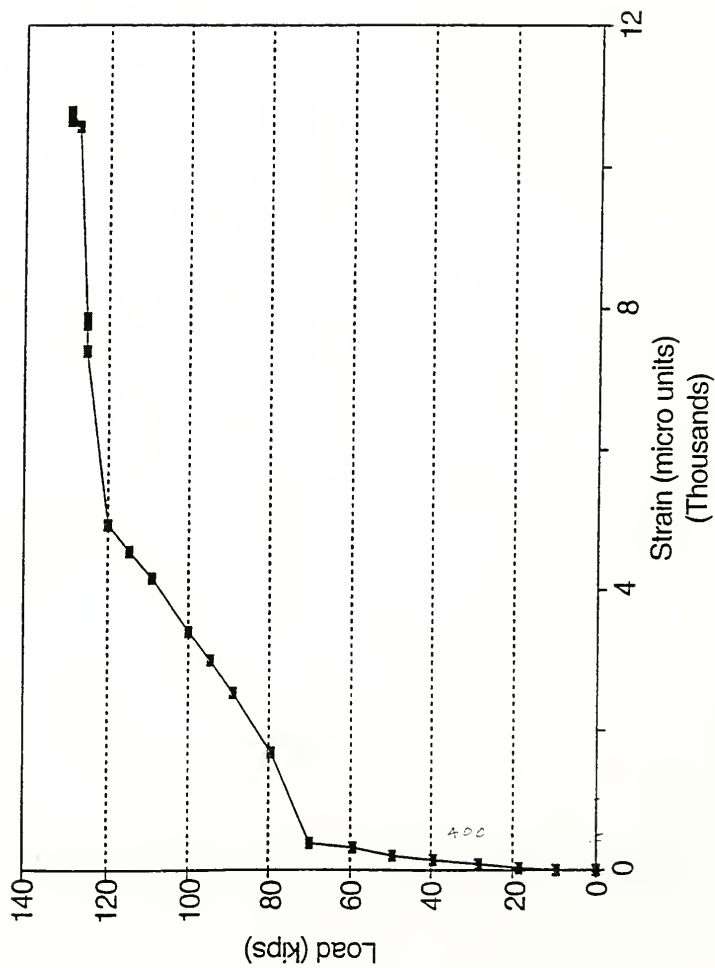


Figure 4.50 Load versus Strain in the strand at #C10 of Specimen 5

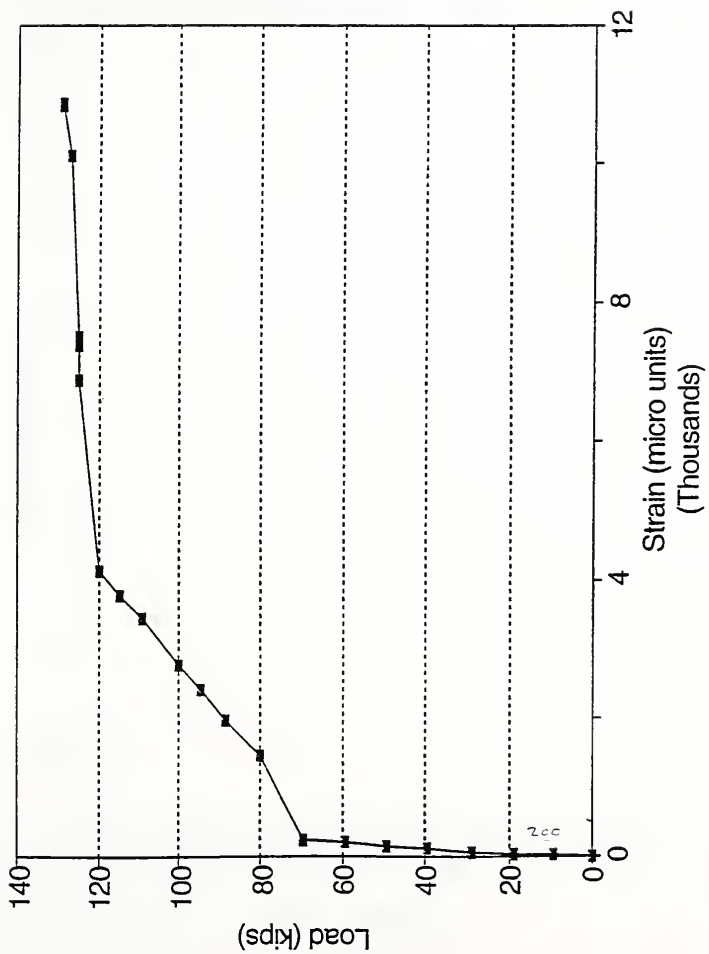


Figure 4.51 Load versus Strain in the strand at #C11 of Specimen 5

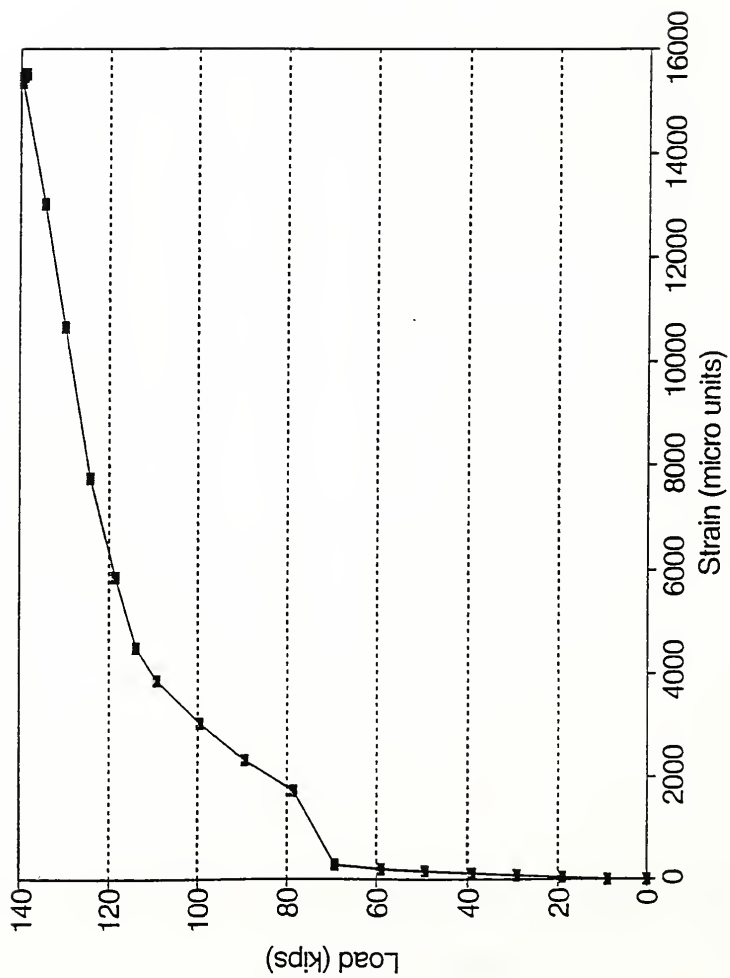


Figure 4.52 Load versus Strain in the strand at #C2 of Specimen 6

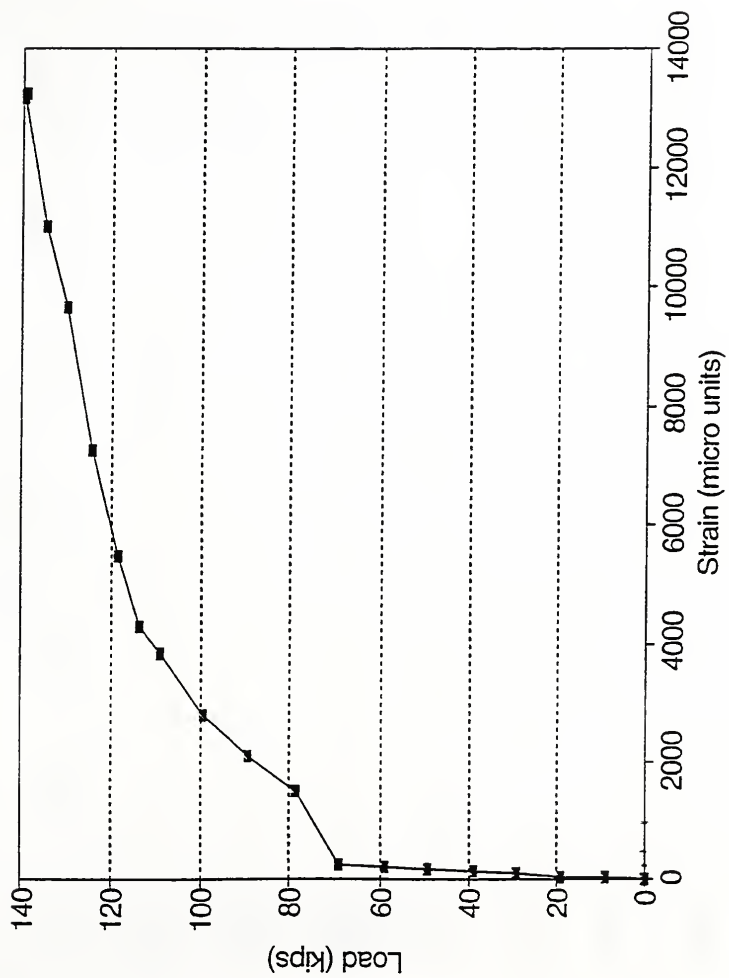


Figure 4.53 Load versus Strain in the strand at #C8 of Specimen 6

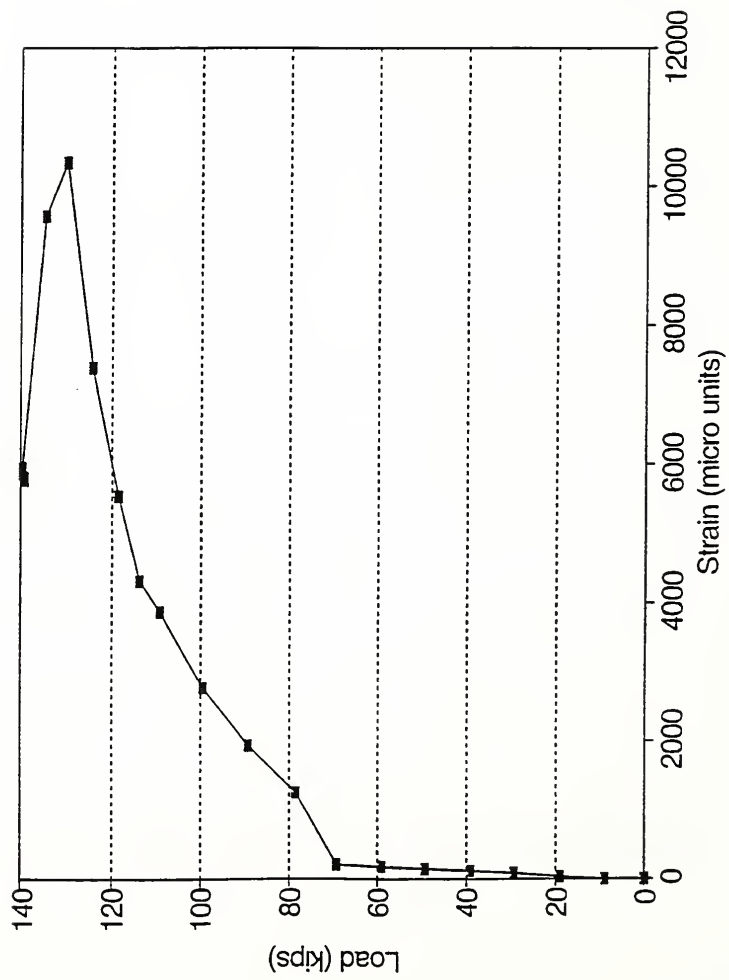


Figure 4.54 Load versus Strain in the strand at #C10 of Specimen 6

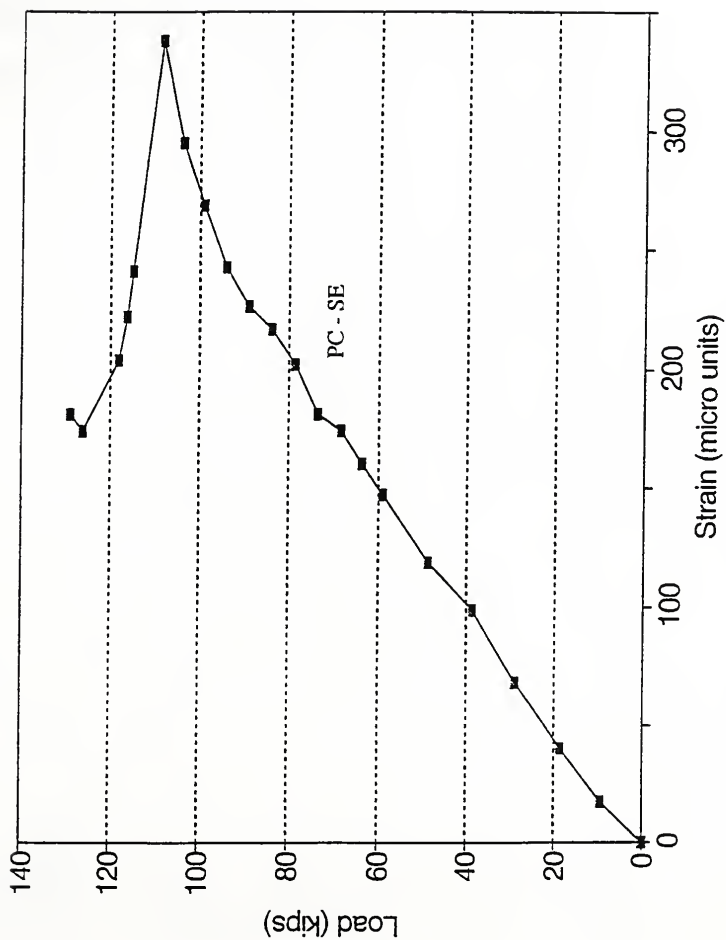


Figure 4.55 Load versus Strain at strand level of Specimen 1

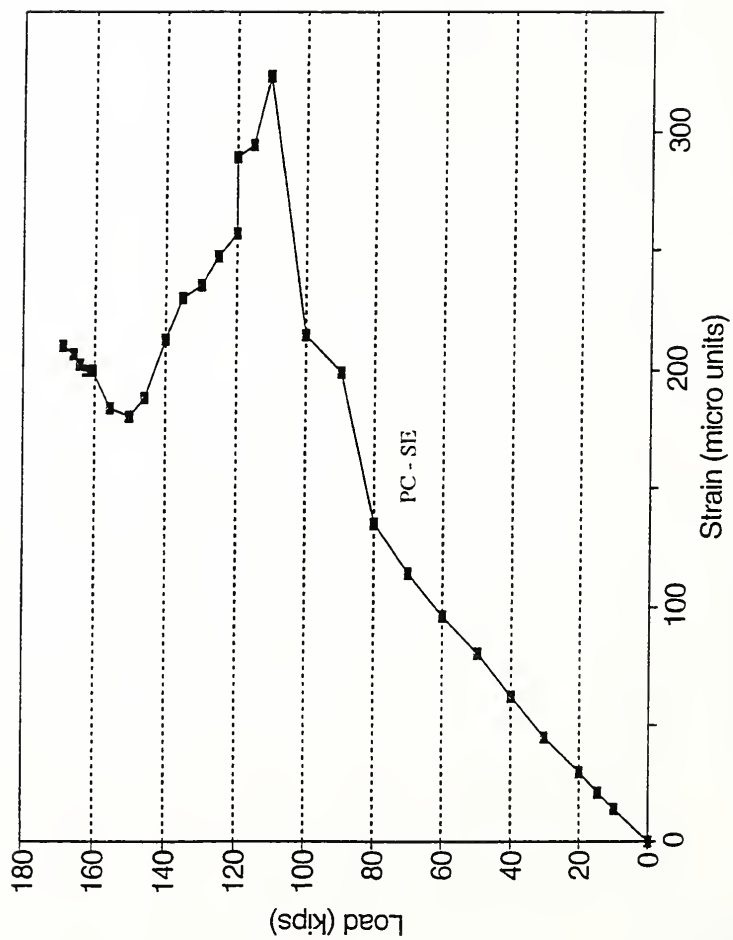


Figure 4.56 Load versus Strain at strand level of Specimen 2

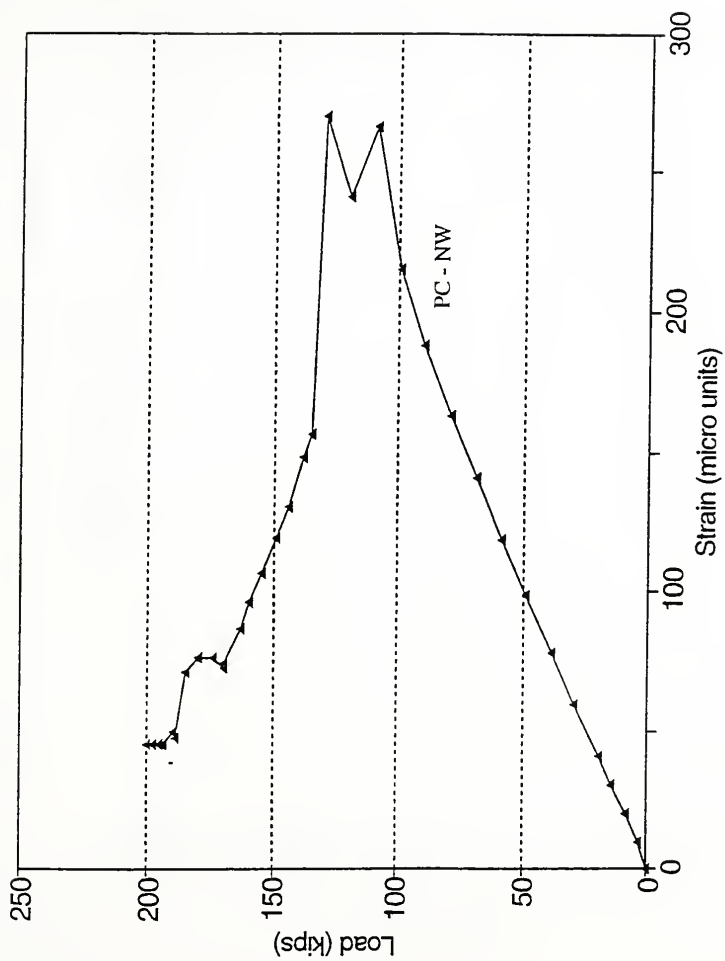


Figure 4.57 Load versus Strain at strand level of Specimen 3

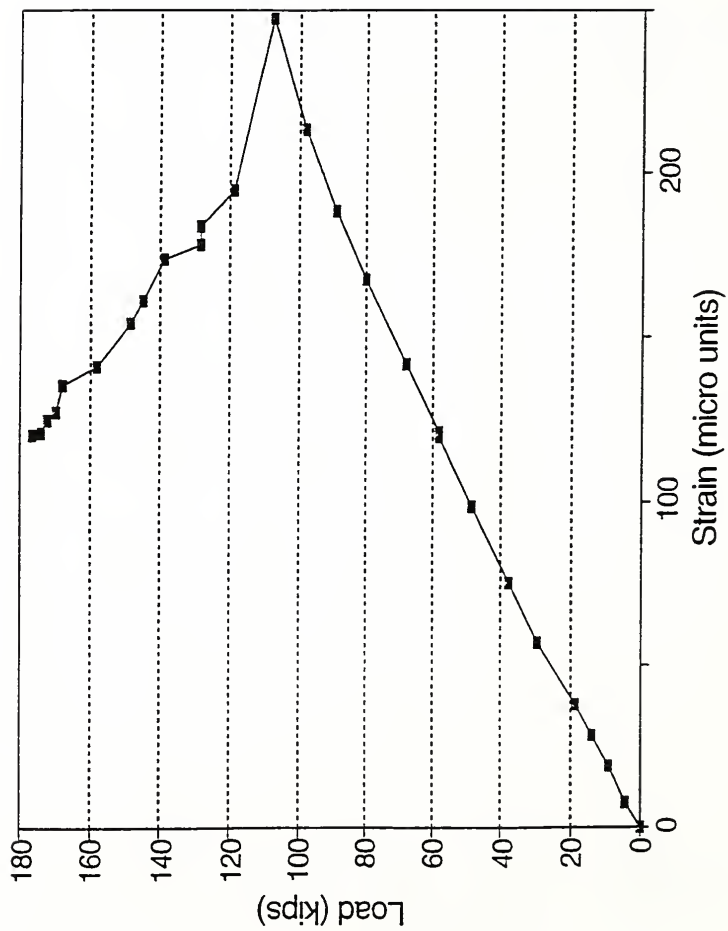


Figure 4.58 Load versus Average strain at strand level of Specimen 4

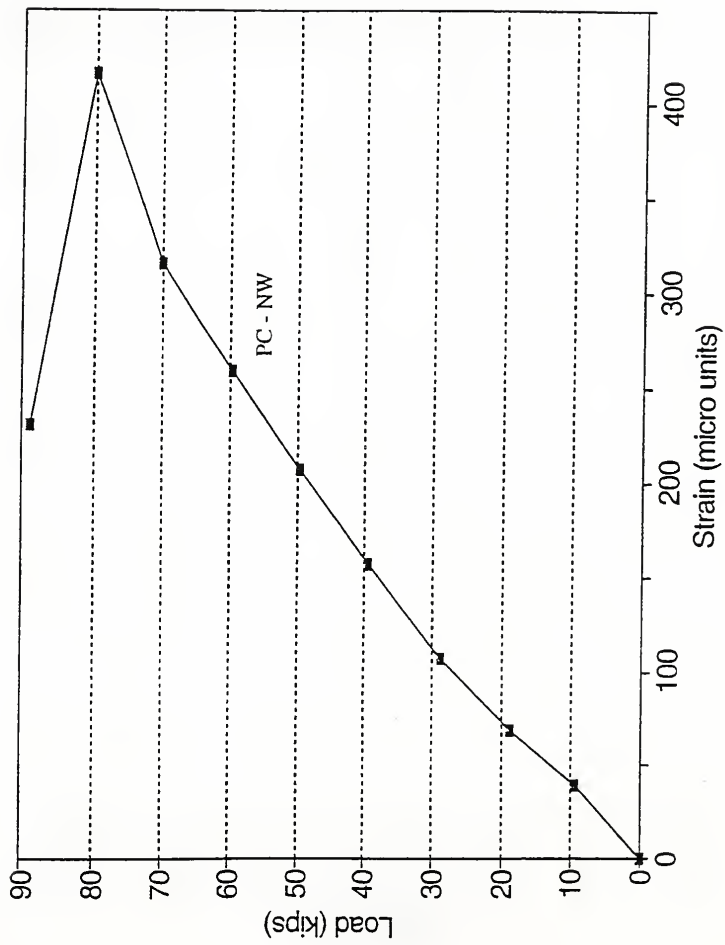


Figure 4.59 Load versus Strain at strand level of Specimen 5

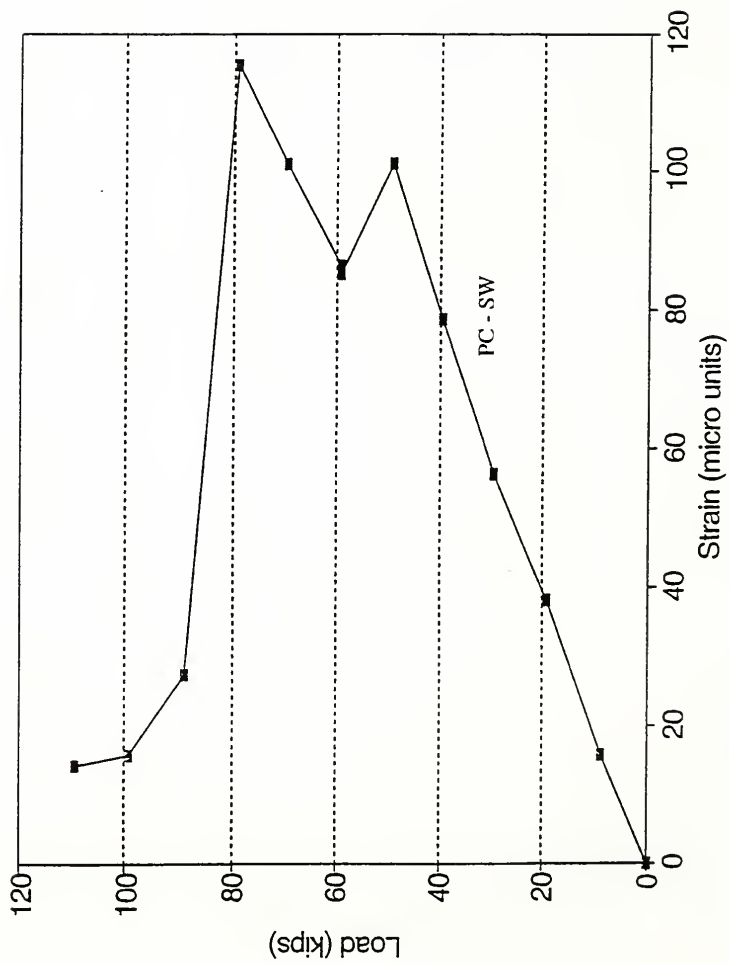


Figure 4.60 Load versus Strain at strand level of Specimen 6

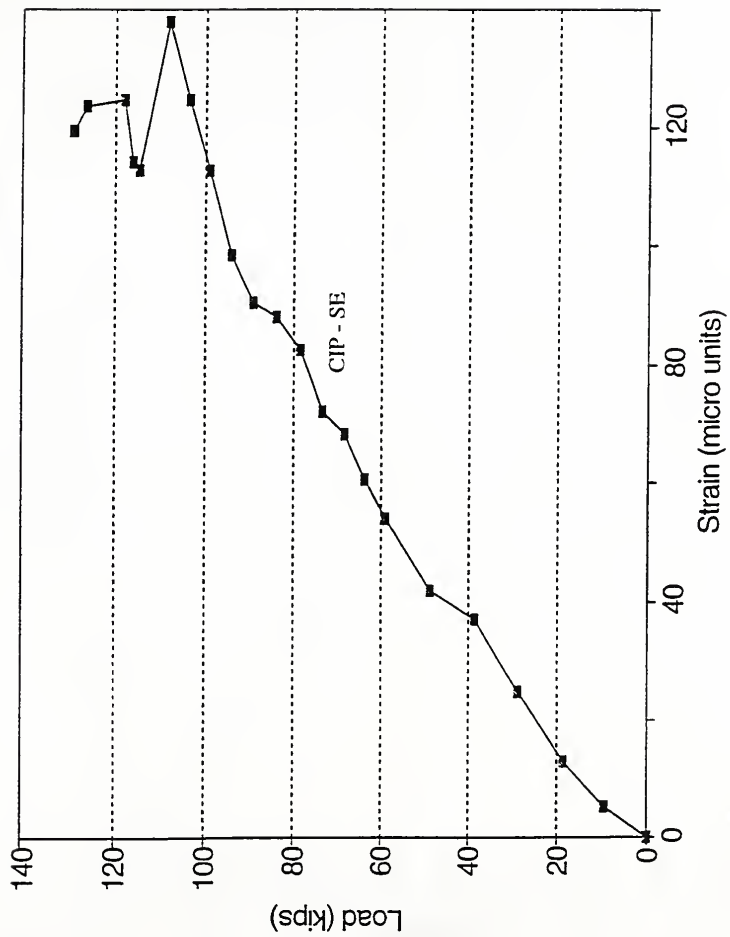


Figure 4.61 Load versus Strain at CIP gage level of Specimen 1

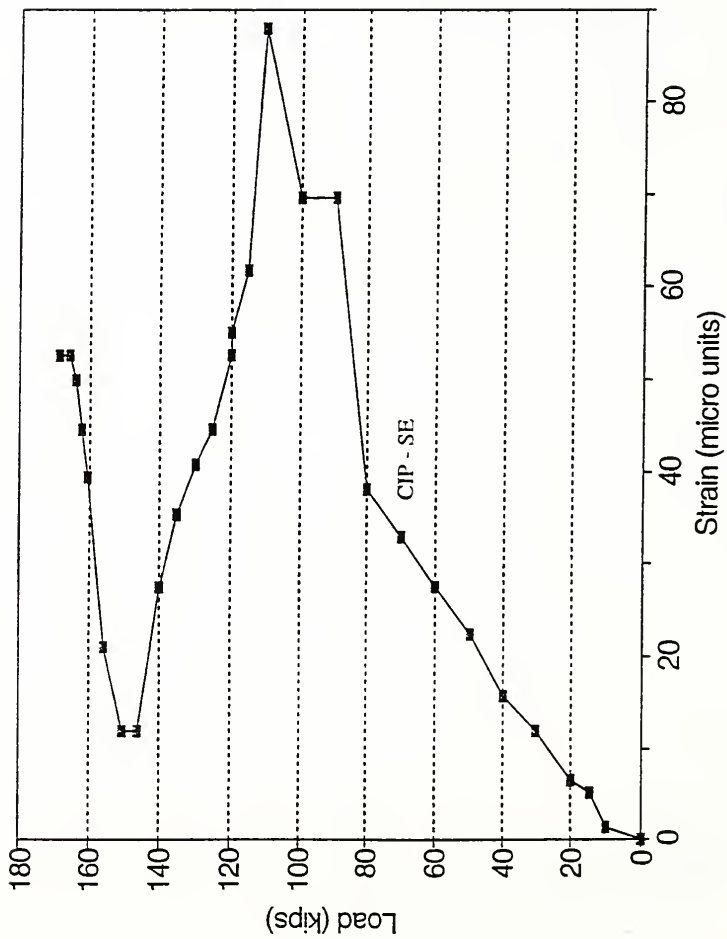


Figure 4.62 Load versus Strain at CIP gage level of Specimen 2

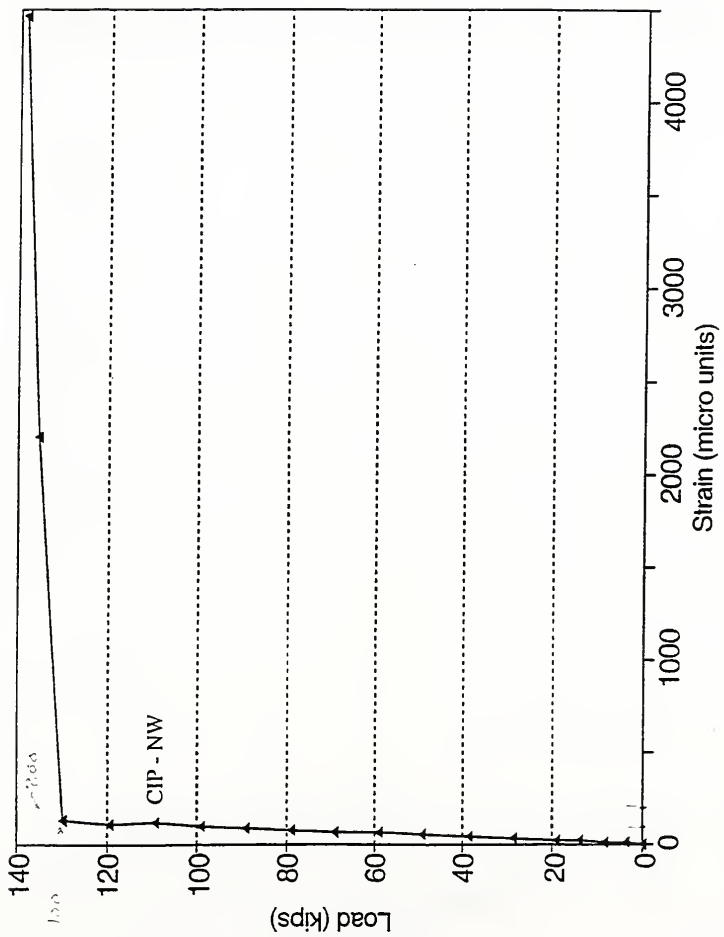


Figure 4.63 Load versus Strain at CIP gage level of Specimen 3

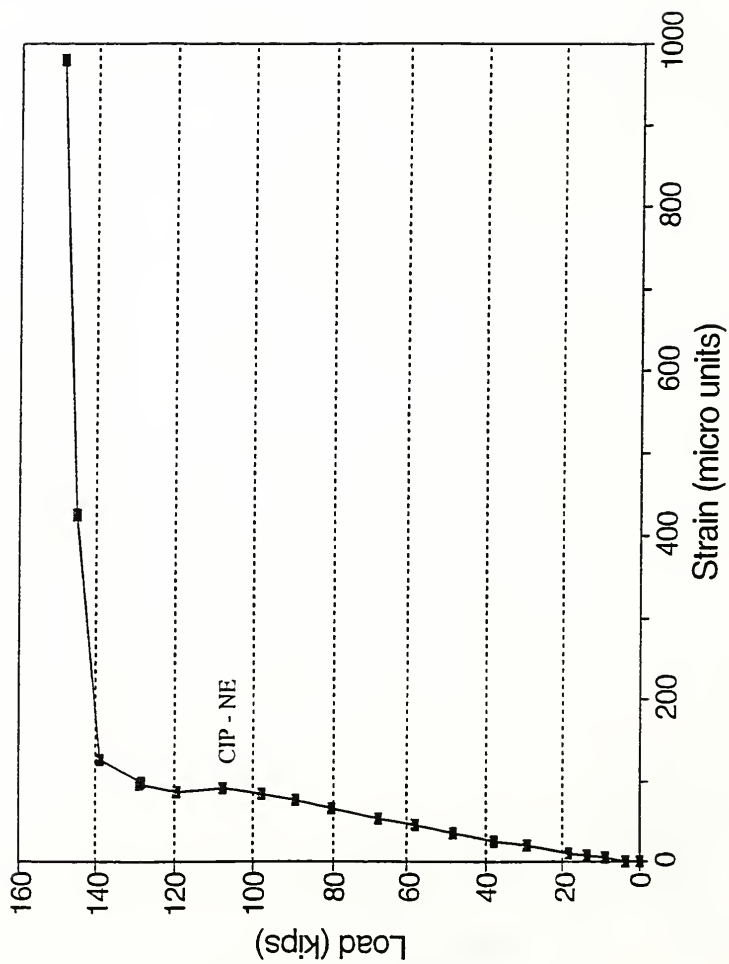


Figure 4.64 Load versus Strain at CIP gage level of Specimen 4

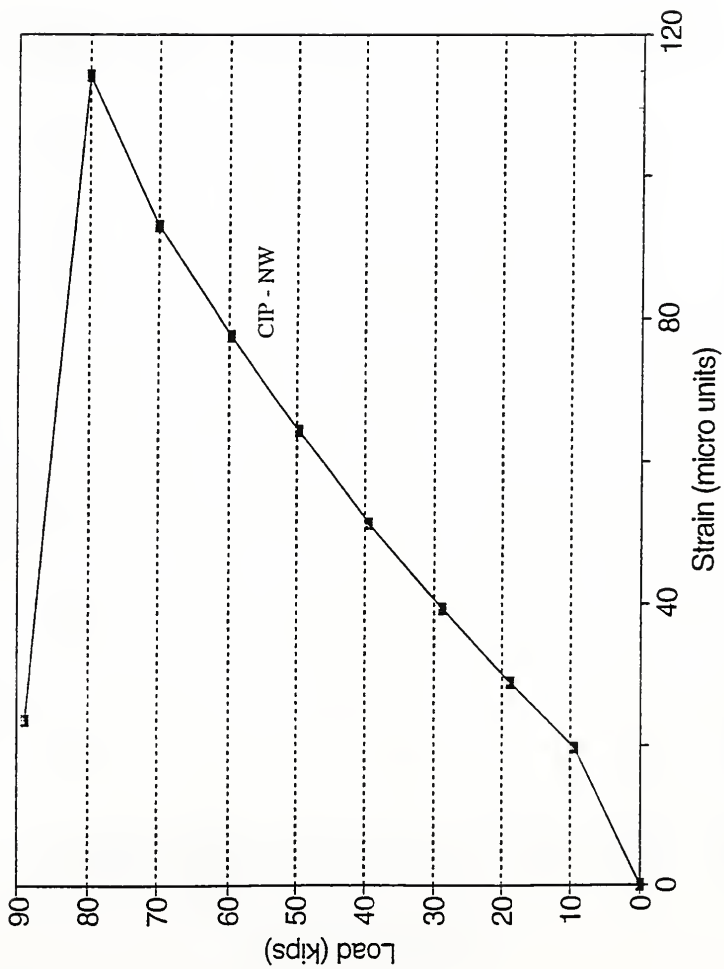


Figure 4.65 Load versus Strain at CIP gage level of Specimen 5

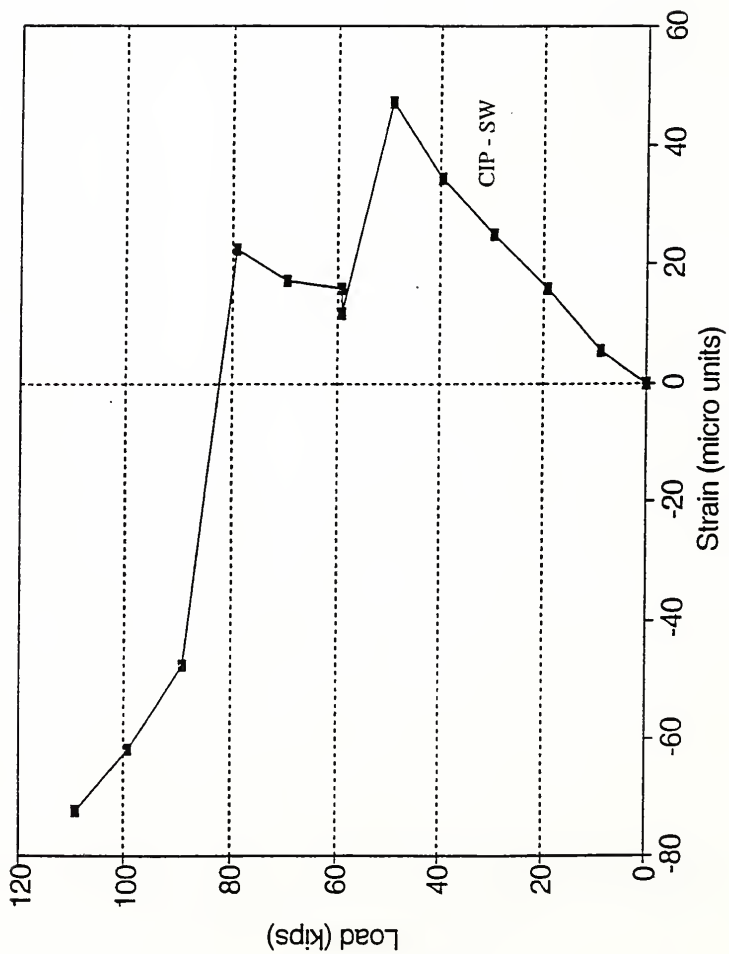


Figure 4.66 Load versus Strain at CIP gage level of Specimen 6

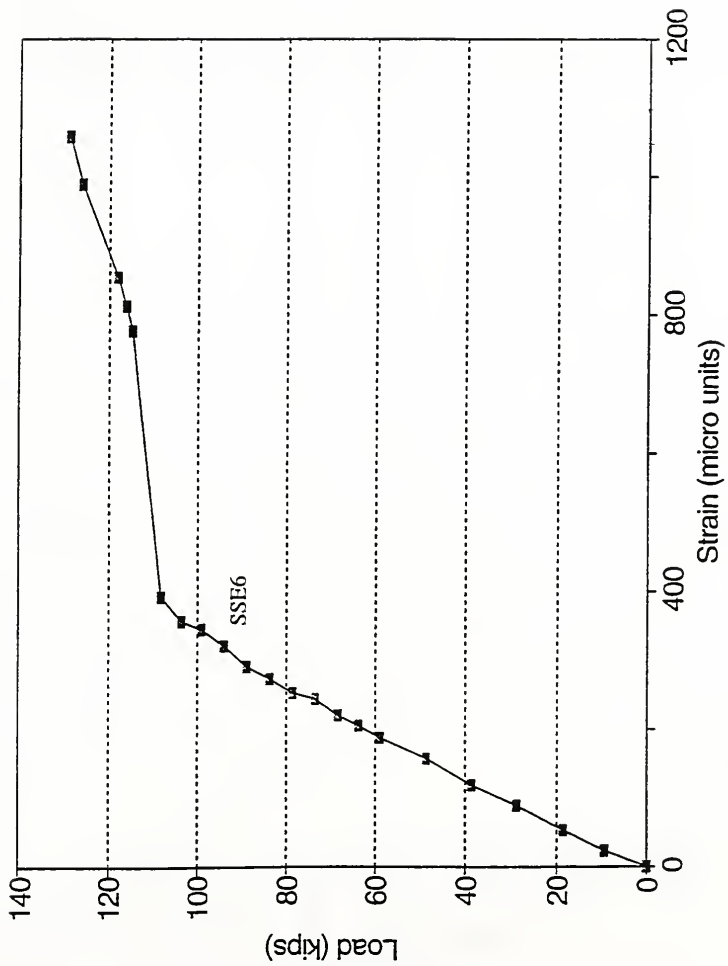


Figure 4.67 Load versus Strain at the top of CIP slab (SSE6) of Specimen I

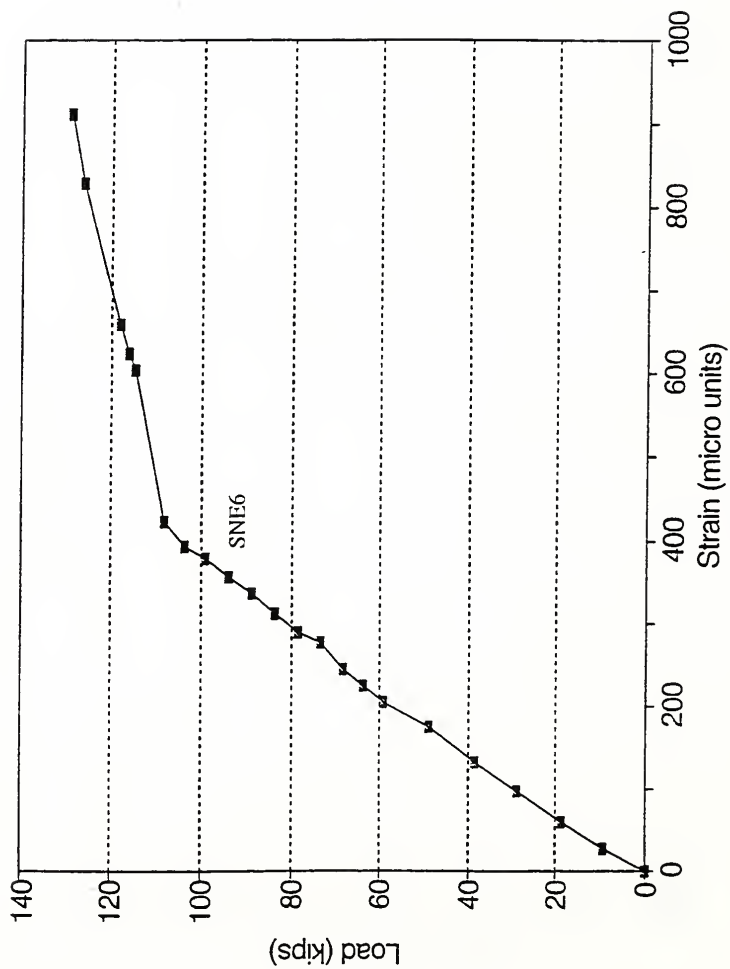


Figure 4.68 Load versus Strain at the top of CIP slab (SNE6) of Specimen I

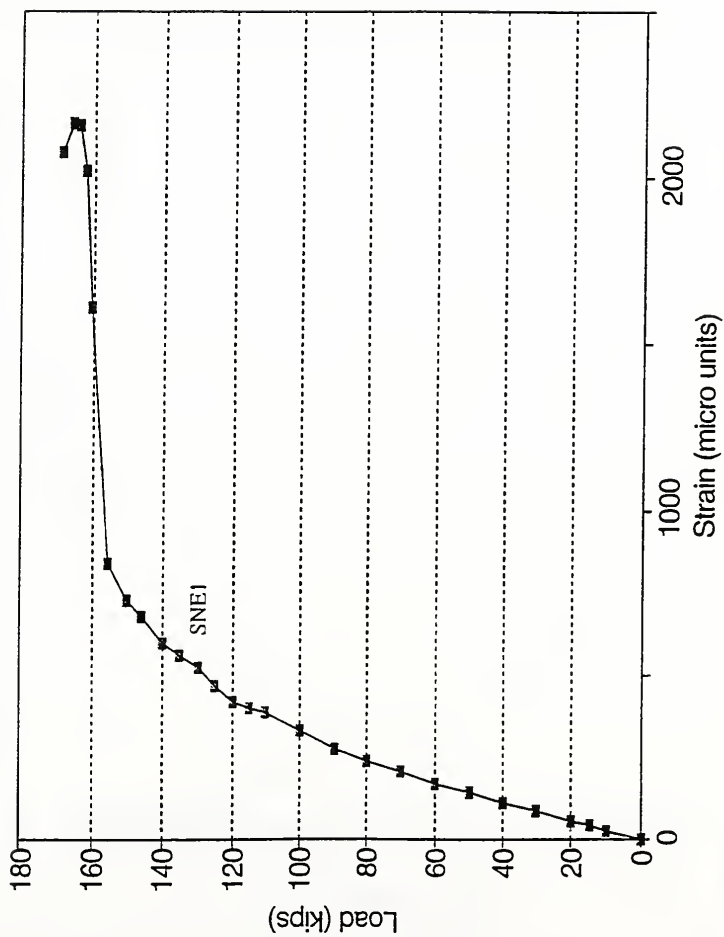


Figure 4.69 Load versus Strain at the top of CIP slab (SNE1) of Specimen 2

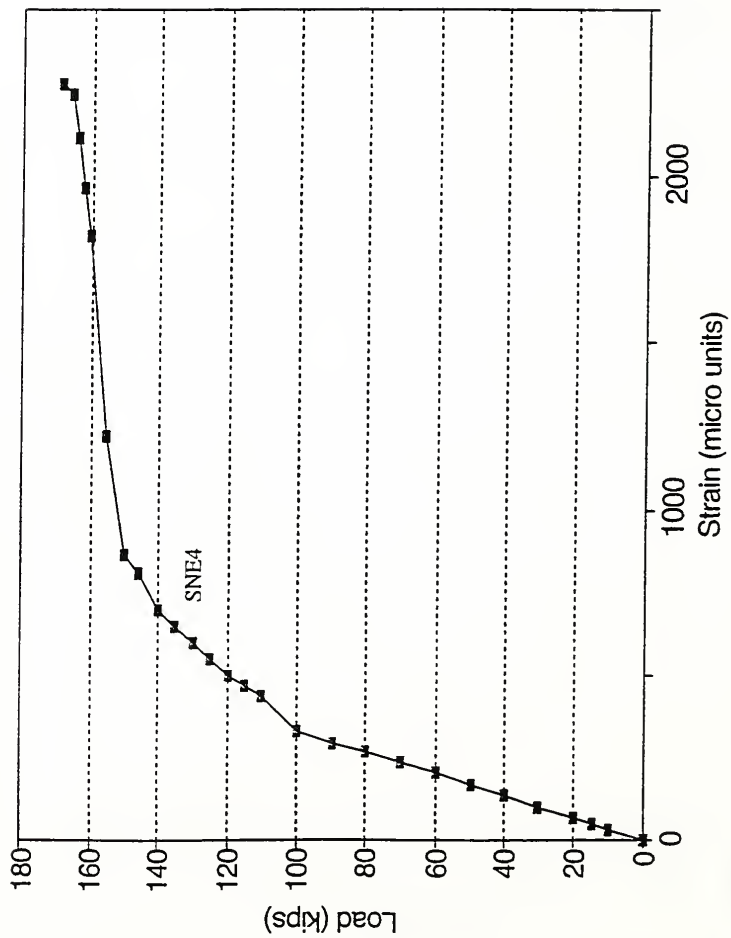


Figure 4.70 Load versus Strain at the top of CIP slab (SNE4) of Specimen 2

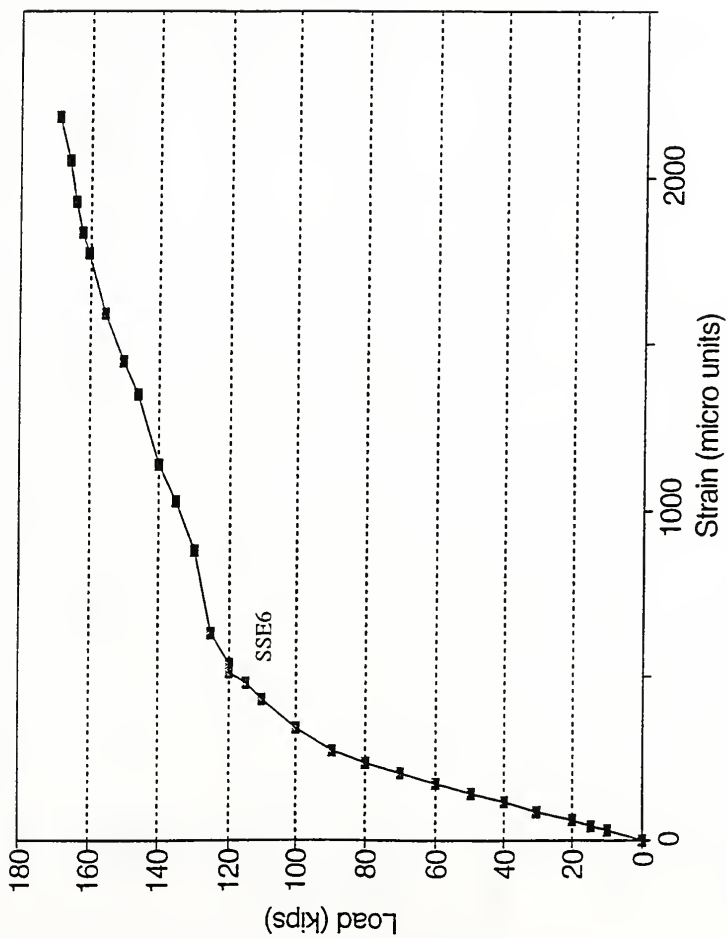


Figure 4.71 Load versus Strain at the top of CIP slab (SSE6) of Specimen 2

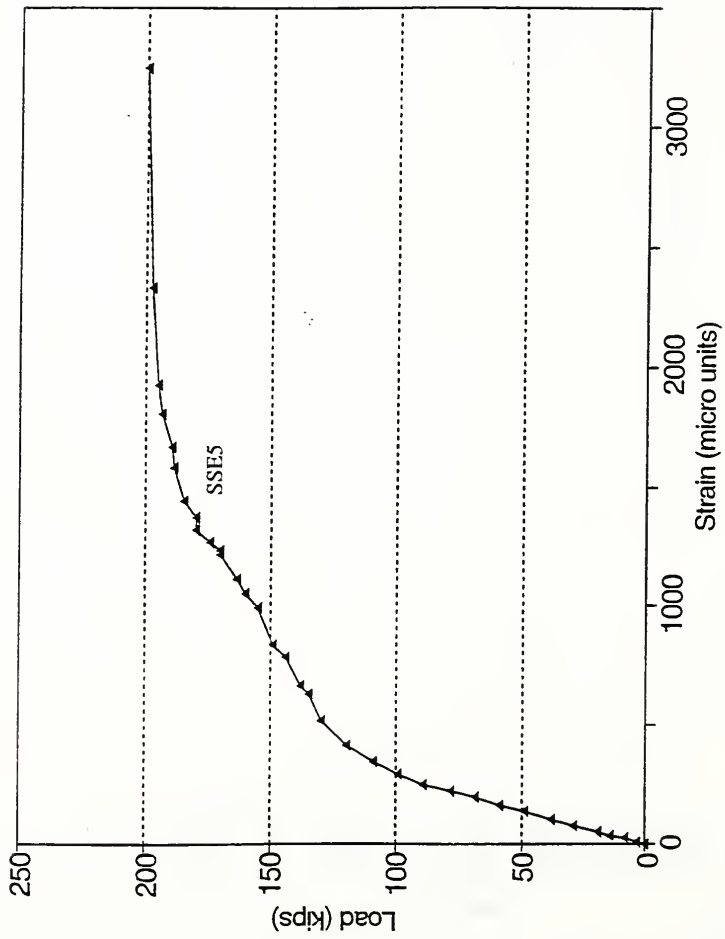


Figure 4.72 Load versus Strain at the top of CIP slab (SSE5) of Specimen 3

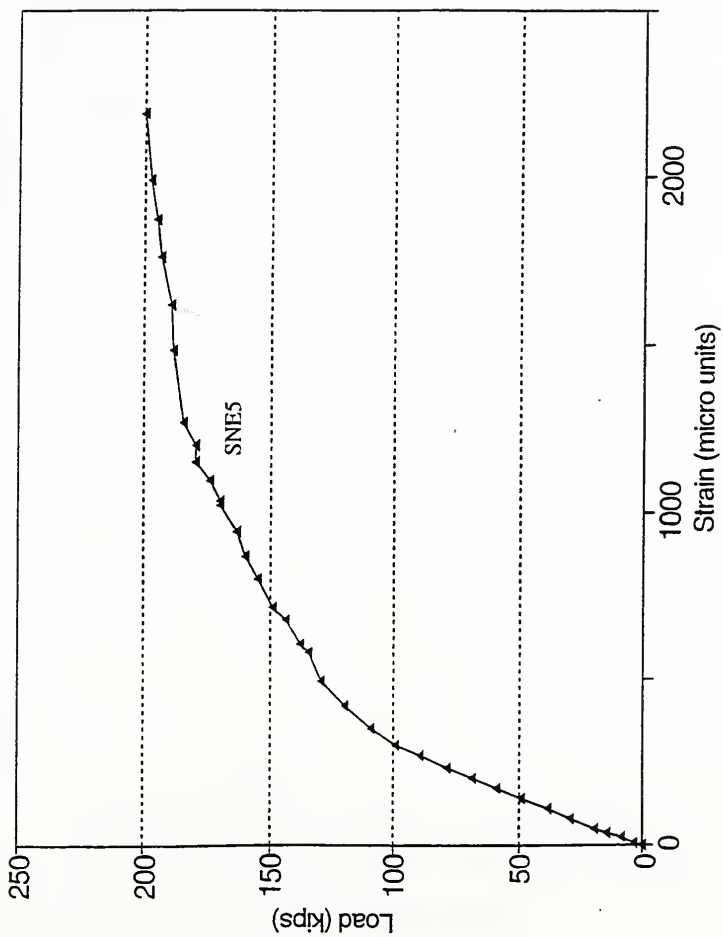


Figure 4.73 Load versus Strain at the top of CIP slab (SNE5) of Specimen 3

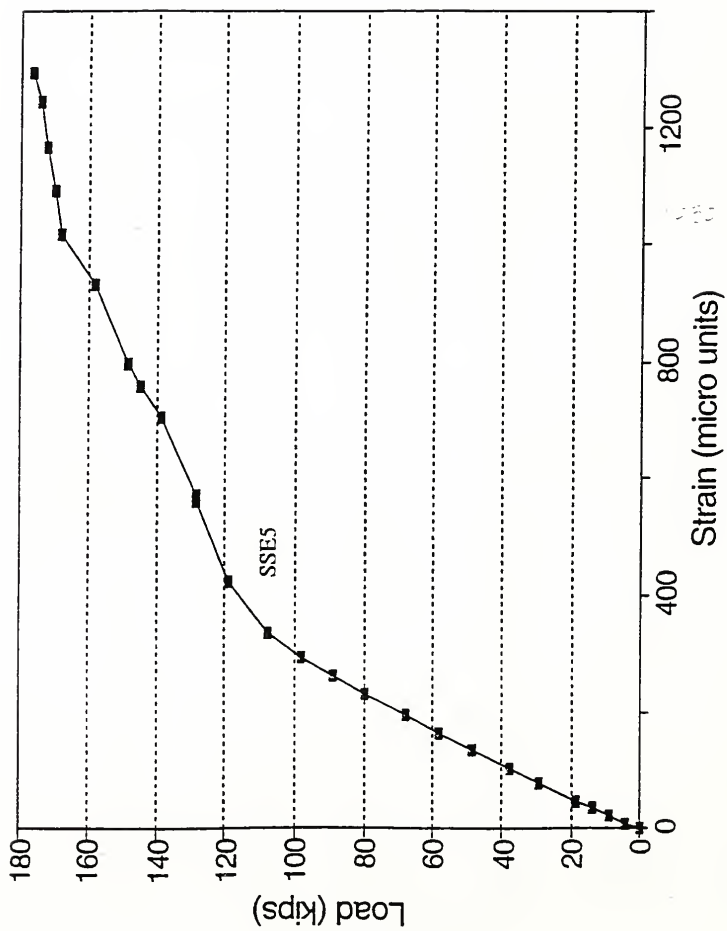


Figure 4.74 Load versus Strain at the top of CIP slab (SSE5) of Specimen 4

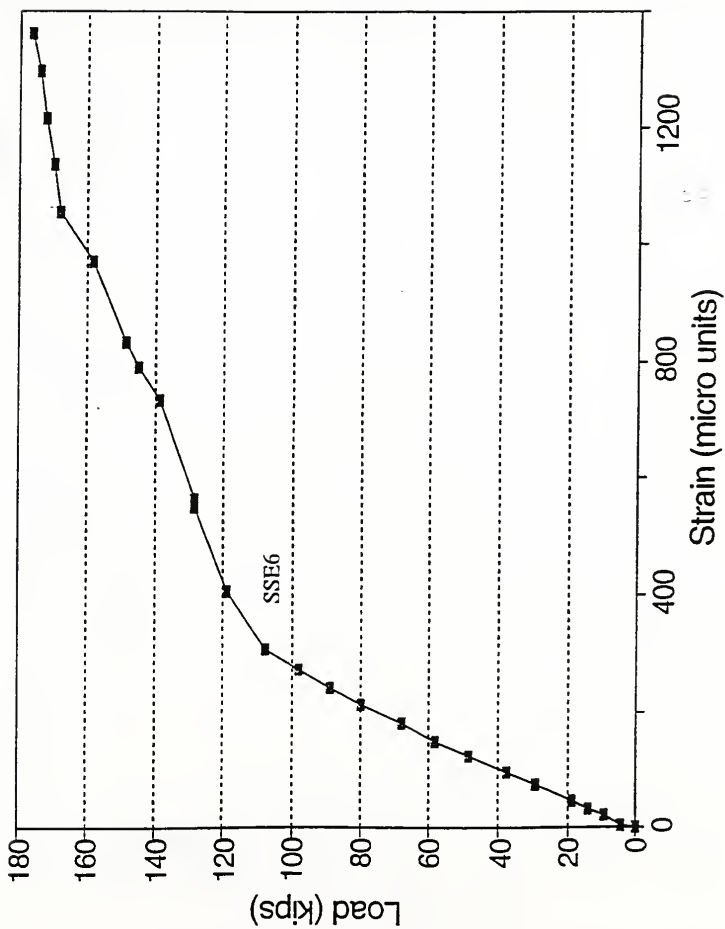


Figure 4.75 Load versus Strain at the top of CLP slab (SSE6) of Specimen 4

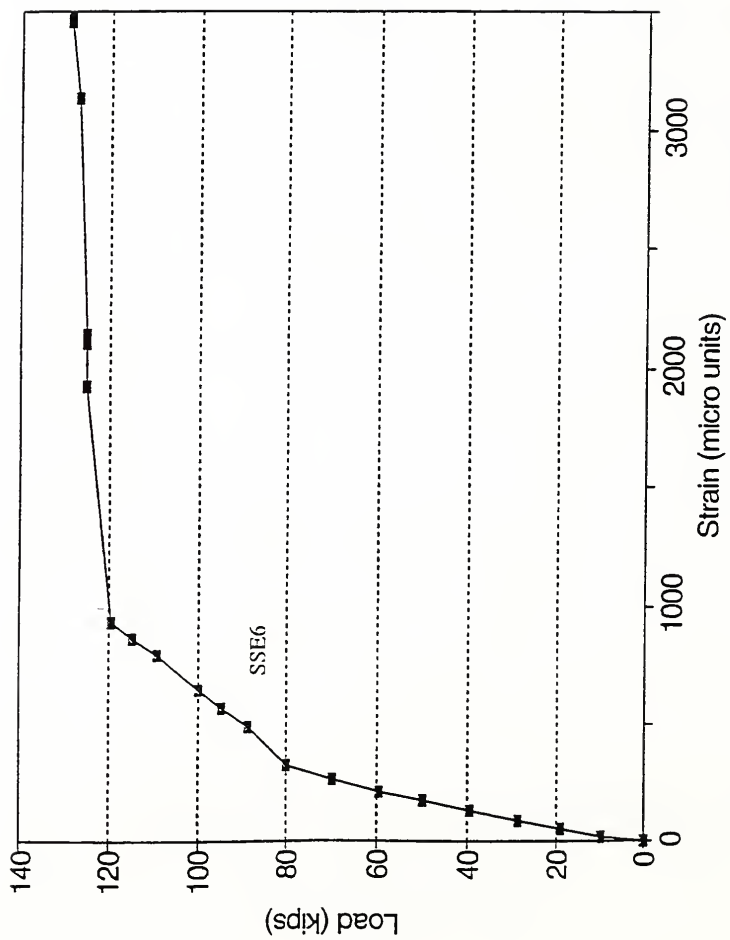


Figure 4.76 Load versus Strain at the top of CIP slab (SSE6) of Specimen 5

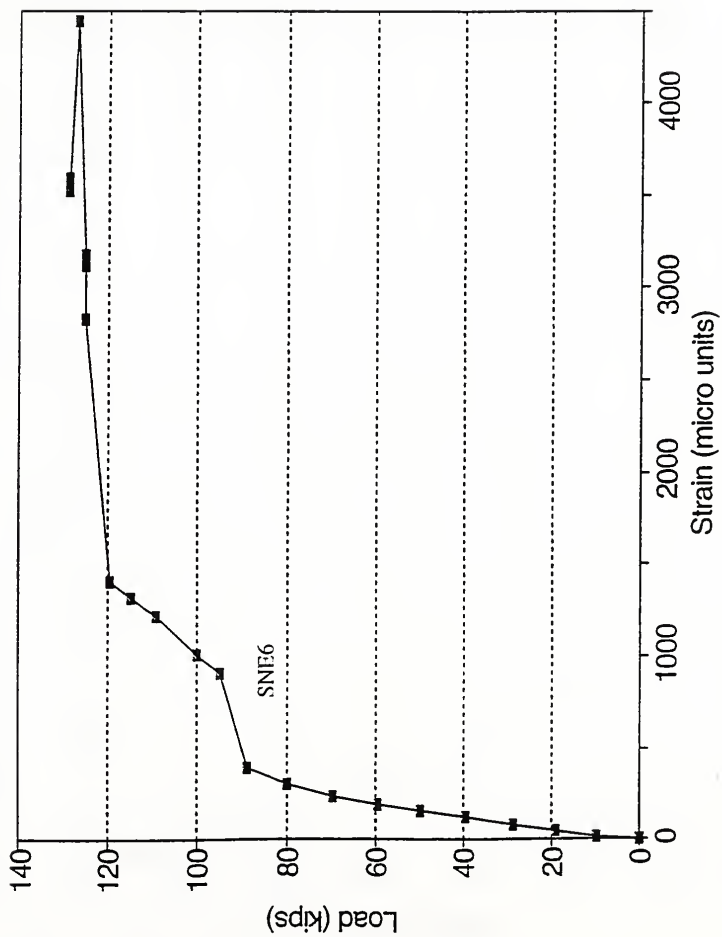


Figure 4.77 Load versus Strain at the top of CIP slab (SNE6) of Specimen 5

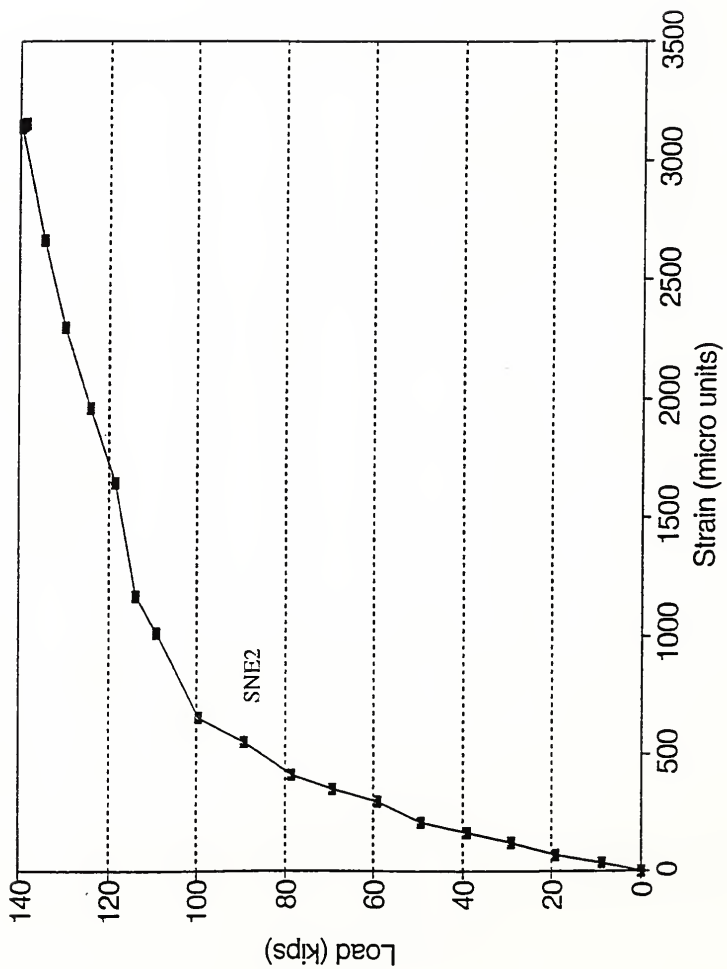


Figure 4.78 Load versus Strain at the top of CIP slab (SNE2) of Specimen 6

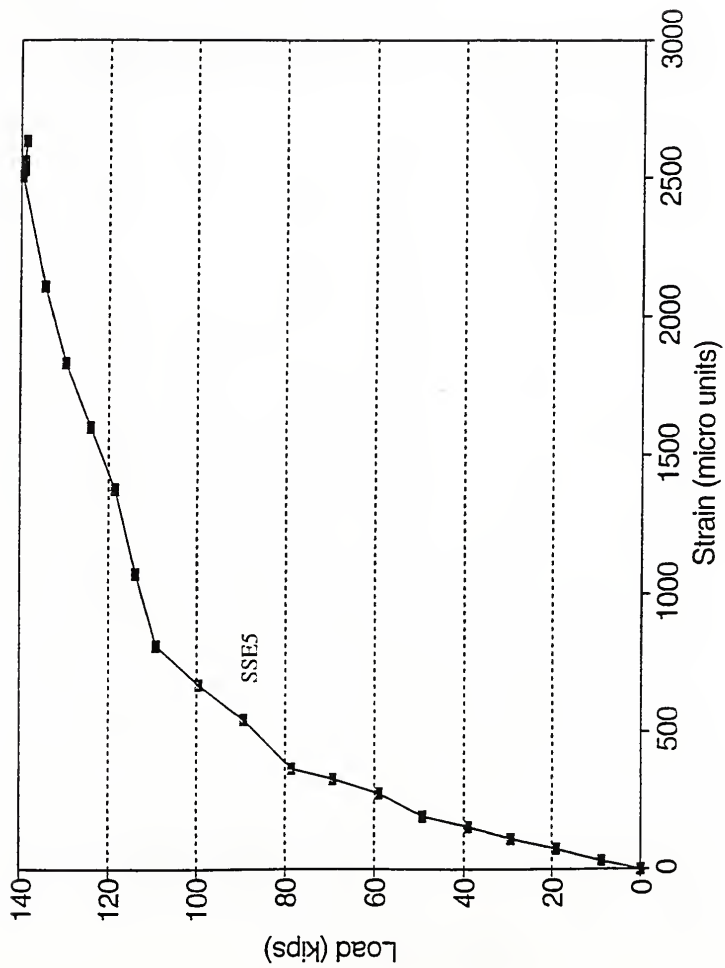


Figure 4.79 Load versus Strain at the top of CIP slab (SSE5) of Specimen 6

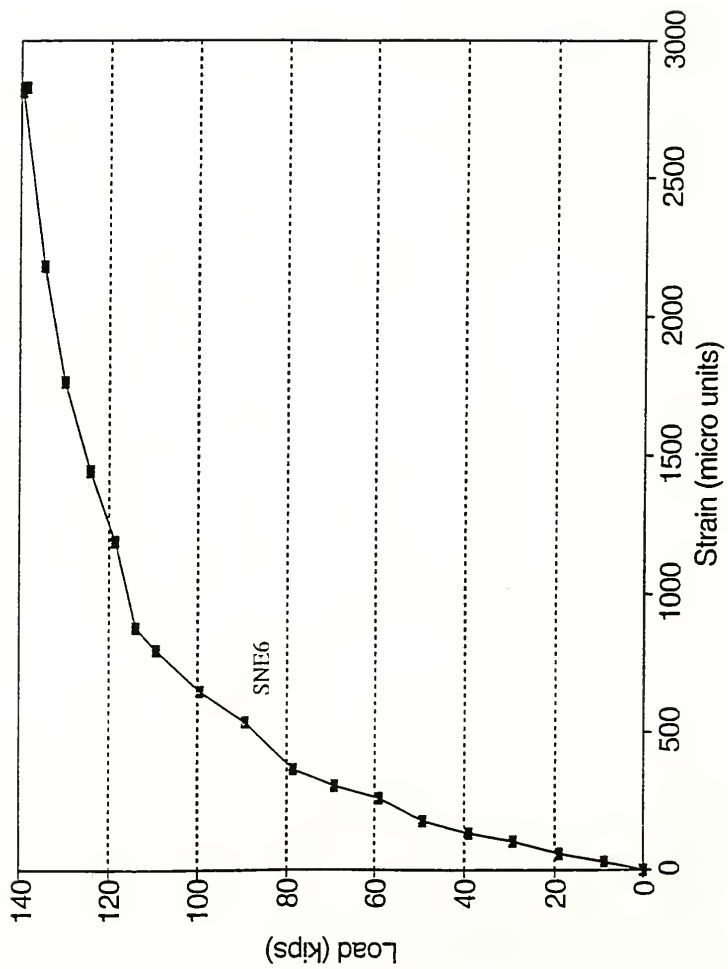


Figure 4.80 Load versus Strain at the top of CIP slab (SNE6) of Specimen 6

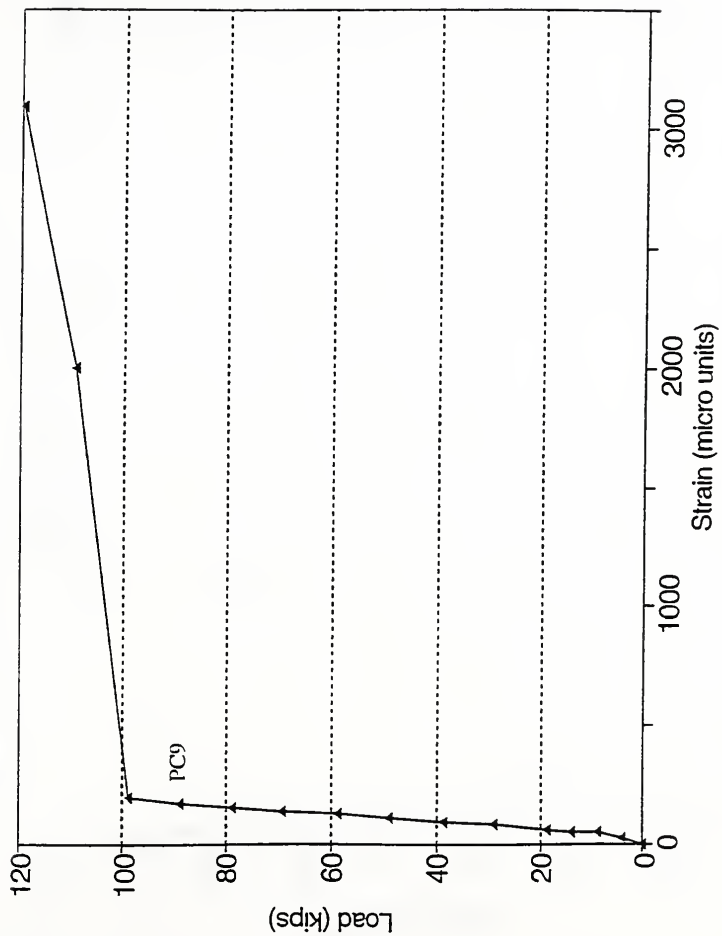


Figure 4.81 Load versus Strain at the interface at #PC9 of Specimen 3

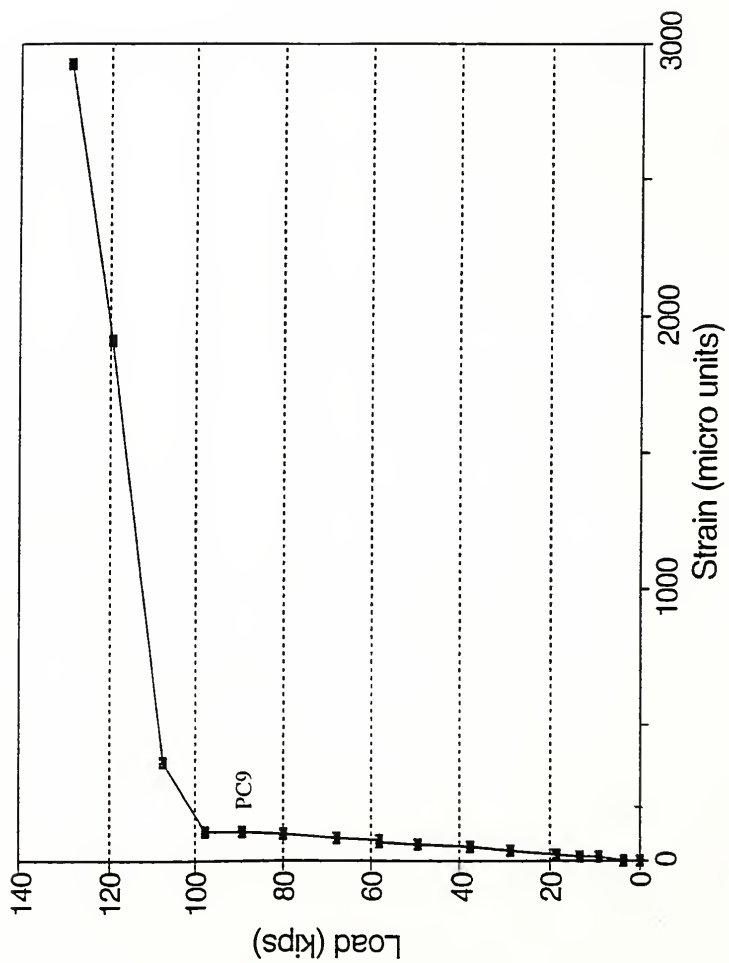


Figure 4.82 Load versus Strain at the interface at #PC9 of Specimen 4

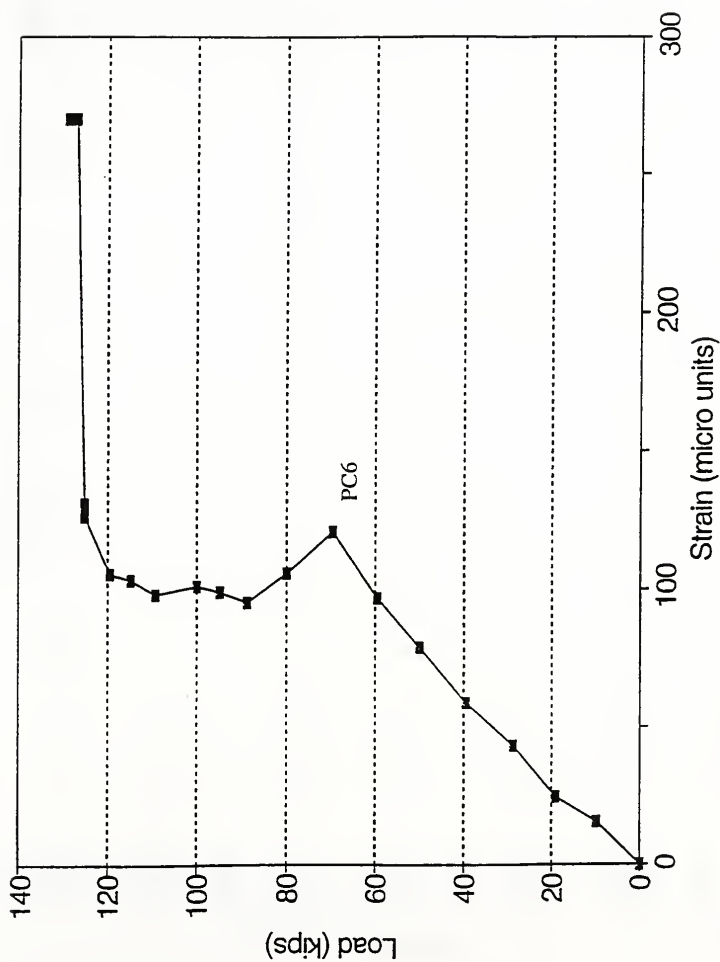


Figure 4.83 Load versus Strain at the interface at #PC6 of Specimen 5

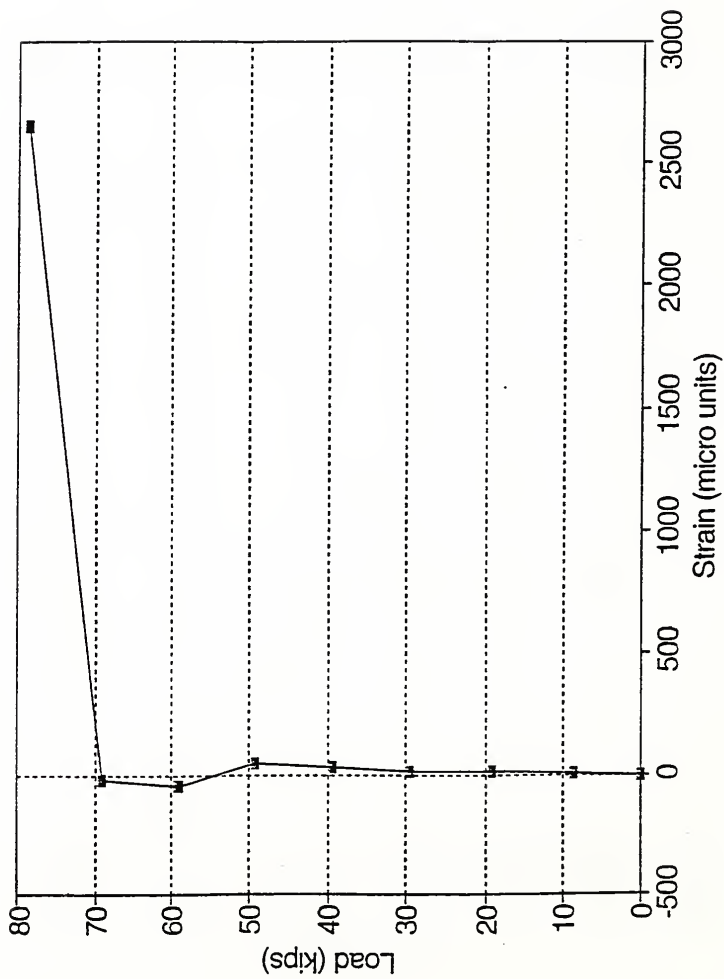


Figure 4.84 Load versus Strain at the interface at #PC2 of Specimen 6

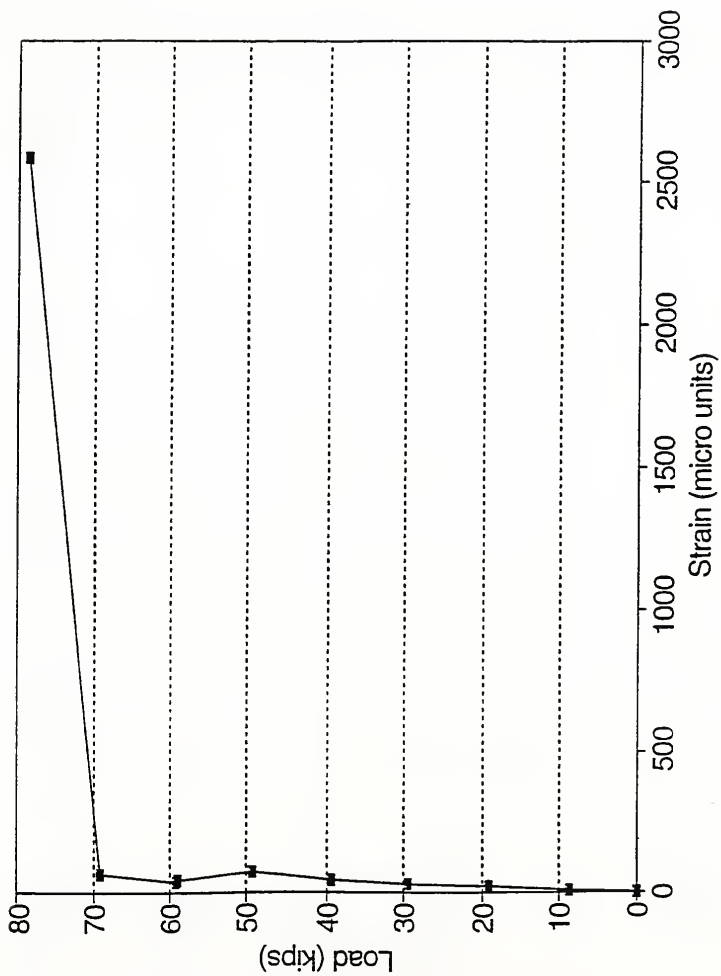


Figure 4.85 Load versus Strain at the interface at #PC3 of Specimen 6

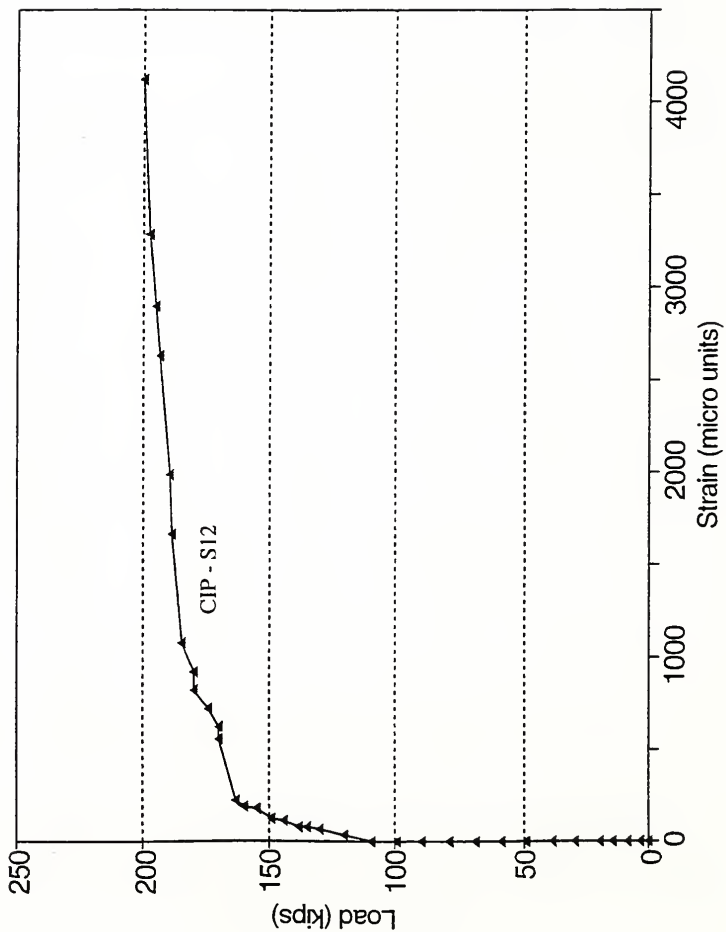


Figure 4.86 Load versus Strain in the CIP Bar on southern side of Specimen 3

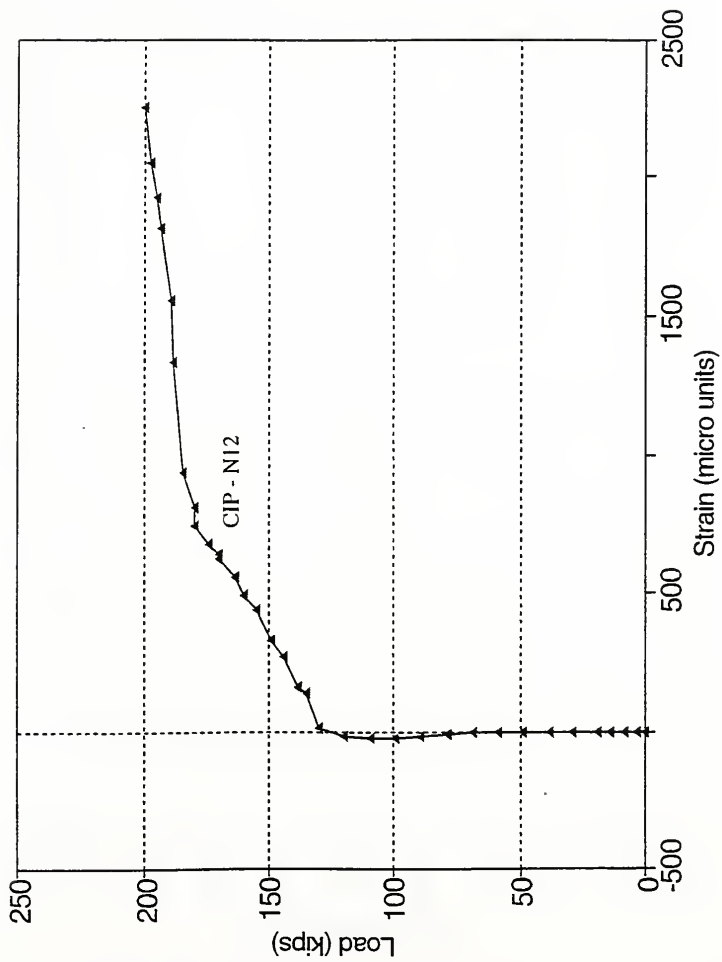


Figure 4.87 Load versus Strain in the CIP Bar on northern side of Specimen 3

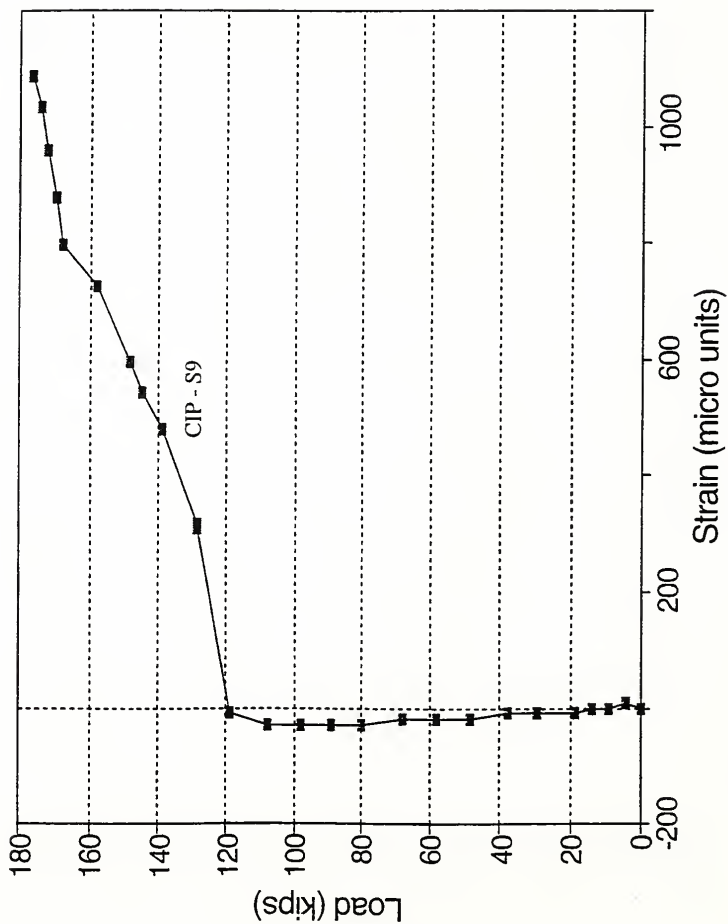


Figure 4.88 Load versus Strain in the CIP Bar on southern side of Specimen 4

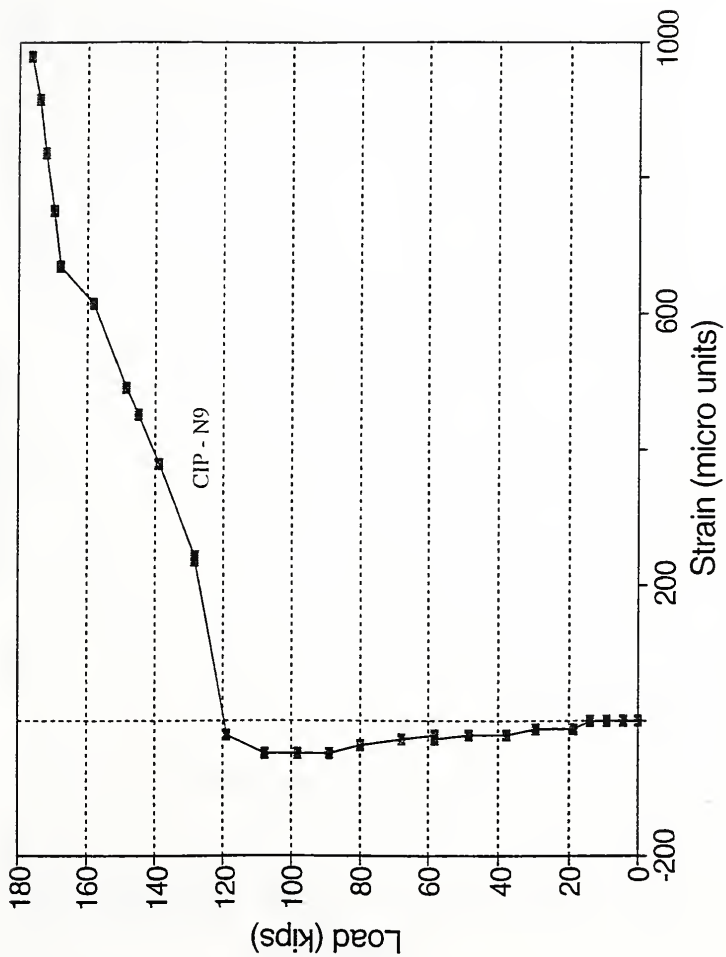


Figure 4.89 Load versus Strain in the CIP Bar on northern side of Specimen 4

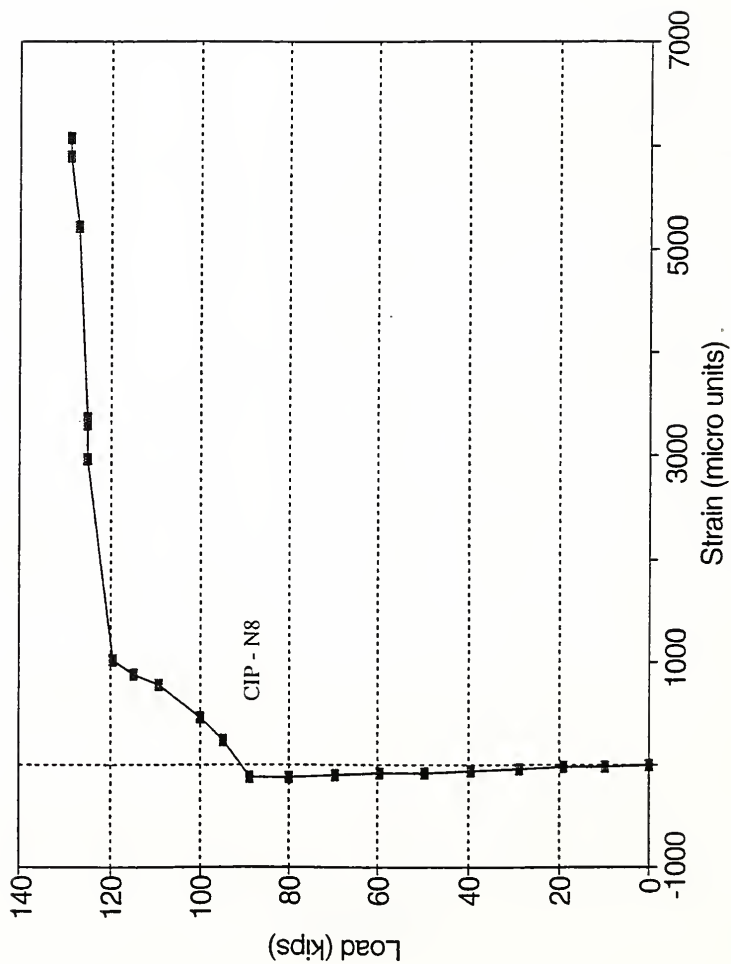


Figure 4.90 Load versus Strain in the CIP Bar on northern side of Specimen 5

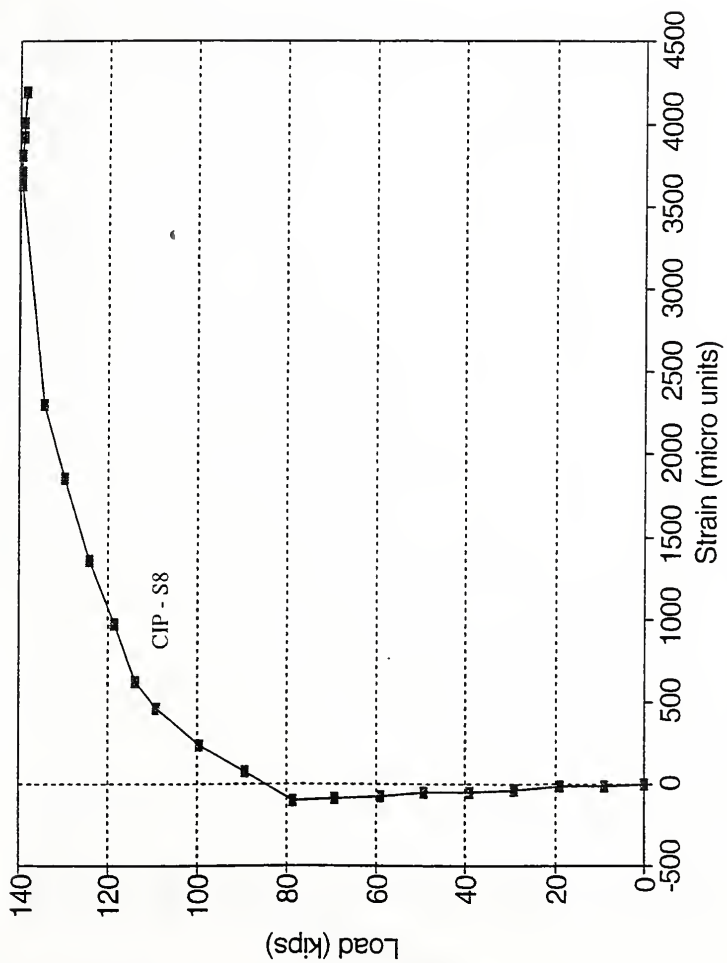


Figure 4.91 Load versus Strain in the CIP Bar on southern side of Specimen 6

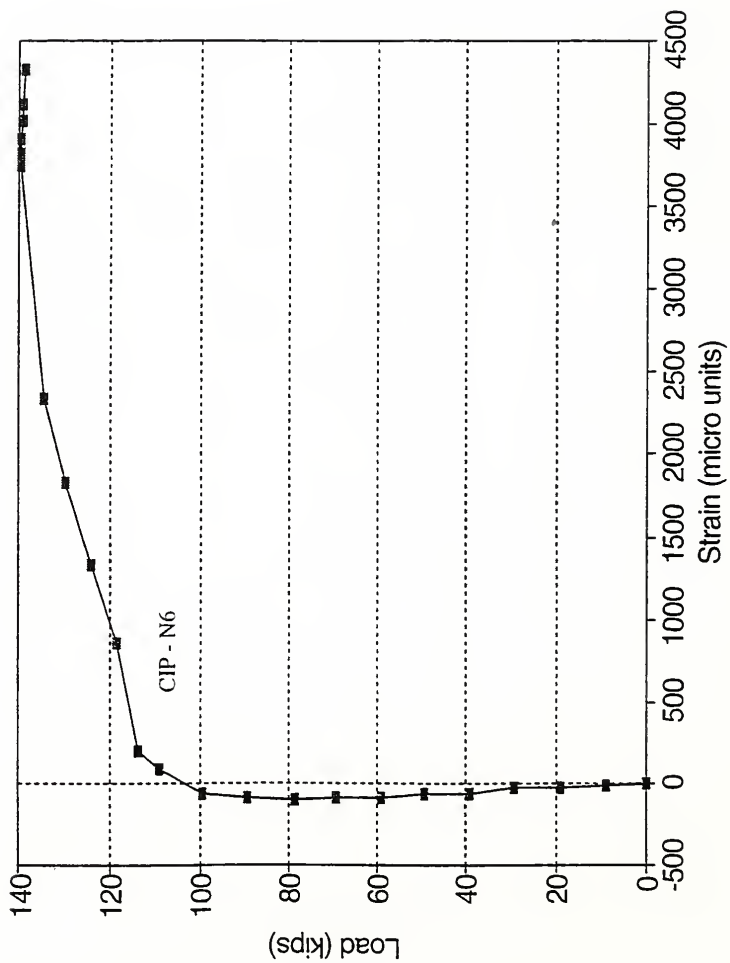


Figure 4.92 Load versus Strain in the CIP Bar on northern side of Specimen 6

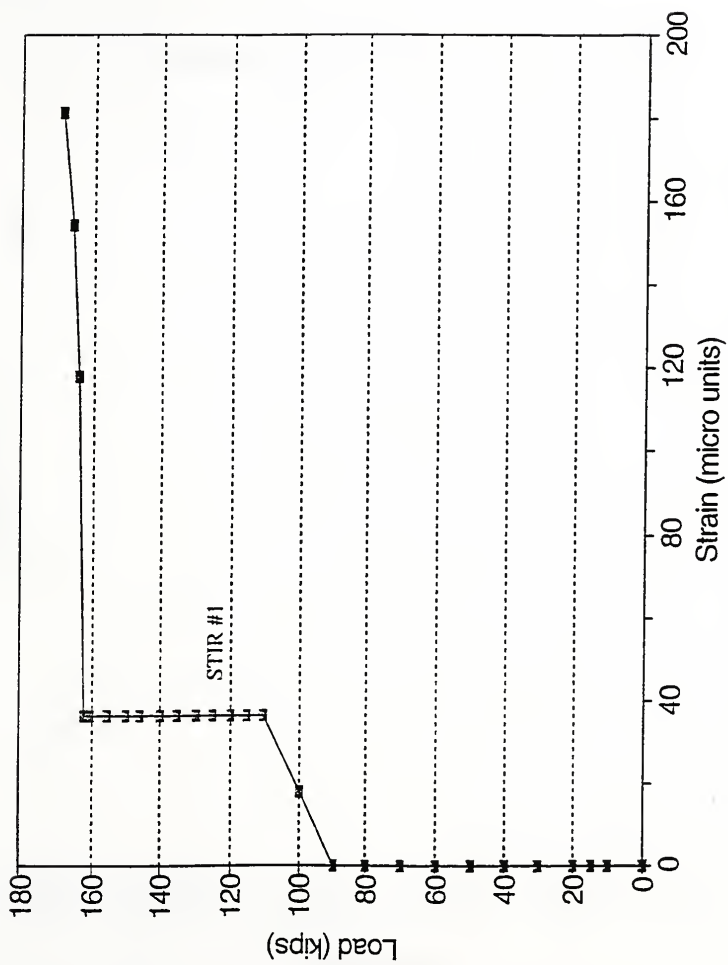


Figure 4.93 Load versus Strain in the horizontal shear connectors of Specimen 2

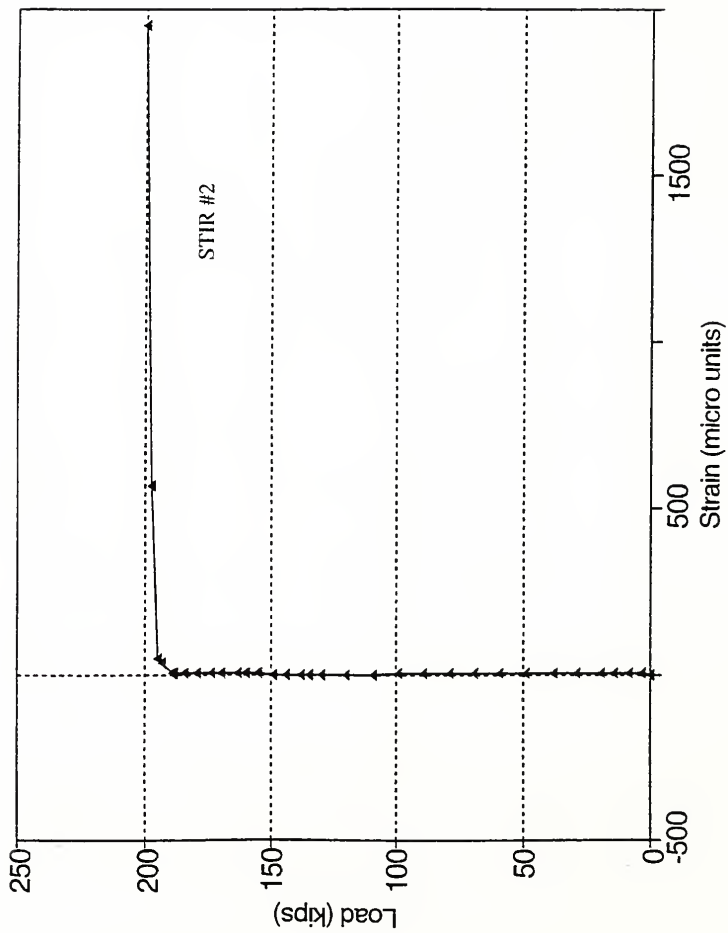


Figure 4.94 Load versus Strain in the horizontal shear connectors of Specimen 3

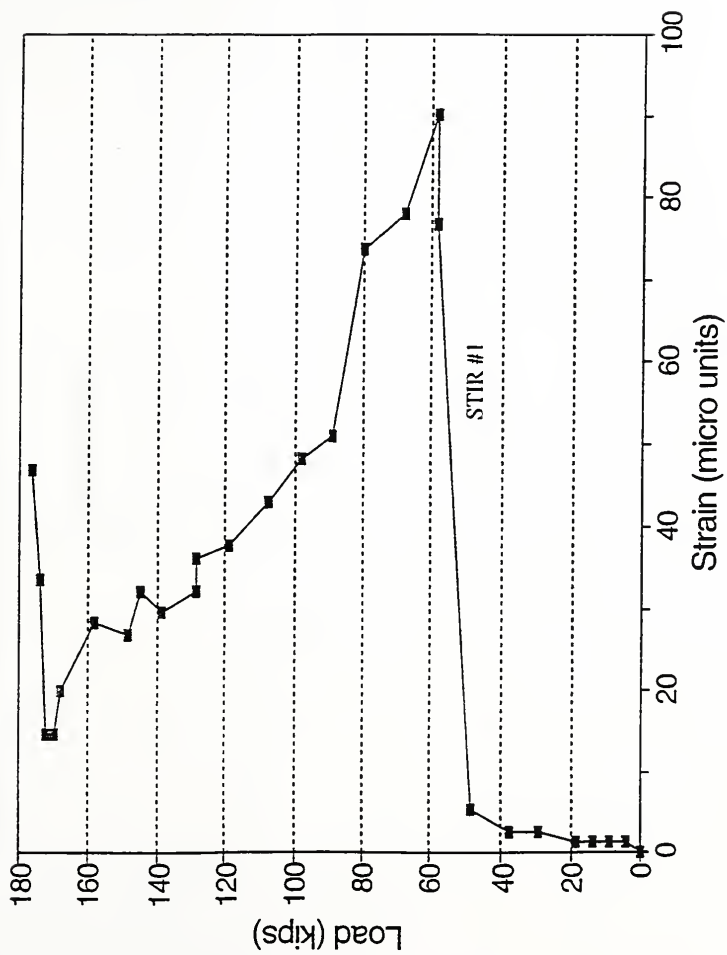
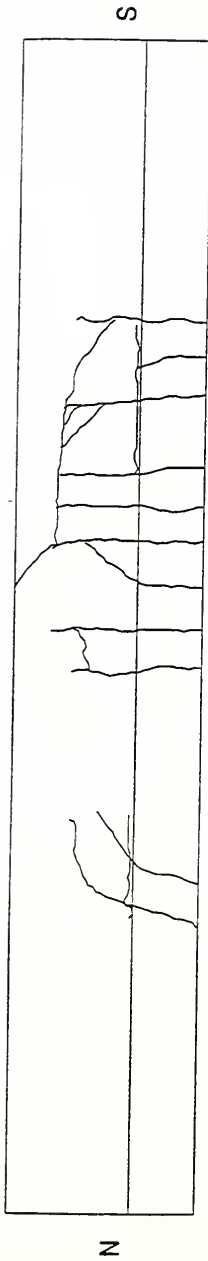
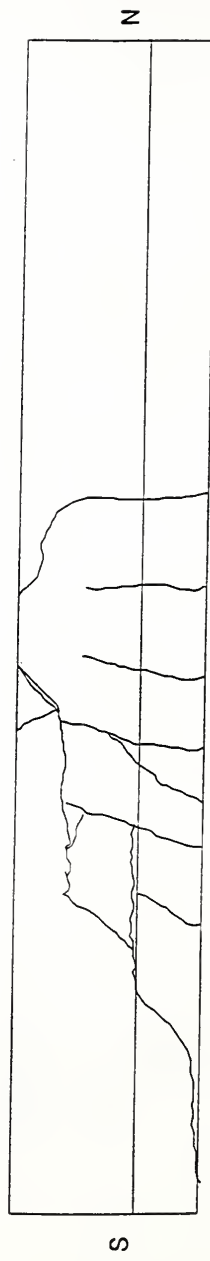


Figure 4.95 Load versus Strain in the horizontal shear connectors of Specimen 4

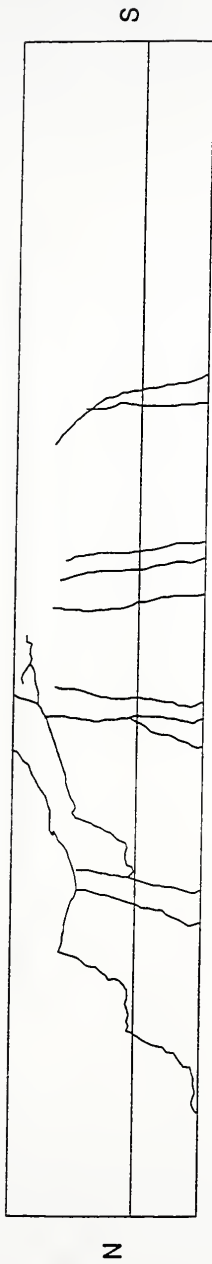


a) West Side View

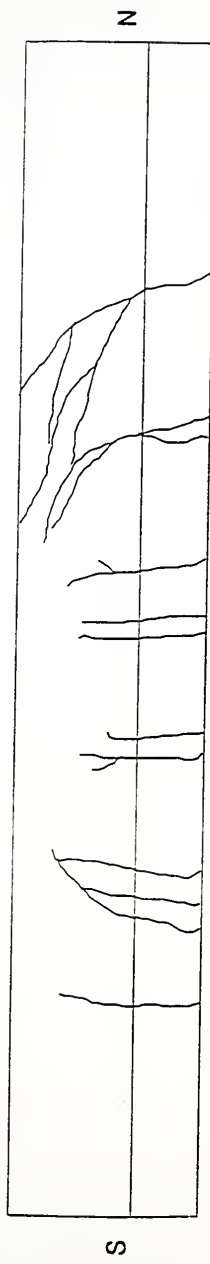


b) East Side View

Figure 4.96 Crack Patterns of Specimen 1 a) West Side View b) East Side View

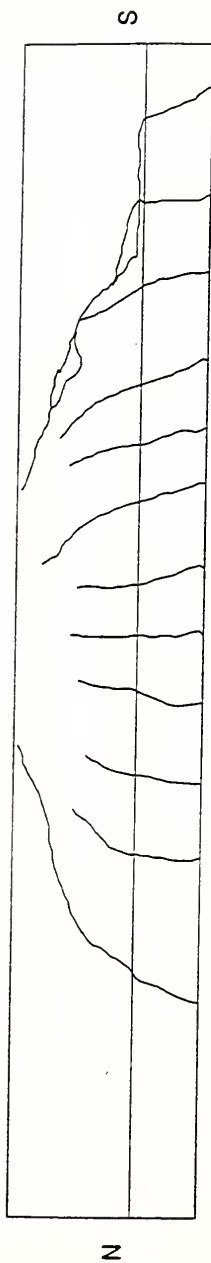


a) West Side View

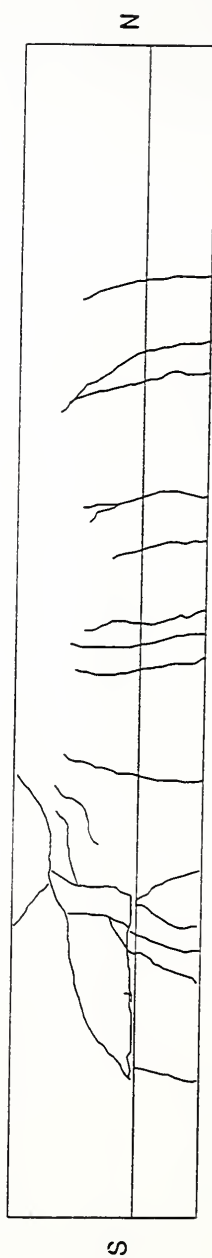


b) East Side View

Figure 4.97 Crack Patterns of Specimen 2 a) West Side View b) East Side View

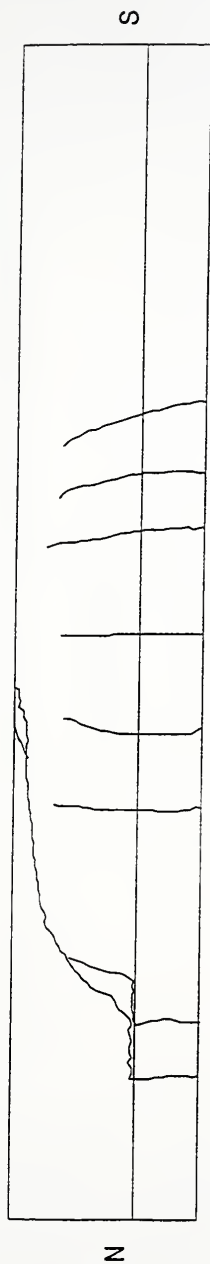


a) West Side View

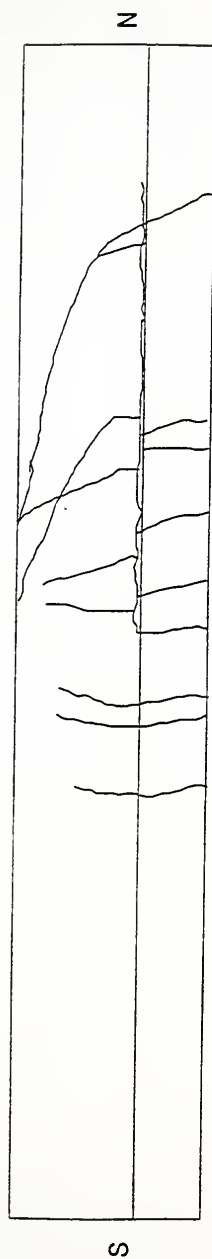


b) East Side View

Figure 4.98 Crack Patterns of Specimen 3 a) West Side View b) East Side View

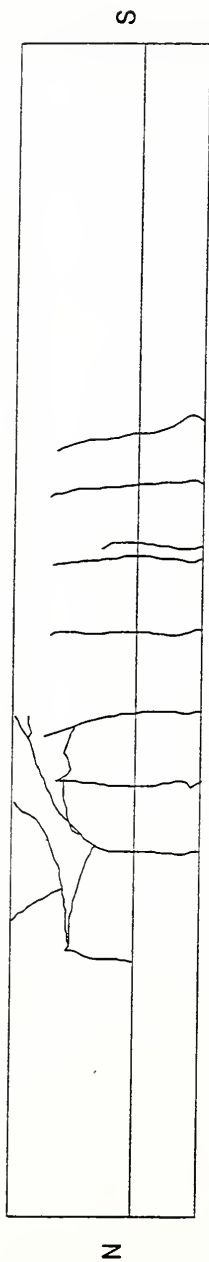


a) West Side View

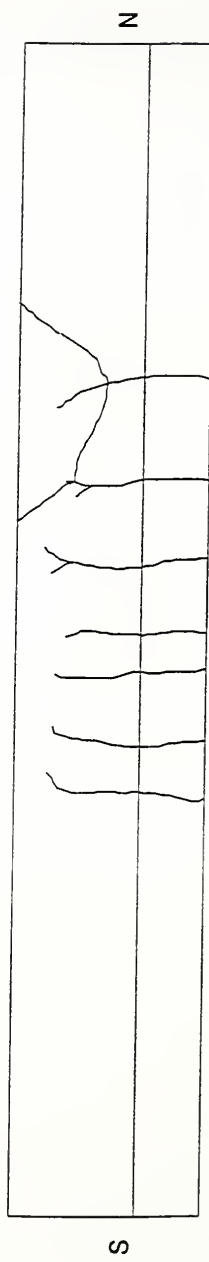


b) East Side View

Figure 4.99 Crack Patterns of Specimen 4 a) West Side View b) East Side View

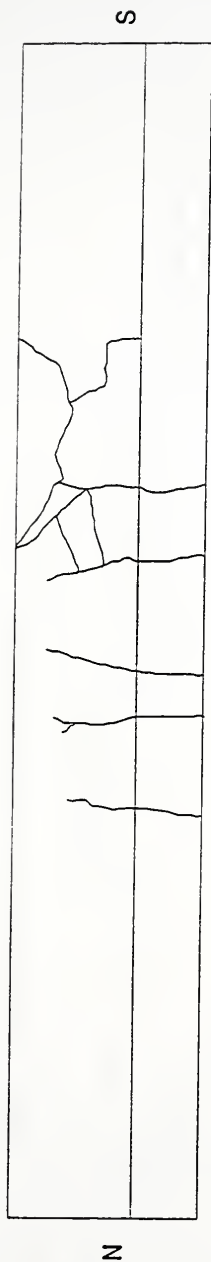


a) West Side View

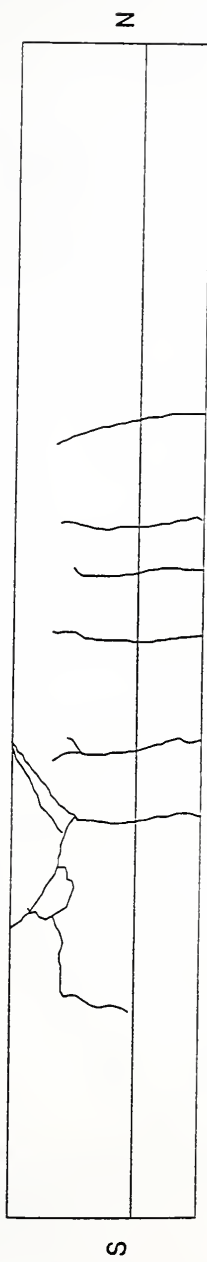


b) East Side View

Figure 4.100 Crack Patterns of Specimen 5 a) West Side View b) East Side View



a) West Side View



b) East Side View

Figure 4.101 Crack Patterns of Specimen 6 a) West Side View b) East Side View

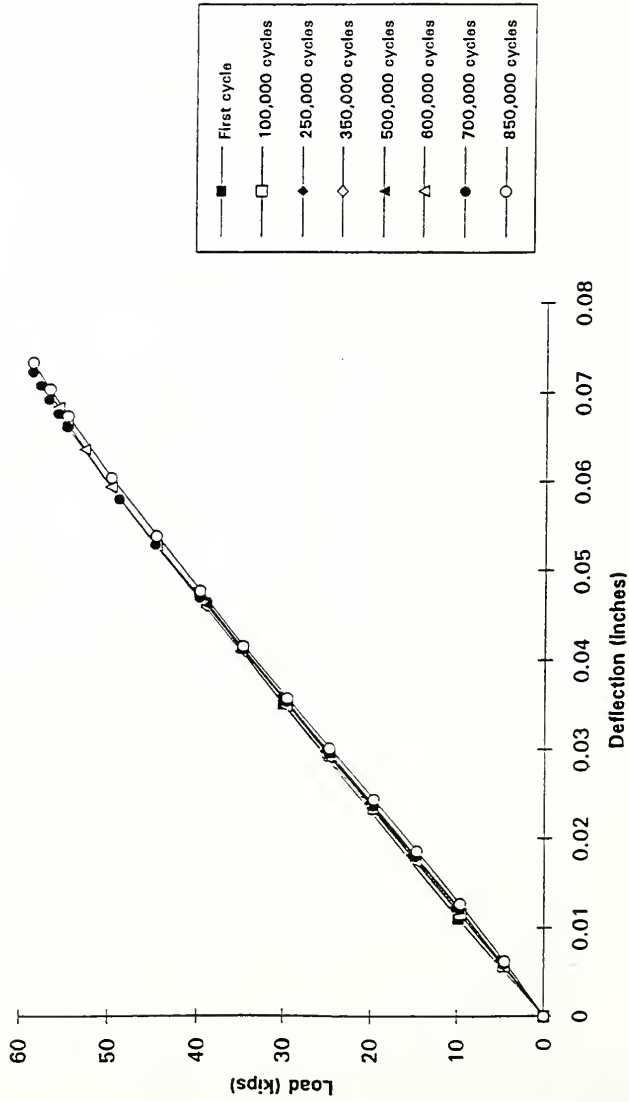


Figure 4.102 Effect of Cyclic Loading on Deflection of Specimen 1

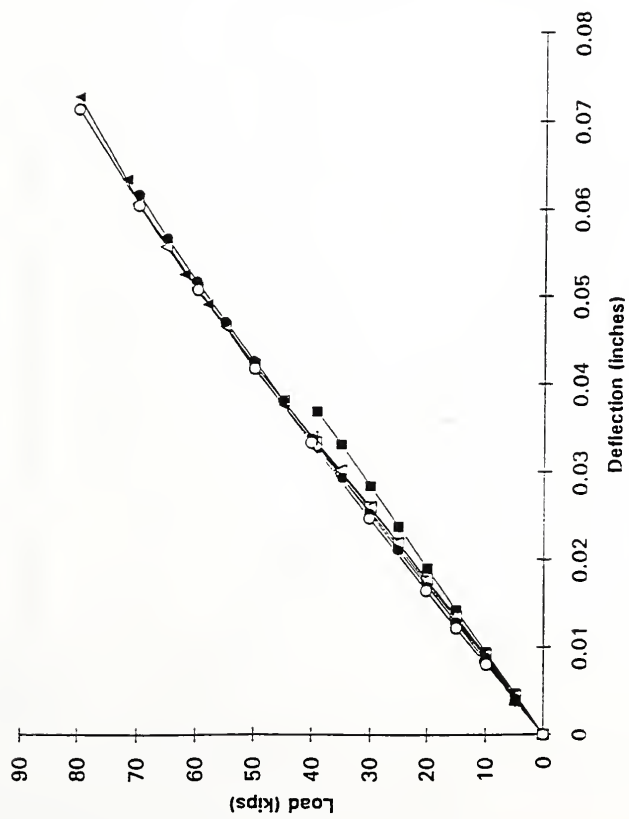


Figure 4.103 Effect of Cyclic Loading on Deflection of Specimen 2

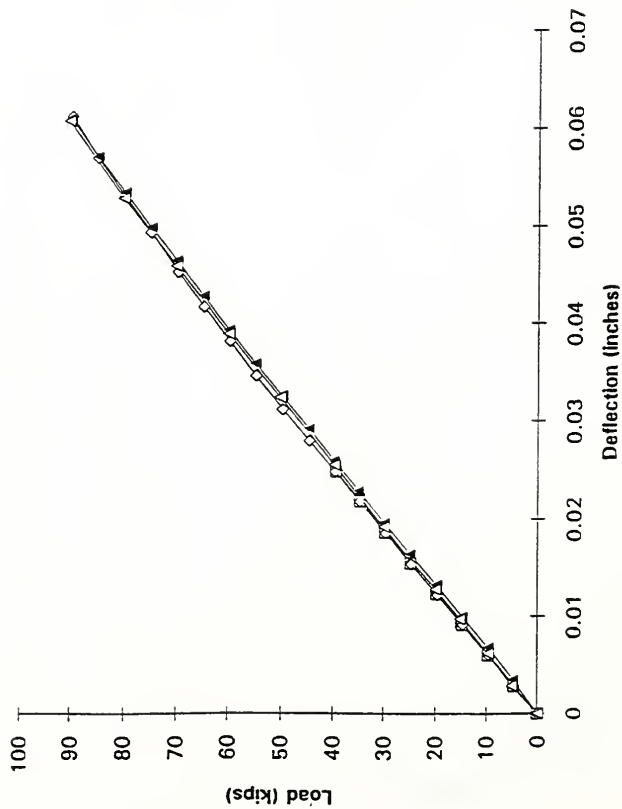


Figure 4.104 Effect of Cyclic Loading on Deflection of Specimen 3

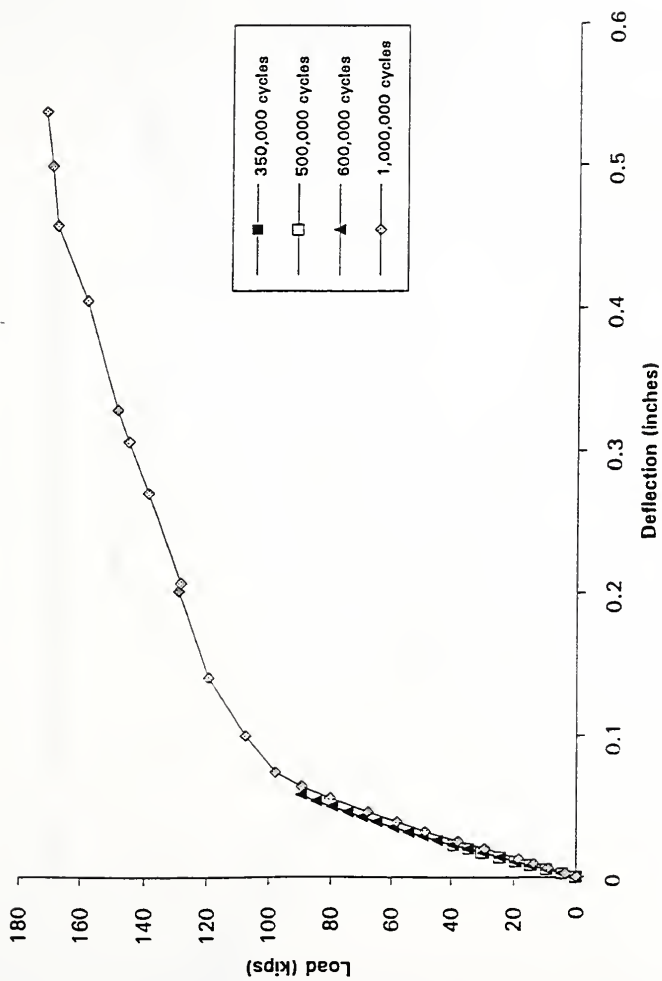


Figure 4.105 Effect of Cyclic Loading on Deflection of Specimen 4

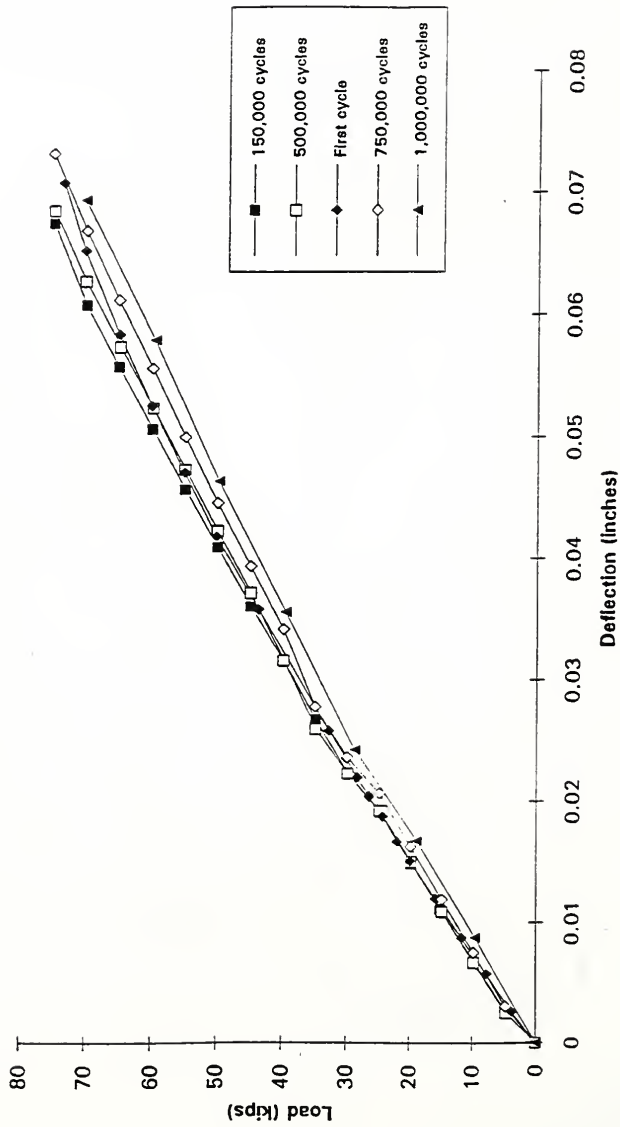


Figure 4.106 Effect of Cyclic Loading on Deflection of Specimen 5

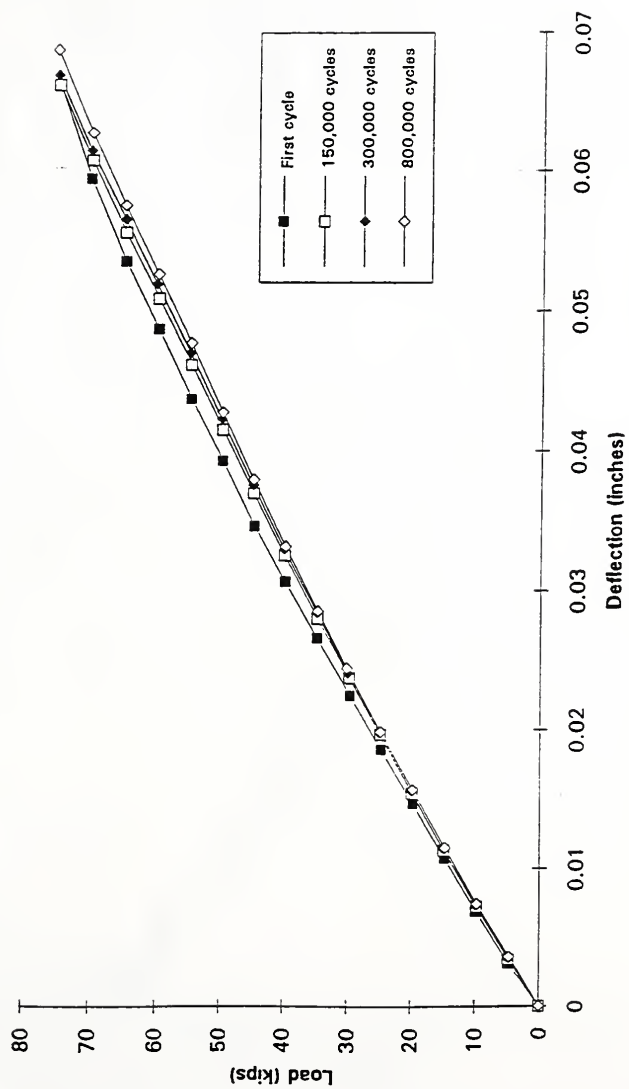


Figure 4.107 Effect of Cyclic Loading on Deflection of Specimen 6

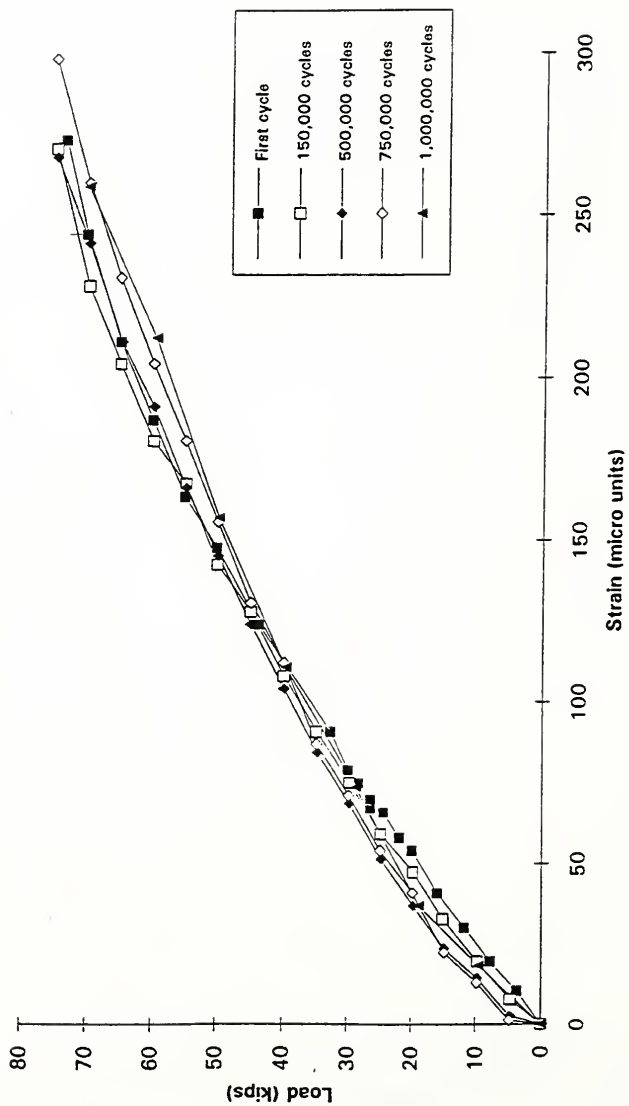


Figure 4.108 Effect of Cyclic Loading on Average strain in strands of Specimen 5

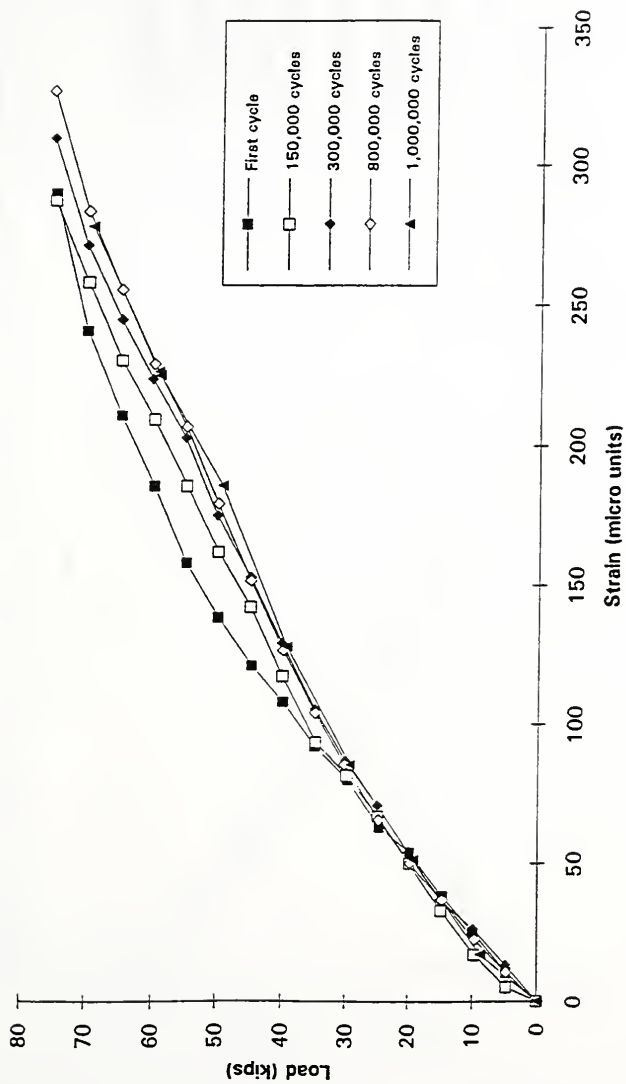


Figure 4.109 Effect of Cyclic Loading on Average strain in strands of Specimen 6

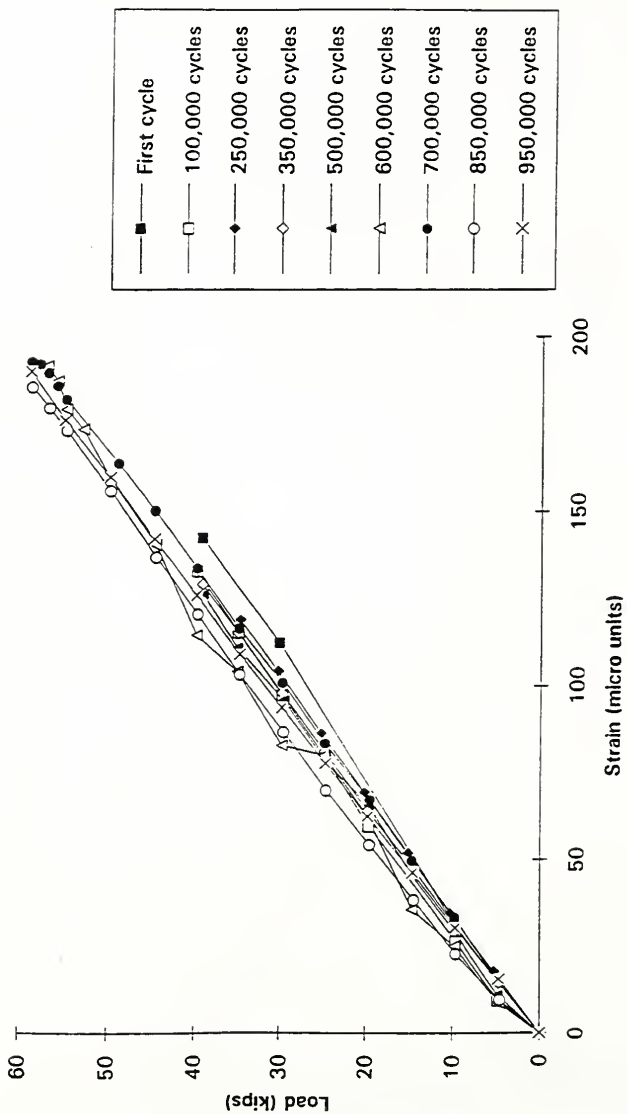


Figure 4.110 Effect of Cyclic Loading on Average strain at the top of CIP slab of Specimen 1

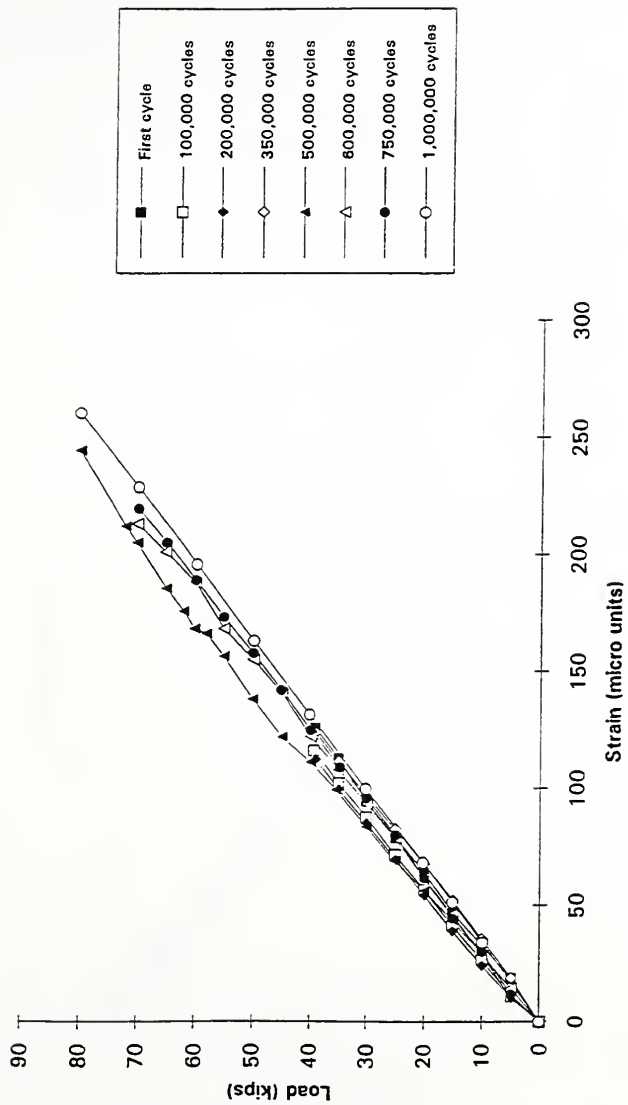


Figure 4.111 Effect of Cyclic Loading on Average strain at the top of CIP slab of Specimen 2

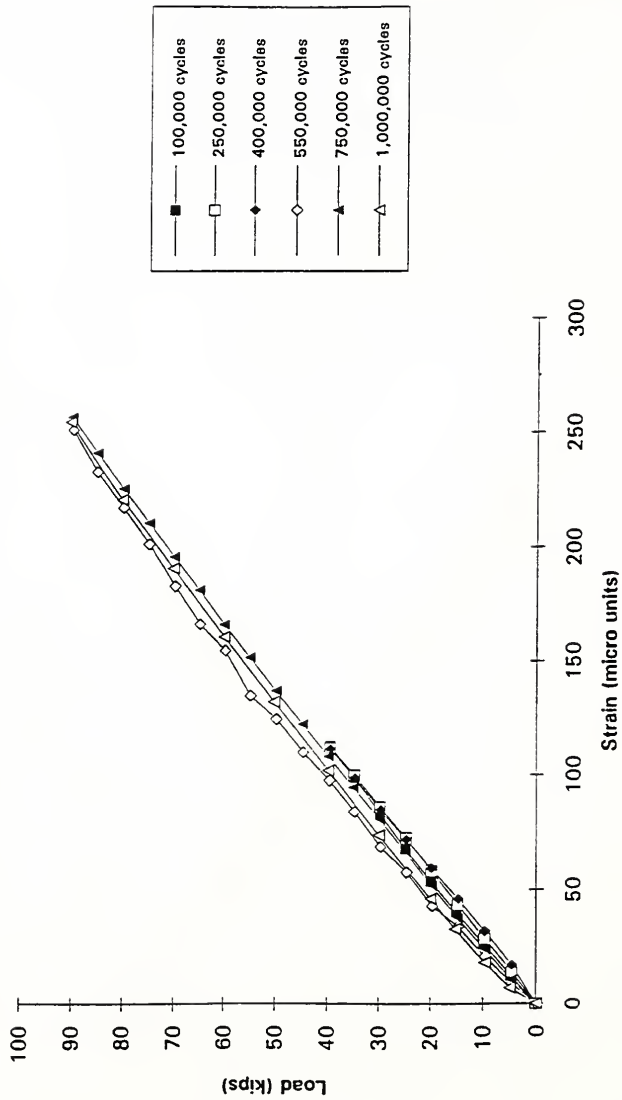


Figure 4.112 Effect of Cyclic Loading on Average strain at the top of CIP slab of Specimen 3

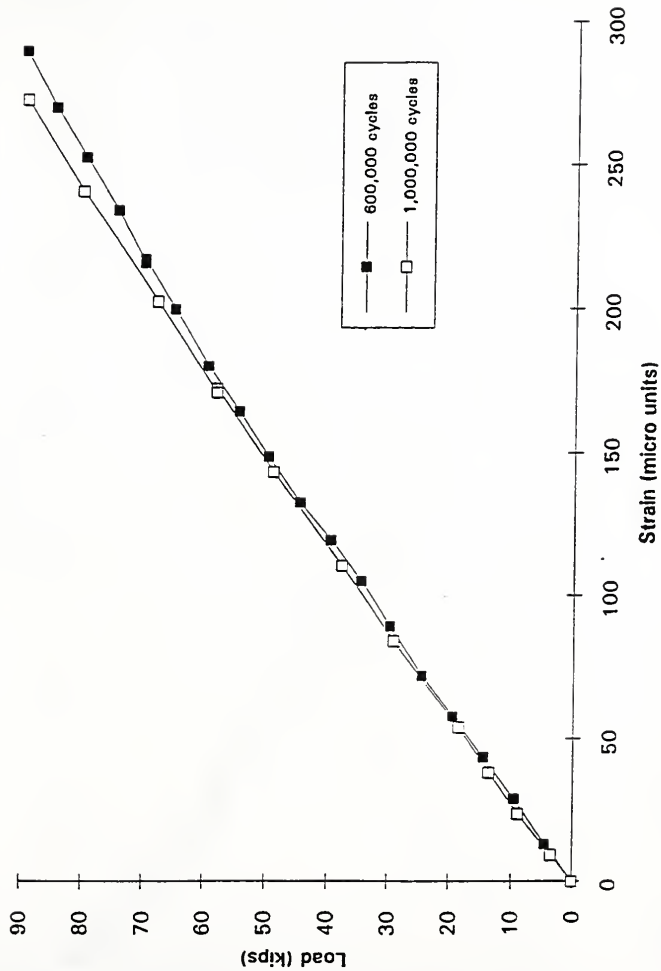


Figure 4.113 Effect of Cyclic Loading on Average strain at the top of CIP slab of Specimen 4

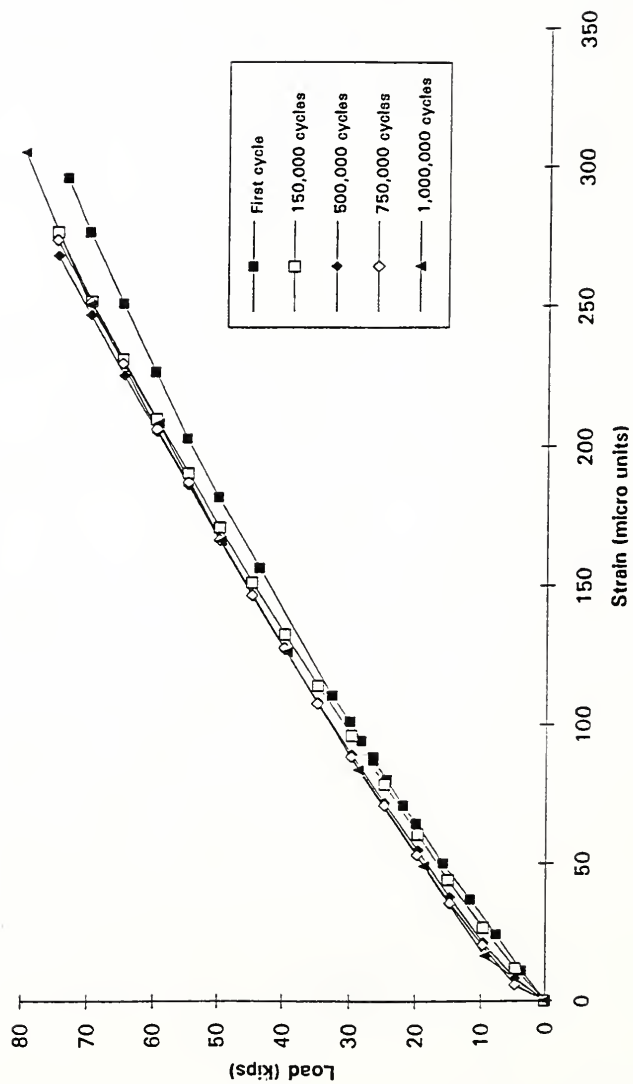


Figure 4.114 Effect of Cyclic Loading on Average strain at the top of CIP slab of Specimen 5

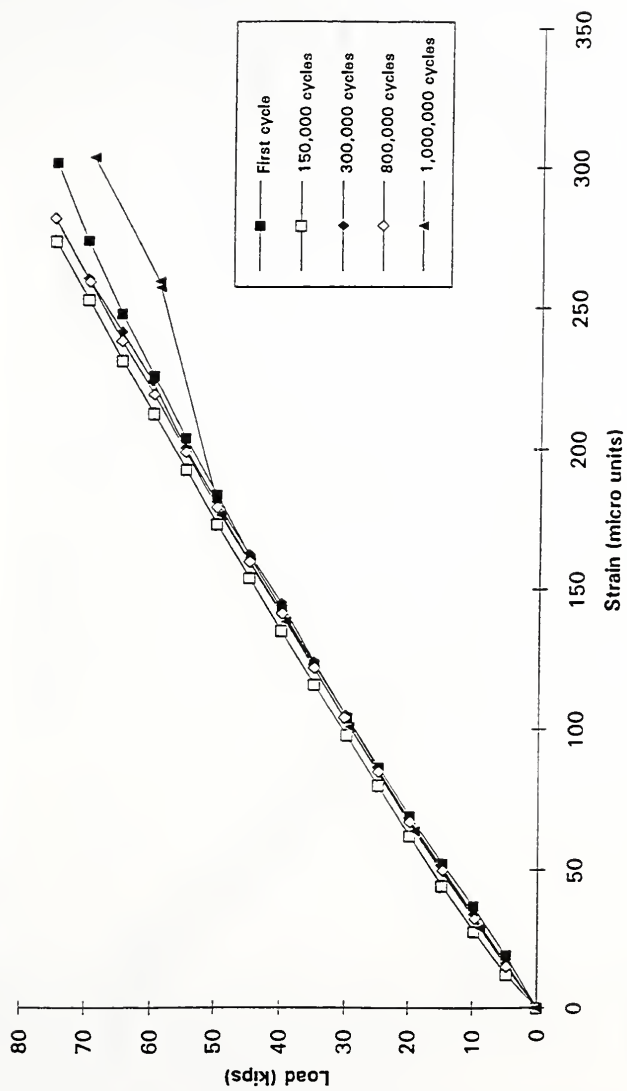


Figure 4.115 Effect of Cyclic Loading on Average strain at the top of CIP slab of Specimen 6

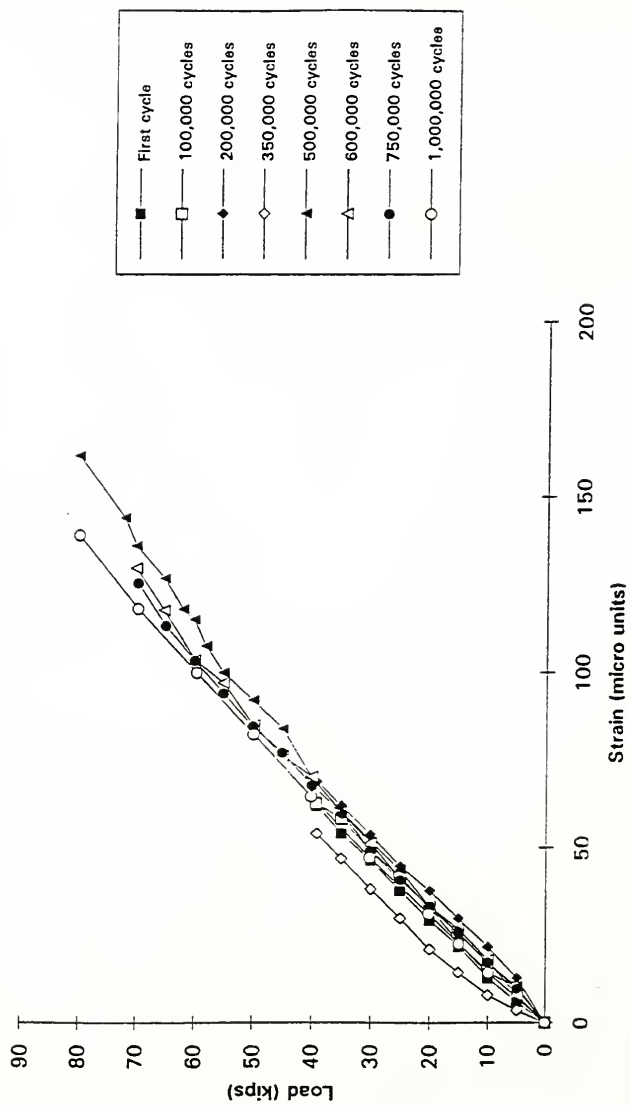


Figure 4.116 Effect of Cyclic Loading on Average strain at strand level of Specimen 2

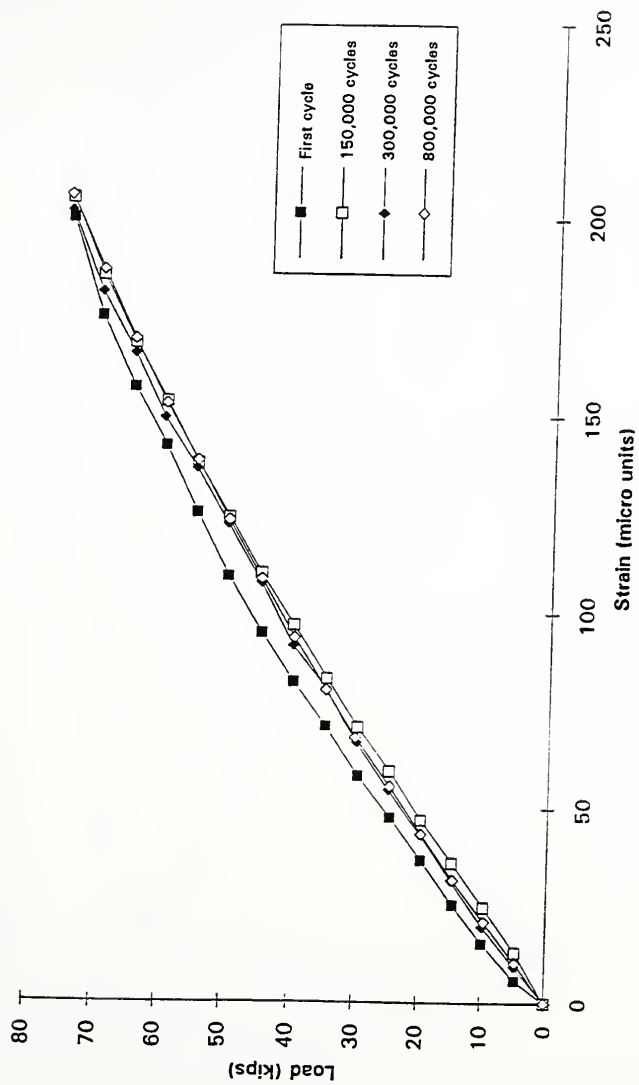


Figure 4.117 Effect of Cyclic Loading on Average strain at strand level of Specimen 6

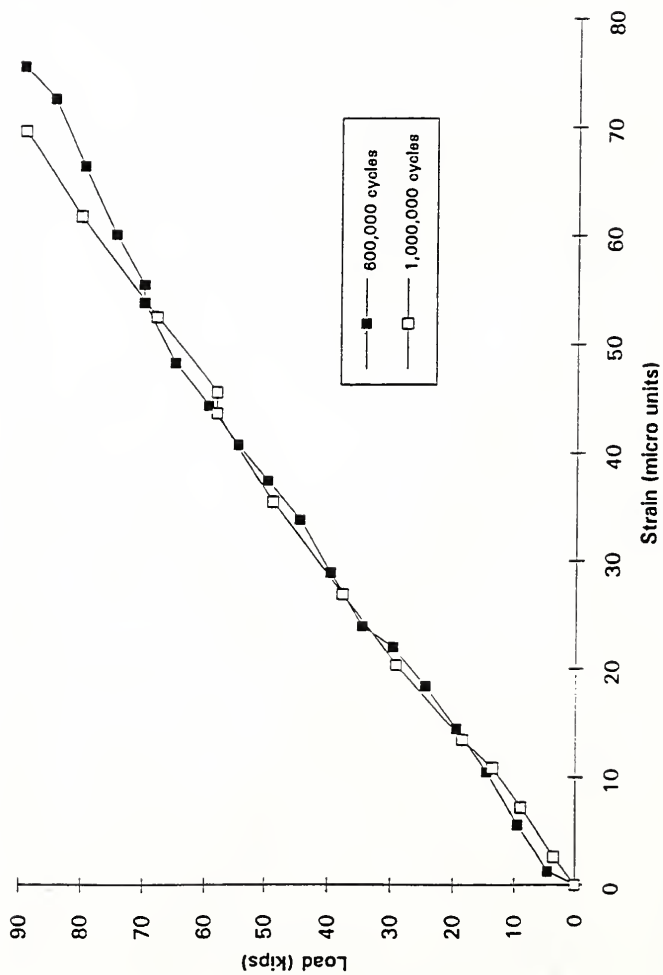


Figure 4.118 Effect of Cyclic Loading on Average strain at CIP gage level of Specimen 4

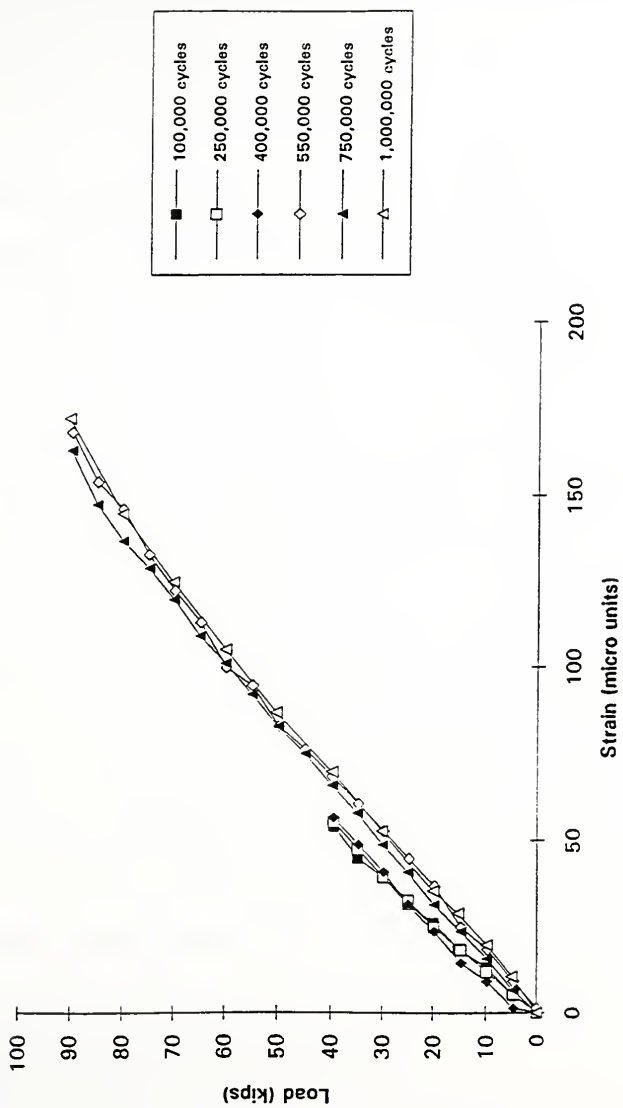


Figure 4.119 Effect of Cyclic Loading on Average strain at the interface of Specimen 3

CHAPTER 5 - SUMMARY, CONCLUSIONS AND RECOMMENDATIONS

5.1 General

The use of precast concrete for new bridge construction and for the rehabilitation of deteriorated bridges is economically and structurally attractive. Durability, ease and speed of construction, together with reduced need for maintenance are all advantages in using precast concrete. Precast prestressed concrete bridge deck panels are used with CIP concrete to provide a convenient and cost effective method of construction for concrete bridge decks. In this study, emphasis is placed on the behavior of stay-in-place precast panels in conjunction with CIP decks under the action of applied loads. During the past 12 years the construction cost of bridge decks in Indiana has been reduced by the use of precast panels as stay-in-place deck forms.

The main objective of this study was to evaluate the horizontal shear friction requirements for prestressed deck panels in bridge construction with broom finished top surface. Currently INDOT requires a total of 20 shear connectors across the interface regardless of panel dimensions. This study addresses the specific INDOT concerns dealing with the number of horizontal shear connectors required in precast panels with broom finished top surface. The issues of potential separation of the precast prestressed panel from the cast-in-place portion of the deck, as well as the adequate development of positive moment and shear capacities of the composite section were examined experimentally.

5.2 Research Program

To accomplish the objective of this study, an experimental program consisting of six full-scale composite stay-in-place deck slabs was conducted. These specimens had different interface characteristics including different amounts of horizontal shear reinforcement across the interface. Specimens 1-4 had 18 prestressing strands representing a practical upper limit on the amount of flexural reinforcement in this type of member. These specimens were tested to evaluate the potential maximum horizontal shear demand. Specimens 5 and 6 had 12 prestressing strands. These last two specimens were used to evaluate the effect of repeated loading due to an increase in mean shear stress at the interface. In addition, these specimens were intended to evaluate the amount of shear to be transferred in deck panels designed according to AASHTO for HS20 loading. Specimens 1 and 5 had no shear connectors. Specimen 4 had a lubricated top surface for the precast panel.

All six composite specimens consisted of a 2.5 in. thick precast prestressed panel with a 5.5 in. thick CIP reinforced concrete topping slab. This provided an 8 in. standard full deck thickness as commonly used in Indiana. The longitudinal dimension of the panel depends on the spacing of longitudinal bridge girders. A panel length equal to 8 ft was chosen as it falls in the range of medium to wide girder spacing. A width of 8 ft. was chosen as it represents the upper practical limit due to handling considerations. The prestressing strands were Lo-Lax, Grade 270, with a 3/8 in. diameter. The mild reinforcing steel in the panel was Grade 60 and met the requirements of ASTM A-615. Welded wire fabric was according to ASTM A-497 requirements. Panels were roughened in the direction parallel to the strands so as to minimize the reduction in

section modulus. The broom finished surface provided deformations with approximately 0.05 to 0.075 in. amplitude. This is less than the raked surface amplitude of 0.25 in. Strands were prestressed to about 17.5 kips (corrected for slip loss which was estimated to be approximately 0.3 kips) approximately equal to $0.75 f_{pu}$, where f_{pu} is the ultimate strand tensile strength. Each panel had a single layer of welded wire fabric located directly on top of the prestressing strands. In addition, these panels contained five #3 reinforcing bars placed at 6 in., 18 in. and 48 in. from either end of the panel.

The reinforcement in the CIP slab was nominal and placed in the concrete to take care of the temperature and shrinkage stresses. The transverse reinforcement consisted of #5 bars spaced at 9 in. on centers supported on 1.75 in. high bar chairs spaced at approximately 2 ft on centers. The bar chairs rested directly on the top surface of the precast panels. The longitudinal reinforcement parallel to the prestressing strands consisted of #5 bars spaced at 6 in. on centers, placed on top of the transverse reinforcement. All reinforcing bars were ASTM A615-90, Grade 60 bars. These bars were not epoxy coated and the clear cover to the top bars was 2.5 inches. End cover was 3 inches. The design concrete compressive strength was 4000 psi.

These specimens were tested under static and cyclic loadings. All loads were applied by hydraulic actuators. Static load tests were performed at regular intervals of repeated loading. The specimens were tested under repeated loading to simulate traffic effects on the horizontal shear strength of the panel at the interface between the precast panel and the cast-in-place portion of the deck. Following cyclic loading, the specimens were monotonically loaded to failure.

When the load is applied over the wheel foot print, it has been found that punching shear usually governs the ultimate strength of the slab in a monotonic loading situation. In these cases

the full flexural capacity of the panels would not be achieved and thus the maximum uniform horizontal shear stress at the interface is not developed across the entire width of the panel. Thus to find the horizontal shear capacity of the panel, the loading area was extended over the entire width of the panel. In this study, horizontal shear capacity was also examined in the limit of flexural failure of the specimen. The load was distributed over an area of 10 in. x 96 in.

The performance of the deck system was obtained by evaluating the following data:

- 1) Load versus deflection characteristics
- 2) Interface slip characteristics
- 3) Load versus strand slip characteristics
- 4) Behavior under cyclic loading
- 5) Load versus strain at various locations of the specimens

To obtain the above data, instrumentation was provided at appropriate locations. During all the static tests, load, strains, and deflection were monitored. To observe the cyclic loading effect on these specimens, intermediate static tests were performed at regular intervals, during these static tests behavior of these specimens was observed. Data collected at the end of each of these intermediate static tests were analyzed to observe the effect of cyclic loading on stiffness and ductility characteristics of steel and concrete elements in the specimen.

5.3 Findings from Experimental Program

5.3.1 Strand Development

Strand development lengths necessary to attain the full strength of strands were not obtained experimentally on a quantitative basis. However, a qualitative evaluation of the strand development lengths were obtained by monitoring the ends of selected strands for their slip

relative to the panel ends. Slippage of prestressing strands was observed in all of the ultimate monotonic loading cycles of the six specimens. Specimens 3 and 4 showed a significant difference in their loads (P_{ssmin}) at which strand slip in the monitored strands was observed, when compared to loads at which strand slip occurred in Specimens 1 and 2. In these specimens, strand slip might have occurred earlier than observed in some of the non-monitored strands. However, in all the specimens a minimum reserve capacity of about 22.5% above that of the strand slip loads observed was noted at failure. The strand slip loads for the first four specimens were within 4.17 to 5.87 times the service load of 26.4 kips (equivalent to standard AASHTO wheel load with a 30% impact factor).

In Specimens 5 and 6 this ratio was 3.60 and 3.79 respectively (see Table 4.9). These ratios in the last two specimens roughly correspond to the same stress level at the strand locations as that of Specimens 1-4.

5.3.2 Interface Slip

Composite behavior between the precast panels and the reinforced concrete topping slab is assumed to exist for conventional analysis of these types of bridge decks. For the equivalent service level wheel load of 26.4 kips, that was applied to all the specimens, and for the equivalent factored wheel load equal to 57.3 kips, interface slip was not observed. In Specimens 1-4, significant slip at the interface occurred only at maximum load levels. In these cases, the minimum ratio of significant slip (0.005 in. as chosen by Hanson [14]) load (obtained from Figs. 4.25 to 4.30) to the ultimate load was about 0.8. No interface slip was observed in Specimens 5 and 6.

5.3.3 Load Deflection Behavior

The load versus deflection behavior of the composite slab specimens was linear elastic at both the equivalent wheel service and factored load levels. The midspan slab deflections were quite small at both of these load levels. Just before the failure of specimens, LVDTs were removed to prevent them from getting damaged. In the case of the first four specimens whose failure occurred in shear mode, the deflections recorded by LVDTs were within a range of 0.4 to 0.55 inches. At failure, deflection recorded by the micro profiler of the controller, was within a range of 0.9 to 1.0 inch. These readings were confirmed with the readings obtained in the case of Specimen 2, where the LVDTs were not removed prior to failure of the specimen. The load-deflection behavior of Specimens 5 and 6 was the same as the previous four panels for the majority of the loading cycle. The behavior was linearly elastic at both the service load level and the factored load level. Just before failure, the measured deflection was about 1.8 inches in both specimens. This larger deflection was due to their ductile flexural mode of failure compared to the sudden beam-shear mode failure in the first four specimens. Load versus deflection behavior in general can be partitioned into three main stages. In Stage 1, deflection varied linearly up to cracking load. In a few cases this crack did not appear over the entire width of the specimen up to a higher load level. In Stage 2, which is post-cracking stage, deflection varied at a much faster rate than in Stage 1. Load versus deflection behavior in this stage can also be roughly described as linear. Near the maximum load level, there was a sudden increase in deflection for very small increments in load. This signified the end of Stage 2 and beginning of Stage 3. In Stage 3, deflection increased rapidly with small increments in load up to failure.

5.3.4 Strains in Reinforcement and Concrete

Strain gages were placed at various locations on the prestressing strands, on the concrete deck and also on the CIP bars. In Specimens 1-4 load versus strand strain characteristics were linear, both at the equivalent wheel service load and at the equivalent wheel factored load levels. Even at the factored load level, strain was below $7000 \mu\epsilon$ which is below the elastic limit of the strand steel. Hence strands were not loaded into their inelastic range at equivalent wheel factored loads. Once the load exceeded cracking levels, as expected, there was a sudden change in strain value. In the strands where slippage was observed, there was either a reduction in strain or constant strain. In the strands where slippage was observed, there was an increase in strain with increasing load level and at the time of failure, the stress in the strands reached almost their ultimate capacity. In Specimens 5 and 6, similar behavior was observed except that at the ultimate load levels, due to ductile flexural behavior, the stress in the strands was much higher. Some of the strands in these last two specimens fractured at failure.

Load versus strain readings from gages located at the top of the CIP slab varied linearly up to the flexural cracking load. With further increase in load, strain increased suddenly. Near maximum load levels, there was a sudden increase in strain, it increased rapidly for very small increments in load up to failure. In Specimens 1-4, failing in beam-shear mode, strain recorded at failure was barely $2800 \mu\epsilon$. In Specimens 5 and 6 failing in flexural mode, the strain recorded at failure was well over $3000 \mu\epsilon$. In fact, the average strain recorded in these specimens on the failure side was about $3500 \mu\epsilon$.

Strain gages were placed on CIP bars parallel to the strands only in Specimens 3, 4, 5 and 6. Load versus strain gage readings located on the CIP bars did not show significant strain value

during the earlier stages of loading. In fact, these bars were under compression up to a load of 110 kips in Specimens 3 and 4. Strain value at this load was about $-50 \mu\epsilon$. With further increase in load, strain in the bars changed from compressive to tensile. This tensile strain in the bars increased non-linearly with increasing load up to near ultimate load level. At ultimate, the strain increased very rapidly and in Specimen 3, of the strain observed at failure on the failure side was well over $3000 \mu\epsilon$, indicating yielding in the bars. In Specimen 4, strain observed at failure was about $950 \mu\epsilon$. This could be due to sudden splitting failure which caused separation at the interface. In Specimens 5 and 6, the bars were under compression up to a load of 80 kips. With further increases in load, these compressive strains became tensile strains. At the ultimate load, the average strain recorded in the bars was about $3500 \mu\epsilon$ with as much as $6000 \mu\epsilon$ in certain bars.

5.3.5 Horizontal Shear Connectors

Specimens 1 and 5 did not have horizontal shear connectors. Specimens 2,3,4 and 6 had four shear connectors. In all the specimens, strain in shear connectors was not significant until a significant slip occurred at the interface. Significant amount of interface slip was observed only in Specimens 1-4 near the ultimate load level and hence the effect of the shear connectors was observed only at the maximum load level. Minimum load at which interface slip occurred in Specimens 1-4 was about 5.68 times the equivalent wheel service load level of 26.4 kips and 2.6 times the factored load of 57.3 kips. Near failure, strain in one of the shear connectors of Specimen 3, reached its yield capacity. This suggests that shear connectors were effective at the ultimate load, though not enough to prevent failure.

5.3.6 Crack Patterns

The crack patterns on either side of the loading point were symmetrical for most of the loading cycles. Near the ultimate load level, a number of cracks appeared on one side of the loading point indicating the impending failure on that side of specimen. In Specimens 1-4, failing in beam-shear mode, the principal diagonal failure crack emanated from one of the preexisting cracks and progressed towards the interface. At the interface, cracks propagated along the interface up to the compressive flow region of the reaction point and from there the bottom tip of this diagonal crack propagated towards the reaction point and the top tip progressed towards the loading point. Propagation of this critical crack occurred suddenly at the maximum load causing this diagonal crack to extend from the bottom fiber near the reaction point to the top fiber near loading point. In Specimens 5 and 6, where failure occurred in a ductile flexural mode, the crack pattern was symmetrical even at the ultimate loads except that crack widths were wider on the failure side. Failure occurred in a typical flexural mode with cracks extending into the concrete flexural compression block and finally causing the crushing of concrete. Some of the prestressing strands were fractured at failure. The crack patterns, indicated that full composite behavior existed between the precast panel and CIP topping slab almost up to failure of specimens.

5.3.7 Effects of Cyclic Loading

Load versus deflection characteristics obtained after each intermediate static test performed during cyclic loading of the specimens showed negligible effect of cyclic loading on the stiffness of the deck slab. During this cyclic loading, specimens stayed below the elastic

limit and hence there was not any significant effect of cyclic loading observed in any of the measurements taken.

5.4 Conclusions

The primary objectives of this study was to evaluate the performance of thin precast prestressed concrete panels with broom finish surface and to determine if horizontal shear friction reinforcement is needed to ensure adequate composite behavior between the panel and the CIP portion of the bridge deck. The issues of potential separation of the precast prestressed panel from the cast-in-place portion of the deck, as well as the adequate development of positive moment and shear capacities of the composite bridge section were examined experimentally.

Failure occurred in beam-shear-compression mode in Specimens 1-4. In Specimens 5 and 6 a ductile flexural mode was observed. The specimens with 18 prestressing strands had a larger flexural capacity than shear capacity, whereas Specimens 5 and 6 with 12 prestressing strands had a lower flexural capacity than shear capacity and hence failure occurred in flexural mode. From the first four specimens, a limit on the nominal horizontal shear strength across the interface with broom finish can be established. This nominal horizontal shear strength across the interface was obtained with the minimum capacity of those specimens which failed in shear mode. Hence from the first specimen capacity of 160 kips, nominal horizontal shear strength obtained was about 123 psi. Based on the minimum load of 150 kips at which interface slip was observed in Specimens 1-4, a lower limit for nominal horizontal shear strength can be established as 115 psi ($= 150 / (2 * 96 * 6.75)$). Therefore, with a broom finish, an interface horizontal shear stress of 115 psi can be transferred without shear connectors.

The following additional conclusions are drawn from the experimental tests:

- 1) Slippage of prestressing strands was recorded during the final monotonic cycle to failure for all specimens. However, an excessive capacity of at least 29% at failure above that of the strand slip loads observed and at least 11% at strand slip loads above the strand slip loads predicted by current AASHTO procedures were observed in all the specimens.
- 2) All the specimens showed composite behavior to failure. Interface slip was not observed at the equivalent service load of 26.4 kips (117.5 kN) nor at the equivalent factored wheel load of 57.3 kips (255 kN). Interface slip in the first four specimens with 18 strands occurred only at failure loads at least 54% above the predicted AASHTO capacity controlled by development length. No interface slips were recorded in Specimens 5 and 6 with 12 strands.
- 3) Specimens with shear connectors were stiffer near ultimate loads than those without shear connectors (Specimens 1 and 5) but having the same number of strands. Specimens 3 and 4 were stiffer than specimens 1 and 2 due to less prestress loss.
- 4) Cyclic loading did not have appreciable effect on the stiffness of deck slabs.

5.5 Recommendations

No shear connectors are needed in stay-in-place precast prestressed deck panels with broom finished surface if the nominal average horizontal shear stress at the interface is less than 115 psi.

5.6 Needed Research

Additional research into the behavior of composite bridge deck slabs constructed with precast prestressed concrete panels includes the following topics :

- 1) Continuity of composite slabs across the bridge girders
- 2) Non-destructive field load tests of a composite bridge deck to monitor behavior
- 3) Non-destructive evaluation of an existing composite bridge deck slab for potential reinforcement corrosion and integrity of composite behavior
- 4) Effects of shrinkage of concrete in the cast-in-place topping slab on the development of cracks in the composite slab.

LIST OF REFERENCES

1. AASHTO. Standard Specifications for Highway Bridges. 13th Edition. The American Association of State Highway and Transportation Officials, Washington, D.C., 1983, and Interim Specifications Bridges (Second Supplement) 1992.
2. ACI Committee 318. Building Code Requirements for Reinforced Concrete. ACI Standard 318-89 (Revised 1992). American Concrete Institute, Detroit, Michigan, 1992.
3. Barker, J. M., "Research, Application and Experience with Precast Prestressed Bridge Deck Panels." PCI Journal, 20, Nov.-Dec., 1975, No. 6, pp. 66 - 85.
4. Mrinmay Biswas, "Precast Bridge Deck Design Systems (special report)", PCI Journal.
5. Ross Bryan Associates, Inc., "Recommended Practice for Precast Prestressed Concrete Composite Bridge Deck Panels." PCI Journal, March-April, 1988, pp. 67 - 109.
6. Armand Gustafarro, Marc A. Hillier, and Jack R. Janney, "Performance of Prestressed Concrete on the Illinois Tollway after 25 Years of Service." PCI Journal, Jan.-Feb., 1983, pp. 51-67.
7. S. Dei Poli, M. Di Prisco and P. G. Gambarova, "Shear Response, Deformations, and Subgrade Stiffness of a Dowel Bar Embedded in Concrete." ACI Structural Journal, Nov.-Dec., 1992, pp. 665 - 675.
8. Mrinmay Biswas, Jerome S. B. Iffland, Russel E. Schofield, URS / Madigam-Praeger, Inc., and Anthony E. Gregory, "Bridge Replacements with Precast Concrete Panels." New York State Thruway Authority, Albany, New York.
9. J. C. Saemann and George W. Washa, "Horizontal Shear Connections Between Precast Beams and Cast-In-Place Slabs." Journal of the American Concrete Institute, Nov., 1964, pp. 1383-1408.
10. PCI Committee on Bridges, "Precast Prestressed Concrete Bridge Deck Panels (special report)", PCI Journal, March-April, 1987, pp. 27-45.
11. Robert L. Reed, "Application and Design of Prestressed Deck Panels." Texas State Department of Highway and Public Transportation.
12. F. Seible and C. T. Latham, "Horizontal Load Transfer in Structural Concrete Bridge Deck Overlays." J. Struct. Engrg., ASCE, 116(10), pp. 2691-2710.
13. F. Seible and C. T. Latham, "Analysis and Design Models for Structural Concrete Bridge Deck Overlays." J. Struct. Engrg., ASCE, 116(10), pp. 2711-2728.

14. Hanson, N. W., "Precast Prestressed Concrete Bridges, 2. - Horizontal Shear Connections." Journal, PCA Research and Development Laboratories, May, 1960, pp. 38-58.
15. Richard E. Klingner and Lee A. Bieschke, "Effects of Transverse Panel Strand Extensions on the Behavior of Precast Prestressed Panel Bridges." PCI Journal, Jan.-Feb., 1988, pp. 69-88.
16. Ralph W. Kluge and Herbert A. Sawyer, "Interacting Pretensioned Concrete Form Panels for Bridge Decks." PCI Journal, May-June, 1975, pp. 35-67.
17. Robert M. Barnoff, James A. Orndorff, Jr., Robert B. Harbaugh, Jr., and Donald E. Rainey, "Full Scale Test of a Prestressed Bridge with Precast Deck Planks." PCI Journal, Sep.-Oct., 1977, pp. 67-83.
18. C. Dale Buckner and H. T. Turner, "Performance of Full-Span Panel-Form Bridges under Repetitive Loading." Transportation Research Record 903, Transportation Research Board, National Research Council, pp. 45-52.
19. R. E. Abendroth, H. Pratanata and B. A. Singh, "Composite Precast Prestressed Concrete Bridge Slabs." Iowa Department of Transportation Research Report HR-310, College of Engineering, Iowa State University, August, 1991.
20. Lin, T. Y., and Burns, N. H., Design of Prestressed Concrete Structures, 3rd Edition, John Wiley and Sons, New York, 1981.
21. Park, R., and Paulay, T., Reinforced Concrete Structures, John Wiley and Sons, New York, 1974.
22. Mattock, A. H., and Kaar, P. H., "Precast Prestressed Concrete Bridges, 4-Shear Tests of Continuous Girders." Journal, PCA Research and Development Laboratories, V.3, No. 1, Jan., 1961, pp. 47-56. PCA Development Bulletin D45.
23. Raths, C. H., Reader Comments on "Design Proposals for Reinforced Concrete Corbels." by Mattock, A. H., PCI Journal, March-April, 1977, pp. 93-98.
24. Walraven, J., Frenay, J., and Puijssers, A., "Influence of Concrete Strength and Load History on the Shear Friction Capacity of Concrete Members." PCI Journal, Jan.-Feb., 1987, pp. 66-84.
25. Mattock, A. H., and Hawkins, N. M., "Shear Transfer in Reinforced Concrete-Recent Research." PCI Journal, March - April, 1972, pp. 55-75.

26. William, J. Krefeld, and Charles W. Thurston, "Contribution of Longitudinal Steel to Shear Resistance of Reinforced Concrete Beams." *Journal of the American Concrete Institute*, March, 1966, pp. 325-343.
27. Robert E. Loov, and Anil K. Patnaik, "Horizontal Shear Strength of Composite Concrete Beams with a Rough Interface."
28. Fagundo, F. E., Tabatabal, H., Soongswang, K., Richardson, J. M., and Callis, E. G., "Precast Panel Composite Bridge Decks." *Concrete International*, V. 7, No. 5, May, 1985, pp. 59-65.
29. Murakami, H., "A Laminated Beam Theory with Interlayer Slip." *J. Appl. Mech., ASME*, 1984, 51 (3), 561-559.
30. Toledano, A., and Murakami, H., "A Shear Deformable Two - Layer Plate Theory with Interlayer Slip." *J. Engrg. Mech. Div., ASCE*, 1988, 114 (4), pp. 604-623.
31. George Z. Voyiadjis, and Mohammed H. Baluch, "Refined Theory for Thick Composite Plates." *J. Engrg. Mech. Div., ASCE*, 1988, 114 (4), pp. 671-687.
32. Birkeland, P. W., and Birkeland, H. W., "Connections in Precast Concrete Construction," *Journal of the American Concrete Institute*, vol. 63, No. 3, March 1966, pp. 345-368.
33. Mast, R. F., "Auxiliary Reinforcement in Concrete Connections," *Proceedings, ASCE*, vol. 94, ST6, June 1968, pp. 1485-1504.
34. Hofbeck, J.A., Ibrahim, I.O., and Mattock, A.H., "Shear Transfer in Reinforced Concrete," *Journal of the American Concrete Institute*, vol. 66, No. 2, Feb. 1969, pp. 119-128.
35. Gaston, J.R., and Kriz, L.B., "Connections in Precast Concrete Structures-Scarf Joints," *Journal of the Prestressed Concrete Institute*, vol. 9, No. 3, June 1964, pp. 37-59.
36. Jones, H. L., and Furr, H. L., "Study of In - Service Bridges Constructed with Prestressed Panel Sub-Decks," *Texas Highway Department, Research Project 2-5-10-145*, July 1970.
37. Paulay, T., Park, R., and Phillips, M. H., "Horizontal Construction Joints in Cast -In - Place Reinforced Concrete," *ACI Special Publication SP-42 : Shear in Reinforced Concrete*, vol. 2, American Concrete Institute, Detroit, pp. 599-611.

APPENDIX A: Sample Calculations

A.1 Introduction

Deck panel behavior is discussed at both service and failure stages. At failure stage, capacities in various failure modes are evaluated. In the design phase, only nominal strengths of steel and concrete are used in designing the deck panels. Failure capacities of the panels tested are evaluated based on the strength of steel and an average compressive strength of concrete. Although observed yield strength of the steel is used, observed maximum strength of the concrete is not used in the calculations due to large variation in the observed concrete strengths. Measured modulus of rupture from concrete flexural beam tests are used in calculating the cracking loads of the specimens.

Next, loading and behavior of composite decks with precast panels in various modes of failure such as flexural, beam-shear, horizontal shear, and punching are discussed together with the cracking load levels.

A.2 Loading

Dead Load:

Panel self weight	w	=	2.5 in. @ 150 pcf	=	31.25 psf
Top slab	w	=	5.5 in. @ 150 pcf	=	68.75 psf
Wearing surface	w	=		=	35.00 psf

Live Load:

Construction Live Load:	w	=	50 psf
Wheel Load HS-20:	P	=	16000 lb

$$\text{Impact factor (AASHTO 8.2):} = 1.3 \text{ (30 \%)}$$

$$M_{DL} = (31.25 + 68.75 + 35) (7.5)^2 / 8 = 950 \text{ lb-ft/ft}$$

$$M_{LL} \text{ (simple)} = (s + 2) / 32 P$$

$$\text{But } s = 7.5 \text{ ft.}$$

$$\text{Hence, } M_{LL} = 4750 \text{ lb-ft/ft}$$

Equivalent simply supported live load corresponding to this live load moment is

$$P_{eq} = (4750 * 8 * 2) / 3.75 = 20266 \text{ lbs}$$

$$M_u = 1.3 [M_{DL} + 1.67 M_{LL+I}] = 14641 \text{ lb-ft/ft}$$

$$M_{u \text{ total}} = (14641 * 8 * 12) / 1000 = 1406 \text{ in.-K}$$

$$\text{Hence equivalent service wheel load} = 1.3 * 20.266 = 26.4 \text{ kips}$$

$$\text{Equivalent factored load} = 1.3 * 1.67 * 1.3 * 20.266 = 57.2 \text{ kips}$$

Note: Load due to wearing surface is not added to the above values. It is assumed to be balanced by the excessive weight of the composite deck resulting from the extra depth of the specimen above 8 inches.

A.3 Flexural Strength

A.3.1 Based on nominal strength values

In this mode, ultimate capacities of the deck panels based on nominal strength characteristics of steel and concrete are evaluated. Contribution from cast-in-place reinforcement (CIP rebars) and wire mesh is not considered.

In specimens 1 to 4 with 18 strands:

Flexural capacity assuming full development length is obtained by (ACI 318/89 - 18.7.2):

$$f_{su} = f_{pu} [1 - \gamma_p / \beta_1 (\rho_p f_{pu} / f'_c)] \quad \text{for } f_{se} > 0.5 (f_{pu}) = 135 \text{ ksi}$$

where $\gamma_p = 0.28$; $\beta_1 = 0.85$ and

$$\rho_p = A_{ps} / (b d) = (0.085 * 18) / (8 * 12 * 6.75) = 0.00236$$

which gives $f_{su} = 255.8 \text{ ksi}$;

Hence the neutral-axis depth based on this stress value is

$$a = (A_{ps} f_{su}) / (0.85 f'_c b) = (1.53 * 255.8) / (0.85 * 4 * 96) = 1.2 \text{ in.}$$

Hence, the nominal positive moment is obtained as

$$M_n^+ = f_{su} A_{ps} (d - a/2) = 2407 \text{ in.-K}$$

Hence the corresponding live load is $P = 107 \text{ kips}$.

Based on development length limitation (AASHTO - 9.17.4), flexural capacity is obtained as:

$$f_{su} = l_x / D + (2/3) f_{se}$$

substituting $D = 0.375 \text{ in.}$ (diameter of 3/8 inch strand), and

$l_x =$ distance from end of prestressing strand to center of panel = 48 inches

gives $f_{su} = 243 \text{ ksi}$, thus

$$a = 1.14 \text{ in.}; \quad M_n^+ = 2298 \text{ in.-K}; \quad P = 102 \text{ kips};$$

In specimens 5 and 6 with 12 strands:

when full development length is assumed

$$a = 0.814 \text{ in.}; \quad M_n^+ = 1685.6 \text{ in.-K}; \quad P = 75 \text{ kips};$$

Based on development length limitation

$$a = 0.759 \text{ in.}; \quad M_n^+ = 1578 \text{ in.-K}; \quad P = 70 \text{ kips};$$

A.3.2 Based on Observed Behavior:

In specimens which failed in flexure, some of the prestressing strands were broken indicating that ultimate strength of the strands was achieved at this stage. This can be inferred from the strain measurements also. Similarly, the CIP rebars indicated strains beyond the yielding and hence the contribution of these CIP rebars along with the wire mesh contribution is added to the ultimate flexural capacity of the specimens. At failure, some of the strands slipped. But the load at which strand slip was observed is not considered as the ultimate failure load of the specimens.

In specimens with 18 strands:

contribution from prestressing strands:

$$\text{total area of steel} = 18 * 0.085 = 1.53 \text{ in}^2$$

$$\text{actual strength @ fracture} = 280 \text{ ksi}$$

$$T_1 = 280 * 1.53 = 428.4 \text{ kips acting @ 6.75 in. from top}$$

contribution from CIP rebars as they were observed to yield at failure:

16, #5 bars @ 6 in. c/c

$$\text{total area of steel} = 16 * 0.31 = 4.96 \text{ in}^2$$

$$\text{yield strength} = 75 \text{ ksi}$$

$$T_2 = 75 * 4.96 = 372 \text{ kips @ 2.5 inches from top}$$

contribution from the wire mesh placed in precast panels:

$$\text{wire mesh} = 3 \times 15 \text{ D7} \times \text{W4}$$

$$\text{nominal area of D7} = 0.07 \text{ in}^2; \quad \text{dia.} = 0.298 \text{ in.}$$

$$\text{total no. of D7s in a 8 ft. wide panel} = (96 / 3) - 2 + 1 = 31 \text{ bars}$$

$$\text{area} = 31 * 0.07 = 2.17 \text{ in}^2;$$

$$T_3 = 2.17 * 60 = 130.2 \text{ kips acting @}$$

$$(8 - 1.25 - 0.375 / 2 - 0.298 / 2) = 6.1425 \text{ in.}$$

average compressive strength of concrete = 5.0 ksi (taken into account the scatter in test values).

Hence the neutral-axis depth is obtained as,

$$a = (T_1 + T_2 + T_3) / (0.85 f'_c b)$$

which gives $a = 2.28 \text{ in.}$;

Moment capacity of the specimen is obtained as

$$M_n^+ = T_1 (d - a/2) + T_2 (d_2 - a/2) + T_3 (d_3 - a/2)$$

where $d = 6.75 \text{ in.}$; $d_2 = 2.5 \text{ in.}$; $d_3 = 6.1425 \text{ in.}$;

substituting the above values:

$$M_n^+ = 3622.5 \text{ in.-K} = 301.8 \text{ ft-kips}$$

Corresponding to this moment the live load can be obtained as, $P = 161 \text{ kips}$

Subtracting the dead load effects, we have

$$P = 161 - 3 = 158 \text{ kips}$$

Note: The depth of neutral-axis observed in the specimens at the time of failure was about an inch to 1.5 inches. This could be due to higher compressive strength of concrete. In any case, usage of actual neutral-axis depth will only increase the M_n^+ of the specimen.

In specimens with 12 strands:

$$T_1 = 280 * 1.02 = 285.6 \text{ kips @ 6.75 in. from top}$$

$$T_2 = 75 * 4.96 = 372 \text{ kips @ 2.5 in. from top}$$

$$T_3 = 2.17 * 60 = 130.2 \text{ kips acting @ 6.4125 in.}$$

which gives

$$a = 1.9 \text{ in.}; \quad M_n^+ = 245.4 \text{ ft.-K}; \quad P = 131 \text{ kips};$$

Subtracting dead load effects,

$$P = 131 - 3 = 128 \text{ kips.}$$

A.4 One-Way Shear Strength

In evaluating the shear strength of the specimens, the nominal concrete compressive strength of $f_c' = 4000 \text{ psi}$ is used.

$$V_c = 2 \sqrt{f_c'} b_w d = 82 \text{ kips}$$

$$V_c = 3.5 \sqrt{f_c'} b_w d = 143 \text{ kips}$$

$$V_c = (1.9 \sqrt{f_c'} + 2500 \rho_w V_u d / M_u) b_w d = 78.4 \text{ kips}$$

From the above three values, estimated shear capacity of specimens is taken as,

$$V_c = 82 \text{ kips}$$

Hence the corresponding live load is given by $P = 82 * 2 = 164$ kips.

Subtracting the dead load effects, we have

$$P = 164 - 6 = 158 \text{ kips.}$$

A.5 Horizontal Shear Strength

According to AASHTO - 9.20.4.3 provisions, if the surface of the precast panel is intentionally roughened but not provided with minimum amount of horizontal shear ties, then the shear strength of such a surface is given by

$$V_{nh} = 80 b_v d$$

Substituting, $b_v = 96$ in. and $d = 6.75$ in., we get

$$V_{nh} = 52 \text{ kips (lowerbound)}$$

In the case of surface not intentionally roughened, but provided with minimum amount of horizontal shear reinforcement according to

$$A_{st \min} = 50 b_w s / f_y = 50 * 8 * 12 * 20 / 60000 = 1.6 \text{ in}^2$$

at every section, then the shear strength of such a surface is also equal to

$$V_{nh} = 80 b_v d$$

Hence, with a minimum of 20 shear connectors, distributed as 4 shear connectors at a spacing of 20 inches, we have

which satisfies the minimum amount of shear reinforcement required. Hence, the shear strength

$$A_{st} = 4 * 2 * 0.2 = 1.6 \text{ in.}^2 \text{ at every section}$$

of a surface with 20 shear connectors is given by $V_{nh} = 52$ kips.

Similarly, the upper bound for such a panel with broom finished surface and 20 shear connectors is given by

$$V_{nh} = 350 b_v d \quad (\text{upperbound})$$

which results in a shear strength of $V_{nh} = 227$ kips. Hence the lower and upper bounds on the live loads after deducting the dead load effects are given by

$$P (\text{lowerbound}) = 2 * 52 - 6 = 98 \text{ kips}$$

$$P (\text{upperbound}) = 2 * 227 - 6 = 448 \text{ kips}$$

A.6 Punching Shear Strength (AASHTO)

$$V_{nc} = (2 + 4 / \beta_c) \sqrt{f_c} b_o d_p$$

where

$$f_c' = 4000 \text{ psi}$$

$$\beta_c = 2.5$$

$$b_o = 2 ((20 + 6.75) + (8 + 6.75)) = 83 \text{ in. (HS-20 wheel footprint)}$$

$$d_p = 6.75 \text{ in.}$$

Hence

$$V_{nc \text{ min}} = 127.6 \text{ kips.}$$

Thus, to evaluate the horizontal shear resistance of a broom finished deck panel surface

in the limit of flexural failure or beam-shear failure mode, punching shear failure of the composite specimens should be eliminated. For this purpose, the total load is spread over the entire width of the panel.

A.7 Service Load Analysis

At this stage, the cracking loads of the specimens are obtained based on the measured modulus of rupture of the concrete. The geometrical characteristics of the deck panel and the composite specimens are given below:

Deck panel characteristics:

$$\text{Area} = 8 * 12 * 2.5 = 240 \text{ in}^2$$

$$S_b \text{ (panel)} = 100 \text{ in}^3$$

Composite deck slab characteristics:

$$n = E_{\text{top slab}} / E_{\text{precast}} = 0.95$$

$$y_b = 3.96 \text{ in.}$$

$$I = 3987 \text{ in}^4$$

$$S_b \text{ (composite)} = 1007 \text{ in}^3$$

In specimens with 18 strands,

stresses at the bottom fiber due to prestress based on 15% losses is

$$= -(1.53 * 172) / 240 = -1.10 \text{ ksi}$$

In specimens with 12 strands,

stresses at the bottom fiber due to prestress based on 15% losses is

$$= -(1.02 * 172) / 240 = -0.731 \text{ ksi}$$

Due to self weight of the panel, stress at the bottom fiber is 0.21 ksi.

Due to the weight of CIP slab, stress at the bottom fiber is 0.46 ksi.

In specimens with 18 strands, modulus of rupture is taken as equal to 0.92 ksi. (p. 36.)

Based on the above values, stress required to crack the bottom fiber is

$$f_{bc} = 0.92 + 1.1 - 0.21 - 0.46 = 1.35 \text{ ksi}$$

which results in an applied live cracking load of 60 kips.

In specimens with 12 strands, modulus of rupture is taken as equal to 0.83 ksi (p. 38.)

Based on the above values, stress required to crack the bottom fiber is obtained as

$$f_{bc} = 0.83 + 0.73 - 0.21 - 0.46 = 0.89 \text{ ksi}$$

which results in an applied live cracking load of 40 kips.

COVER DESIGN BY ALDO GIORGINI